Polyphase Structure-Based Approaches for FIR *M*th-band Filters and Constrained Filter Banks: Design, Implementation and Applications

Chao Wu

A Thesis

in

The Departement

of

Electrical and Computer Engineering

Presented in Partial Fulfillment of the Requirements
for the Degree of Doctor of Philosophy at
Concordia University
Montreal, Quebec, Canada

November 2007

Your file Votre référence
ISBN: 978-0-494-37759-8
Our file Notre référence
ISBN: 978-0-494-37759-8

ABSTRACT

Polyphase Structure-Based Approaches for FIR *M*th-band Filters and Constrained Filter Banks: Design, Implementation and Applications

Chao Wu, Ph. D.

Concordia University, 2007

Multirate systems, including *M*th-band filters and filter banks, have greatly facilitated the analysis, understanding and compression of signals. Polyphase structure plays an important role in the study of multirate systems due to the fact that it provides a parallel and very efficient implementation architecture. In this dissertation, some polyphase structure-based approaches for the design and implementation of *M*th-band filters as well as filter banks are presented. The emphasis is placed on the development of new structures that satisfy certain constraints and having low computational complexity.

A design algorithm for *M*th-band filters is first presented based on the generalized polyphase (GP) structure. Both the interpolation and linear-phase conditions are incorporated in the proposed GP realization of *M*th-band filters. By deriving a closed-form frequency response specification for each of the constituent filters in the GP structure, the design of the original large-tap FIR filter is simplified to the design of short-length constituent filters to reduce the overall design complexity. The GP-based approach is then extended for the design of *M*th-band filters meeting certain regularity requirements. To show the wide applicability of the proposed method, the design of 2-D *M*th-band filters via the GP structure is also considered. It is shown that by applying the singular-value decomposition (SVD) to each 2-D subfilter in the GP structure, the

implementation complexity of the overall 2-D filter can be significantly reduced without introducing a large error.

The second part of the dissertation is concerned with the development of new lattice structures for perfect reconstruction filter banks (PRFBs) with certain constraints, such as the linear-phase (LP) and the mirror-image symmetry (MIS). The innovative work is based on the polyphase matrix representation of the analysis and synthesis filters, and a key idea of devising basic building blocks that are capable of propagating the desirable symmetry properties while being cascaded to generate the required lattice structures. Due to the added constraints, the resulting lattice structures have fewer parameters, leading to a speedy optimization design and a reduction in the heavy implementation burden.

It is proved that there exists a complete and minimal lattice structure for MIS-PRFBs. It is shown that a class of well-known filter banks, namely, the cosine-modulated filter banks (CMFBs), is a subclass of MIS-PRFBs, whose non-singular matrices are of sparse coefficients. By introducing more prototype filters, in conjunction with a proper modulation, new CMFBs with more parameters are generated. Combining the linear-phase and mirror-image symmetries, a lattice structure with further reduced number of parameters is also developed for MIS-LPPRFB. The designed MIS-LPPRFB is then utilized as a block transform for image compression coding. Simulation results show that the MIS-LPPRFB, despite its reduced number of parameters, offers a competitive performance in terms of both the visual quality and the peak signal-to-noise ratio for various images under a wide range of compression ratios.

To my loving family

ACKNOWLEDGEMENTS

It is a time to draw a period of my Ph. D. studies. I would like to take this precious opportunity to thank all the wonderful people around me. First and foremost, I would like to express my deepest gratitude and heartfelt thanks to my supervisors, Dr. Wei-Ping Zhu and Dr. M. N. S. Swamy, for their guidance and support throughout the span of this research. I have benefited a lot from their detailed advices, valuable feedback and very careful correction of the thesis chapters. Without their encouragement, it would not have been possible to complete this thesis.

It is my pleasure to thank my friends and colleagues at the Centre for Signal Processing and Communications, Dept. of Electrical and Computer Engineering. I appreciate the moral support and friendship from Dr. Gui Xie, Rajeev Yadav, Nikhil Gupta, Wei Wu, Shahaz Celia, Fattah Shaikh, Hong-Xiang Wang, Bhuiyan Mohammad, and Feng Wan.

Above all, I am indebted to my parents in China for their unconditional support, care, and love. My deepest gratitude goes to my wife Liping Yang who showed infinite patience and understanding during my lengthy study. The love and encouragement only she can offer help me through those hard times.

Contents

List of Figures

List of Tables

List of Abbreviations

BOLT	Biorthogonal Lapped Transform
CMFB	Cosine-Modulated Filter Bank
DCT	Discrete Cosine Transform
DOF	Degree-One Factorization
DFT	Discrete Fourier Transform
DFB	Directional Filter Bank
EBCOT	Embedded Block Coding with Optimized Truncation
EZW	Embedded Zero-Tree Wavelet
FB	Filter Bank
FIR	Finite-Impulse Response
FRM	Frequency-Response Masking
GenLBT	Generalized Lapped Biorthogonal Transform
GenLOT	Generalized Lapped Orthogonal Transform
GP	Generalized Polyphase
IFIR	Interpolated Finite-Impulse Response
IIR	Infinite-Impulse Response
JPEG	Joint Photographic Experts Group
LOT	Lapped Orthogonal Transform
LP	Linear Phase
LUT	Lapped Unimodular Transform
MIS	Mirror-Image Symmetry
MPEG	Moving Picture Experts Group
OOF	Order-One Factorization
PM	Parks-McClellan
PR	Perfect Reconstruction
PSNR	Peak Signal-to-Noise Ratio
PU	Paraunitary

QMF	Quadrature Mirror Filter
SDF	Symmetric-Delay Factorization
SDP	Semidefinite Programming
SPIHT	Spatial Partitioning of Images into Hierarchical Trees
SVD	Singular-Value Decomposition

Chapter 1

Introduction

1.1 General

Over the past two decades, there has been a tremendous growth of research activities in the area of multirate signal processing. Multirate systems [1]-[5] have found a wide range of applications in many engineering fields, such as telecommunications, electronics, and speech and image processing. The most frequent applications of multirate systems are fractional sampling-rate alternation [1] and subband coding [2], [4], in which the Mth-band filter and filter banks play a key role. For example, with a fractional sampling-rate alternation, we may scale a speech, image, or video sequence to different resolutions for various purposes. As such, the design and implementation of the Mth-band filters and filter banks have received a great deal of research attention over the last two decades.

Fig. 1.1 shows a simple, yet typical, multirate system that changes the input sampling rate by L_u / L_d, where L_u and L_d represent the factors of the expander and decimator, respectively, and $H(z)$ is a low-pass filter with a cutoff frequency specified by $M = \max\{L_u, L_d\}$. Hence, $H(z)$ is often called the Mth-band filter, which is used to get rid of the duplicated images caused by the expander as well as to prevent the occurrence

of the aliasing due to the subsequent decimation. Ideally, an Mth-band filter should have a sinc function type impulse response $h[n] = \dfrac{\sin(n\pi / M)}{n\pi}$. Clearly, this impulse response has an important feature that it gives a zero-crossing every M samples, namely, $h[nM] = \frac{1}{M}\delta[n]$. The above property is particularly useful when the Mth-band filter is employed in signal interpolation by a factor of M, where M-1 new samples are generated between every two consecutive input samples while leaving the original samples unchanged. Thus, the property $h[nM] = \frac{1}{M}\delta[n]$ is often referred to as the interpolation condition. Although the interpolation property is desirable in multirate signal processing, it is in general difficult to be accommodated in filter design. Most of the filter design algorithms available in the literatures give only an approximation to the desired frequency response, while very few methods concern about time-domain constraints such as the interpolation condition. Therefore, it is necessary to develop a design method satisfying both the desired frequency response and the time-domain condition.

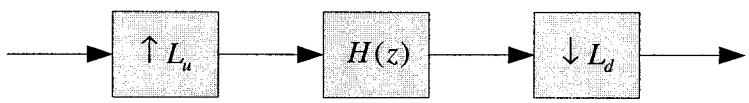

Figure 1.1: Sampling rate conversion by a factor of L_u / L_d

It is well known that the polyphase structure is essential in multirate signal processing applications due to its computational efficiency. The polyphase structure decomposes an original direct-form filter into a number of parallel subfilters having sparse coefficients. Taking the signal interpolation by a factor of two as an example, in which a half-band filter $H(z)$ is used after the expander, one can rewrite $H(z)$ in polyphase structure as

$H(z) = z^{-1}E_0(z^2) + E_1(z^2)$, giving a two-branch polyphase structure as shown in Fig. 1.2(a). This implementation is not efficient since half of the coefficients in $H(z)$ are zeros. By invoking the Noble identity [5], this scheme can be redrawn as a more efficient implementation in Fig. 1.2(b). Clearly, the filters in (b) operate at a rate which is one-half of that of the filters in (a) while both the structures have the same number of coefficients. Another advantage of the polyphase structure is that the interpolation condition can easily be satisfied by implementing one of its parallel branches as $\frac{1}{M}\delta(n)$.

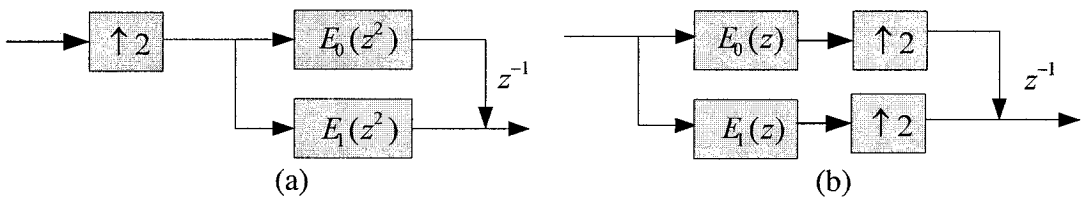

Figure 1.2: The implementation of interpolation filter.
(a) Polyphase structure. (b) Efficient implementation.

Another important application of multirate systems is the subband coding, which is widely used in speech and image compression. Most of physical signals in the real world contain dominant low-frequency components and attenuate gradually as frequency increases, as shown in Fig. 1.3. This unevenly distributed frequency spectrum can be exploited for signal compression: one can split the entire signal into a number of subband signals in the frequency domain using a multirate system and then adopt different coding techniques to each of the subband signals. The coded subband signals can be synthesized by another multirate system to reconstruct the overall compressed signal. In this way, a large compression ratio can be achieved by allocating a different bit rate to each subband according to the energy distribution.

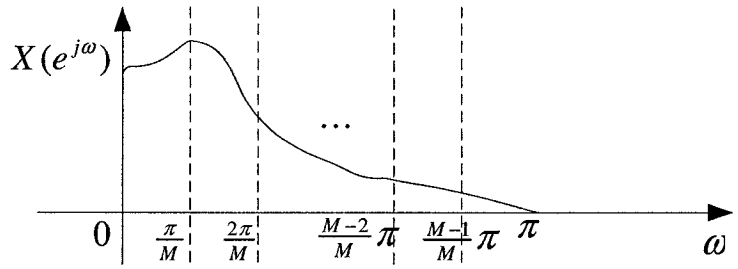

Figure 1.3: A typical signal with its energy concentrated in the low frequency region

The division and reconstruction of the subband signals is performed by a set of analysis and synthesis filters, which constitute a so-called filter bank, as shown in Fig.1.4. The input signal $x[n]$ is separated to M subband signals by M analysis filters $H_i(z)$ with frequency-selective bandpass responses. These band-limited subband signals are then decimated by M so that the total number of samples per unit time is the same as the input rate of $x[n]$. At the receiver end, i.e., the right-hand part of Fig. 1.4, the subband signals are upsampled and combined by a set of synthesis filters $F_i(z)$ to form the reconstructed signal $\hat{x}[n]$. Generally speaking, the reconstructed signal $\hat{x}[n]$ is only an approximation of the original input $x[n]$. The error can be of two types: one is the aliasing and distortion error from the analysis and synthesis parts as well as the corresponding expander and decimator, the other being the quantization error from the intermediate processing.

One of the major developments in filter banks is the recognition of the fact that, through a proper design of the analysis and synthesis filters, all the errors apart from the quantization can be completely eliminated. This feature is called *perfect reconstruction*, which implies that the reconstructed signal is exactly the same as the input one except for a delay, i.e., $\hat{x}[n] = x[n-D]$, if the errors caused by the processing of the subband signals

are ignored. Obviously, perfect reconstruction is a desirable and very attractive feature in view of practical applications. It has been intensively studied, and various approaches [41]-[50] have been proposed to guarantee the perfect reconstruction property. Similar to the implementation of the Mth-band filters, filter banks can also be efficiently realized in the form of polyphase structure. It was recognized, by Vetterli [41] and Vaidyanathan [48] independently, that the polyphase representation results in a considerable simplification of the theory of perfect reconstruction filter banks.

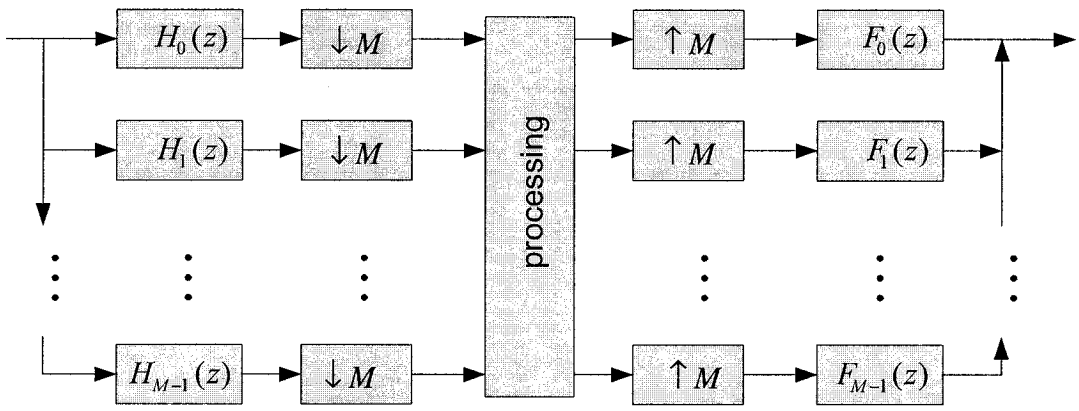

Figure 1.4: An M-channel maximally decimated filter bank

The polyphase representation of the M-channel filter banks is depicted in Fig. 1.5, where M analysis and synthesis filters are now represented by the respective polynomial matrices $\mathbf{E}(z)$ and $\mathbf{R}(z)$. In the polyphase representation, the perfect reconstruction can be equivalently expressed in a simple form, $\mathbf{E}(z)\mathbf{R}(z) = z^{-l}\mathbf{I}$. Moreover, based on the polyphase structure, a lattice factorization has been developed for PRFBs [41, 48], where the polyphase matrices are decomposed into a cascade form of invertible matrices and delay matrices. In the lattice factorization, the perfect reconstruction is structurally satisfied, while all the free coefficients are contained in the invertible matrices. With the

invertible matrices being characterized by a set of parameters, we can design a good performance filter bank by optimizing the free parameters. The lattice factorization approach not only exploits an unconstrained optimization technique for the design of PRFBs, but also provides a robust and efficient implementation.

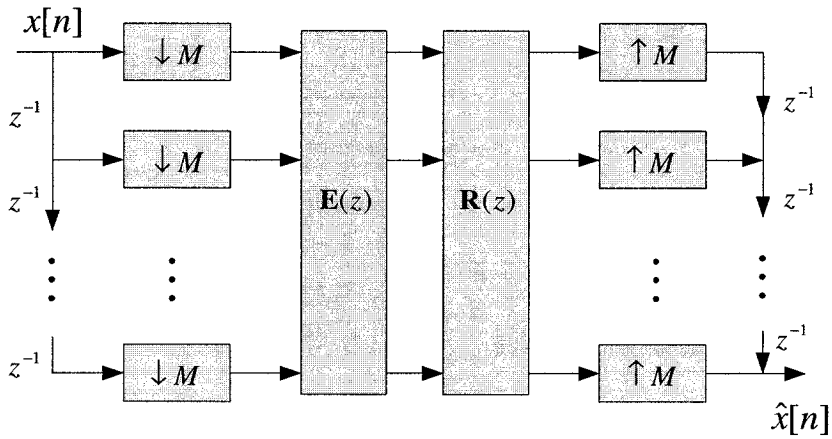

Figure 1.5: Polyphase representation of the M-channel filter banks

Although the lattice factorization enjoys many advantages, it is, in general, not complete for PRFBs. The lattice factorization is said to be complete if and only if any given PRFB can be factorized in the lattice form. The completeness guarantees all the PRFBs are covered by the lattice structure and the "best" PRFB could be reached by unconstrained optimization, at least in theory. The completeness is proved to be true only for a subclass of PRFBs, namely, the PUFB (paraunitary FB) [53]-[55]. As such, researchers have turned their attention to a class of PRFBs satisfying certain constraints, such as linear-phase and pairwise mirror-image symmetry in the frequency response. The linear-phase PUFBs have important applications in image processing and are intensively studied in [68]-[74]. The mirror-image symmetry was first introduced by Nguyen *et al.* [49] to reduce the complexity of filter banks. A complete and minimal lattice structure

was proposed for MIS-PUFBs in [50]. Compared to the linear-phase characteristic, the mirror-image symmetry is a mild constraint, imposing very little limit on the choice of the filter length and the type of symmetry. With only one-half of the number of parameters in general PUFBs, the MIS-PUFB provides a similar performance. Based on the development of an order-one building block, which enables to propagate both linear-phase and perfect reconstruction property, Tran *et al.* have extended the popular linear-phase paraunitary filter bank (LPPUFB) to the linear-phase perfect reconstruction filter bank (LPPRFB) in [74]. Although Tran's structure has been proved to be not complete [82], his idea has inspired us to study other types of constrained PRFBs.

With the above observation in mind, in this thesis, we would like to develop the structure-based design and implementation techniques for Mth-band filters as well as filter banks. The first part of the thesis focuses on the design of FIR filters, with an emphasis on Mth-band filters having time-domain constraints, using the generalized polyphase structure. The second part deals with the design and implementation of a class of PRFBs with certain constraints, such as mirror-image symmetric PRFBs and linear-phase PRFBs, with an objective of obtaining a complete and minimal lattice realization structure.

1.2 State of the Art Techniques

In this section, we will review some of the typical techniques, which has been widely used in the filter and filter bank design. This literature review not only serves as a necessary background material in this field, but also supports the motivation of the proposed work.

1.2.1 Design of General FIR Filters

Although we mainly focus on the design of Mth-band FIR filters in this thesis, it would be helpful to briefly review some of the commonly used methods for the design of general FIR filters. We will then point out the limitations of these methods and state why they fail to design Mth-band FIR filters. Also, these methods may serve as good references for the comparison of the performances of the filters designed via different techniques including the proposed algorithm.

Window method [6], [7] is probably the simplest way to obtain an FIR filter, wherein the impulse response of the ideal filter is truncated with a window function. Kaiser window [6], which is actually a family of windows spanned by a parameter β, offers a systematic way to design filters with various degrees of tradeoff between the transition band, error ripples and filter length. Since the impulse response is obtained from the ideal filter, the interpolation condition is automatically satisfied. However, the window method is in general not optimal in any sense.

Optimal FIR filters should give the best approximation to the desired frequency response under certain criterion with finite coefficients. Two commonly used optimal criteria are the mini-max error and the least-squares error. A filter optimal in the mini-max sense minimizes the maximum errors in the passband as well as in the stopband. According to the optimization theory, the minimized maximum error tends to be evenly distributed over the entire frequency band of interest, either passband or stopband, and thus, has an equiripple frequency response. For filters designed in the least-squares sense, the error energy, i.e., the square of the difference between the ideal and actual responses, is minimized. Generally speaking, the filter designed in the mini-max sense avoids the

"overshooting" response near the cutoff frequency points, which quite often occurs in the least-squares design. However, the least-squares design outperforms the mini-max one in terms of the algorithmic complexity.

Based on the alternation theorem [15], Parks and McClellan [16] have proposed a mini-max design algorithm, yielding equiripple linear phase filters. This method is very efficient and allows us to systematically design a large family of linear-phase FIR filters including differentiators and Hilbert transformers. Unfortunately, this method is not flexible and fails to design filters with extra constraints.

Later, Vaidyanathan and Nguyen [17]-[18] proposed the eigenfilter approach, which is optimal in the least squares sense. By formulating the objective function as the sum of the passband and stopband errors, the optimal filter coefficients can be obtained from an eigenvector of an appropriately formulated matrix. Moreover, the interpolation condition can be satisfied by deleting the corresponding coefficients from the eigenvectors.

FIR filter design is basically an optimization problem. From linear programming [8], [9] to the recent semidefinite programming (SDP) [10]-[13], the development of the optimization algorithms makes it possible to design more complicated filters with large taps and/or various time/frequency-domain constraints. SDP is primarily concerned with minimizing a linear or convex quadratic objective function subject to linear matrix inequality-type constraints. The wide applicability of SDP is attributed to several reasons. (1) Most of the filter design problems, regardless of 1-D or 2-D, FIR or IIR, the minimax design or the least-sqaures one, can be formulated as an SDP optimization problem. (2) The extra constraints, such as the flatness and interpolation condition, can be well accommodated by means of a linear matrix inequality. (3) An efficient and user-friendly

software implementation of various SDP algorithms is available. However, this optimization method still has several uncertain issues such as the convergence, numerical precision and the computational complexity.

1.2.2 Structure-based Filter Design and *M*th-band Filters

Another major focus on FIR filter design is to develop fast and efficient algorithms with an objective of reducing the computations for its design as well as implementation. One of the successful ideas in fast filter design and implementation is to use the structural decomposition.

Neuvo *et al.* have introduced the concept of interpolated FIR (IFIR) filter [19], where a subfilter with sparse coefficients is cascaded by a relatively simple interpolator. With the unwanted images of the subfilter being suppressed by the interpolator, IFIR is capable of realizing large-tap narrow-band FIR filters with a less computational cost. However, the IFIR concept only works for narrow-band filters.

To overcome this limitation, Lim *et al.* [20], [21] have proposed the frequency-response masking (FRM) technique, which involves two complementary subfilters and the corresponding interpolators. Using this idea, large computational savings can be achieved, especially for filters with a sharp transition-band. In both the IFIR and FRM methods, the expander has been used to give a sharp transition with a shorter filter length.

Observing that there also exists expander in the polyphase structure, Mitra *et al.* [22], [23] have proposed the generalized polyphase (GP) structure, which can be regarded as an IFIR with M branches. Through the insertion of a pair of Hadamard transform matrices in the conventional polyphase structure, the original filter is realized by parallel branches, each branch consisting of a so-called interpolator and an upsampled constituent

filter in cascade connection. The authors have also investigated the frequency selective property of the interpolators and provided a framework for obtaining the constituent filter, the interpolator and the original filter.

In the design and implementation of 2-D filters, a parallel structure using singular-value decomposition (SVD) has attracted a great deal of research attention [24]-[27]. By applying SVD to the sampled frequency response matrix in the frequency-domain or the impulse response matrix in the time-domain, a 2-D filter is decomposed into a set of 1-D filters. In many cases, only the first few branches of the SVD realization are significant. Therefore, those branches with small contributions can be neglected with a little sacrifice in the designed frequency response.

At the same time, the *M*th-band filter has attracted considerable attention for its important role in interpolation, wavelets and filter banks. Mintzer [28], was the first one to arrive at the necessary requirements in the frequency domain for the interpolation condition. It was Vaidyanathan who realized that the interpolation condition can be exploited to reduce the number of unknown coefficients and expedite the design process. In [29], a half-band filter is designed based on the polyphase structure, where only one-half of the coefficients need to be determined. The 'trick' of this method is that the interpolation condition imposed on one subfilter contributes an ideal constant frequency response and the frequency response of the overall filter is then fully determined by the the other subfilter to be designed. Therefore, as long as the subfilter is designed to be equiripple, the overall half-band filter is also equiripple. However, this result is not available for general *M*th-band filters, since there are more than one subfilter to be determined.

Noticing that the eigenfilter approach can be used to design optimal Mth-band filters in the least-squares sense, an iterative procedure [30] was proposed to reach an optimal Mth-band filter in the minimax sense. At each step, a weighting function is used to adjust the error ripples of the eigenfilters. The design of Mth-band filters has also been extended to the nonlinear-phase case [31], [32] as well as the 2-D case [33]. Some fast design methods have also been proposed to generate a family of Mth-band filters from one prototype Mth-band filter through modulation [34], [35].

1.2.3 Design and Implementation of General PRFBs

After the analysis and synthesis filtering in the filter bank together with the decimator and expander operations, the reconstructed signal differs from the original input signal due to three error sources: aliasing, amplitude distortion and phase distortion. It was shown by Smith and Barnwell [36], and Mintzer [37] that for a quadrature mirror filter (QMF) bank, a special two-channel filter bank, all the three distortions mentioned above can be eliminated through a proper choice of the analysis and synthesis filters, leading to a perfect reconstruction result. For the case of M channel filter banks, the conditions for aliasing cancellation and perfect reconstruction are much more complicated. The general principle of perfect reconstruction in the M channel case has been developed by a number of authors [38]-[48]. The most commonly used PR condition is given by $\mathbf{R}(z)\mathbf{E}(z) = cz^{-l}\mathbf{I}$. Since then, the design and implementation of the PRFBs has been intensively studied and several approaches have been proposed. In [42], the perfect reconstruction condition is formulated as constraints in the time-domain. With the help of polynomial matrix analysis, various decomposition methods, such as the lifting scheme, LU decomposition and singular-value decomposition [43]-[47], have been proposed to

attain PRFBs. The most popular way of designing and implementing the PRFBs is through the lattice factorization [48]-[55], which decomposes the polyphase matrix of FB into a cascade form of invertible matrices and delay matrices. While it is easy to verify that the lattice structure gives a PRFB, it is in general not complete, i.e., not all PRFBs can be factorized into the lattice structure. As mentioned earlier, the lattice structure has been proved to be complete for a subclass of PRFBs, namely, the PUFBs, whose analysis polyphase matrix satisfies $\mathbf{E}^H(z^{-1})\mathbf{E}(z) = \mathbf{I}$. Obviously, the PUFB is of perfect reconstruction with a synthesis polyphase matrix as given by $\mathbf{R}(z) = z^{-K}\mathbf{E}^H(z^{-1})$, where K is the highest order of $\mathbf{E}(z)$. Vaidyanathan *et al.* [48] proposed a complete and minimal structure which is based on the *degree-one factorization* (DOF) and peels off a PU building block of McMillan degree-one from the polyphase matrix. The DOF is more suitable for systems with a fixed degree. However, the McMillan degree represents a minimum delay number as required by the system, which is usually not predetermined. In practice, one may more often have a system with a fixed filter length instead of the degree. Therefore, the order-based factorization is a more reasonable choice. For some constrained PUFBs, such as linear-phase or pairwise mirror-image symmetry, complete and minimal lattice structures have been developed based on *order-one factorization* (OOF) [50]-[52]. In these structures, approximately one-half of the entries in the delay matrices are pure delays. Observing this fact, the symmetry delay factorization [53] was proposed, which covers both linear-phase and pairwise mirror-image symmetric PUFBs as well as the CMFBs. In these structures, the building blocks reduce the order of polyphase matrix instead of the McMillan degree. More recently, based on the SVD, Gao *et al.* [54] have proved for the first time that the OOF is complete for a general PUFB

without any constraints. Moreover, they have pointed out that there are redundant parameters in the previous lattice structures and provided a simplified structure with the number of parameters reduced almost by one-half. This structure was then further simplified by Gan *et al* in [55].

1.2.4 Design and Implementation of PRFBs with certain Constraints

In addition to general PUFBs, those with certain constraints, such as linear-phase and the pairwise mirror-image symmetry, have also been widely investigated. Linear-phase PUFBs have very important applications in image processing and have been studied in [68]-[86]. The study of LPPRFBs started from the two-channel case [56]. Although a lot of effort has been made to obtain a solution for two-channel LPPRFBs, there are still some open questions for the M-channel case. The famous DCT transform, which is widely used in international standards for image compression, is a special case of the M-channel FBs with a zero order. The lapped orthogonal transform (LOT) [68] of order one, and the LPPUFBs [70] of an arbitrary order were then subsequently developed for higher order LPPRFBs. A much simplified version of the LPPUFBs, called the GenLOT, was proposed by de Queiroz [71], which includes the DCT and LOT as special cases. Trac *et al.* then investigated the LPPRFBs with a variable length and obtained the necessary condition for the existence of LPPRFB [72], [73]. Based on the development of an order-one building block, which enables to propagate both the linear-phase and the perfect reconstruction properties, Tran *et al.* have extended the popular linear-phase paraunitary filter bank (LPPUFB) to the linear-phase perfect reconstruction filter bank (LPPRFB) in [74]. From the block transform perspective, the LPPRFBs can be viewed as a family of the generalized lapped biorthogonal transforms (GenLBT). The relaxation of the

orthogonal constraint allows the GenLBT to have different analysis and synthesis filters, which can be tailored appropriately to fit a particular application.

A general PRFB can be achieved through a lattice structure, however, the considerable number of free parameters and the highly complicated nonlinear optimization have made the design and implementation a formidable task. Therefore, certain constraints have been introduced to reduce the number of parameters. In Fig.1.6, typical frequency responses of the analysis filters are illustrated. With the symmetry in the frequency response, two types of filter banks have been proposed: one is the pairwise image symmetric filter banks (MIS-FBs), the other is the cosine-modulated filter banks (CMFBs). For the MIS-FBs, a constraint denoted as $H_k(z) = \tilde{H}_{M-1-k}(z^{-1})$ is imposed so that the frequency response of the analysis filters are pairwise symmetric with respect to the center $\pi/2$. This constraint is introduced to reduce the parameters of the filter banks and to expedite the design procedure with a mild sacrifice in the performance [49], [50]. To further reduce the number of parameters, a class of cosine-modulated filter banks (CMFBs), which has a more stringent constraint, has been proposed [87]-[89]. Since the frequency response of the analysis filters can be regarded as shift versions of one another, it is possible to generate all the analysis filters from one low-pass prototype filter through modulation. With only one filter to be designed instead of all the M analysis filters, the design/implementation complexity of CMFBs has been significantly reduced. The cosine modulated pseudo QMF systems were first proposed in [87], where the analysis and synthesis filters are chosen so that only the "adjacent-channel aliasing" is canceled, and the distortion is approximately a delay. Later, cosine-modulated filter banks with perfect reconstruction property have been independently developed by Malvar [88], and

Koilpillai [89]. These paraunitary systems retain both the simplicity and economy of the pseudo QMF systems, yet possess the perfect reconstruction property. A more general CMFB family with arbitrary filter lengths, biorthognal frame, and linear-phase, is then further studied in [90]-[97].

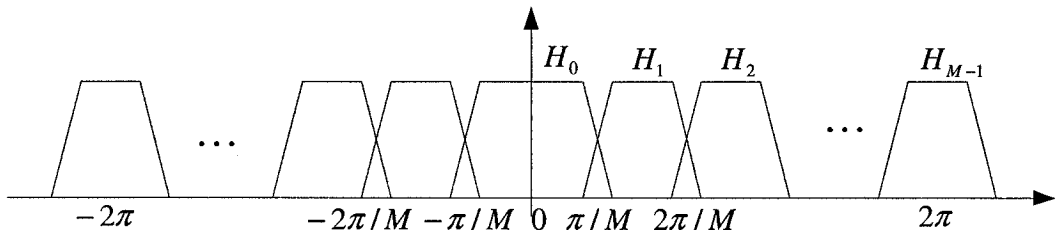

Figure 1.6: Typical frequency response of analysis bank

1.3 Motivations and Objectives

An important advancement in multirate systems is the invention of the polyphase representation. This permits great simplification of theoretical results and also leads to computationally efficient implementation. Based on the polyphase representation, many algorithms have been proposed to obtain a fast and efficient structure for the design of filters/filter banks satisfying certain constraints. Some of the advantages of the structural decomposition-based techniques are as follows.

1. A large complicated system is decomposed into several small easy-to-handle subsystems.
2. The resulting structure suits for a parallel and modular processing, which is favorable in hardware implementation.
3. Additional constraints can be easily accommodated and structurally satisfied.
4. Part of the structure can be set to zero or discarded without severely jeopardizing the performance, leading to a simplified realization structure.

From the earlier review, we know that the interpolation condition is hard to accommodate in most of the existing filter design methods, thus making very few methods available for the design of Mth-band filters. As for filter banks, although great success has already been achieved in the lattice factorization of the polyphase matrix for PUFBs, as to whether there is a complete lattice structure for general PRFBs, or for those with certain constraints, is still an open question. The success of the polyphase structure inspires us to proceed with the structural decomposition-based design and implementation methodologies for the FIR Mth-band filters and MIS-PRFBs.

Although the polyphase structure may elegantly satisfy the interpolation condition for the Mth-band filters, a direct design based on the polyphase structure faces some difficulties. First, for a linear-phase filter, the subfilters in the polyphase structure are no longer linear-phase, making it difficult to exploit the symmetry of the coefficients. Second, the polyphase structure decomposes the overall filter into several branches, each containing partial coefficients to be determined. Directly designing these subfilters instead of the overall filter requires the frequency specifications for these subfilters, which is the key issue to be solved for the polyphase-based design.

The first difficulty can be overcome under the GP framework, where the linear-phase property is restored for the constituent filters. Therefore, it is possible to design these linear-phase constituent filters without worrying about the phase distortion. However, in [22], the GP structure is based on the Hadamard transform, which limits the branch number to be of a power-of-two. Besides, it has been suggested in [22] that these constituent filters be designed separately, i.e., only one subfilter is optimized at a time while the others are kept unchanged. This scheme requires time-consuming iterations

before reaching a final stable solution, since the optimization of each constituent filter may depend on the other constituent filters. In order to design these constituent filters independently, the frequency response specification for each of them should be determined, and this is the key to the GP-based design technique. As such, it is necessary to further study the GP structure with regard to the following aspects.

1. To construct new transform matrices as generalizations of the Hadamard matrix, so that they enable the use of arbitrary number of branches.
2. To study the relationship between the original filter, the interpolators and the constituent filters from the frequency response perspective, and derive, if possible, a closed-form expression for the frequency specification for each of the constituent filters.
3. To incorporate the interpolation constraint in the GP structure.

In the design of filter banks, although the perfect reconstruction property has been thoroughly studied and many efficient approaches have been proposed for its realization, these methods are in general not complete. Until now, the lattice structure has been proved to be complete only for a special class of PRFB, namely, the parauintary filter banks (PUFBs), and that for general PRFBs is complete for order-one only. Since there is no lattice structure for a general PRFB, we would like to limit our study to a class of PRFBs with certain constraints. In particular, we will focus on the study of MIS-PRFBs and linear-phase PRFBs.

The MIS filter banks are of particular interest for the following reasons. (1) The MIS constraint can be elegantly expressed in the polyphase form and imposes certain symmetry property to the corresponding polyphase matrices. This kind of symmetry,

further exploited by the lattice structure, can significantly reduce the complexity of the filter bank. (2) The MIS is such a mild constraint that it loses almost nothing compared to an optimal filter bank. What is more, unlike the linear-phase constraint which imposes certain conditions on the choice of the filter length, MIS is valid for filter banks with arbitrary length. This makes it possible to combine the MIS with other types of filter banks so that the number of parameters can be further reduced. (3) Both the CMFBs and the MIS-FBs utilize the symmetry property of the frequency response of the analysis filters, except that the former is a more strong condition than the latter. It would be also interesting to investigate the relationship between these two types of filter banks.

In this thesis, we focus our study on the development of lattice structures for constrained PRFBs with the following objectives:

1. to investigate the completeness of the lattice structure for mirror-image symmetric filter banks,
2. to reveal the relationship between CMFB and MIS-PRFB and generate a framework encompassing both FBs, and
3. to develop a lattice structure with fewer parameters by combining the constraints of linear-phase and mirror-image symmetry.

Another objective of this thesis is to apply the designed Mth-band filters and filter banks to image interpolation and compression, by using the Mth-band filters to resize the resolution of images and to study the application of the proposed filter banks as the lapped transform in image compression coding.

1.4 Organization of the Thesis

The thesis is organized as follows. In Chapter 2, we briefly review the background material concerning filters and filter banks. Some of the state of the art techniques for the design of FIR filters and filter banks are also presented. In Chapter 3, a new approach for the design of FIR filters based on the GP structure is developed with an emphasis on a class of Mth-band filters satisfying certain constraints such as the interpolation and regularity conditions. This GP-based approach is then extended for the design of 2-D filters in Chapter 4. A simplified realization structure as a combination of the GP structure and SVD is also developed. Chapters 5-7 focus on the lattice structure-based design techniques for PRFBs with certain symmetry constraints. In Chapter 5, a complete and minimal lattice structure is proposed for mirror-image symmetric PRFBs. The lattice structure is based on an order-one building block that enables the propagation of both the mirror-image symmetry and the perfect reconstruction from a lower-order filter bank to a higher order one. In Chapter 6, cosine-modulated filter banks (CMFBs) are revealed as a special case of mirror-image symmetric PUFBs with a sparse bidiagonal matrix. In Chapter 7, the linear-phase and mirror-image symmetry constraints are combined together to give a more simplified PRFB with fewer parameters. The resulting filter bank is functioned as a lapped transform in the image compression application. Finally, the main contributions of the thesis are summarized in Chapter 8, together with possible future research directions.

1.5 Main Contributions

The main contributions of the thesis work can be summarized as follows.

First, a GP-based design method is proposed for FIR filters. Several new transform matrices are proposed as seed matrices to obtain a GP structure with arbitrary number of branches. These matrices overcome the limitation of the commonly-used Hadamard transform whose length is restricted to be a power of two. Then, an in-depth study of the components in the GP structure is undertaken, yielding a closed-form frequency specification for the design of constituent filters. With the derived amplitude specifications, the constituent filters can be designed independently, thus simplifying the design problem of a large-tap FIR filter to that of a number of short-length constituent FIR filters. It is shown that using the derived specification along with a semidefinite programming (SDP) optimization technique, a wide range of filters including general FIR filters, Mth-band filters and those with certain regularities can be well designed by the proposed GP-based approach.

The GP-based design is also extended for 2-D filters. A realization scheme that combines the singular-value decomposition (SVD) and the generalized polyphase (GP) structure is proposed for 2-D linear-phase FIR filters. With a small number of extra additions, a high-order 2-D FIR filter is converted to several lower-order 2-D subfilters. These subfilters are then realized using the SVD, yielding a parallel implementation structure for each 2-D subfilter. Due to the energy compaction of the SVD and the frequency-selective property of the GP structure, the number of parallel branches in each 2-D subfilter is significantly reduced without introducing a large error. It is also shown that the various symmetries of 2-D filters, such as the quadrantal symmetry and the central symmetry, are well preserved in the proposed GP-SVD structure.

A complete lattice structure for perfect reconstruction mirror-image symmetric filter banks is presented. An order-one building block is first developed to construct a higher-order polyphase matrix of a class of perfect reconstruction filter banks (PRFBs). The proposed building block is capable of propagating both the perfect reconstruction and mirror-image symmetry properties during the order update of the polyphase matrix. Based on a cascade of such building blocks, it is then shown that the lattice structure is complete for a class of PRFBs that satisfy the mirror-image symmetry.

The cosine-modulated filter bank (CMFB) is also investigated as a special case of PUFBs with mirror-image symmetry. CMFB is formulated as a cascade of a modulation matrix and a polyphase matrix with a bidiagonal structure. Several new CMFBs are developed by using multiple prototype filters in conjunction with a proper modulation scheme. It is shown that when M prototype filters are used, a full polyphase matrix representing a general PUFB can be obtained, thus providing a bridge connecting CMFBs and PUFBs. It is also shown that with more free parameters involved in the CMFBs, one can achieve a tradeoff between the performance of the filter bank and its design/implementation complexity.

The application of the constrained filter banks in image compression is also investigated. All the desirable properties, such as perfect reconstruction, mirror-image symmetry, and linear-phase constraints are guaranteed by the proposed lattice structure. Despite all these constraints and the reduced number of parameters, the filter bank obtained from the proposed lattice structure still offers a competitive performance in both visual quality and the peak signal-to-noise ratio (PSNR).

Chapter 2

Background and Literature Review

This chapter introduces some basic notations and concepts involved in the development of filters and filter banks. Some state of the art literature relating to the proposed work are also reviewed, providing the necessary details of the relevant existing design methods for the development of new approaches in later chapters.

2.1 Fundamentals of Multirate Systems

A traditional single-rate signal processing system includes basic elements like multipliers, adders, and delay elements. In a multirate system, there are two more elements, the decimator (downsampler) and expander (upsampler), as depicted in Fig.2.1. With two new operations of downsampling and upsampling, the sampling rate of an input signal can be rationally changed.

(a) (b)

Figure 2.1: Multirate system. (a) M-fold expander. (b) M-fold decimator.

Expander

An M-fold expander or upsampler takes an input sequence $x[n]$ and inserts M-1 zeros between two neighboring input samples. The output sequence $y_E[n]$ can be written as

$$y_E[n] = \begin{cases} x[n/M], & \text{if } n \text{ is a multiple of } M, \\ 0, & \text{otherwise.} \end{cases} \tag{2.1}$$

In z-transform, the relationship of the output sequence and input sequence after the expander can be obtained as

$$Y_E(z) = X(z^M). \tag{2.2}$$

From (2.2), we have $Y_E(e^{j\omega}) = X(e^{jM\omega})$. This means that $Y_E(e^{j\omega})$ is an M-fold compressed version of $X(e^{j\omega})$, as seen from Fig.2.2(a) and Fig.2.2(b). The multiple copies of the compressed spectrum are called images.

Decimator

An M-fold decimator or downsampler takes an input sequence $x[n]$ and retains only every M-th sample in the output sequence. The output $y_D[n]$ is given by

$$y_D[n] = x[Mn]. \tag{2.3}$$

For the M-fold decimator, the frequency response of the output, $Y_D(e^{j\omega})$, can be expressed in terms of the frequency response of the input $X(e^{j\omega})$ as

$$Y_D(e^{j\omega}) = \frac{1}{M}\sum_{k=0}^{M-1} X\left(e^{j(\omega-2\pi k)/M}\right). \tag{2.4}$$

The above frequency response is illustrated in Fig. 2.2(a) and Fig. 2.2(c). The graphical interpretation is as follows: (a) stretch $X(e^{j\omega})$ by a factor of M to obtain $X(e^{j\omega/M})$, (b) create M-1 copies of the stretched version by shifting it uniformly in successive amounts

of 2π, and (c) add all these shifted stretched versions to the unshifted version $X(e^{j\omega/M})$, and divide it by M.

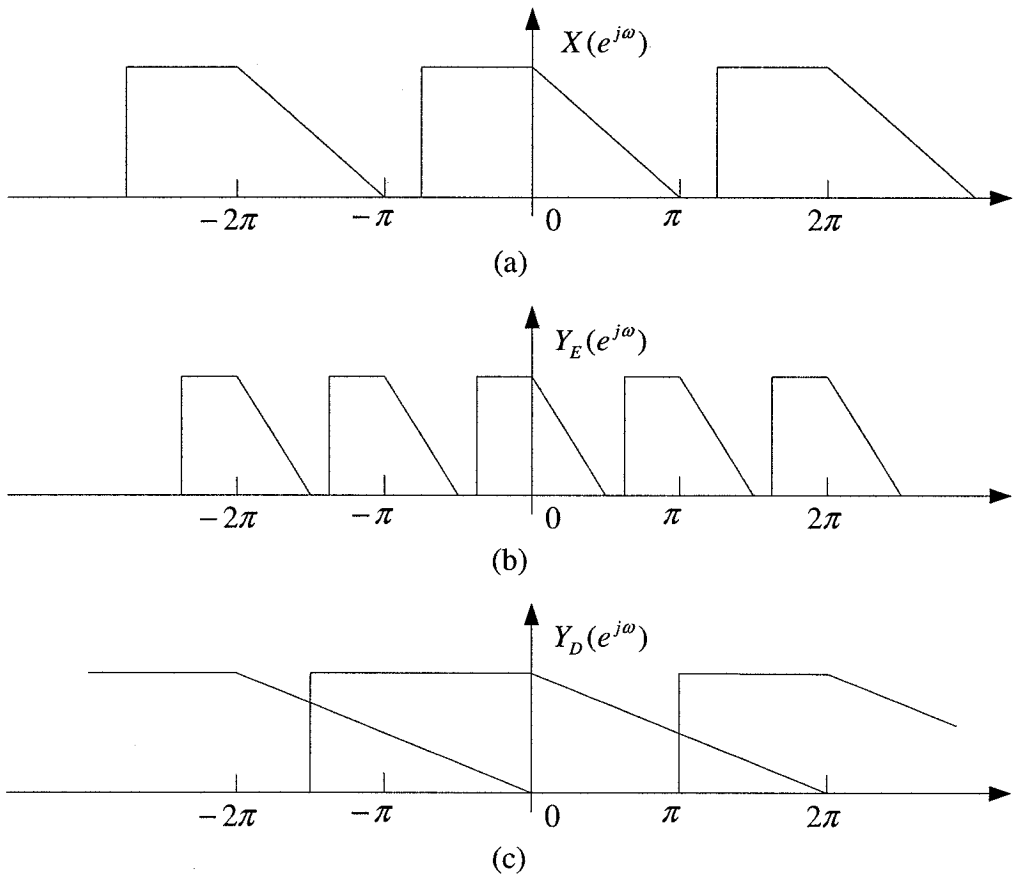

Figure 2.2: Frequency-domain effects of the expander and decimator. The Fourier transform of (a) the input signal $x[n]$, (b) the expanded signal $y_E[n]$ (M=2), and (c) the decimated signal $y_D[n]$ (M=2).

Nobel Identities

The expander and decimator can be cascaded with a linear time-invariant system. In Fig. 2.3(a), a filter follows a decimator, and in Fig. 2.3(c), a filter precedes an expander. If the filter has a rational system function $H(z)$, we may get equivalent implementations of Fig.2.3(a) and (c) as shown in Fig. 2.3(b) and (d), respectively. Notice that the filters in Fig. 2.3 (a) and (c) operate at a lower rate, and therefore, they are more efficient than that

in Fig. 2.3 (b) and (d). These relationships, called *Nobel Identities,* are very useful in the analysis and implementation of multirate systems.

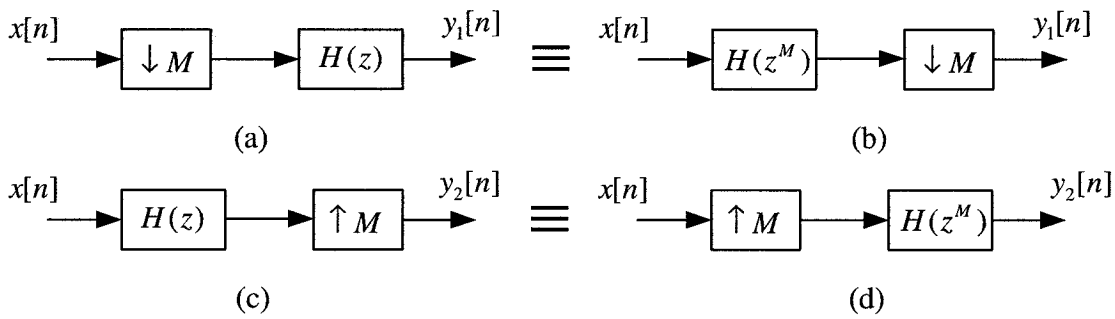

Figure 2.3: Nobel identity. (a) A decimator followed by a filter. (b) Equivalent structure of (a). (c) A filter precedes an expander. (d) Equivalent structure of (c).

Polyphase Structure

An important advancement in multirate systems is the invention of the polyphase representation, which greatly simplifies the theoretical results and yields a computationally efficient implementation. For a given filter $H(z)$, we can always decompose it as

$$H(z)=\sum_{n=-\infty}^{\infty}h[n]z^{-n}=\sum_{l=0}^{M-1}z^{-l}\sum_{n=-\infty}^{\infty}h[Mn+l]z^{-nM}=\sum_{l=0}^{M-1}z^{-l}E_l(z^M) \qquad (2.5)$$

where

$$E_l(z)=\sum_{n=-\infty}^{\infty}h[Mn+l],\ 0\le l\le M-1$$

Equation (2.5) is called the Type I polyphase representation. A variation of (2.5) is given by

$$H(z)=\sum_{l=0}^{M-1}z^{-(M-1-l)}R_l(z^M) \qquad (2.6)$$

where

$$R_l(z) = \sum_{n=-\infty}^{\infty} h[Mn + M - 1 - l] = E_{M-1-l}(z)$$

Equation (2.6) is called Type II polyphase representation, whose components $R_l(z)$ are permutations of $E_l(z)$.

2.2 FIR Filter Design

2.2.1 SDP-based Filter Design

The semidefinite programming (SDP) is a recent major progress in the optimization theory [11]. Some of the features of SDP include the following. 1. SDP is a convex optimization which covers many available methods, such as the linear programming, as special cases. 2. SDP can be efficiently solved through the method of interior points, which outperforms others methods as a more powerful optimization tool. 3. In signal processing, SDP has already been used to design a large class of 1-D and 2-D filters with arbitrary frequency responses [10]. 4. Extra linear equality or inequality constraints can be easily accommodated in SDP.

A typical SDP problem can be expressed as

$$\text{minimize} \quad \mathbf{c}^T\mathbf{x} \tag{2.7a}$$

$$\text{subject to:} \quad \mathbf{F}(\mathbf{x}) \succeq \mathbf{0} \tag{2.7b}$$

$$\mathbf{F}(\mathbf{x}) = \mathbf{F}_0 + \sum_{i=1}^{n} x_i \mathbf{F}_i \tag{2.7c}$$

where $\mathbf{c}$ is a known vector, $\mathbf{x} = [x_1 \quad \cdots \quad x_n]^T$ is the unknown vector to be determined, and $\mathbf{F}_i$ are known symmetric matrices and $\mathbf{F}(\mathbf{x}) \succeq \mathbf{0}$ denotes that $\mathbf{F}(\mathbf{x})$ is positive

semidefinite at $\mathbf{x}$. Note that the constraint matrix $\mathbf{F}(\mathbf{x})$ in (2.7) is affine with respect to $\mathbf{x}$. In [10], the authors have shown that the filter design problem under either mini-max or least-squares sense can be formulated as the SDP problem given in (2.7). Assume $H_d(e^{j\omega_i})$ to be the desired amplitude response. Define the impulse coefficients and Fourier transform vectors as

$$\mathbf{h} = [h(0) \quad h(1) \quad \cdots \quad h(N-1)]^T \tag{2.8a}$$

$$\mathbf{g}(e^{j\omega}) = [1 \quad e^{-j\omega} \quad \cdots \quad e^{-j(N-1)\omega}]^T \tag{2.8b}$$

Then the relevant parameters in (2.7) for the mini-max design are given by

$$\mathbf{x} = [\delta_1 \ \mathbf{h}^T]^T \tag{2.9a}$$

$$\mathbf{c} = [1,0,\cdots 0]^T \tag{2.9b}$$

$$\mathbf{F}(\mathbf{x}) = diag\{\mathbf{\Lambda}(\omega_1), \mathbf{\Lambda}(\omega_2), \cdots, \mathbf{\Lambda}(\omega_K)\} \tag{2.9c}$$

where δ_1 is the largest error at the sampled frequency ω_i, $(i = 1,2,\ldots,K)$ and $\mathbf{\Lambda}(\omega_i)$ is given by

$$\mathbf{\Lambda}(\omega_i) = \begin{bmatrix} \delta_1 & \mathbf{h}^T\mathbf{g}(e^{j\omega_i}) - H_d(e^{j\omega_i}) \\ \mathbf{h}^T\mathbf{g}(e^{j\omega_i}) - H_d(e^{j\omega_i}) & 1 \end{bmatrix}$$

For the optimal filter design in the least-squares sense, the corresponding matrices can be obtained as

$$\mathbf{x} = [\delta_2 \ \mathbf{h}^T]^T \tag{2.10a}$$

$$\mathbf{c} = [1,0,\cdots 0]^T \tag{2.10b}$$

$$\mathbf{F}(\mathbf{x}) = \begin{bmatrix} \delta_1 + \gamma & \mathbf{h}^T\mathbf{U}^{1/2} - (\mathbf{U}^{1/2}\mathbf{q})^T \\ (\mathbf{h}^T\mathbf{U}^{1/2} - (\mathbf{U}^{1/2}\mathbf{q})^T)^T & \mathbf{I} \end{bmatrix} \tag{2.10c}$$

with

$$\mathbf{U} = \int_0^{\pi} \mathbf{g}(e^{j\omega})\mathbf{g}^H(e^{j\omega})d\omega,$$

$$\mathbf{q} = \int_0^{\pi} H_d(e^{j\omega})\mathbf{g}(e^{j\omega})d\omega$$

$$\gamma = \left\|\mathbf{U}^{1/2}\mathbf{q}\right\|^2 - \int_0^{\pi} \left|H_d(e^{j\omega})\right|^2 d\omega$$

where δ_2 is the total squared error in both pass and stop bands.

2.2.2 Eigenfiler Approach

The eigenfilter design method for a discrete time filter involves the determination of the filter coefficients as the eigenvector of a particular Hermitian positive definite matrix. As opposed to other filter design algorithms such as the least-squares approach, which requires the computation of a matrix inverse, the eigenfilter method only requires the computation of a single eigenvector. Consider a low-pass filter with a passband frequency ω_p and stopband ω_s, whose desired response is

$$H_d(\omega) = \begin{cases} 1, & 0 \le \omega \le \omega_p \\ 0, & \omega_s \le \omega \le \pi \\ \text{don't care}, & \omega_p < \omega < \omega_s \end{cases} \tag{2.11}$$

To approximate $H_d(\omega)$ as given in (2.11), two quantities are considered, a stopband error ξ_s and a passband error ξ_p. Both errors are measured in the mean-squared sense, namely,

$$\xi_s = \frac{1}{\pi}\int_{\omega_s}^{\pi} \mathbf{b}^T\mathbf{c}(\omega)\mathbf{c}^T(\omega)\mathbf{b}d\omega = \mathbf{b}^T\mathbf{P}_s\mathbf{b} \tag{2.12a}$$

$$\xi_p = \frac{1}{\pi}\int_0^{\omega_p} \mathbf{b}^T\left[\mathbf{1} - \mathbf{c}(\omega)\right]\cdot\left[\mathbf{1} - \mathbf{c}(\omega)\right]^T\mathbf{b}d\omega = \mathbf{b}^T\mathbf{P}_p\mathbf{b} \tag{2.12b}$$

where $\mathbf{P}_s$ and $\mathbf{P}_p$ are real, symmetric, positive definite matrices

$$\mathbf{P}_s = \frac{1}{\pi}\int_{\omega_s}^{\pi} \mathbf{c}(\omega)\mathbf{c}^T(\omega)d\omega \tag{2.13a}$$

$$\mathbf{P}_p = \frac{1}{\pi}\int_{0}^{\omega_p} [\mathbf{1}-\mathbf{c}(\omega)]\cdot[\mathbf{1}-\mathbf{c}(\omega)]^T d\omega \tag{2.13b}$$

Vectors $\mathbf{b}$ and $\mathbf{c}(\omega)$ are the corresponding impulse response coefficients and the frequency response vectors of linear-phase FIR filters, defined as

$$\mathbf{b} = [h(M) \quad 2h(M-1) \quad \cdots \quad 2h(1)]^T \tag{2.14a}$$

$$\mathbf{c}(\omega) = [1 \quad \cos\omega \quad \cdots \quad \cos M\omega]^T \tag{2.14b}$$

The overall error is a linear summation of these two errors

$$\xi = \alpha\xi_s + (1-\alpha)\xi_p = \mathbf{b}^T(\alpha\mathbf{P}_s + (1-\alpha)\mathbf{P}_p)\mathbf{b} \ , \ 0 \le \alpha \le 1 \tag{2.15}$$

where α is a tradeoff parameter between the stopband and the passband performances. Since the Hermitian matrix $\mathbf{P} = \alpha\mathbf{P}_s + (1-\alpha)\mathbf{P}_p$ measures the error energy over both the passband and the stopband, the optimal solution to the filter coefficients corresponds to the vector $\mathbf{b}$ that gives the minimum value for ξ. Note that $\mathbf{P}$ is a real, symmetric, positive definite matrix, the optimal $\mathbf{b}$ which minimizes ξ in (2.15) is simply the eigenvector corresponding to the minimum eigenvalue of $\mathbf{P}$ by Rayleigh's principle.

2.2.3 SVD Structure

For the design and implementation of 2-D filters, a parallel structure using singular-value decomposition (SVD) has attracted a great deal of research attention [24-27]. By applying SVD to the sampled frequency response matrix in the frequency-domain or the impulse response matrix in the time-domain, a 2-D filter is decomposed into a set of 1-D filters, namely,

$$\mathbf{A} = \mathbf{USV}^H = \sum_{k=1}^{r} \sigma_k \mathbf{u}_k \mathbf{v}_k^H = \sum_{k=1}^{r} \mathbf{f}_k \mathbf{g}_k^H \tag{2.16}$$

where $\mathbf{A}$ represents the impulse response or the frequency response of a 2-D filter, $\mathbf{u}_k$ and $\mathbf{v}_k$ represent the kth column eigenvectors and σ_k is the corresponding eigenvalue. From (2.16), the 2-D FIR filter can be realized by a set of 1-D subfilters, as shown in Fig. 2.4.

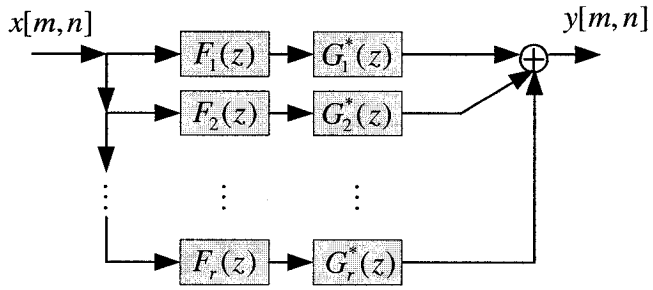

Figure 2.4: SVD-based realization structure

This SVD-based approach has many advantages.

1. A 2-D filter design problem can be simplified to the problem of designing 1-D subfilters.
2. The SVD-based structure is very suitable for a parallel and modular implementation, which speeds up the processing of 2-D signals as well as reduces the computational cost.
3. With a properly chosen SVD, only the first few branches corresponding to the larger singular values need to be retained, yielding a significantly simplified SVD realization.
4. A 2-D linear-phase FIR filter often has symmetric magnitude response. This symmetry property can be exploited in the SVD structure to get linear-phase 1-D subfilters and to further simplify the implementation structure.

2.2.4 Generalized Polyphase Structure

The generalized polyphase (GP) implementation of FIR filters can be expressed as [22], [23]

$$H(z)=\begin{bmatrix}1 & z^{-1} & \cdots & z^{-L+1}\end{bmatrix}\mathbf{PQ}\begin{bmatrix}H_0(z^L)\\H_1(z^L)\\\vdots\\H_{L-1}(z^L)\end{bmatrix}=\sum_{k=0}^{L-1}F_k(z)G_k(z^L) \tag{2.17}$$

where L represents the number of branches, **P** and **Q** are a pair of $L\times L$ inverse matrices, $H_k(z^L)$ are the subfilters in the conventional polyphase structure, and $F_k(z)$, $G_k(z^L)$ represent, respectively, the interpolators and constituent filters of the GP structure. Obviously, $F_k(z)$ and $G_k(z)$ can be written in terms of **P** and **Q** as

$$F_k(z)=\sum_{l=0}^{L-1}P(l,k)z^{-l}$$

$$G_k(z)=\sum_{l=0}^{L-1}Q(k,l)H_l(z)$$

Fig. 2.5 shows the GP realization structure of an FIR filter, where the constituent filters are implemented in the upsampled form. Hadamard transforms have been employed in [22] to obtain the interpolators and constituent filters due to their computational simplicity and frequency-selective property. Another advantage of the Hadamard transform is that for linear-phase filters, unlike the subfilters in a conventional polyphase realization, the constituent filters in the GP structure are symmetric.

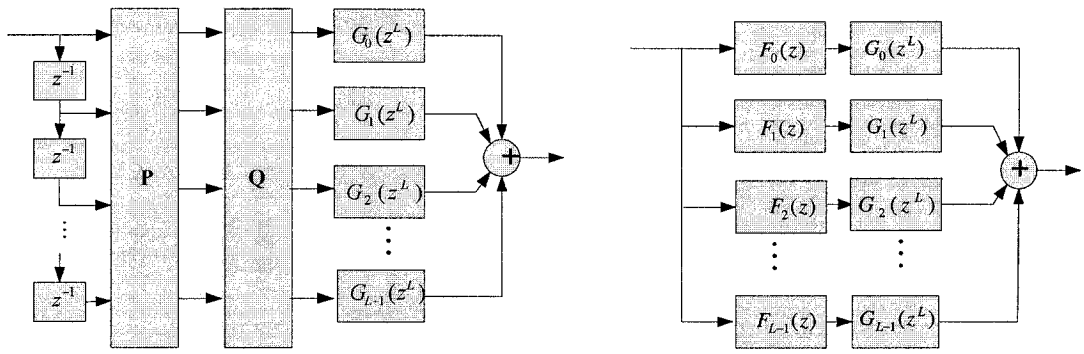

Figure 2.5: Generalized polyphase structure of an FIR filter

2.3 Lattice Structure of FIR Filter Banks

2.3.1 Filter Banks and Polyphase Representation

A filter bank is a collection of digital filters, with a common input and a common output, as depicted in Fig. 2.6. The left-hand part of Fig. 2.6 is called the *analysis bank*, where the input signal $x[n]$ is passed through M analysis filters $H_i(z)$, which have frequency-selective bandpass responses. The input $x[n]$ is then divided by analysis filters into several *subband signals* according to their frequency spectrum. These band-limited subband signals are usually decimated to a lower sampling rate. The decimated subband signals are then processed, via quantization, encoding, transmission *etc.*, according to the requirements of the particular application at hand. The right-hand part of Fig. 2.6 is called the synthesis bank, where all the subbands are combined by a set of expanders and synthesis filters $F_i(z)$ to form the reconstructed signal $\hat{x}[n]$. If all decimators have the same downsampling ratio, the system is called a *uniform filter bank*, otherwise it is said to be *nonuniform*. On the other hand, the system is labeled to be *critically sampled* or *maximally sampled* if $\sum_{i=0}^{M-1}\frac{1}{N_i}=1$, and *oversampled* if $\sum_{i=0}^{M-1}\frac{1}{N_i}>1$. For many

applications, especially data compression, critical sampling is desired since it provides a nonexpansive representation of the input. An oversampled filter bank has some redundancy and thus is more robust, which is useful in digital communications systems. In this dissertation, we focus on the *maximally decimated uniform* filter bank, where $N_0 = N_1 \cdots = N_{M-1} = M$.

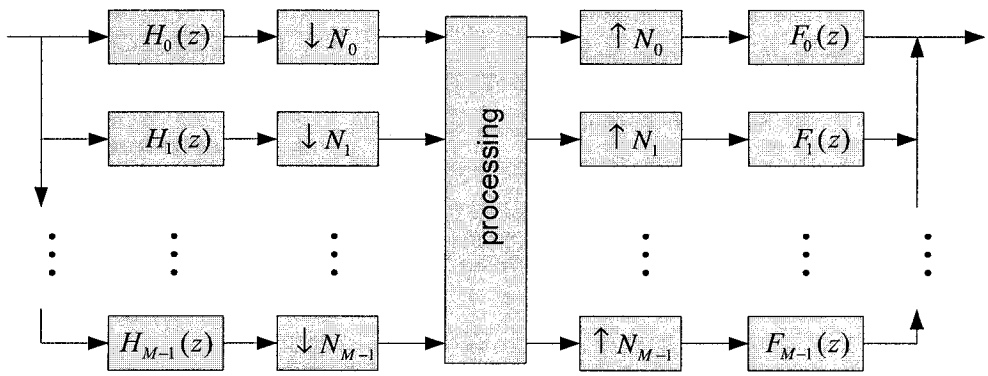

Figure 2.6: A general multirate digital filter bank

The filter bank in Fig. 2.6 is not efficient, since all the filters operate at high sampling rate. Using Nobel Identities in Fig. 2.2, a more efficient FB implementation, namely, the *polyphase representation*, can be obtained,

$$\begin{bmatrix} H_0(z) \\ H_1(z) \\ \vdots \\ H_{M-1}(z) \end{bmatrix} = \underbrace{\begin{bmatrix} E_{0,0}(z^M) & E_{0,1}(z^M) & \cdots & E_{0,M-1}(z^M) \\ E_{1,0}(z^M) & E_{1,1}(z^M) & \cdots & E_{1,M-1}(z^M) \\ \vdots & \vdots & \ddots & \vdots \\ E_{M-1,0}(z^M) & E_{M-1,1}(z^M) & \cdots & E_{M-1,M-1}(z^M) \end{bmatrix}}_{\mathbf{E}(z^M)} \begin{bmatrix} 1 \\ z^{-1} \\ \vdots \\ z^{-(M-1)} \end{bmatrix} \tag{2.18}$$

where $\mathbf{E}(z)$ is referred to as the *analysis polyphase matrix*. Similarly, the synthesis bank can be written as

$$[F_0(z) \quad F_0(z) \quad \cdots \quad F_{M-1}(z)] =$$

$$[z^{-(M-1)} \quad z^{-(M-2)} \quad \cdots \quad 1] \underbrace{\begin{bmatrix} R_{0,0}(z^M) & R_{0,1}(z^M) & \cdots & R_{0,M-1}(z^M) \\ R_{1,0}(z^M) & R_{1,1}(z^M) & \cdots & R_{1,M-1}(z^M) \\ \vdots & \vdots & \ddots & \vdots \\ R_{M-1,0}(z^M) & R_{M-1,1}(z^M) & \cdots & R_{M-1,M-1}(z^M) \end{bmatrix}}_{\mathbf{R}(z^M)} \tag{2.19}$$

where $\mathbf{R}(z)$ is called the *synthesis polyphase matrix.*

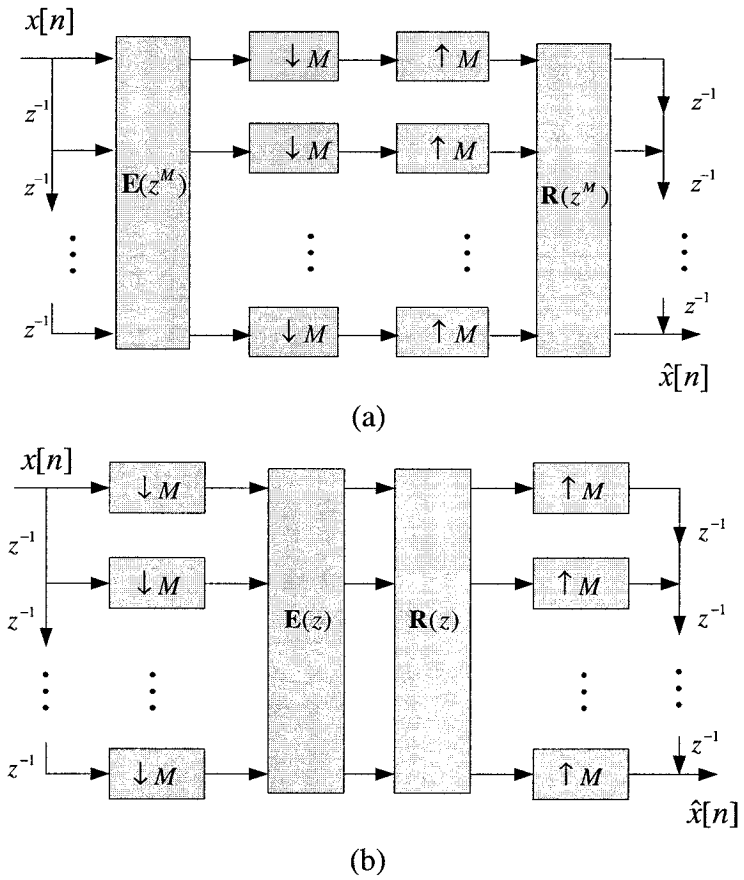

Figure 2.7: Equivalent polyphase representations of an M-channel filter bank. (a) Before applying Nobel Identity. (b) After applying Nobel Identity

Thus, the M-channel maximally decimated filter bank in Fig. 2.6 can be represented by Fig. 2.7 (a), which, by applying the noble identities, can then be simplified to Fig. 2.7 (b), the *polyphase representation.* The filters are now operating at a lower rate. Notice that the k-th row of $\mathbf{E}(z)$ contains the polyphase components of $H_k(z)$, whereas k-th column

of $\mathbf{R}(z)$ is comprised of the polyphase components of $F_k(z)$. The combination of the delay chain and the decimators at the analysis stage works as a serial-to-parallel converter, whereas the expanders and the delay chain at the synthesis side act as the parallel-to-serial conversion.

2.3.2 Prefect Reconstruction and Paraunitary Filter Banks

By ignoring the processing block in the middle of the filter bank, from Fig.2.7, the reconstruction signal $\hat{X}(z)$ can be expressed in terms of the input signal $X(z)$ as

$$\hat{X}(z) = \sum_{l=0}^{M-1} A_l(z) X(ze^{j2\pi l/M}) \tag{2.20}$$

where

$$A_l(z) = \frac{1}{M} \sum_{k=0}^{M-1} H_k(ze^{j2\pi l/M}) F_k(z), \; 0 \le l \le M-1 \tag{2.21}$$

Comparing the original input signal with the reconstructed one in (2.21), one can find three types of errors introduced by the filter bank, the *aliasing and imaging*, the *amplitude distortion*, and the *phase distortion*. The shifted version $X(ze^{j2\pi l/M})$ is due to the decimation and interpolation operations. We may say that $X(ze^{j2\pi l/M})$ is the *l*th aliasing term and $A_l(z)$ the corresponding gain. The frequency responses of these shifted versions would contaminate the original signal, causing aliasing and imaging. Even if the aliasing error is cancelled, the original signal is still corrupted by the distortion function $A_0(z)$. If $|A_0(z)|$ is not a constant, we say there is an amplitude distortion, and if $A_0(z)$ is not of linear-phase we say that there is a phase distortion. If analysis filters $H_k(z)$ and synthesis filters $F_k(z)$ are deliberately chosen such that (a) aliasing is completely canceled, and (b) the distortion function is a pure delay, (i.e., $A_0(z) = cz^{-n_0}$, $c \neq 0$, n_0 is

an integer), then the system is free of aliasing, amplitude and phase distortions. Such a system satisfies $\hat{x}[n] = cx[n-n_0]$, and is said to be *perfect reconstruction.*

With the polyphase representation, a filter bank is said to be perfect reconstruction if its polyphase matrices $\mathbf{R}(z)$ and $\mathbf{E}(z)$ satisfy,

$$\mathbf{R}(z)\mathbf{E}(z) = z^{-l}\mathbf{I}. \tag{2.22}$$

Further, if the synthesis polyphase matrix is chosen as $\mathbf{R}(z) = z^{-K}\mathbf{E}^H(z^{-1})$, where K is the highest order of $\mathbf{E}(z)$, such that

$$\mathbf{R}(z)\mathbf{E}(z) = \mathbf{E}^H(z^{-1})\mathbf{E}(z) = \mathbf{I}, \text{ for all } z \tag{2.23}$$

a special class of PRFB, called *paraunitary filter bank*, is obtained. The term z^{-K} is to ensure that the synthesis bank is causal. The popular DFT and DCT both belong to the PUFB. The following remarks regarding PUFBs can be made.

1. Paraunitariness is not necessary for perfect reconstruction. But if $\mathbf{E}(z)$ is paraunitary, the choice $\mathbf{R}(z) = cz^{-K}\tilde{\mathbf{E}}(z)$ results in perfect reconstruction.
2. The condition $\mathbf{R}(z) = cz^{-K}\tilde{\mathbf{E}}(z)$ is equivalent to

   $$f_k[n] = ch_k[MK + M - 1 - n]$$

   That is, the synthesis filters are the time reversed versions of the analysis filters.
3. PUFBs can be factorized into the lattice structure.
4. If the analysis filters are causal and stable, the synthesis filters will also be causal and stable.
5. PUFBs can be used to generate orthogonal transforms.
6. The function $\tilde{H}_k(z)H_k(z)$ is an Mth-band filter.
7. The analysis filters are power complementary, namely,

$$\sum_{k=0}^{M-1}\left|H_k(e^{j\omega})\right|^2 = \text{nonzero constant}.$$

2.3.3 Lattice Factorization

One of the most efficient ways for the implementation and design of PRFBs is via the lattice factorization [49]-[55]. The lattice structure decomposes $\mathbf{E}(z)$ of PRFBs into a cascade form of invertible matrices and delay matrices. This approach provides a fast, efficient, and robust implementation structure as well as an unconstrained optimization means for the design problem. There are mainly two kinds of factorization approaches, one is based on the McMillan degree, called *degree-one factorization*, and the other based on the order of the polyphase matrix, called *order-one factorization*.

Degree-One Factorization

The degree-one building block is defined as

$$\mathbf{G}(z) = \mathbf{I} - \mathbf{u}\mathbf{u}^H + z^{-1}\mathbf{u}\mathbf{u}^H \tag{2.24}$$

where $\mathbf{u}^H\mathbf{u} = 1$. The corresponding inverse building blocks are given by

$$\mathbf{G}^{-1}(z) = \mathbf{I} - \mathbf{u}\mathbf{u}^H + z\mathbf{u}\mathbf{u}^H, \tag{2.25}$$

Since $\mathbf{u}$ is a nonzero vector, one can always find M-1 linearly independent vectors $\hat{\mathbf{u}}_m$ $(m = 1\cdots M-1)$ so that $\mathbf{u}^H\hat{\mathbf{u}}_m = 0$. Using vectors $\hat{\mathbf{u}}_m$ together with $\mathbf{u}$, we may form an invertible matrix $\mathbf{U}$ such that

$$\mathbf{G}(z) = \mathbf{U}\begin{bmatrix}\mathbf{I}_{M-1} & \mathbf{0}\\ \mathbf{0} & z^{-1}\end{bmatrix}\mathbf{U}^H, \tag{2.26}$$

where $\mathbf{U} = [\hat{\mathbf{u}}_1 \quad \hat{\mathbf{u}}_2 \quad \cdots \quad \hat{\mathbf{u}}_{M-1} \quad \mathbf{u}]$ is a non-singular matrix. The properties of the degree-one building block can be summarized as follows:

1. It contains one unitary matrix and one diagonal matrix with a delay element;

2. The transfer function is causal and has an anticausal inverse;

3. The transfer matrix is of degree-one.

With the degree-one building block, we can generate a more complicated PRFB with degree r as,

$$\mathbf{E}(z) = \mathbf{G}_r(z)\cdots\mathbf{G}_2(z)\mathbf{G}_1(z)\mathbf{G}_0 \tag{2.27}$$

Order-One Factorization

The above degree-one factorization is based on the McMillan degree, which is usually undetermined in real applications. In practice, we often have a system with fixed filter length instead of the McMillan degree. Thus, the order-based factorization is more applicable. In the degree-one factorization in (2.27), if the vectors $\{\mathbf{u}_j\}$ $(j=1,\cdots r)$ of different $\mathbf{G}_j(z)$ are linearly independent, we may merge them together, leading to a general formulation of the *order-one factorization* (OOF) lattice structure as given below

$$\mathbf{E}(z) = \prod_{i=K-1}^{1}(\mathbf{U}_i\mathbf{\Lambda}_i(z))\mathbf{U}_0 \tag{2.28}$$

where $\mathbf{U}_i$ is an invertible matrix separated by the delay matrix $\mathbf{\Lambda}_k(z) = \mathrm{diag}(\mathbf{I}_{M-r_i}, z^{-1}\mathbf{I}_{r_i})$, $(0 \le r_i \le M)$, as shown in Fig. 2.8. For PUFBs with some constraints, such as the linear-phase or pairwise mirror-image symmetry, complete and minimal lattice structures have been developed based on the order-one factorization [50], [53], [70]. In these structures, the order of $\mathbf{E}(z)$ instead of its McMillan degree is reduced by one at each stage. More recently, based on the singular-value decomposition (SVD), Gao *et al.* [54] have proved that for a general PUFB without any constraint, the order-one factorization is complete. Moreover, by exploiting the Hermitian symmetry of each building block, they have

derived a simplified structure with reduced number of parameters. Later, the number of parameters in the lattice structure of PUFB has been further reduced by Gan *et al.* in [55].

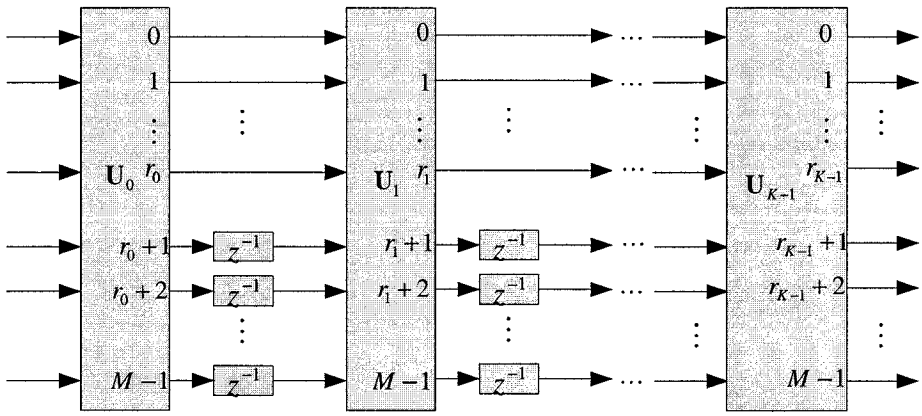

Figure 2.8: Order-one factorization of the polyphase matrix

2.3.4 Parameterization

Parameterization represents a way to completely characterize the invertible matrix $\mathbf{U}_i$ by a set of parameters. These parameters can then be optimized to give a filter bank according to the performance requirement. Several general requirements should be taken into account to develop a good parameterization method. 1) The matrix should always be invertible, even when the lattice coefficients are quantized. This is to avoid singular or near-singular matrices during the optimization process. 2) The parameterization should provide a fast implementation which has fewer multiplication and addition operations. 3) Costly matrix inversion should be avoided. There are two good candidates for the parameterization of the invertible matrix. One is the *Givens Rotations*, which used for a unitary matrix, and the other is *Lifting Scheme*, which deals with an invertible matrix.

A unitary matrix with real coefficients reduces to an orthogonal matrix. An $M \times M$ orthogonal matrix can be completely characterized by $M(M-1)/2$ rotation angles $\theta_{i,j}$ and M sign parameters as depicted in Fig. 2. 9.

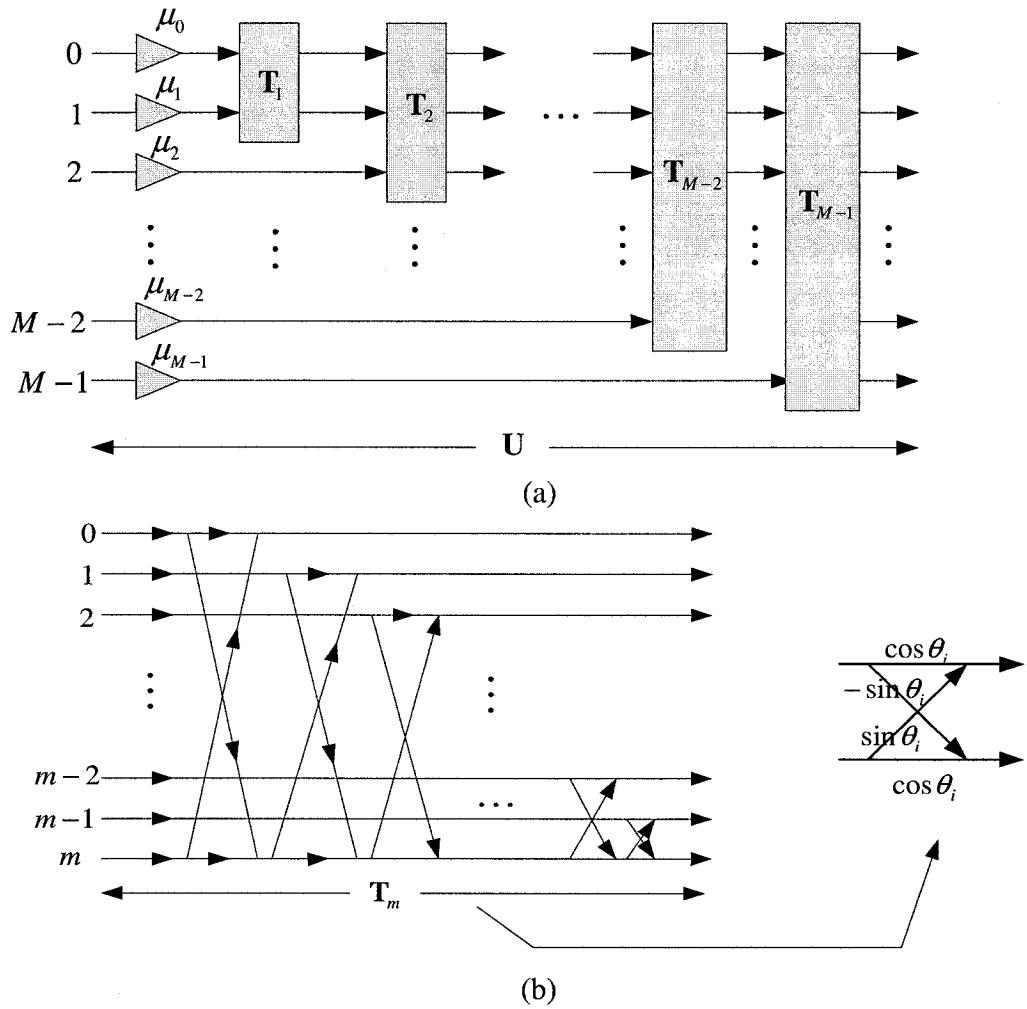

Figure 2.9: Parameterization of a matrix. (a) Complete representation of $M \times M$ orthogonal matrix. (b) Details of $\mathbf{T}_m$ in which each criss-cross is a Givens Rotation.

As for the lifting scheme, with the Gauss-Jordan elimination process, it is not difficult to prove that any $M \times M$ invertible matrix can be completely characterized by $M(M-1)$ lift steps a_i, b_i and M scaling factors α_i, as depicted in Fig. 2. 10.

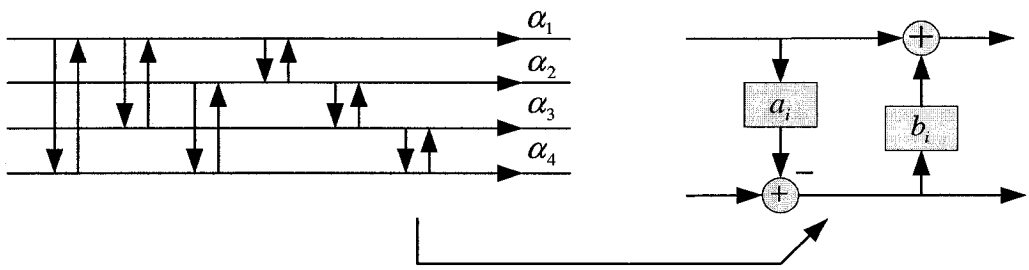

Figure 2.10: Parameterization of an invertible matrix via lifting steps

Although unitary matrix is parameterized by rotation planes, we can still realize the unitary matrix in the lifting scheme, which is proved to be a more efficient implementation. A plane rotation can be rewritten as two lifting steps,

$$\begin{bmatrix} \cos\theta & -\sin\theta \\ \sin\theta & \cos\theta \end{bmatrix} = \begin{bmatrix} 1 & a \\ 0 & 1 \end{bmatrix} \begin{bmatrix} 1 & 0 \\ b & 1 \end{bmatrix} \begin{bmatrix} \alpha & 0 \\ 0 & \beta \end{bmatrix} \tag{2.29}$$

where $a = -\sin\theta/\cos\theta$, $b = \sin\theta\cos\theta$, $\alpha = 1/\cos\theta$ and $\beta = \cos\theta$. With α and β being folded into the final scaling coefficients, the realization of a rotation plane is simplified from four multipliers and two adders to two multipliers and two adders. In practice, to avoid the occurrence of unacceptable large value when $\cos\theta$ is close to zero, three lifting steps, rather than two, are normally adopted

$$\begin{bmatrix} \cos\theta & -\sin\theta \\ \sin\theta & \cos\theta \end{bmatrix} = \begin{bmatrix} 1 & a \\ 0 & 1 \end{bmatrix} \begin{bmatrix} 1 & 0 \\ b & 1 \end{bmatrix} \begin{bmatrix} 1 & a \\ 0 & 1 \end{bmatrix} \tag{2.30}$$

where $a = (1-\cos\theta)/\sin\theta$, $b = \sin\theta$. The implementation cost is then three multipliers and three adders, which is still better than the four multipliers and two adders required for the rotation plane.

2.3.5 Completeness

It is evident that the lattice structure (2.28) results in a PR system, with the inverse $\mathbf{R}(z)$ being given by

$$\mathbf{R}(z) = [\mathbf{E}(z)]^{-1} = \mathbf{U}_0^{-1} \prod_{i=1}^{K-1} \left(\mathbf{\Lambda}_i(z^{-1}) \mathbf{U}_i^{-1} \right). \tag{2.31}$$

Conversely, a tough question remains, namely, is the lattice structure complete or is there always a factorized form (2.28) for any given PRFBs? The completeness of the lattice structure is a crucial issue in filter bank design and has been intensively studied by many researchers. Generally speaking, the lattice structure is not complete for any PRFB. The completeness was first proved to be true for the PUFBs in which the invertible matrices $\mathbf{U}_k$ in (2.28) are constrained to be unitary. Vaidyanathan *et al.* [48] proposed a complete and minimal structure that uses the DOF to peel off a PU building block with one McMillan degree from $\mathbf{E}(z)$. Later, for some PUFBs subject to certain constraints, such as the linear-phase or pairwise mirror-image symmetry, complete and minimal lattice structures have been developed based on the so-called *symmetric-delay factorization* (SDF) [53]. In these structures, the building blocks reduce the order of $\mathbf{E}(z)$ instead of the McMillan degree. More recently, based on the singular-value decomposition (SVD), Gao *et al.* [54] have proved that the OOF given by (2.28) is complete for a general PUFB without any constraint.

Although the lattice structure has been proved to be complete for PUFBs, it is not true for a general PRFB. The degree-one factorization has been extended to the PRFB case, resulting in lattice structures of the biorthogonal lapped transform (BOLT) [51], [52] and the lapped unimodular transform (LUT) [46], [47]. However, the lattice structure of PRFBs is complete for BOLT of order-one only. As such, researchers have turned their efforts to a class of PRFBs meeting certain constraints. As an example, the linear-phase perfect reconstruction filter bank (LPPRFB) has been studied by Tran *et al.* in [74], which is an extension of the popular linear-phase paraunitary filter bank (LPPUFB). The

relaxation of the PU constraint to PR brings a degree of flexibility in the design of the synthesis bank.

2.4 Filter Banks with Constraints

Depending on different application purposes, some extra properties are desirable. For example, in image processing, all analysis and synthesis filters are expected to be of linear-phase. To tradeoff between the complexity and the performance, some extra constraints, such as MIS and cosine modulation are artificially introduced. Specific lattice structures are developed such that these properties, together with the PR condition, are automatically satisfied. Here, we introduce three constrained filter banks, linear-phase filter banks, filter banks with mirror-image symmetric analysis filters, and CMFBs.

2.4.1 Linear-Phase Filter Banks

A filter bank is said to be linear-phase if all of its filters are either symmetric or anti-symmetric, i.e., $h_k[n] = \pm h_k[N-1-n]$, where N is the filter length. In the case where all the filters having the same length $N=KM$, the linear-phase property can be written in terms of the polyphase representation as

$$\mathbf{E}(z) = z^{-(K-1)}\mathbf{D}\mathbf{E}(z^{-1})\mathbf{J} \tag{2.32}$$

where $\mathbf{D}$ is a diagonal matrix with entries ± 1. It has been shown in [71] that the even channel LPPUFBs with the polyphase matrix given by (2.32) can always be factorized as

$$\mathbf{E}(z) = \prod_{i=K-1}^{1}\left(\mathbf{\Phi}_i\mathbf{W}\mathbf{\Lambda}(z)\mathbf{W}\right)\mathbf{E}_0 = \prod_{i=K-1}^{1}\mathbf{G}_i(z)\mathbf{E}_0 \tag{2.33}$$

where

$$\mathbf{E}_0 = \frac{1}{\sqrt{2}}\begin{bmatrix}\mathbf{U}_0 & \mathbf{0}\\ \mathbf{0} & \mathbf{V}_0\end{bmatrix}\begin{bmatrix}\mathbf{I} & \mathbf{J}\\ \mathbf{J} & -\mathbf{I}\end{bmatrix}, \tag{2.34a}$$

$$\mathbf{\Phi}_i = \begin{bmatrix}\mathbf{I} & \mathbf{0}\\ \mathbf{0} & \mathbf{V}_i\end{bmatrix}, \mathbf{\Lambda}(z) = \begin{bmatrix}\mathbf{I} & \mathbf{0}\\ \mathbf{0} & z^{-1}\mathbf{I}\end{bmatrix}, \tag{2.34b}$$

$$\mathbf{W} = \frac{1}{\sqrt{2}}\begin{bmatrix}\mathbf{I} & \mathbf{I}\\ \mathbf{I} & -\mathbf{I}\end{bmatrix}. \tag{2.34c}$$

In (2.34), $\mathbf{U}_0$ and $\mathbf{V}_i$ are the unitary matrices to be determined, $\mathbf{\Lambda}(z)$ is a diagonal delay matrix, and $\mathbf{W}$ the butterfly structure. The lattice structure of (2.34) is illustrated in Fig. 2.11.

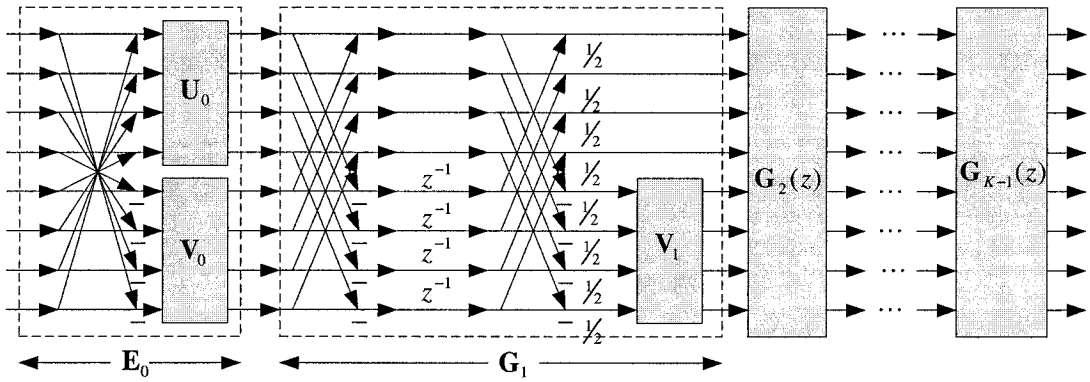

Figure 2.11: Lattice structure of linear-phase paraunitary filter bank

2.4.2 Mirror-Image Symmetric Filter Banks

Mirror-image symmetry imposes that the frequency responses of the analysis filters $H_k(z)$ are symmetric about $\pi/2$. Let us consider a mirror-image symmetric filter bank whose analysis polyphase matrix is given by

$$H_{M-1-k}(z) = \begin{cases} z^{-(L-1)}H_k(-z^{-1}), & \text{even } M \\ H_k(-z), & \text{odd } M \end{cases}, \tag{2.35}$$

where $0 \le k \le M-1$. When M is even, i.e., the even-channel case, assuming that all the analysis filters have the same length $L=KM$, and the associated polyphase matrix has the highest order (K-1), the symmetry constraint in (2.35) can be equivalently written as

$$\mathbf{E}(z) = z^{-(K-1)}\mathbf{D}\mathbf{E}(z^{-1})\mathbf{T} \tag{2.36}$$

where

$$\mathbf{D} = \begin{bmatrix} \mathbf{0} & -\mathbf{I}_{M/2} \\ \mathbf{I}_{M/2} & \mathbf{0} \end{bmatrix}, \quad \mathbf{T} = \begin{bmatrix} \mathbf{0} & -\mathbf{D}_t\mathbf{J}_{M/2} \\ \mathbf{J}_{M/2}\mathbf{D}_t & \mathbf{0} \end{bmatrix},$$

$$\mathbf{D}_t = \begin{bmatrix} 1 & & & \\ & -1 & & \\ & & \ddots & \\ & & & (-1)^{M/2-1} \end{bmatrix}$$

For a mirror-image symmetric PUFB [50], the polyphase matrix satisfying (2.36) can always be factorized as

$$\begin{aligned} \mathbf{E}(z) &= \mathbf{G}_{K-1}(z)\mathbf{G}_{K-2}(z)\cdots\mathbf{G}_1(z)\mathbf{G}_0 \\ &= \prod_{i=K-1}^{1}(\mathbf{\Phi}_i\mathbf{\Lambda}(z)\mathbf{W})\mathbf{G}_0 \end{aligned} \tag{2.37}$$

where

$$\mathbf{\Phi}_i = \begin{bmatrix} \mathbf{U}_i & -\mathbf{V}_i \\ \mathbf{V}_i & \mathbf{U}_i \end{bmatrix}, \mathbf{E}_0 = \begin{bmatrix} \mathbf{U}_0 & -\mathbf{V}_0 \\ \mathbf{V}_0 & \mathbf{U}_0 \end{bmatrix}\begin{bmatrix} \mathbf{I}_{M/2} & \mathbf{0} \\ \mathbf{0} & \mathbf{D}_t\mathbf{J}_{M/2} \end{bmatrix} \tag{2.38}$$

The lattice structure characterized by (2.38) is depicted in Fig. 2.12.

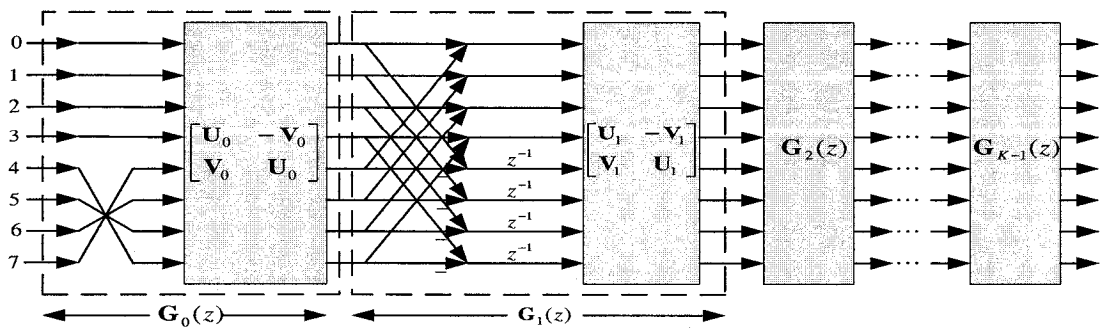

Figure 2.12: Lattice structure of mirror-image symmetric PUFB

2.4.3 Cosine-Modulated Filter Banks

In this case, the impulse responses of the analysis and synthesis filters in a CMFB are obtained from a prototype filter $h[n]$ through the cosine modulation, namely,

$$h_k[n]=2h[n]\cos\left[(2k+1)\frac{\pi}{2M}\left(n-\frac{N-1}{2}\right)+(-1)^k\frac{\pi}{4}\right], \tag{2.39}$$

$$f_k[n]=2h[n]\cos\left[(2k+1)\frac{\pi}{2M}\left(n-\frac{N-1}{2}\right)-(-1)^k\frac{\pi}{4}\right], \tag{2.40}$$

$$n=0,1,\cdots,N-1,\ k=0,1,\cdots,M-1$$

where $h[n]$ is a linear-phase filter with length $N=2mM$. Note that the cosine modulation has a periodicity of $2M$, the corresponding analysis polyphase matrix can be written as

$$\mathbf{E}(z)=\sqrt{M}\mathbf{C}_M^{IV}\left[(\mathbf{I}-\mathbf{J})\quad -(\mathbf{I}+\mathbf{J})\right]\begin{bmatrix}\mathbf{G}_0(-z^2)\\ z^{-1}\mathbf{G}_1(-z^2)\end{bmatrix} \tag{2.41}$$

where

$$\left[\mathbf{C}_M^{IV}\right]_{k,l}=\sqrt{\frac{2}{M}}\cos\left(\frac{\pi}{M}\left(k+\frac{1}{2}\right)\left(l+\frac{1}{2}\right)\right)$$

$$\mathbf{G}_0(z)=\mathrm{diag}\left(G_0(z)\quad G_1(z)\quad\cdots\quad G_{M-1}(z)\right)$$

$$\mathbf{G}_1(z)=\mathrm{diag}\left(G_M(z)\quad G_{M+1}(z)\quad\cdots\quad G_{2M-1}(z)\right)$$

Note that $G_l(z)$ represents the polyphase decomposition of the prototype filter. It is easy to check that the synthesis filters are time-reversal of the analysis filters and the necessary and sufficient condition for the cosine-modulated FB to be perfect reconstruction is then given by [89]

$$\tilde{G}_k(z)G_k(z)+\tilde{G}_{M+k}(z)G_{M+k}(z)=\frac{1}{2M},\quad 0\le k\le M/2-1 \tag{2.42}$$

Obviously, condition (2.42) can be fulfilled by employing the following lattice structure of cascade form,

$$\begin{bmatrix} G_k(z) \\ G_{M+k}(z) \end{bmatrix} = \prod_{k=0}^{m-1} \left(\begin{bmatrix} \cos\theta_k & \sin\theta_k \\ \sin\theta_k & -\cos\theta_k \end{bmatrix} \begin{bmatrix} 1 & 0 \\ 0 & z^{-1} \end{bmatrix} \right) \begin{bmatrix} 1 \\ (-1)^m \end{bmatrix} \tag{2.43}$$

With (2.42) and (2.43), the realization of the paraunitary cosine-modulated FB is then completed as shown in Fig. 2.13.

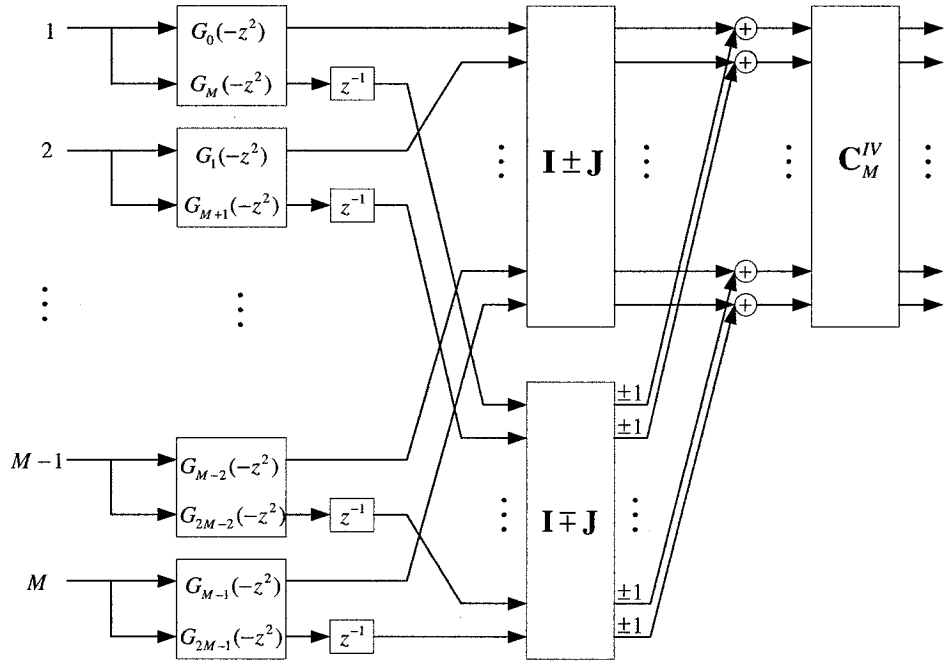

Figure 2.13: Implementation of cosine-modulated filter bank with perfect reconstruction

2.5 Conclusion

In this chapter, we briefly present the background knowledge necessary for the following discussions. Some of the literature works have been summarized as the benchmark of our contributions. For general filter design, the PM method, eigenfilter approach, and the SDP, provide an optimal solution under certain criteria, while

structure-based methods, such as IFIR filter, FRM technique, and GP structure, give a fast and efficient way in the design and implementation. *M*th-band filter, a particular interest in the thesis, is discussed in detail. To meet the interpolation condition of *M*th-band filter brings difficulty in the filter design. For the filter bank, most of the papers are related to the lattice factorization of the polyphase matrix. The success of lattice factorization in structurally satisfying different properties, has been proved in the PUFBs, LPPRFBs, CMFBs, and MIS-PUFBs. Analyzing the success and drawbacks of these works, we now proceed to propose our contributions.

Chapter 3

Design of Linear-Phase FIR *M*th-band Filters based on Generalized Polyphase Structure

3.1 Introduction

Over the past decades, design of digital filters has been one of the most important subjects in the area of digital signal processing, and digital filters have been extensively used in many engineering fields such as telecommunications, electronics, speech and image processing. In many applications, finite-duration impulse response (FIR) filter is attractive in view of its inherent stability, linear-phase and being free of limit cycles. However, the major drawback of an FIR filter is its large number of taps, which in turn requires a large number of computations for its design as well as implementation. Another concern is that for many applications, there are some particular constraints for the desired filters. For example, an *M*th-band filter should meet the time-domain interpolation constraint $h(Mn) = \frac{1}{M}\delta(n)$ in addition to its low-pass frequency response. This class of filters has many important applications such as image interpolation and frame rate conversion of video sequence [32]-[34]. The time-domain constraint makes most of the existing design methods including the powerful Parks-McClellan (PM)

method [16] invalid, since this extra constraint has not been taken into account in these methods.

In this chapter, a GP structure based filter design algorithm is presented with emphasis on the *M*th-band filters. It is known that the time-domain constraint of *M*th-band filters can be easily realized by setting one of the subfilters as $h_l(n) = \frac{1}{M}\delta(n)$ in the M branch of the polyphase structure. Noticing that the GP structure is a transformed version of the traditional polyphase structure, the time-domain constraint can be equivalently expressed in the GP structure. Moreover, as the constituent filters in the GP structure remain to be linear-phase and have a significantly reduced length, they can be designed independently and easily provided that proper frequency specifications are available for these constituent filters. Therefore, the key to the GP-based design algorithm is to determine the desired frequency specification for the constituent filters [31] and to incorporate the time-domain constraint in the final design problem.

3.2 *M*th-band Filter Design

An *M*th-band filter has an ideal frequency response given by

$$H(e^{j\omega}) = \begin{cases} 1, & 0 \le \omega \le \pi / M \\ 0, & \text{elsewhere} \end{cases},$$

which leads to a sinc function type impulse response

$$h[n] = \frac{\sin(n\pi / M)}{n\pi}.$$

Clearly, an important feature of that the impulse response is there exists a zero-crossing every M samples in $h[n]$, namely,

$$h[nM] = \frac{1}{M}\delta[n] \tag{3.1}$$

The above property is particularly useful when the Mth-band filter is employed in signal interpolation by a factor of M, where M-1 new samples are generated between every two consecutive input samples while leaving the original input samples unchanged. Hence, the property described by (3.1) is often referred to as the interpolation condition.

Although the interpolation condition (3.1) is desirable in multirate signal processing, it is in general difficult to be accommodated in filter design. For example, the most commonly used PM method [16] for optimal FIR filter design utilizes the Remez search algorithm based on the orthogonal space $\{\cos(k\omega), k = 0,1,\cdots\}$. Having the interpolation condition imposed on the impulse response of the FIR filter, however, the linear independency of the basis function $\cos(k\omega)$ would be broken, making the PM method invalid due to the failure of the Remez search. Similar to the PM method, most of the existing design approaches are not applicable for the Mth-band filter design. Although the design problem of the Mth-band filters satisfying the interpolation condition could be solved by a constrained optimization technique, the incorporation of the extra constraint might bring about some issues such as the convergence, numerical precision and computational complexity of the optimization method. In [17] and [30], the Mth-band filter has been designed by the eigenfilter approach, in which the optimal filter coefficients obtained in the least-square sense are given as the eigenvector of the squared error matrix corresponding to the smallest eigenvalue. Then, the interpolation constraint is satisfied by deleting the related columns and rows from the squared error matrix.

3.2.1 Half-band Filters based on Polyphase Structure

It is well known that the polyphase structure plays a key role in multirate processing and interpolation due to its computational efficiency. Another advantage of the polyphase structure is that the interpolation condition can easily be satisfied by implementing one of its parallel branches as $\frac{1}{M}\delta(n)$. Thus, it is intuitive to pursue the polyphase structure-based design method for Mth-band filters. In what follows, we begin with a brief review of the design problem of linear-phase half-band FIR filters based on polyphase structure [28], showing that the subfilters of the half-band filter are still linear-phase and thus can be designed separately and easily without phase distortion. We will then point out the linear-phase feature of the subfilters is not obtainable when the polyphase structure is applied to the design of general Mth-band filters, necessitating the development of a generalized polyphase structure-based design technique.

With the interpolation condition on the impulse response, we can easily verify that for a zero phase half-band filter, its length must be odd ($2N+1$). Writing the impulse response into a two-branch polyphase structure, we have

$$h(n) = h(2n) + h(2n+1) = h_0(n) + h_1(n) \tag{3.2}$$

Obviously, both the subfilters $h_0(n)$ and $h_1(n)$ are of linear-phase, with lengths $N+1$ and N, respectively. The time-domain constraint of half-band filters are now imposed only on the first subfilter, i.e., $h_0(n) = \frac{1}{2}\delta(n)$, yielding a fixed impulse response with respect to a half-unity frequency response. Thus, all the parameters to be designed are contained in the second subfilter $h_1(n)$. Note that this subfilter can readily be designed using an existing optimization technique, such as the PM method [16], so that the upsampled frequency response of $h_1(n)$ satisfies

$$\tilde{H}_1(e^{j2\omega}) = \begin{cases} 1/2, & 0 \le \omega < \pi/2 \\ -1/2, & \pi/2 \le \omega < \pi \end{cases}.$$

Then, the sum of $h_0(n)$ and $h_1(n)$ would give a low-pass frequency response. Obviously, the overall half-band filter has an equiripple frequency response provided that $h_1(n)$ is equiripple. The whole idea is illustrated in Fig.3.1, where (a), (c) and (e) represent $h_0(n)$, $h_1(n)$ and $h(n)$, while (b), (d) and (f) are the corresponding frequency responses, respectively. It is observed that the overall filter exhibits an equiripple frequency response as a result of equiripple $h_1(n)$.

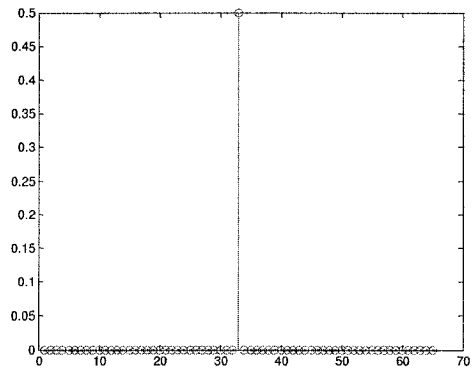

(a)

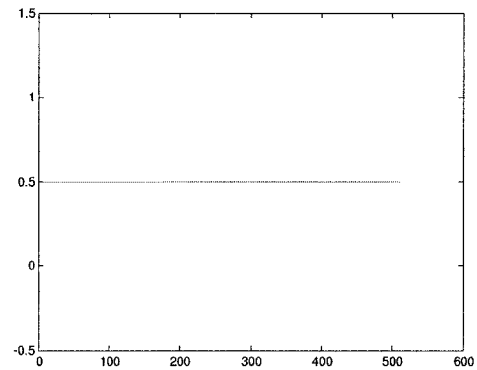

(b)

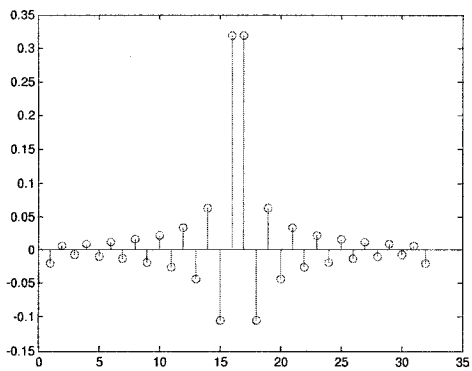

(c)

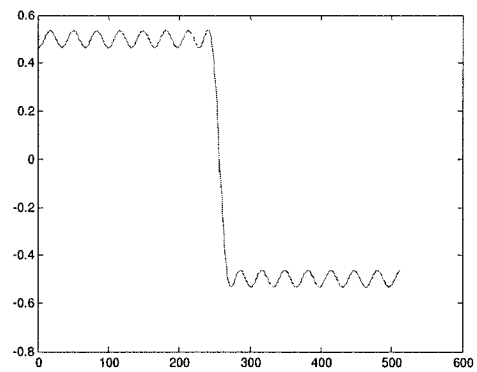

(d)

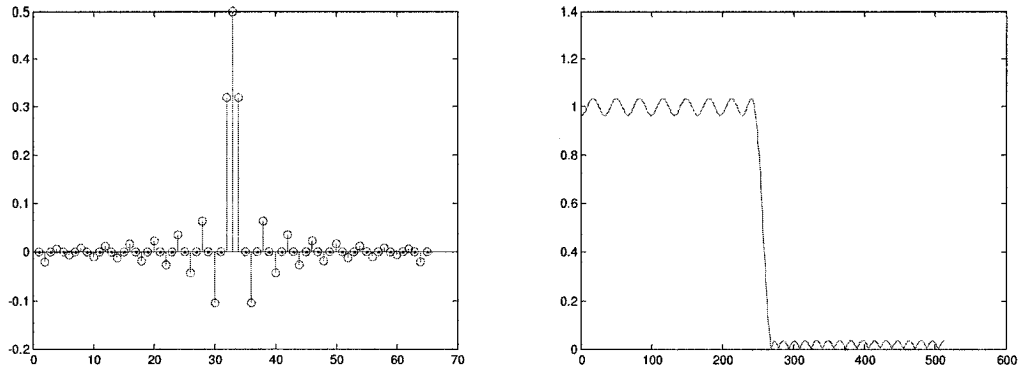

(e) (f)

Figure 3.1: Half-band filter design based on the polyphase structure.
(a), (c) and (e) at left column are the impulse response of $h_0[n]$, $h_1[n]$ and $h[n]$, respectively. (b), (d) and (f) at the right column are their corresponding frequency responses.

Unfortunately, the above polyphase structure-based design is only available for half-band filters and cannot be extended to an arbitrary Mth-band filter. One of the reasons behind the failure of polyphase structure approach is that the subfilters of Mth-band filters are no longer linear-phase in the polyphase decomposition. In [22], it has been shown that the linear-phase can be restored in the GP structure. Therefore, it is straightforward to extend the above polyphase structure-based approach to the GP structure and apply it for the design of Mth-band filters.

3.2.2 Generalized Polyphase Structure

The generalized polyphase (GP) implementation of FIR filters can be expressed as [22], [23]

$$H(z)=\begin{bmatrix}1 & z^{-1} & \cdots & z^{-L+1}\end{bmatrix}\mathbf{PQ}\begin{bmatrix}H_0(z^L)\\H_1(z^L)\\\vdots\\H_{L-1}(z^L)\end{bmatrix}=\sum_{k=0}^{L-1}F_k(z)G_k(z^L) \tag{3.3}$$

where L represents the number of branches, $\mathbf{P}$ and $\mathbf{Q}$ are a pair of $L \times L$ inverse matrices, $H_k(z^L)$ are the subfilters in the conventional polyphase structure, and $F_k(z)$ and $G_k(z^L)$ represent, respectively, the interpolators and constituent filters of the GP structure. Obviously, $F_k(z)$ and $G_k(z)$ can be written in terms of $\mathbf{P}$ and $\mathbf{Q}$ as

$$F_k(z) = \sum_{l=0}^{L-1} P(l,k) z^{-l} \tag{3.4}$$

$$G_k(z) = \sum_{l=0}^{L-1} Q(k,l) H_l(z) \tag{3.5}$$

Hadamard transforms have been employed in [22] to obtain the interpolators and constituent filters due to their computational simplicity and frequency-selective property. Another advantage of the Hadamard transform is that for linear-phase filters, unlike the subfilters in a conventional polyphase realization, the constituent filters in the GP structure are linear-phase.

On the other hand, there are a few issues to be addressed in the GP structure-based filter design using the Hadamard transform. First, since the size of the Hadamard matrix is restricted to be even, the Hadamard transform-based decomposition applies only to a small class of parallel structures with even number of branches. Therefore, it is imperative to develop other transforms in order to obtain a general GP realization structure with an arbitrary number of branches. Another issue of the GP technique is the design of the constituent filters. It has been suggested in [22] that these constituent filters be designed separately, that is, only one subfilter be optimized at a time while the others are kept unchanged. However, this scheme requires time-consuming iterations before reaching a final stable solution, since the optimization of each constituent filter may depend on the other constituent filters. Moreover, in order to design these constituent

filters independently, the frequency response specification for each of them should be determined, and this is the key to the GP-based design technique.

Bearing these issues in mind, in what follows, we will develop a GP structure-based design method for Mth-band FIR filters by proposing general transform matrices, as well as deriving closed-form frequency specifications for the constituent filters. It will be shown in the proposed method that the constituent filters of the GP structure can be designed separately and the interpolation condition can easily be satisfied.

3.3 Proposed Transform Matrices

3.3.1 Seed Matrix

Although Hadamard matrix enjoys many desirable features such as simplicity and frequency selectivity, the fact that the matrix order has to be even limits its applications. Observing that the Hadamard matrix is constructed based on a simple 2×2 matrix, we would like to propose some basic seed matrices of prime order, with which a general higher-order matrix can be constructed using the Kronecker product. For the seed matrix, the following requirements should be taken into consideration.

1. As linear-phase is a desirable property in many applications and is preferred in FIR filter design, we would like to retain this property in the decomposed constituent filters. Accordingly, the impulse response of each constituent filter resulting from the proposed seed matrix should be either symmetric or antisymmetric.

2. To reduce the implementation complexity of the GP structure, the seed matrix should be as simple as possible. It is expected that the transform matrix contains only the elements 0, 1 or -1 to avoid multiplications.
3. As in the case of the Hadamard matrix, we would like the resulting interpolators to be frequency selective. This frequency selectivity introduces the "subband" meaning for each branch and measures the significance of the associated subfilter on the overall frequency response of the FIR filter.
4. The seed matrix should be invertible. This requirement is obvious as both **P** and its inverse $\mathbf{Q}= \mathbf{P}^{-1}$ are employed in the GP structure.

It is easy to verify that in order for the constituent filters to be of linear phase, the column vectors of the transform matrix should be either symmetric or antisymmetric. Let a $q \times q$ (q is prime) transform matrix be of the general form,

$$\mathbf{R}_q = \mathbf{A}\begin{bmatrix} \mathbf{U}_{(q+1)/2} & \mathbf{0} \\ \mathbf{0} & \mathbf{V}_{(q-1)/2} \end{bmatrix}\mathbf{\Sigma} \tag{3.6}$$

where $\mathbf{U}_{(q+1)/2}$ and $\mathbf{V}_{(q-1)/2}$ are nonsingular matrices of order $(q+1)/2$ and $(q-1)/2$, respectively, $\mathbf{\Sigma}$ is a nonsingular matrix of compatible dimension. By choosing $\mathbf{\Sigma}$ properly, the symmetry of the row vectors of $\mathbf{R}_q$ can be guaranteed. Here, the elementary matrix $\mathbf{A}$ is introduced to interchange the row vectors of $\mathbf{R}_q$ such that its column vectors are also symmetric. In particular, we would like $\mathbf{A}$ to convert the row vectors of $\mathbf{U}_{(q+1)/2}$ to the odd row vectors of $\mathbf{R}_q$ and that of $\mathbf{V}_{(q-1)/2}$ to the even row vectors of $\mathbf{R}_q$. For example, if $\mathbf{R}_q$ is of order three, $\mathbf{A} = \begin{bmatrix} 1 & 0 & 0 \\ 0 & 0 & 1 \\ 0 & 1 & 0 \end{bmatrix}$. Then, the second row vector of $\mathbf{U}_{(q+1)/2}$

now forms the third row vector of $\mathbf{R}_3$ and the first row vector of $\mathbf{V}_{(q-1)/2}$ becomes the second one in $\mathbf{R}_3$. Similarly, to obtain $\mathbf{R}_5$, the following fifth-order matrix $\mathbf{A}$ can be used,

$$\mathbf{A}=\begin{bmatrix}1 & 0 & 0 & 0 & 0\\ 0 & 0 & 0 & 1 & 0\\ 0 & 1 & 0 & 0 & 0\\ 0 & 0 & 0 & 0 & 1\\ 0 & 0 & 1 & 0 & 0\end{bmatrix}.$$

From (3.6), the inverse of $\mathbf{R}_q$ can be written as

$$\mathbf{R}_q^{-1}=\mathbf{\Sigma}^{-1}\begin{bmatrix}\mathbf{U}_{(q+1)/2}^{-1} & \mathbf{0}\\ \mathbf{0} & \mathbf{V}_{(q-1)/2}^{-1}\end{bmatrix}\mathbf{A}^{-1} \tag{3.7}$$

It is expected that both $\mathbf{U}$ and $\mathbf{V}$ be chosen as simple matrices and $\mathbf{\Sigma}$ be selected appropriately such that both $\mathbf{R}_q$ and $\mathbf{R}_q^{-1}$ have symmetric or antisymmetric columns. Here, $\mathbf{\Sigma}$ is chosen as,

$$\mathbf{\Sigma}=\begin{bmatrix}\mathbf{I}_{(q-1)/2} & 0 & \mathbf{J}_{(q-1)/2}\\ 0 & 1 & 0\\ \mathbf{J}_{(q-1)/2} & 0 & -\mathbf{I}_{(q-1)/2}\end{bmatrix} \tag{3.8}$$

It is noted that the matrix given by (3.8) is the famous butterfly structure, which makes the columns of $\mathbf{R}_q$ and $\mathbf{R}_q^{-1}$ either symmetric or antisymmetric. As such, we only need to determine $\mathbf{U}$ and $\mathbf{V}$ in order to obtain $\mathbf{R}_q$ and $\mathbf{R}_q^{-1}$. To make the transform matrix to be both simple and frequency-selective, one may choose Hadamard matrices for $\mathbf{U}$ and $\mathbf{V}$. For example, by selecting $\mathbf{U}_2=\begin{bmatrix}1 & 1\\ 1 & -1\end{bmatrix}$ and $\mathbf{V}_1=1$, one may get a 3rd-order seed matrix which can be used for a 3-branch GP decomposition:

$$\mathbf{R}_3 = \begin{bmatrix} 1 & 1 & 1 \\ 1 & 0 & -1 \\ 1 & -1 & 1 \end{bmatrix} \text{ and } \mathbf{R}_3^{-1} = \frac{1}{4}\begin{bmatrix} 1 & 2 & 1 \\ 2 & 0 & -2 \\ 1 & -2 & 1 \end{bmatrix} \tag{3.9}$$

In a similar manner, one may construct a 5th-order seed matrix by choosing $\mathbf{U}_3 = \mathbf{R}_3$ and $\mathbf{V}_2$ as the 2nd-order Hadamard matrix, yielding

$$\mathbf{R}_5 = \begin{bmatrix} 1 & 1 & 1 & 1 & 1 \\ 1 & 1 & 0 & -1 & -1 \\ 1 & 0 & -1 & 0 & 1 \\ 1 & -1 & 0 & 1 & -1 \\ 1 & -1 & 1 & -1 & 1 \end{bmatrix} \text{ and } \mathbf{R}_5^{-1} = \frac{1}{8}\begin{bmatrix} 1 & 2 & 2 & 2 & 1 \\ 2 & 2 & 0 & -2 & -2 \\ 2 & 0 & -4 & 0 & 2 \\ 2 & -2 & 0 & 2 & -2 \\ 1 & -2 & 2 & -2 & 1 \end{bmatrix} \tag{3.10}$$

It can be verified that the proposed seed matrices $\mathbf{R}_3$ and $\mathbf{R}_5$ possess all the above-mentioned properties. For example, the interpolators generated by $\mathbf{R}_3$ and $\mathbf{R}_5$ have the frequency-selective property as shown in Fig. 3.2. The transform matrix contains only the elements 1, -1 and 0. The elements of the inverse matrix are also simple, being 0 or $\pm 2^{-K}$, ($K = 0,1,2,\cdots$). It is also observed from (3.9) and (3.10) that both the transform matrix and its inverse have the same sign and zero patterns, which may be exploited to simplify the implementation.

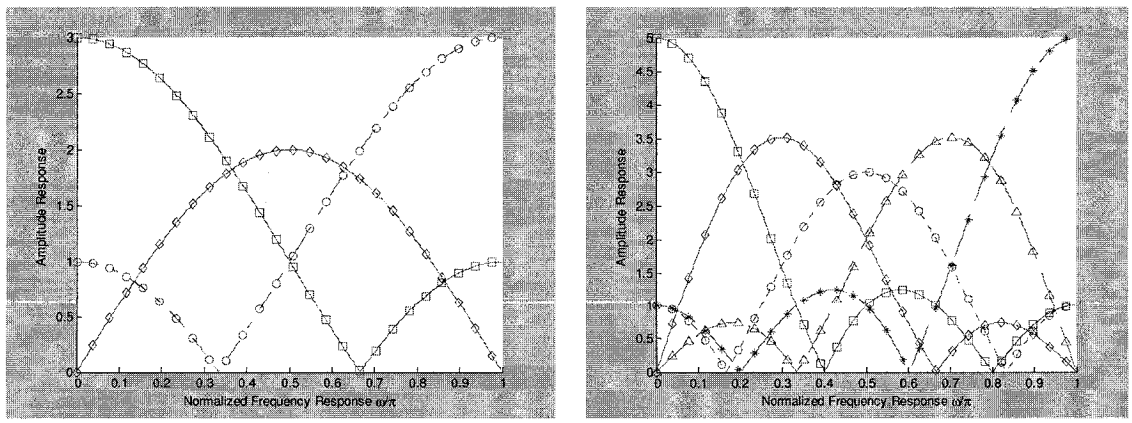

(a) (b)

Figure 3.2: Frequency response of the interpolators in the GP structure.
(a) 3-branch decomposition. (b) 5-branch decomposition.

3.3.2 High-Order Transform Matrix

In a manner similar to the way that $\mathbf{R}_3$ and $\mathbf{R}_5$ are developed, one can get more seed matrices of different prime orders. Using these basic seed matrices in conjunction with the 2nd-order Hadamard matrix, a general high-order transform matrix can be obtained using the Kronecker product, namely,

$$\mathbf{R}_N = \underbrace{\mathbf{R}_{q_1} \otimes \cdots \otimes \mathbf{R}_{q_1}}_{\mu_1 \text{ terms}} \underbrace{\otimes \mathbf{R}_{q_2} \otimes \cdots \otimes \mathbf{R}_{q_2}}_{\mu_2 \text{ terms}} \cdots \underbrace{\mathbf{R}_{q_K} \otimes \cdots \otimes \mathbf{R}_{q_K}}_{\mu_K \text{ terms}} \tag{3.11}$$

where $\mathbf{R}_{q_k}$ $(k = 1, 2, \cdots, K)$ represents the individual seed matrix of order q_k. At the same time, the inverse of (3.11) is readily given by

$$\mathbf{R}_N^{-1} = \underbrace{\mathbf{R}_{q_1}^{-1} \otimes \cdots \otimes \mathbf{R}_{q_1}^{-1}}_{\mu_1 \text{ terms}} \underbrace{\otimes \mathbf{R}_{q_2}^{-1} \otimes \cdots \otimes \mathbf{R}_{q_2}^{-1}}_{\mu_2 \text{ terms}} \cdots \underbrace{\mathbf{R}_{q_K}^{-1} \otimes \cdots \otimes \mathbf{R}_{q_K}^{-1}}_{\mu_K \text{ terms}} \tag{3.12}$$

Obviously, (3.12) reduces to the generation of Hadarmard transform only when the 2nd-order Hadamard matrix is used as the basic element. It is clear that the higher-order matrices thus generated still possess all the desired properties that the seed matrices do. For example, with the 2×2 Hadamard matrix and the proposed 3×3 seed matrix, a 6×6 matrix can be built as given below,

$$\mathbf{R}_6 = \mathbf{R}_2 \otimes \mathbf{R}_3 = \begin{bmatrix} 1 & 1 & 1 & 1 & 1 & 1 \\ 1 & 0 & -1 & 1 & 0 & -1 \\ 1 & -1 & 1 & 1 & -1 & 1 \\ 1 & 1 & 1 & -1 & -1 & -1 \\ 1 & 0 & -1 & -1 & 0 & 1 \\ 1 & -1 & 1 & -1 & 1 & -1 \end{bmatrix}$$

$$\mathbf{R}_6^{-1} = \mathbf{R}_2^{-1} \otimes \mathbf{R}_3^{-1} = \frac{1}{8}\begin{bmatrix} 1 & 2 & 1 & 1 & 2 & 1 \\ 2 & 0 & -2 & 2 & 0 & -2 \\ 1 & -2 & 1 & 1 & -2 & 1 \\ 1 & 2 & 1 & -1 & -2 & -1 \\ 2 & 0 & -2 & -2 & 0 & 2 \\ 1 & -2 & 1 & -1 & 2 & -1 \end{bmatrix} \tag{3.13}$$

It should be noted that the transform matrices meeting the aforementioned requirements are not unique. For example, exchanging the order of the two matrices in (3.13) would generate another transform matrix with similar properties.

Based on the proposed transform matrices, we can obtain a GP structure with an arbitrary number of branches whose constituent filters are of linear-phase. Although there are some other methods to generate a parallel structure such as [59], which is able to restore the symmetric property of the polyphase structure, our approach based on the proposed transform matrices provides a more systematic way of obtaining the GP struture. Moreover, besides the restoration of the symmetry property, more desirable features, such as the frequency-selectivity of the interpolators, are achieved in our method. The proposed transform matrices could be regarded as an extension of the even-order Hadamard matrix.

3.3.3 Incorporation of Interpolation Condition

We now proceed to incorporate the interpolation constraint into the GP structure. The combination of the linear-phase property and the interpolation constraint requires the filter length to be odd. Notice that in the above GP structure, we have assumed that every subfilter has the same length and thus the overall filter is of length $N = MK$. Accordingly, there are some requirements on the choice of N and M. Depending on the parity of M, the discussion is divided into two cases: even or odd M.

For odd M, it is feasible to have an odd N as long as K is odd. The interpolation condition can easily be satisfied in the conventional M-branch polyphase structure by setting one subfilter as $h_{(M-1)/2}[n] = \frac{1}{M}\delta[n - \frac{K-1}{2}]$. From (3.5), we know that the constituent filters in the GP structure and the subfilters in the conventional polyphase structure are associated through the matrix equation

$$\mathbf{H}(z) = \mathbf{P}\mathbf{G}(z) \tag{3.14}$$

where

$$\mathbf{H}(z) = [H_0(z) \quad H_1(z) \quad \cdots \quad H_{M-1}(z)]^T$$

$$\mathbf{G}(z) = [G_0(z) \quad G_1(z) \quad \cdots \quad G_{M-1}(z)]^T$$

By taking the inverse Z-transform on both sides of (3.14) and applying the interpolation constraint on the conventional polyphase structure, we obtain

$$\sum_{k=0}^{M-1} P(\tfrac{M-1}{2}, k) g_k(n) = h_{(M-1)/2}(n) = \tfrac{1}{M}\delta(n) \tag{3.15}$$

The above equation imposes a constraint on the design of the constituent filters $g_k(n)$. Clearly, this constraint can easily be satisfied by designing the first (M-1) constituent filters independently while leaving the last one as

$$g_{M-1}(n) = \frac{1}{P(l', M-1)}\left[\frac{1}{M}\delta(n) - \sum_{k=0}^{M-2} P(l', k) g_k(n)\right] \tag{3.16}$$

As for even M, one cannot find any integer K such that N=MK is odd. However, we can still obtain a slightly different GP structure by allowing the constituent filters to have non-identical filter lengths. For example, let the overall filter length be $N = MK + 1$, where K is odd, we now have M-1 subfilters of length K in the polyphase structure except for $H_0(z)$ of length $K+1$. The subfilter $H_0(z)$ has a fixed impulse response determined

by the time-domain constraint and thus can be singled out and treated separately. The rest of the subfilters with the same length K are then transformed into the constituent filters in the GP structure. Notice that the transform matrix to be employed to obtain the GP structure should have an odd order M-1.

3.4 Frequency Response Specifications for Constituent Filters

With Hadamard or the proposed seed matrices, it is straightforward to construct a transform matrix and obtain a GP realization structure for a known FIR filter. On the other hand, in order to simplify the design problem of a large-tap FIR filter, it is necessary to derive the frequency response specifications for the constituent filters. Unlike the conventional polyphase structure in which the subfilters are, in general, not linear-phase, the GP decomposition leads to linear-phase constituent filters. This feature also motivates us to design the length-reduced constituent filters directly without causing any phase distortion. It is expected that these filters be designed separately and easily. In what follows, a systematic way is developed to find the desired frequency specifications for the constituent filters. Our discussion begins with the design of Mth-band filters, and is then extended to general FIR filters.

3.4.1 Frequency Specification for Mth-band Filters

In this chapter, we assume that an Mth-band filter is decomposed into M branches using the GP structure so as to get a closed-form expression for the amplitude specifications of the constituent filters. Let us consider a low-pass Mth-band filter first. As seen from (3.3), each constituent filter $G_k(e^{j\omega})$ is upsampled M times, which

generates M compressed images. To get an ideal low-pass frequency response of the overall filter, we expect the desired constituent filters $\tilde{G}_k(e^{j\omega})$ to satisfy

$$\tilde{H}(e^{j\omega}) = \sum_{k=0}^{M-1} F_k(e^{j\omega})\tilde{G}_k(e^{jM\omega}) = \begin{cases} 1, & 0 \le \omega \le \pi/M \cup (2M-1)\pi/M \le \omega \le 2\pi \\ 0, & \pi/M \le \omega \le 3\pi/M \\ \vdots & \vdots \\ 0, & (2M-3)\pi/M \le \omega \le (2M-1)\pi/M \end{cases} \tag{3.17}$$

To this end, we define a set of functions $E_k(e^{j\omega})$ as

$$E_k(e^{j\omega}) = \frac{1}{M}\sum_{l=0}^{M-1} Q(k,l)\exp(jl\omega). \tag{3.18}$$

Let $\tilde{G}_k(e^{j\omega})$ be given by

$$\tilde{G}_k(e^{j\omega}) = E_k(e^{j\omega/M}), \; -\pi \le \omega \le \pi \tag{3.19}$$

Note that the upsampled version of $\tilde{G}_k(e^{j\omega})$ can be expressed as

$$\tilde{G}_k(e^{jM\omega}) = \begin{cases} E_k(e^{j\omega}), & 0 \le \omega \le \pi/M \cup (2M-1)\pi/M \le \omega \le 2\pi \\ E_k(e^{j(\omega-2\pi/M)}), & \pi/M \le \omega \le 3\pi/M \\ \vdots & \vdots \\ E_k(e^{j[\omega-2\pi(M-1)/M]}), & 2\pi - 3\pi/M \le \omega \le 2\pi - \pi/M \end{cases} \tag{3.20}$$

Substituting (3.20) into the first equation of (3.17) and noting that $\sum_{k=0}^{M-1} E_k(e^{j(\omega-2\pi n/M)})F_k(e^{j\omega}) = \delta(m)$, one can verify that the second equation in (3.17) is satisfied, which implies that (3.20) gives exactly the desired specifications for the constituent filters.

We now investigate the design of band-pass Mth-band filters. Considering that the passband can be any of the M bands in the entire frequency domain, we have two types of expressions for the ideal frequency response, namely

$$\tilde{H}(e^{j\omega}) = \begin{cases} 1, & 2i\pi/M \le |\omega| \le (2i+1)\pi/M \\ 0, & \text{elsewhere} \end{cases}, \quad i = 0,1,\cdots,\lfloor (M-1)/2 \rfloor \tag{3.21}$$

or,

$$\tilde{H}(e^{j\omega}) = \begin{cases} 1, & (2i+1)\pi/M \le |\omega| \le 2(i+1)\pi/M \\ 0, & \text{elsewhere} \end{cases}, \quad i = 0,1,\cdots,\lceil (M-1)/2 \rceil - 1 \tag{3.22}$$

where $\lfloor x \rfloor$ and $\lceil x \rceil$, respectively, denote the nearest integer less than or equal to x, and the nearest integer larger than or equal to x. Obviously, (3.21) includes the low-pass Mth-band filter as a special case when i=0. Using (3.19), it can be shown that the specification of the constituent filters with respect to (3.21) is given by

$$\tilde{G}_k(e^{j\omega}) = \begin{cases} E_k(e^{j(\omega+2i\pi)/M}), & 0 \le \omega \le \pi \\ E_k(e^{j(\omega-2i\pi)/M}), & -\pi \le \omega \le 0 \end{cases} \tag{3.23}$$

and that with regard to (3.22) is given by

$$\tilde{G}_k(e^{j\omega}) = \begin{cases} E_k(e^{j(\omega-2i\pi)/M}), & 0 \le \omega \le \pi \\ E_k(e^{j(\omega+2i\pi)/M}), & -\pi \le \omega \le 0 \end{cases} \tag{3.24}$$

3.4.2 Frequency Specification for General Linear-Phase Filters

Although our focus is on the Mth-band filter design, the proposed GP-based design approach is also applicable to general FIR filters. In this case, the band edges may not be exactly $k\pi/M$, and three typical situations are considered depending on the location of the cutoff frequencies of the desired overall filter. Although the following discussions are focused on low-pass filters, the results can easily be extended for the case of high-pass and band-pass filters.

Situation 1: Consider a low-pass filter with the passband edge ω_p and the stopband edge ω_s subject to $\omega_p + \omega_s = 2\pi/M$. The transition-band width is then $\Delta\omega = \omega_s - \omega_p$. It can easily be verified that the amplitude specification for the constituent filters is given by

$$\tilde{G}_k(e^{j\omega}) = \begin{cases} E_k(e^{j\omega/M}), & 0 \le \omega \le M\omega_p \\ \text{don't care}, & M\omega_p \le \omega \le \pi \end{cases}, \tag{3.25}$$

where the region $M\omega_p \le \omega \le \pi$ of $\tilde{G}_k(e^{j\omega})$ falls within the transition band of the overall filter.

Situation 2: If the low-pass filter in question has a stopband edge as $\omega_s < \pi/M$, then the region $\omega_s \le \omega \le \pi/M$ of $H(e^{j\omega})$, which corresponds to $M\omega_s \le \omega \le \pi$ of $\tilde{G}_k(e^{j\omega})$ falls into the stopband. Therefore, the desired amplitude response $\tilde{G}_k(e^{j\omega})$ can be modified as

$$\tilde{G}_k(e^{j\omega}) = \begin{cases} E_k(e^{j\omega/M}) & 0 \le \omega \le M\omega_p \\ \text{don't care}, & M\omega_p \le \omega \le M\omega_s \\ 0, & M\omega_s \le \omega \le \pi \end{cases} \tag{3.26}$$

Situation 3: A low-pass filter with its passband larger than π/M, namely, $R\pi/M \le \omega_p \le \omega_s \le (R+1)\pi/M$, where $R \ge 1$ is an integer, is considered. In this case, the overall frequency response can be regarded as an addition of R+1 parts, namely,

$$\tilde{H}^{(i)}(e^{j\omega}) = \begin{cases} 1, & i\pi/M \le \omega \le (i+1)\pi/M \\ 0, & \text{elsewhere} \end{cases}, (i = 0,1,\cdots,R-1) \tag{3.27a}$$

and

$$\tilde{H}^{(R)}(e^{j\omega}) = \begin{cases} 1, & R\pi/M \le \omega \le \omega_p \\ \text{don't care}, & \omega_p \le \omega \le \omega_s \\ 0, & \text{elsewhere} \end{cases} \tag{3.27b}$$

Let the specification with respect to each part in (3.27) be $\tilde{G}_k^{(i)}(e^{j\omega})$, $(i=0,1,\cdots,R)$. As the overall filter is equivalent to a sum of R+1 filters, the specifications for the constituent filters would be the summation of all $\tilde{G}_k^{(i)}(e^{j\omega})$. As for (3.27a), the specifications corresponding to these band-pass Mth-band filters are given by (3.23) or (3.24). With regard to (3.27b), the frequency specification corresponding to the passband of the overall filter can be determined from either (3.23) or (3.24) depending on the parity of R while that corresponding to the stopband is always zero, i.e.,

$$\tilde{G}_k^{(R)}(e^{j\omega}) = \begin{cases} E_k(e^{j(\omega+R\pi)/M}), & 0 \le \omega \le M\omega_p - R\pi \\ \text{don't care} & M\omega_p - R\pi \le \omega \le M\omega_s - R\pi \\ 0, & M\omega_s - R\pi \le \omega \le \pi \end{cases} \tag{3.28a}$$

when R is even, and

$$\tilde{G}_k^{(R)}(e^{j\omega}) = \begin{cases} 0, & 0 \le \omega \le (R+1)\pi - M\omega_s \\ \text{don't care}, & (R+1)\pi - M\omega_s \le \omega \le (R+1)\pi - M\omega_p \\ E_k(e^{j(\omega-(R+1)\pi)/M}), & (R+1)\pi - M\omega_p \le \omega \le \pi \end{cases} \tag{3.28b}$$

when R is odd. Thus, the total frequency specification for each constituent filter is given by

$$\tilde{G}_k(e^{j\omega}) = \sum_{i=0}^{R} \tilde{G}_k^{(i)}(e^{j\omega}) \tag{3.29}$$

According to the above discussions, we have been able to convert the design problem of a large-tap FIR filter into that of M lower-order filters. As the transform matrix $\mathbf{Q}$ has symmetric or antisymmetric column vectors, it is clear that the design of lower-order constituent filters belongs to the category of linear-phase filter design. Since the design complexity of FIR filters is, in general, of the order of $O(N^2)$, where N is the filter length, the proposed method is able to reduce the computational complexity by a factor of

M compared to a direct design of the original filter. It should be mentioned that although the proposed GP-based method needs the calculation of the frequency specifications for the constituent filters, this additional computation, with the help of the above closed-form expression, is negligible in comparison to the overall design complexity.

3.5 *M*th-band Filters with certain Regularities

In some applications, one has to deal with filters that satisfy special requirements in time and/or frequency domain. For instance, interpolation filters with certain regularity are of particular interest in the construction of wavelets and have been extensively studied [61]. A filter is referred to as an interpolation filter of K-regularity if (i) its impulse response satisfies $h[Mn]=\frac{1}{M}\delta[n]$, where M represents the interpolation factor, and (ii) the amplitude response $H(\omega)$ as well as its first (K-1) derivatives have zeros at the aliasing frequency points $\omega = 2\pi q / M$, $(q = 0,1,\ldots,M-1)$. In this section, we present a GP-based design method for this class of filters with an emphasis on deriving a set of time-domain constraints for the constituent filters in the GP implementation. Then, the design of the constituent filters turns out to be a constrained optimization problem.

As the constituent filters in the GP structure are related to the subfilters in the polyphase structure, our discussion is conducted first for the conventional polyphase structure. We will then extend the resulting constraints for the constituent filters. Let us consider an N-tap causal FIR filter, whose conventional polyphase realization is given by

$$H(z)=\sum_{l=0}^{M-1} z^{-l} \sum_{n=0}^{N/M-1} h[Mn+l]z^{-Mn} = \sum_{l=0}^{M-1} z^{-l} \sum_{n=0}^{N/M-1} h_l[n]z^{-Mn} \tag{3.30}$$

where N is assumed to be a multiple of M and l is the subfilter index. The regularity constraints for the subfilters $h_l[n]$ are given by the following theorem.

Theorem 3.1: A linear-phase filter is K-regular *iff* the impulse response of each subfilter in (3.30) satisfies

$$\sum_{n=0}^{N/M-1}(n-\beta)^r h_l[n]=(\alpha-l)^r/M^{r+1}, \tag{3.31}$$

$$(r=0,1,\ldots,K-1;l=0,1,\ldots,M-1)$$

where

$$\alpha=(M-1)/2,\ \beta=(N/M-1)/2 \tag{3.32}$$

As the constraint is given in the form of the moment of the impulse response, it can be termed as the moment constraint.

Proof: We first prove the necessity by mathematical induction. From the regularity definition, for $r=0$, we have

$$H(\omega)=\begin{cases}1, & \omega=0\\ 0, & \omega=2\pi q/M, q=1,\ldots,M-1\end{cases} \tag{3.33}$$

As the filter is of linear-phase, its amplitude response can be written in the polyphase decomposition form as

$$\begin{aligned}H(\omega)&=\sum_{n=0}^{N-1}h[n]e^{-j\omega(n-(N-1)/2)}\\ &=e^{-j\omega(N-1)/2}\sum_{l=0}^{M-1}e^{-j\omega l}\sum_{n=0}^{N/M-1}h_l[n]e^{-j\omega M n}\end{aligned} \tag{3.34}$$

From (3.33) and (3.34), we get

$$\mathbf{W}_M \cdot \begin{bmatrix} \sum_{n=0}^{N/M-1} h_0[n] \\ \sum_{n=0}^{N/M-1} h_1[n] \\ \vdots \\ \sum_{n=0}^{N/M-1} h_{M-1}[n] \end{bmatrix} = \begin{bmatrix} 1 \\ 0 \\ \vdots \\ 0 \end{bmatrix} \tag{3.35}$$

where $\mathbf{W}_M$ is the M-point DFT matrix, whose elements are given by $[\mathbf{W}_M]_{p,q} = \exp(-j2\pi pq/M)$, $(p,q = 0,1,\ldots M-1)$. Solving (3.35) leads to

$$\sum_{n=0}^{N/M-1} h_l[n] = 1/M \ , \ (l = 0,1,\ldots,M-1) \tag{3.36}$$

which obviously satisfies (3.31) for r=0.

For $r=1$, we need to calculate the first derivative of the amplitude response,

$$\begin{aligned} \frac{d}{d\omega}H(\omega) &= -j\sum_{n=0}^{N-1}(n-(N-1)/2)h[n]e^{-j\omega(n-(N-1)/2)} \\ &= -je^{j\omega(N-1)/2}\sum_{l=0}^{M-1}e^{-j\omega l}\left(\sum_{n=0}^{N/M-1}M(n-\beta)h_l[n]e^{-j\omega Mn} + \sum_{n=0}^{N/M-1}(l-\alpha)h_l[n]e^{-j\omega Mn}\right) \end{aligned} \tag{3.37}$$

In obtaining (3.37), we have used the fact $M\beta+\alpha=(N-1)/2$. From the regularity definition with regard to the first derivative, we have

$$\left.\frac{d}{d\omega}H(\omega)\right|_{\omega=2\pi q/M} = 0, \ (q = 0,1,\ldots,M-1). \tag{3.38}$$

Using (3.37) in (3.38) gives

$$\mathbf{W}_M \cdot \left(\begin{bmatrix} \vdots \\ \sum_{n=0}^{N/M-1} M(n-\beta)h_l[n] \\ \vdots \end{bmatrix} + \begin{bmatrix} \vdots \\ (l-\alpha)\sum_{n=0}^{N/M-1} h_l[n] \\ \vdots \end{bmatrix} \right) = \mathbf{0} \tag{3.39}$$

Substituting into (3.39) the result from (3.36) with respect to $r=0$, we have

$$\sum_{n=0}^{N/M-1}(n-\beta)h_l[n]=(\alpha-l)/M^2,\ (l=0,1,\ldots,M-1). \tag{3.40}$$

Thus, we have completed the proof of (3.31) for $r=1$.

We now assume that (3.31) holds till $r=k-1$, namely,

$$\sum_{n=0}^{N/M-1}(n-\beta)^r h_l[n]=(\alpha-l)^r/M^{r+1},\quad (l=0,1,\ldots,M-1;r=0,1,\ldots,k-1) \tag{3.41}$$

and prove that it is also true for $r=k$. Clearly, the (k-1)th derivative of $H(\omega)$ is given by

$$\begin{aligned}\frac{d^{k-1}}{d\omega^{k-1}}H(\omega)&=(-j)^{k-1}e^{-j\omega(N-1)/2}\sum_{n=0}^{N-1}(n-M\beta-\alpha)^{k-1}h[n]e^{-j\omega n}\\&=(-j)^{k-1}e^{-j\omega(N-1)/2}\sum_{l=0}^{M-1}e^{-j\omega l}\sum_{n=0}^{N/M-1}\left[M(n-\beta)+(l-\alpha)\right]^{k-1}h_l[n]e^{-j\omega M n}\end{aligned} \tag{3.42}$$

By using the binomial expansion,

$$\left[M(n-\beta)+(l-\alpha)\right]^{k-1}=\sum_{q=0}^{k-1}C_{k-1}^{q}\left[M(n-q)\right]^{q}(l-\alpha)^{k-1-q}$$

and the regularity definition $\left.\frac{d}{d\omega^r}H^r(\omega)\right|_{\omega=2\pi q/M}=0$, (3.42) can be rewritten in matrix form as

$$\mathbf{W}_M\cdot\left(\begin{bmatrix}\vdots\\ \sum_{n=0}^{N/M-1}\left[M(n-\beta)\right]^{k-1}h_l[n]\\ \vdots\end{bmatrix}+\begin{bmatrix}\vdots\\ \sum_{q=1}^{k-1}C_{k-1}^{q}(l-\alpha)^{q}\sum_{n=0}^{N/M-1}\left[M(n-\beta)\right]^{k-1-q}h_l[n]\\ \vdots\end{bmatrix}\right)=\mathbf{0} \tag{3.43}$$

which leads to

$$\sum_{n=0}^{N/M-1}\left[M(n-\beta)\right]^{k-1}h_l[n]=-\sum_{q=1}^{k-1}C_{k-1}^{q}(l-\alpha)^{q}\sum_{n=0}^{N/M-1}\left[M(n-\beta)\right]^{k-1-q}h_l[n] \tag{3.44}$$

Substituting (3.41) into the right side of (3.44), one obtains

$$\sum_{n=0}^{N/M-1}(n-\beta)^{k-1}h_l[n]=(\alpha-l)^{k-1}/M^k \quad (l=0,1,\ldots,M-1), \tag{3.45}$$

which implies that (3.31) holds for $r=k$. The induction can be continued up to the $(K-1)$th derivative of the amplitude response as required by a filter with K-regularity.

On the other hand, by using (3.31) in (3.35), (3.39) and (3.43), one can verify that the first (K-1) derivatives have zeros at aliasing frequency points, implying that (3.31) is also a sufficient condition for a filter with K-regularity. □

Using (3.29) and (3.31), we can get the regularity constraints for constituent filters in the GP structure, as stated in the following corollary.

Corollary 3.1: A linear-phase filter is K-regular *iff* the constituent filters $g_k[n]$ in its GP implementation satisfy

$$\sum_{n=0}^{N/M-1}(n-\beta)^r g_k[n]=\sum_{l=0}^{M-1}Q(k,l)(\alpha-l)^r/M^{r+1} \tag{3.46}$$

$$(r=0,1,\ldots,K-1;\ k=0,1,\ldots,M-1)$$

Remarks:

1. Due to the symmetry or antisymmetry of the columns of $\mathbf{Q}$, the corresponding constituent filters $G_k(z)$ are either symmetric (even k) or antisymmetric (odd k). Exploiting this symmetry property, we may further reduce the number of constraints in (3.46) by one-half. Recalling that $\alpha=(M-1)/2$ and $\beta=(N/M-1)/2$, both sequences $(n-\beta)^r$ and $(\alpha-l)^r$ are symmetric when r is even, or antisymmetric when r is odd. As such, for odd k and even r, both sides of (3.46) sum to zero. Similarly, (3.46) is trivial when k is even and r odd. Therefore, only one-half of the constraints in (3.46) need to be incorporated in the

design of the constituent filters $G_k(z)$.

2. With the constraints in (3.46), the design of the constituent filters is converted to a constrained optimization problem, namely,

$$\begin{aligned} &\min_{g_k(n)} \delta = \left| \sum_n g_k(n) e^{-j\omega n} - \tilde{G}_k(\omega) \right| \\ &s.t. \quad \sum_{n=0}^{N/M-1} (n-\beta)^r g_k[n] = \sum_{l=0}^{M-1} Q(m,l)(\alpha-l)^r / M^{r+1} \end{aligned} \tag{3.47}$$

with $k+r$ being odd. When the first M-1 constituent filters are solved using (3.47), the last one can be readily determined from (3.16).

3.6 Simulation Results

In this section, several linear-phase FIR filters and Mth-band filters are designed based on the proposed GP structure. The design results are compared to those obtained by the direct SDP design and the eigenfilter approach in terms of the maximum error as well as the design complexity. It is shown that our GP-based design gives a nearly optimal performance with considerable savings on the computational complexity. The designed Mth-band filter is also employed as an interpolation filter for image resizing.

3.6.1 Design Examples

According to the discussions in the previous sections, the proposed design method mainly contains the following steps.

(1) Choose a transform matrix of a proper order in accordance with the length and type of the filter to be designed.

(2) Determine the desired frequency specifications for each constituent filter of the GP structure.

(3) Incorporate the time-domain interpolation condition in Mth-band filter design.

(4) Include the regularity condition for Mth-band filters, if required, as part of the constraints for the optimization problem.

(5) Solve the constrained optimization problem using an existing optimization technique.

Since the frequency specifications of the constituent filters may have arbitrary shape instead of the normal piece-wise constant shape, the semidefinite programming (SDP) proposed in [10] is employed for the design of the constituent filters. As a powerful optimization tool, SDP covers a large class of 1-D and 2-D filters with arbitrary frequency responses and can easily accommodate extra linear equality or inequality constraints. By utilizing a user-friendly Matlab software for the implementation of the SDP optimization technique [98, 99], several design examples are completed in order to validate the proposed GP-based design approach.

Example 3.1:

In the first example, a conventional low-pass linear-phase FIR filter is designed to validate the derived closed-form frequency specifications for the constituent filters. Assume that the filter is of length 64 with the passband and stopband frequencies given by $\omega_p = 0.3\pi$ and $\omega_s = 0.34\pi$ and a two-branch GP structure is employed for its realization. As the stopband cutoff frequency ω_s is smaller than π/M ($M = 2$), the frequency specification in *Situation 2* of Section 3.4 should be applied. Using (3.25) and the second-order Hadamard matrix, we obtain

$$\tilde{G}_0(\omega) = \begin{cases} \frac{1}{2}\cos(\omega/4), & |\omega| \le 0.6\pi \\ 0, & 0.68\pi \le |\omega| \le \pi \end{cases} \tag{3.48a}$$

$$\tilde{G}_1(\omega) = \begin{cases} \frac{1}{2}\sin(\omega/4), & |\omega| \le 0.6\pi \\ 0, & 0.68\pi \le |\omega| \le \pi \end{cases} \tag{3.48b}$$

The resulting amplitude responses of the designed filters $G_0(\omega)$ and $G_1(\omega)$ are depicted along with the ideal frequency specifications in Fig. 3.3(a) and 3.3(b), respectively. Since the maximum error is minimized, one can see that the amplitude error is equiripple. The frequency contribution from each branch $F_k(\omega)G_k(2\omega)$ is depicted in Fig. 3.3(c). It is noted that the two frequency contributions add to unity in the passband and to zero in the stopband. The overall frequency response of the designed filter as well as that obtained directly from the Parks-McClellan (PM) minimax design is given in Fig. 3.3(d). The maximum amplitude approximation error is 0.00139 for the PM method and 0.00141 for the GP method, clearly indicating a similar performance of the two methods. A brief analysis of the approximation error of the proposed method and its comparison with the optimal PM method are provided at the end of this section. It is observed that the GP-based design does not yield an equiripple amplitude response, especially in the stopband even though each constituent filter is designed in the minimax error sense. This is due to the frequency response images generated from the upsampling of the constituent filters with respect to the transition band, which cannot cancel each other completely. However, this phenomenon of amplitude fluctuation in the stopband can be improved by slightly modifying the frequency specification for one of the constituent filters as seen in the next example.

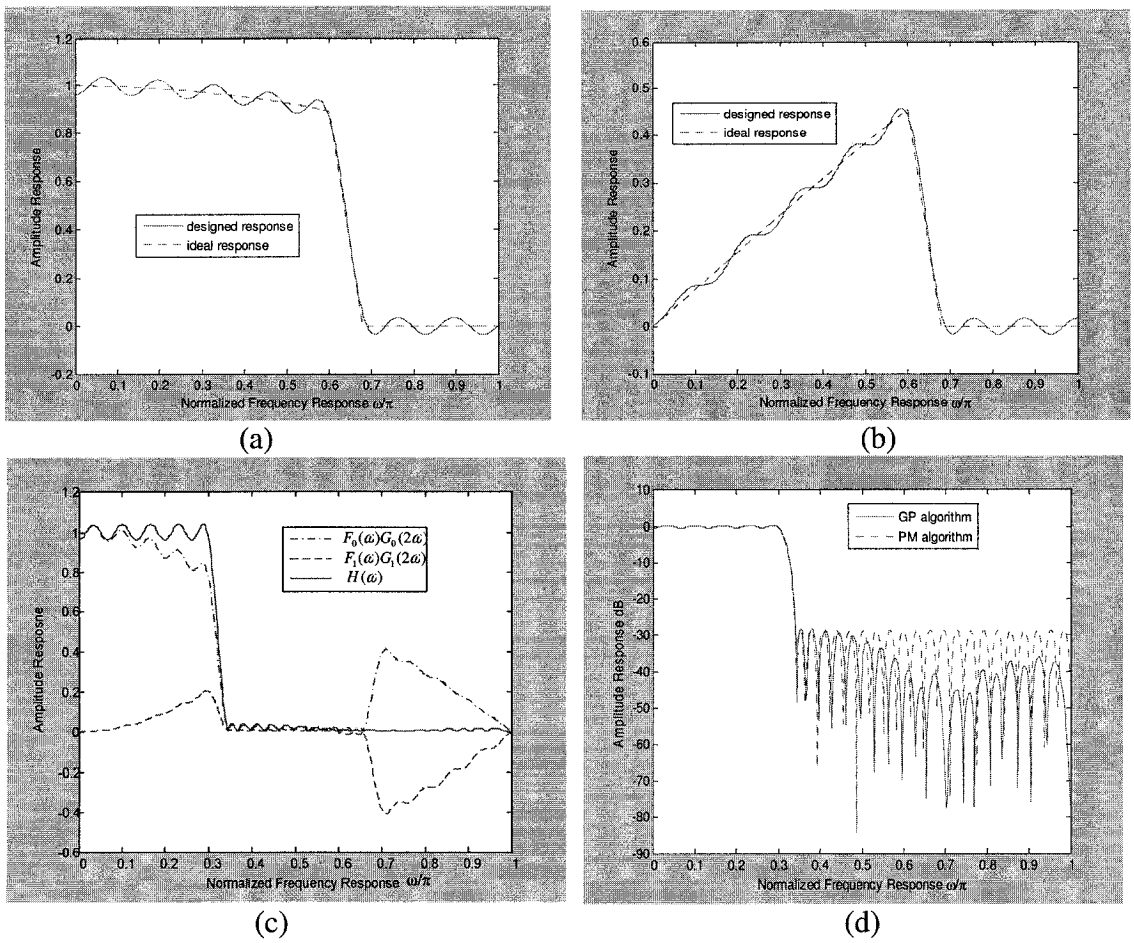

Figure 3.3: Frequency responses of the filters in *Example 3.1.* (a) Designed $G_0(\omega)$ vs. its frequency specification. (b) Designed $G_1(\omega)$ vs. its frequency specification. (c) Contributions from two branches. (d) The overall filter vs. that designed by PM method.

Example 3.2:

Here, we consider a highpass 4th-band filter of length 119 with a sharp-transition specified by $\omega_s = 0.7\pi, \omega_p = 0.8\pi$. From the discussion in Section 3.3, the 4-branch GP structure must have one 29-tap constituent filter with the fixed impulse response $g_3[n] = \delta[n-14]$ and three 30-tap linear-phase constituent filters to be designed. Using the 3rd-order transform matrix in (3.9), the frequency specifications for the constituent filters are readily given by

$$\tilde{G}_0(\omega) = 1/4(\cos((\omega - 6\pi)/4) + 1/2),$$

$$\tilde{G}_1(\omega) = 1/4\sin((\omega - 6\pi)/4), \tag{3.49}$$

$$\tilde{G}_2(\omega) = 1/4(\cos((\omega - 6\pi)/4) - 1/2)$$

$$\omega \in (0, 0.8\pi)$$

As mentioned in *Example 1*, the "don't-care" region corresponding to the transition band of the constituent filters would cause the amplitude response of the designed filter to fluctuate in the stopband. In order to alleviate this problem, one can use a modified specification of the last constituent filter once other filters have been designed. For example, when $G_0(z)$ and $G_1(z)$ are designed according to the above specifications, their actual frequency response can then be taken into account in the design of $G_2(z)$. The frequency specification of $G_2(z)$ is modified as

$$\tilde{G}_2(\omega) = \begin{cases} 1/4(\cos((\omega - 6\pi)/4) - 1/2), & 0 \le \omega < 0.8\pi \\ [1/4(\cos((\omega - 6\pi)/4) - 1/2) - G_0(\omega) - G_1(\omega)] & 0.8\pi \le \omega < \pi \end{cases} \tag{3.50}$$

This modification helps to reduce the peak design error in the stopband of the overall filter that is contributed by the transition band of the constituent filters. The amplitude response of the designed filter, which is almost equiripple, is shown in Fig. 3.4. As pointed out earlier, most of the existing design algorithms do not consider the interpolation constraint. To make a fair comparison, we also design the overall fourth-band interpolation filter via SDP. The frequency response of 4th-band filter directly designed by SDP is depicted in Fig. 3.5. The time-domain constraint is imposed as the additional equality constraint to the SDP problem. It is seen that the directly designed fourth-band filter has a maximum error of 1.5662e-005. Compared with the optimal filter, the maximum error of our GP-based fourth-band filter is 2.1063e-005. Since the overall

filter is given by the synthesis of the constituent filters through the transform matrix, the overall response is no longer optimal in the minimax sense, even though the constituent filters are designed to be optimal in the minimax sense. However, except for the mirror images of the narrow transition band, the errors at most of the frequency band are comparable to the optimum. We should also point out that in the direct design, the time-domain constraint is just numerically satisfied and brings extra burden to the optimization algorithm, while in our GP-based approach, the time-domain constraint is structurally satisfied with fewer coefficients to be determined. In our simulation, under the Pentinum 2.4GHz and 769M memory environment, the execution time for the direct approach is 4.2656 seconds while only 2.4844 seconds for the GP-based approach. This saving in the execution time is due to two aspects. First, instead of imposing the extra time-constraint in the direct SDP, the interpolation condition is structurally satisfied and used to reduce the free coefficients. Second, the design of the shorter length constituent filters would be easier than that of the large-length original filter. The maximum errors and execution times for highpass fourth-band filters with different lengths designed via GP-based approach are compared with those achieved by the direct SDP method in Table 3.1.

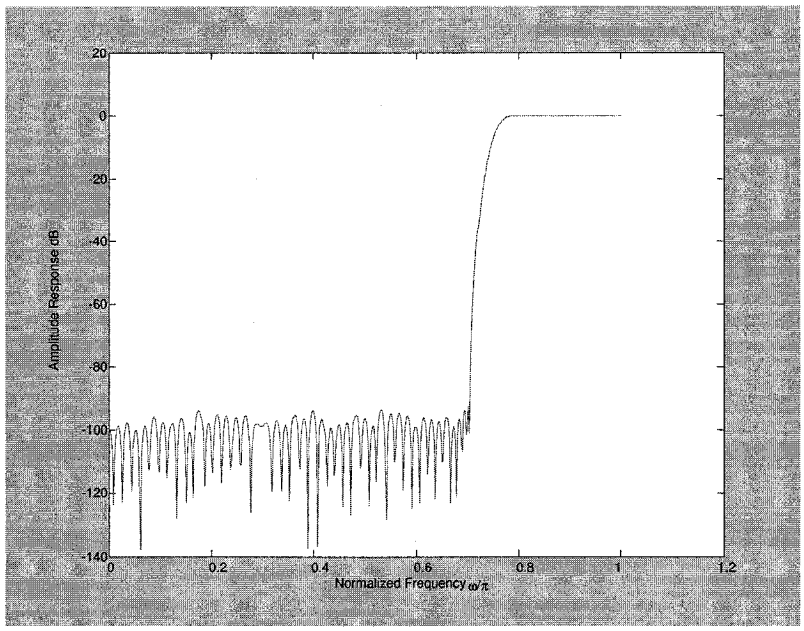

Figure 3.4: Frequency response of the high-pass 4th-band filter in *Example 3.2*, designed by GP-base approach

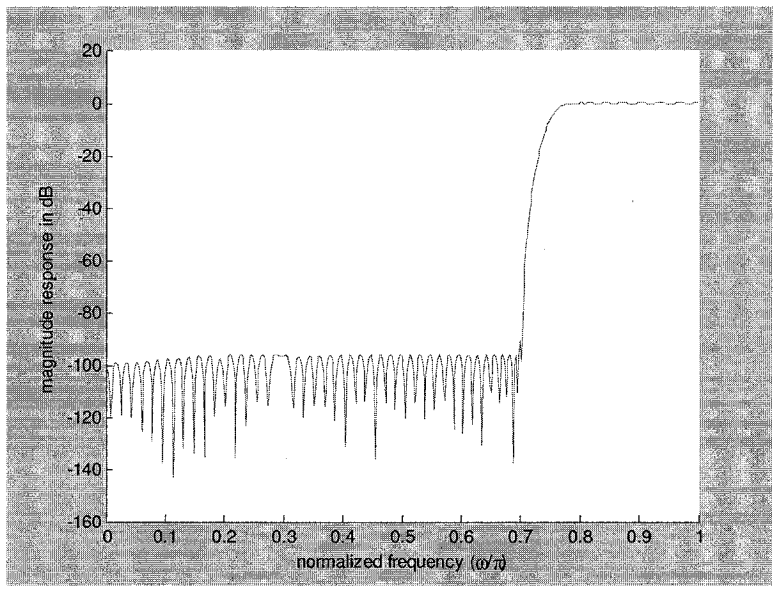

Figure 3.5: Frequency response of the high-pass 4th-band filter in *Example 3.2* designed directly by SDP

Table 3.1: Comparison of maximum errors and execution times for highpass 4th-band filter designed via the direct SDP and the GP-based approaches

	Maximum error		Execution time (seconds)	
Filter length	Direct SDP	GP-based	Direct SDP	GP-based
119	1.5662e-005	2.1063e-005	4.2656	2.4844
99	9.6670e-005	10.2658e-005	3.2813	1.5256
79	4.2118e-004	4.8965e-004	2.9688	1.0484
59	0.0026	0.0027	2.1719	0.9566
39	0.0122	0.0123	2.0469	0.8755

Example 3.3:

In this example, a set of 75-tap fifth-band interpolation filters with different regularities is designed. The cutoff frequencies are $\omega_p = 0.18\pi$ and $\omega_s = 0.22\pi$. Each of the filters to be designed is decomposed into five branches with the transform matrix given by (3.10). According to *Situation 1*, we get the amplitude specification for each of the constituent filters as

$$\begin{aligned}
\tilde{G}_0(\omega) &= \tfrac{1}{5} + \tfrac{2}{5}\cos(\omega/5) + \tfrac{2}{5}\cos(2\omega/5) \\
\tilde{G}_1(\omega) &= -\tfrac{2}{5}\sin(\omega/5) - \tfrac{2}{5}\sin(2\omega/5) \\
\tilde{G}_2(\omega) &= -\tfrac{1}{5} + \tfrac{2}{5}\cos(2\omega/5) \\
\tilde{G}_3(\omega) &= \tfrac{2}{5}\sin(\omega/5) - \tfrac{2}{5}\sin(2\omega/5) \\
\tilde{G}_4(\omega) &= \tfrac{1}{5} - \tfrac{2}{5}\cos(\omega/5) + \tfrac{2}{5}\cos(2\omega/5)
\end{aligned} \tag{3.51}$$

$$|\omega| \le 0.9\pi$$

Using the above specifications in conjunction with the equality constraint in (3.46) pertaining to different regularities, each constituent filter can be designed by the SDP optimization technique. In order to satisfy the interpolation condition, only the first four constituent filters need to be designed and the last one is readily given by (3.16). The resulting overall frequency responses of the designed filters with regularities 1, 2 and 3

are depicted in Fig. 3.6(a). The frequency responses in the passband are zoomed in Fig. 3.6(b). It is seen that the degree of flatness near $\omega = 0$ and the attenuation at the aliasing frequency points $\omega = 0.4\pi$ and 0.8π are dictated by different regularities. It is noted that both the flatness of the passband and the attenuation at the aliasing points of the stopband significantly improve when the regularity is increased from 1 to 2, while room for further improvement from regularity 2 to 3 is limited for the filter designed under the current specification. For the purpose of comparison, we have also designed the same 75-tap filter using the eigenfilter method [17], but without the regularity constraint. The resulting frequency response is illustrated in Fig. 3.7. The maximum frequency error of the filter designed by the proposed method is 0.0365, whereas that for the eigenfilter approach without regularity is 0.0869. It is also clear that the proposed approach gives a nearly equiripple frequency response in the stopband except at the frequencies of $k\pi / M$ ($k = 2,3,4$) in contrast to the eigenfilter method. This is due to the fact that the constituent filters in the GP structure are designed in the minimax error sense with the SDP technique.

Table 3.2 gives a comparison of the maximum error of various filters with different taps designed via the proposed method constrained by regularity 1, as well as the eigenfilter approach without the regularity constraint. It is seen that the proposed method always gives a smaller maximum error despite the additional regularity constraint. It should be emphasized that even though a high regularity is imposed in our approach, a similar maximum error can be achieved which is consistently superior to that of the eigenfilter method.

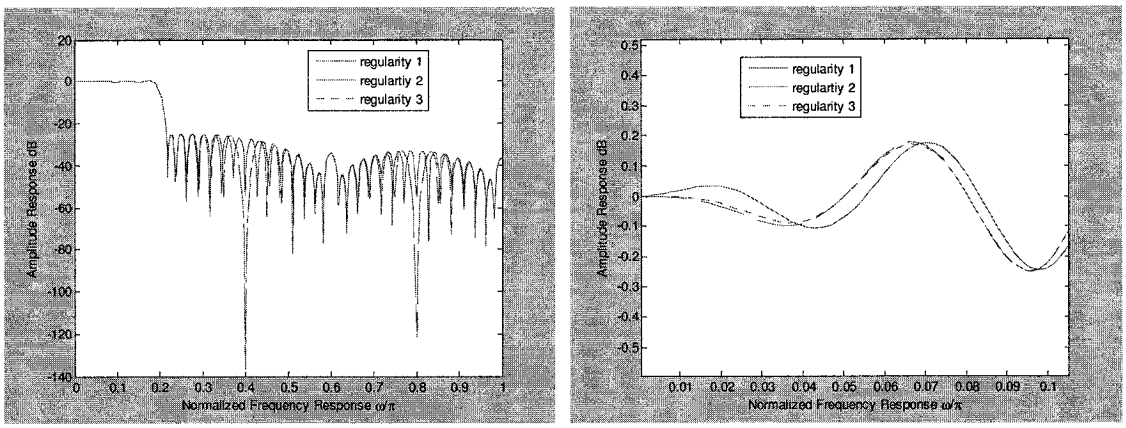

(a) (b)

Figure 3.6: Frequency response of the 5th-band interpolation filter in *Example 3.3* with different regularities. (a) Overall response. (b) Low-pass details.

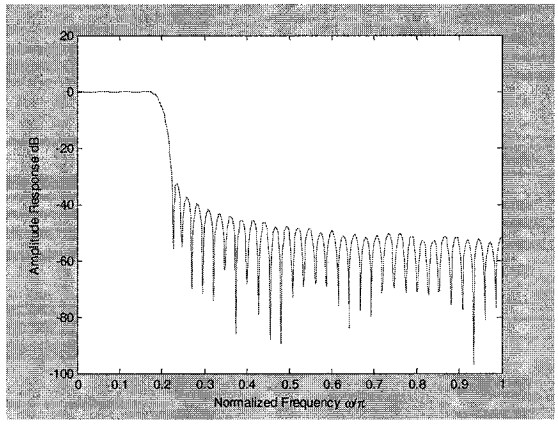

Figure 3.7: Frequency response of 5th-band low-pass filter in *Example 3.3* designed by eigenfilter method.

Table 3.2: Comparison of maximum errors for the lowpass 5th-band filter designed in *Example 3.3* via the GP-based and eigenfilter approaches

Filter length	Maximum error	
	GP-based	Eigenfilter
95	0.0227	0.0458
85	0.0283	0.0645
75	0.0365	0.0869
65	0.0492	0.1064
55	0.0698	0.1402

3.6.2 Error Analysis

In order to evaluate the design accuracy of the proposed method, the error performance of our method is now compared to that of the direct design of the overall filter.

Taking the 1-D filter design as an example, the approximation error of the kth constituent filter can be written as

$$\varepsilon_k(e^{j\omega}) = G_k(e^{j\omega}) - \tilde{G}_k(e^{j\omega}) \tag{3.52}$$

Then, the resulting design error in the overall frequency response is given by

$$\varepsilon(e^{j\omega}) = H(e^{j\omega}) - \tilde{H}(e^{j\omega}) = \sum_{k=0}^{L-1} F_k(e^{j\omega})\varepsilon_k(e^{j\omega}) \tag{3.53}$$

It is known that in the mini-max design of a low-pass filter using the PM method, the maximum error is a function of the product of the filter length N and the transition bandwidth $\Delta\omega$. In the GP-based design, considering the fact that the filter length of constituent filters is reduced by a factor of L while their transition bandwidth expanded L times in comparison with the original direct-form filter, we infer that the maximum design error of the constituent filters should be comparable to that of the original large-tap filter provided that the mini-max design error criterion is employed for the constituent filters as we have done. The frequency specifications of the constituent filters have a smaller abrupt drop in the transition band in contrast to a regular low-pass or high-pass filter, which drops from one to zero. Taking this into account, we may estimate the peak error of the kth constituent filter by

$$\varepsilon_k \approx \left|\tilde{G}_k(\omega_p) - \tilde{G}_k(\omega_s)\right|\varepsilon_{dir} = \tilde{G}_k(\omega_p)\varepsilon_{dir} \tag{3.54}$$

where ε_{dir} is the maximum error from the mini-max design of the original direct-form filter. Using (3.54) in (3.53), we can obtain

$$\begin{aligned}\left|\varepsilon(e^{j\omega})\right| &\approx \left|\sum_{k=0}^{L-1} F_k(e^{j\omega})\varepsilon_k\right| \le \sum_{k=0}^{L-1}\left|F_k(e^{j\omega})\varepsilon_k\right| \approx \sum_{k=0}^{L-1}\left|F_k(e^{j\omega})\tilde{G}_k(\omega_p)\right|\varepsilon_{dir} \\ &= \tfrac{1}{L}\left|\mathbf{w}^T(e^{j\omega})\mathbf{PQ}\mathbf{w}(e^{j\omega_p})\right|\varepsilon_{dir} \le \tfrac{1}{L}\|\mathbf{w}\|_2\left\|\mathbf{w}(\omega_p)\right\|_2\varepsilon_{dir} = \varepsilon_{dir}\end{aligned} \tag{3.55}$$

where $\mathbf{w}(e^{j\omega}) = [1 \quad e^{-j\omega} \quad \cdots \quad e^{-j(L-1)\omega}]^T$. The above equation indicates that the maximum error of the GP-based design is not greater than that of a direct mini-max design method. Although (3.54) and (3.55) are not strictly-proven error bounds, we have found that they give a pretty accurate estimation result. Table 3.3 lists the peak errors estimated using (3.54) for the constituent filters in *Examples 3.1-3.3* along with those from the actual SDP design of each filter. It is seen that they are quite consistent.

Table 3.3: Comparison of the estimated and actual design errors of the designed constituent filters

		Estimated peak error	Actual design error
Example 3.1	ε_0	0.0165	0.0155
	ε_1	0.0084	0.0084
Example 3.2	ε_0	0.0137	0.0168
	ε_1	0.0136	0.0125
	ε_2	0.0012	0.0015
	ε_3	0.0077	0.0087
Example 3.3	ε_0	0.0048	0.0046
	ε_1	0.0144	0.0178
	ε_2	0.0508	0.0491
	ε_3	0.1226	0.1171
	ε_4	0.0501	0.0485
	ε_5	0.0117	0.0146

3.6.3 Image Interpolation using 5th-Band Filter

Images and video sequences often have to be scaled to different resolutions for various purposes. The resolution of a digital image is determined by the number of pixels and naturally, image interpolation can be employed to increase the resolution/size of an image. We now use the 5th-band interpolation filter designed by the proposed GP-based method to resize a test image. A 15-tap fifth-band interpolation filter is designed. The passband and the stopband cutoff frequencies are $\omega_p = 0.15\pi$ and $\omega_s = 0.25\pi$, respectively. The impulse and frequency responses of the designed filters are depicted in Fig. 3.8, which obviously meets the requirement of the 5th-band filter in both time and frequency domains.

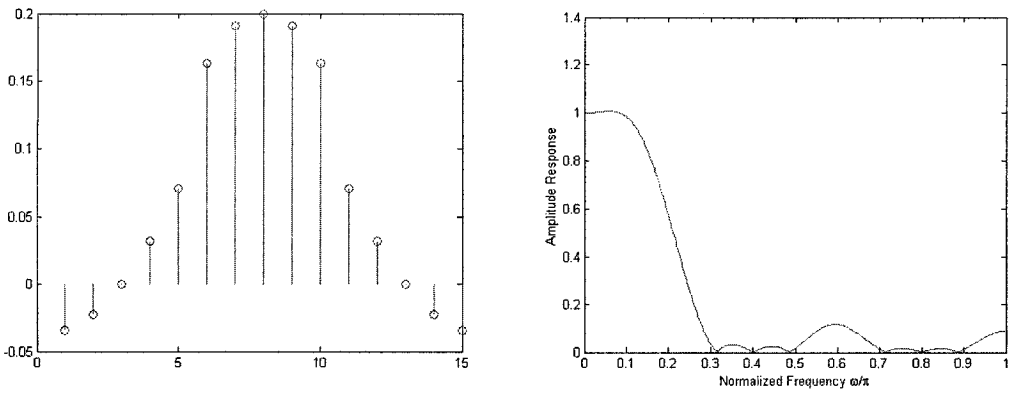

(a) (b)

Figure 3.8: 5th-band interpolation filter. (a) Impulse response. (b) Frequency response.

The images are taken at two resolutions, one at 480-by-640 (image1) and the other at 1200-by-1600 (image 2). Image 1 that has a lower resolution is interpolated to generate an image with a higher resolution. Image 2 can be regarded as the original image to judge the quality of the interpolated image. Image 1 is upsampled by a factor of 5, followed by the designed fifth-band filter and then downsampled by 2. The sampling ratio is then 5/2,

giving the resized image a resolution of 1200-by-1600. The interpolated image is depicted in Fig. 3.9 and the difference of the interpolated image and the original image 2 is shown in Fig. 3.10, which clearly shows a high interpolation quality.

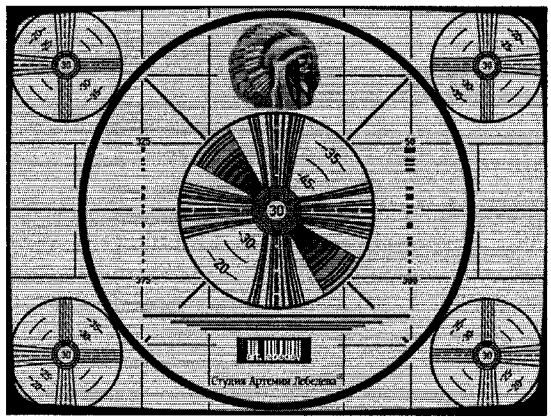

Figure 3.9: Interpolation result of a test image

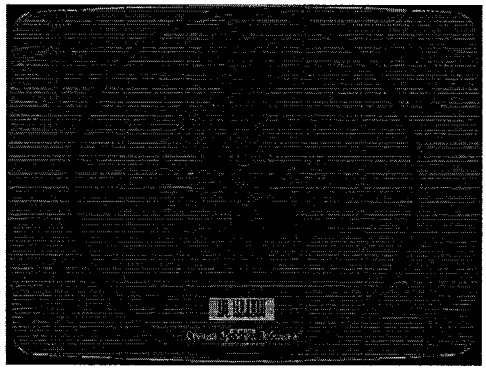

Figure 3.10: Difference of the interpolated image 1 and image 2

To demonstrate the effect of the designed Mth-band filter on image interpolation, the test image is also interpolated via the cubic spline method [100] and the Mth-band filter designed using the eigenfilter approach [17]. With image 2 as the reference image, the peak signal-to-noise ratios (PSNR) of the three interpolated images achieved through cubic spline method, Mth-band filter designed by eigenfilter approach and Mth-band filter designed by GP-based approach, are 29.28dB, 31.16dB and 31.16dB, respectively.

Obviously, the proposed interpolation approach outperforms the cubic spline method. Although the proposed GP-based interpolation gives a PSNR similar to that achieved by the eigenfilter method, the former performs better in visual quality. The detailed difference between the two images is amplified by 8 times in Fig. 3.11. It is seen that our filter yields a much more clear edge whereas the eigenfilter method suffers from ringing artifacts at the vicinity of major edges.

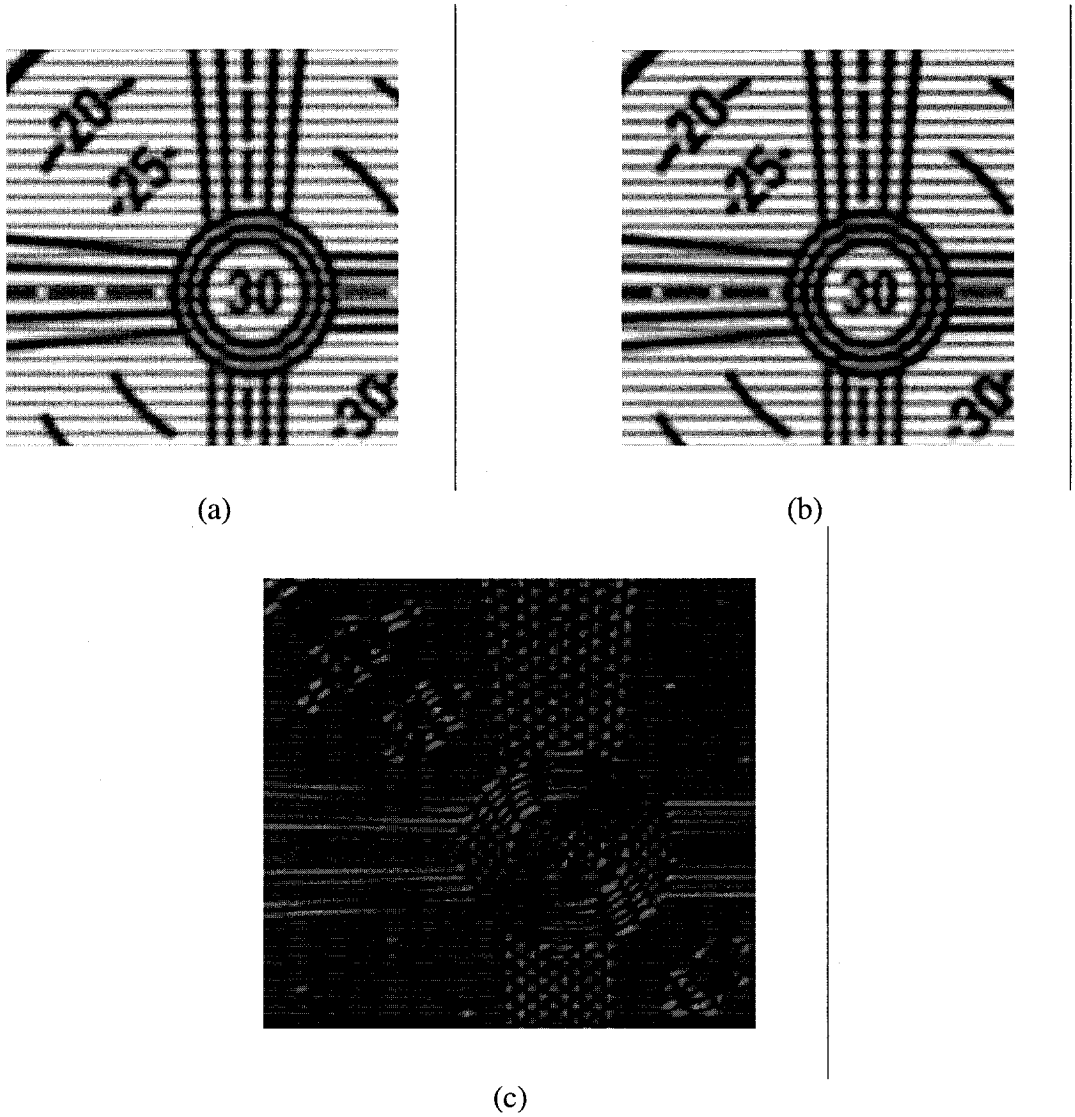

(a) (b)

(c)

Figure 3.11: Details of the interpolated images. (a) Eigenfilter approach. (b) GP-based method. (c) Difference of (a) and (b).

3.7 Conclusions

A GP structure-based method for the design of linear-phase Mth-band FIR filters satisfying the time-domain interpolation condition has been presented. Some new transform matrices have been developed as an extension of the commonly-used Hadamard matrix, allowing for the use of arbitrary number of branches in the GP structure. Closed-form frequency specifications for constituent filters in the GP realization have been obtained, making an independent and fast design of short-length constituent filters possible. The proposed GP-based method has also been extended for the design of a class of interpolation filters with certain regularities. Using the SDP optimization technique, the proposed method has been validated through various design examples and compared with a direct mini-max design of the original large-tap FIR filter as well as the eigenfilter approach. It has been shown that the GP-based design yields an approximation error similar to that obtained from a direct design of the overall filter by the same optimization algorithm, while reducing the computational time to a considerable degree. The designed 5th-band filter has been applied to the interpolation of a test image and compared to the cubic spline interpolation method as well as the 5th-band filter designed via the eigenfilter approach. Our simulation has shown that the proposed GP-based Mth-band filter gives the best interpolation result in terms of the PSNR and the visual quality.

Chapter 4

Design and Realization of 2-D Linear-Phase FIR Filters based on Generalized Polyphase Structure

4.1 Introduction

In the proposed GP-based design technique, the overall filter is decomposed into several constituent filters which can be designed separately. Since the design of short length constituent filters is in general easier than that of the large-length original filter, we would like to extend this method to the case of designing 2-D filters in which the computational complexity is a more critical issue. With the basic ideas such as sampling and polyphase decomposition that are well established in the multidimensional multirate systems [5], we will develop in this chapter the GP structures for 2-D FIR filters and extend the GP-based design method for 2-D Mth-band filters. Most of the material developed in Chapter 3, including the transform matrix and the closed-form expressions for constituent filters, can be extended for the 2-D case. We will also investigate a joint GP and SVD (singular-value decomposition) realization structure for 2-D Mth-band filters.

4.2 Design of 2-D *M*th-band Filters based on GP Structure

In this section, we extend the 1-D GP structure for the design of 2-D FIR filters. Similar to the 1-D filter design discussed in Chapter 3, our objective here is to obtain closed-form frequency specifications for 2-D constituent filters. For the sake of notational simplicity in specifying a 2-D passband, our discussion is focused on a class of 2-D filters, namely, *M*th-band FIR filters.

4.2.1 2-D Generalized Polyphase Structure

A 2-D FIR filter whose impulse response is given by $h[\mathbf{n}]$, where $\mathbf{n} = [n_1 \quad n_2]^T$, has a *Z*-transform of the form

$$H(\mathbf{z}) = \sum_{\mathbf{n} \in \mathcal{N}} h[\mathbf{n}] \mathbf{z}^{(-\mathbf{n})} \tag{4.1}$$

where $\mathbf{z} = [z_1 \quad z_2]^T$, $\mathbf{z}^{(\mathbf{n})} = z_1^{n_1} z_2^{n_2}$, and $\mathcal{N}$denotes a set of two-dimensional integer vectors within the support region of the filter. Unlike 1-D signal sampling, the theory behind sampling of a 2-D signal is fundamentally more complicated because of many different ways to choose the sampling geometry. While the sampling of 1-D sign can be fully determined by a scalar *M*, the sampling of 2-D signal is based on a 2-by-2 sampling matrix **M**. For example, given the sampling matrix $\mathbf{M} = \begin{bmatrix} 1 & -1 \\ 1 & 2 \end{bmatrix}$, the sampled points would be $\mathbf{t} = \begin{bmatrix} t_0 \\ t_1 \end{bmatrix} = \begin{bmatrix} 1 & -1 \\ 1 & 2 \end{bmatrix} \begin{bmatrix} n_0 \\ n_1 \end{bmatrix}$. The sample locations are given by vector **t**, which are integer linear combinations of the columns of the sampling matrix. The graphical illustration of the above sampling is demonstrated in Fig. 4.1. The original signals are dotted in Fig. 4.1(a) and the downsampled version is marked with red in Fig. 4.1(b).

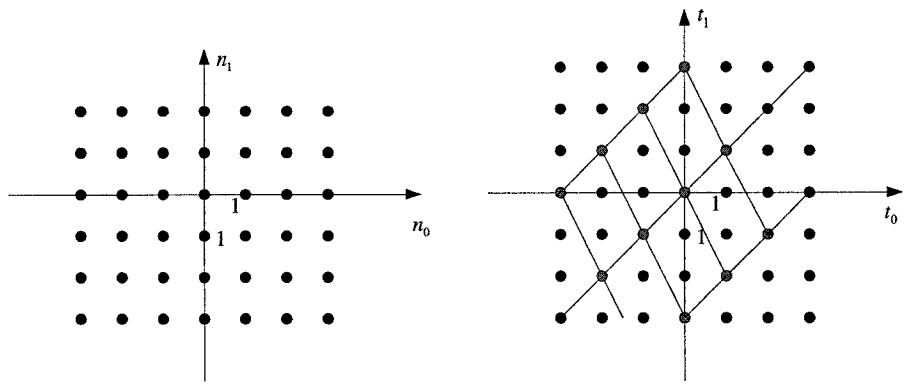

Figure 4.1: The set of sample points. (a) Before sampling. (b) After sampling.

With the introduction of the sample matrix, one can establish all the concepts, such as expander, decimator and polyphase structure, for the 2-D signals. By using a 2×2 nonsingular sampling matrix of integers, $\mathbf{M}=\begin{bmatrix}\alpha_1 & \alpha_2\\ \alpha_3 & \alpha_4\end{bmatrix}$, one can get a polyphase realization of 2-D filters as [5],

$$H(\mathbf{z})=\sum_{\mathbf{k}\in\mathcal{N}(\mathbf{M}^T)} H_{\mathbf{k}}\left(z_1^{\alpha_1}z_2^{\alpha_3}, z_1^{\alpha_2}z_2^{\alpha_4}\right)\mathbf{z}^{(-\mathbf{k})} \tag{4.2}$$

where $\mathbf{k}=[k_1 \quad k_2]^T$ and $\mathcal{N}(\mathbf{M}^T)$ is the set of all integer vectors in the parallelogram area generated by $\mathbf{M}^T\mathbf{x}$, as seen in Fig 4.1(b), with $\mathbf{x}\in[0,1)^2$. The number of integer vectors in $\mathcal{N}(\mathbf{M}^T)$, namely, the number of subfilters, is determined by $L=|\det(\mathbf{M})|$.

Based on (4.2), the L-branch GP structure of a 2-D filter can be constructed as

$$H(\mathbf{z})=\left[\mathbf{z}^{(-\mathbf{k}_0)} \quad \mathbf{z}^{(-\mathbf{k}_1)} \quad \cdots \quad \mathbf{z}^{(-\mathbf{k}_{L-1})}\right]\mathbf{PQ}\begin{bmatrix} H_{\mathbf{k}_0}(z_1^{\alpha_1}z_2^{\alpha_3}, z_1^{\alpha_2}z_2^{\alpha_4}) \\ H_{\mathbf{k}_1}(z_1^{\alpha_1}z_2^{\alpha_3}, z_1^{\alpha_2}z_2^{\alpha_4}) \\ \vdots \\ H_{\mathbf{k}_{L-1}}(z_1^{\alpha_1}z_2^{\alpha_3}, z_1^{\alpha_2}z_2^{\alpha_4}) \end{bmatrix}$$

$$= \sum_{k=0}^{L-1} F_k(\mathbf{z}) G_k(z_1^{\alpha_1} z_2^{\alpha_3}, z_1^{\alpha_2} z_2^{\alpha_4}) \tag{4.3}$$

where

$$F_k(\mathbf{z}) = \sum_{l=0}^{L-1} P(l,k)\mathbf{z}^{(-\mathbf{k}_l)}$$

represents the 2-D interpolators and

$$G_k(z_1^{\alpha_1} z_2^{\alpha_3}, z_1^{\alpha_2} z_2^{\alpha_4}) = \sum_{l=0}^{L-1} Q(k,l) H_{\mathbf{k}_l}(z_1^{\alpha_1} z_2^{\alpha_3}, z_1^{\alpha_2} z_2^{\alpha_4})$$

the 2-D constituent filters. In particular, when $\mathbf{M}$ is a diagonal matrix, the interpolators are separable and (4.3) can be simplified as

$$\begin{aligned} H(z_1, z_2) &= \begin{bmatrix} 1 & z_1^{-1} & \cdots & z_1^{-(\alpha_1-1)} \end{bmatrix} \mathbf{P}_1 \mathbf{Q}_1 \mathbf{H}(z_1^{\alpha_1}, z_2^{\alpha_4}) \mathbf{Q}_2 \mathbf{P}_2 \begin{bmatrix} 1 \\ z_2^{-1} \\ \vdots \\ z_2^{-(\alpha_4-1)} \end{bmatrix} \\ &= \sum_{k=0}^{\alpha_1-1} \sum_{l=0}^{\alpha_4-1} F_{1,k}(z_1) G_{kl}(z_1^{\alpha_1}, z_2^{\alpha_4}) F_{2,k}(z_2) \end{aligned} \tag{4.4}$$

In what follows, we focus on the design of 2-D *M*th-band filters based on the GP structure given by (4.3).

4.2.2 Frequency Specification for 2-D *M*th-band Filters

With the realization of 2-D GP structure, we need to get the frequency specification for each constituent filter such that it can be designed separately. The passband region of a 2-D *M*th-band filter can be specified by a symmetric parallelogram $SPD(\pi\mathbf{M}^{-T})$, generated by $\pi\mathbf{M}^{-T}\mathbf{x}$, with $\mathbf{x} \in [-1,1)^2$ and $|\det(\mathbf{M})| = M$. In order to get a closed-form frequency specification, we define a set of 2-D functions

$$E_k(e^{j\boldsymbol{\omega}}) = \sum_{l=0}^{M-1} Q(l,k) e^{j\mathbf{k}_l^T \boldsymbol{\omega}} \qquad (k = 0,1,\cdots,M-1) \tag{4.5}$$

where $\boldsymbol{\omega} = [\omega_1 \quad \omega_2]^T$. Letting

$$\mathbf{e}(\boldsymbol{\omega}) = \left[E_0(e^{j\boldsymbol{\omega}}) \quad E_1(e^{j\boldsymbol{\omega}}) \quad E_2(e^{j\boldsymbol{\omega}}) \quad \cdots \quad E_{M-1}(e^{j\boldsymbol{\omega}})\right]^T$$

$$\mathbf{f}(\boldsymbol{\omega}) = \left[F_0(e^{j\boldsymbol{\omega}}) \quad F_1(e^{j\boldsymbol{\omega}}) \quad F_2(e^{j\boldsymbol{\omega}}) \quad \cdots \quad F_{M-1}(e^{j\boldsymbol{\omega}})\right]^T$$

it can be shown that

$$\mathbf{f}^T(\boldsymbol{\omega})\mathbf{e}(\boldsymbol{\omega} - 2\pi\mathbf{M}^{-T}\mathbf{n}) = \sum_{\mathbf{k}\in\mathcal{N}(\mathbf{M}^T)} \exp\left(j2\pi\mathbf{k}^T\mathbf{M}^{-T}\mathbf{n}\right) = M\delta(\mathbf{n}) \tag{4.6}$$

Assume that the constituent filters have the following frequency response

$$\tilde{G}_k(e^{j\boldsymbol{\omega}}) = \frac{1}{M} E_k(e^{j\mathbf{M}^{-T}\boldsymbol{\omega}}) \tag{4.7}$$

Substitution of (4.7) into (4.4) and the use of (4.6) lead to the corresponding overall frequency response given by

$$\begin{aligned}
\tilde{H}(e^{j\boldsymbol{\omega}}) &= \tilde{G}_k(e^{j\mathbf{M}^T\boldsymbol{\omega}}) F_k(e^{j\boldsymbol{\omega}}) \\
&= \begin{cases}
\displaystyle\sum_{k=0}^{M-1} E_k(e^{j\boldsymbol{\omega}}) F_k(e^{j\boldsymbol{\omega}}) = 1, & \boldsymbol{\omega} \in SPD(\pi\mathbf{M}^{-T}) \\
\displaystyle\sum_{k=0}^{M-1} E_k(e^{j(\boldsymbol{\omega}-2\pi\mathbf{M}^{-T}\mathbf{n}_1)}) F_k(e^{j\boldsymbol{\omega}}) = 0, & \boldsymbol{\omega} \in SPD(\pi\mathbf{M}^{-T}) + 2\pi\mathbf{M}^{-T}\mathbf{n}_1 \\
\vdots & \vdots \\
\displaystyle\sum_{k=0}^{M-1} E_k(e^{j(\boldsymbol{\omega}-2\pi\mathbf{M}^{-T}\mathbf{n}_{M-1})}) F_k(e^{j\boldsymbol{\omega}}) = 0, & \boldsymbol{\omega} \in SPD(\pi\mathbf{M}^{-T}) + 2\pi\mathbf{M}^{-T}\mathbf{n}_{M-1}
\end{cases} \\
&= \begin{cases}
1, & \boldsymbol{\omega} \in SPD(\pi\mathbf{M}^{-T}) \\
0, & \text{elsewhere}
\end{cases}
\end{aligned} \tag{4.8}$$

Since (4.8) is the desired frequency response of a 2-D *M*th-band filter, we conclude that (4.7) gives the frequency specification of 2-D constituent filters exactly. As such, the design problem of *M*th-band 2-D filters is now converted to that of a number of lower-order 2-D constituent filters.

Example 4.1:

Consider a 16×16 2-D diamond filter with a transition bandwidth of 0.1π. Note that this filter can be obtained from a 2-D half-band filter with a sampling matrix $\mathbf{M} = \begin{bmatrix} 1 & -1 \\ 1 & 1 \end{bmatrix}$. The amplitude response of the 2-D filter can be written in the GP form as

$$H(\omega_1,\omega_2) = 2\cos(\omega_1/2)G_0(\omega_1+\omega_2,-\omega_1+\omega_2) - 2\sin(\omega_1/2)G_1(\omega_1+\omega_2,-\omega_1+\omega_2) \qquad (4.9)$$

From (4.7), we obtain the amplitude specifications for the two constituent filters as

$$\tilde{G}_0(e^{j\omega}) = \cos[(\omega_1-\omega_2)/4]/2 \qquad (4.10a)$$

$$\tilde{G}_1(e^{j\omega}) = -\sin[(\omega_1-\omega_2)/4]/2 \qquad (4.10b)$$

Using (4.10) and the SDP optimization technique, the two constituent filters are designed, giving their amplitude responses, as shown in Fig. 4.2(a) and 4.2(b). The resulting amplitude response of the designed diamond filter is depicted in Fig. 4.2(c). The maximum approximation errors produced by the SDP for $G_0(e^{j\omega})$ and $G_1(e^{j\omega})$ are 0.017 and 0.013, respectively, which yield a maximum design error of 0.023 for the overall diamond filter. We have also designed the diamond filter directly by the SDP optimization and have found that the maximum error in the passband is 0.021 and that in the stopband is 0.017. It is also found that the execution times for designing the two constituent filters are 7.9689 and 8.3439 seconds, respectively, whereas that for direct design of the overall filter is 26.0469 seconds, implying a nearly 40% reduction in computational time is achieved by using the proposed method. Note that this computational saving is more appealing as the size of the filter and the number of branches in the GP structure increase.

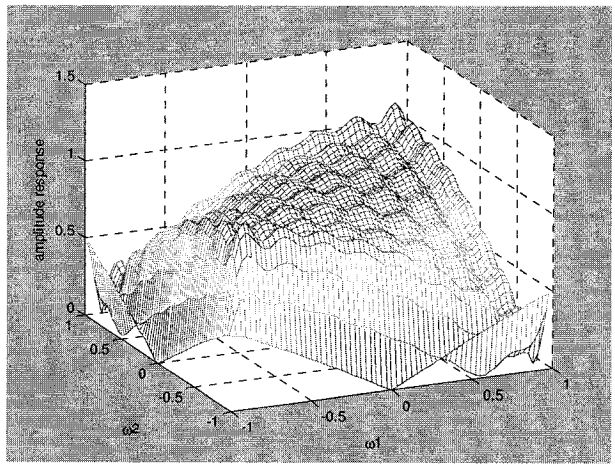

(a)

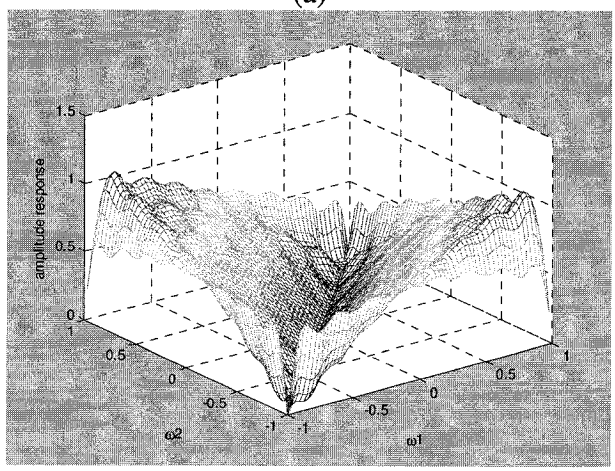

(b)

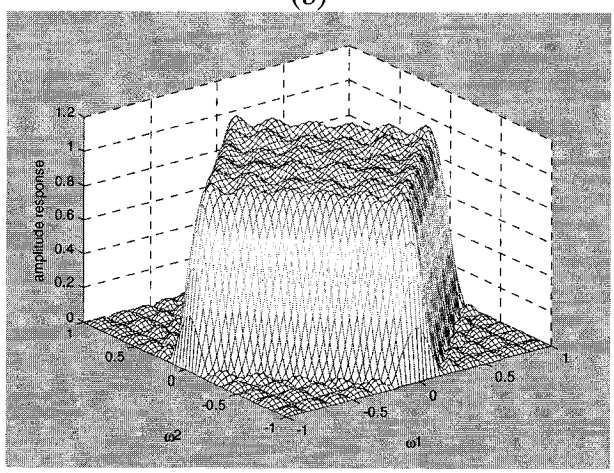

(c)

Figure 4.2: Frequency response of the 2-D diamond filter in *Example 4.1*.
(a) $G_0(\boldsymbol{\omega})$, (b) $G_1(\boldsymbol{\omega})$, and (c) $H(\boldsymbol{\omega})$.

4.3 Realization of GP Structure combined with SVD

For the design and implementation of 2-D filters, a parallel structure using the singular-value decomposition (SVD) has attracted a great deal of research attention [24], [27]. By applying the SVD to the impulse response matrix in the time-domain or the frequency response matrix in the frequency-domain for the design problem, a 2-D filter is decomposed into a set of 1-D filters. The SVD-based approaches have many advantages. One of them is to exploit the energy compaction of the SVD and utilize only a few branches corresponding to the largest singular values, yielding a significantly simplified SVD realization. Generally, a filter is frequency-selective. However, this property is not exploited in the SVD simplification. Recall that in the GP structure, if the interpolators are frequency-selective, each branch would have a limited subband frequency contribution to the overall filter. In this section, a new GP structure using SVD is proposed for 2-D filter realization [103]. In the new structure, the 2-D constituent filters in the GP structure are further decomposed via the SVD. The proposed structure prevails in the following aspects:

1. The various symmetry properties normally available in a 2-D impulse-response matrix can be exploited and elegantly realized in the corresponding 1-D constituent filters by using the SVD. This symmetry can be used to save computing storage and arithmetic operations for filter coefficients and succeeding processing.
2. The GP structure forms a frequency-selective subband for each constituent filter. This feature can be well combined with the energy compaction property of the SVD so as to further reduce the number of branches in the SVD realization.

4.3.1 2-D Separable GP Structure with SVD

Consider a 2-D impulse response $h(m,n)$ of size $M \times N$ with its z-transform $H(z_1, z_2)$. In order to obtain a separable GP structure, let the sampling matrix be given by $\mathbf{M} = \begin{bmatrix} K & 0 \\ 0 & L \end{bmatrix}$, where both K and L are positive integers. Assuming M to be a multiple of K and N a multiple of L, then separable interpolators are obtained, and (4.3) can be simplified as

$$\begin{aligned} H(z_1, z_2) &= \begin{bmatrix} 1 & z_1^{-1} & \cdots & z_1^{-(K-1)} \end{bmatrix} \mathbf{P}_1 \mathbf{Q}_1 \mathbf{H}(z_1^K, z_2^L) \mathbf{Q}_2 \mathbf{P}_2 \begin{bmatrix} 1 \\ z_2^{-1} \\ \vdots \\ z_2^{-(L-1)} \end{bmatrix} \\ &= \sum_{k=0}^{K-1} \sum_{l=0}^{L-1} E_k(z_1) G_{kl}(z_1^K, z_2^L) F_l(z_2) \end{aligned} \tag{4.11}$$

where $\mathbf{H}(z_1^K, z_2^L)$ is a rectangular matrix with elements of 2-D subfilters,

$$\mathbf{H}(z_1^K, z_2^L) = \begin{bmatrix} H_{00}(z_1^K, z_2^L) & \cdots & H_{0(L-1)}(z_1^K, z_2^L) \\ \vdots & \ddots & \vdots \\ H_{(K-1)0}(z_1^K, z_2^L) & \cdots & H_{(K-1)(L-1)}(z_1^K, z_2^L) \end{bmatrix} \tag{4.12}$$

The pre- and post- interpolators and the constituent filters, $E_k(z_1)$, $F_l(z_2)$ and $G_{kl}(z_1^K, z_2^L)$, are given by

$$E_k(z_1) = \sum_{i=0}^{K-1} P_1(i,k) z_1^{-i}, \quad F_l(z_2) = \sum_{j=0}^{L-1} P_2(l,j) z_2^{-j} \tag{4.13a}$$

$$G_{kl}(z_1^K, z_2^L) = \sum_{i=0}^{K-1} \sum_{j=0}^{L-1} Q_1(k,i) H_{ij}(z_1^K, z_2^L) Q_2(j,l) \tag{4.13b}$$

With the transform matrices $\{\mathbf{P}_i, \mathbf{Q}_i\}$ $(i = 1,2)$ being two pairs of inverse matrices, the delay chains corresponding to z_1 and z_2 are then transformed into the column and row

interpolators, denoted as $E_k(z_1)$ and $F_l(z_2)$ in the above, respectively. The original 2-D filter is then divided into KL 2-D constituent filters $G_{kl}(z_1^K, z_2^L)$ of size $(M/K)\times(N/L)$. From (4.11), it is easy to verify that if the original 2-D filter is of linear-phase and the column vectors of the transform matrices $\mathbf{P}_1$ and $\mathbf{P}_2$ are symmetric or antisymmetric, then the corresponding 2-D constituent filters are also of linear-phase.

Performing the SVD on $G_{kl}(z_1, z_2)$ and up-sampling z_1 by K and z_2 by L, we obtain

$$G_{kl}(z_1^K, z_2^L) = \sum_{i=0}^{r-1} \Phi_{kl}^i(z_1^K)\left(\Psi_{kl}^i(z_2^L)\right)^* \tag{4.14}$$

where $\Phi_{kl}^i(z_1^K)$ and $\Psi_{kl}^i(z_2^L)$ are the column vectors of the corresponding unitary matrices. Using (4.14) into (4.11) yields a new realization structure for the overall 2-D filter, namely,

$$H(z_1, z_2) = \sum_{k=0}^{K-1}\sum_{l=0}^{L-1}\sum_{i=0}^{r-1} E_k(z_1)\Phi_{kl}^i(z_1^K)\left(\Psi_{kl}^i(z_2^L)\right)^* F_l(z_2) \tag{4.15}$$

The proposed realization structure is depicted in Fig.4.3 in which a 2-D filter is eventually implemented with a set of 1-D filters. Some advantages can be observed from the proposed realization structure. First, the computational complexity of the SVD implementation of the lower-order constituent filters is much lower than that of the original high-order 2-D filter. Accordingly, the overall computational cost can be reduced by performing the SVD on each constituent filter in the 2-D GP structure. Second, as will be shown, the linear-phase and other symmetry properties of 2-D FIR filters can be well retained in the 2-D constituent filters. Third, with the frequency-selective property of the interpolators in the GP structure and the energy compaction feature of the SVD, more 1-

D subfilters/branches can be discarded without causing a large error in comparison with a direct SVD realization of the original FIR filter.

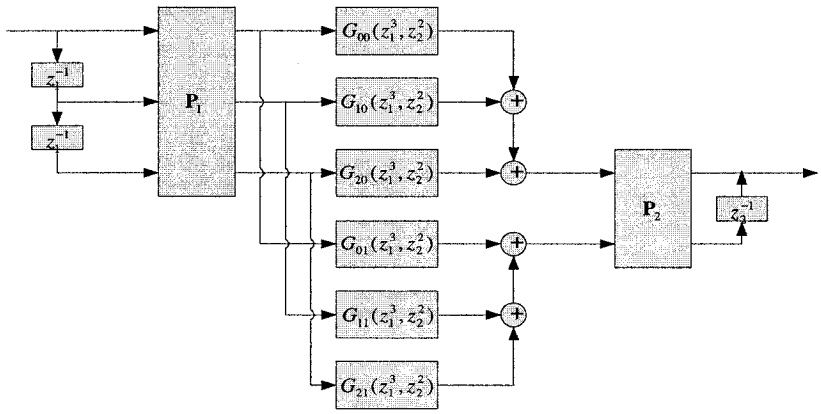

Figure 4.3: A 3×2 GP structure of 2-D filters combined with SVD

In [25], some SVD expressions for the impulse response matrix of 2-D linear-phase filters have been obtained by exploiting various symmetry properties and appropriate matrix transforms. Those SVDs are capable of producing 1-D linear-phase subfilters with similar symmetries. By applying the matrix transforms proposed in [25] to the 2-D constituent filters in the GP structure, one can easily verify that the linear-phase and symmetry features of the original 2-D FIR filter are well preserved in the resulting 1-D subfilters in the proposed GP-SVD realization.

4.3.2 Design Examples

A few examples are presented in this section to demonstrate the performance of the proposed realization technique. The 2-D filters to be realized are designed by the least-squares design method [10]. The designed filters are then realized with the proposed GP-SVD structure, each containing a number of branches. The insignificant branches are neglected, which will significantly reduce the implementation cost while causing only a

small approximation error. The maximum error resulting from the omission of those sections will be computed and compared with the direct SVD with the same realization cost.

Example 4.2: A Quadrantally Symmetric Fan-Shaped Filter:

A 16×16 quadrantally symmetric fan-shaped filter is designed. The magnitude specification is depicted in Fig.4.4, with 1 indicating the passband and 0 the stopband. A 2×2 GP decomposition is carried out based on the Hadamard matrix given by

$$\mathbf{R}_2 = \begin{bmatrix} 1 & 1 \\ 1 & -1 \end{bmatrix} \text{ and } \mathbf{R}_2^{-1} = \frac{1}{2}\begin{bmatrix} 1 & 1 \\ 1 & -1 \end{bmatrix} \tag{4.16}$$

With (4.11) and (4.16), we can get the 2-D constituent filters as

$$\begin{cases} g_{11}[m,n] = h[2m,2n] + h[2m,2n+1] + h[2m+1,2n] + h[2m+1,2n+1] \\ g_{12}[m,n] = h[2m,2n] - h[2m,2n+1] + h[2m+1,2n] - h[2m+1,2n+1] \\ g_{21}[m,n] = h[2m,2n] + h[2m,2n+1] - h[2m+1,2n] - h[2m+1,2n+1] \\ g_{22}[m,n] = h[2m,2n] - h[2m,2n+1] - h[2m+1,2n] + h[2m+1,2n+1] \end{cases} \tag{4.17}$$

Since the filter to be designed is of quadrantal symmetry, its impulse response must have

$$h[m,n] = h[M-1-m,n] = h[m,N-1-n] = h[M-1-m,N-1-n] \tag{4.18}$$

Using (4.18) in (4.17), we can verify that the impulse responses $g_{ij}[m,n]$ possess four types of quadrantal symmetry,

$$\text{Type I: } \mathbf{A} = \begin{bmatrix} \mathbf{A}_1 & \mathbf{A}_1\mathbf{J} \\ \mathbf{J}\mathbf{A}_1 & \mathbf{J}\mathbf{A}_1\mathbf{J} \end{bmatrix}; \qquad \text{Type II: } \mathbf{A} = \begin{bmatrix} \mathbf{A}_1 & -\mathbf{A}_1\mathbf{J} \\ \mathbf{J}\mathbf{A}_1 & -\mathbf{J}\mathbf{A}_1\mathbf{J} \end{bmatrix};$$

$$\text{Type III: } \mathbf{A} = \begin{bmatrix} \mathbf{A}_1 & \mathbf{A}_1\mathbf{J} \\ -\mathbf{J}\mathbf{A}_1 & -\mathbf{J}\mathbf{A}_1\mathbf{J} \end{bmatrix}; \qquad \text{Type IV: } \mathbf{A} = \begin{bmatrix} \mathbf{A}_1 & -\mathbf{A}_1\mathbf{J} \\ -\mathbf{J}\mathbf{A}_1 & \mathbf{J}\mathbf{A}_1\mathbf{J} \end{bmatrix}. \tag{4.19}$$

Next, we show that the quadrantal symmetry can be elegantly realized with the SVD. Since all the four types of symmetry are closely related, we only investigate Type I

symmetry. In this case, the symmetric matrix $\mathbf{A}$ in (4.19) is similar to $\mathbf{B}$ through an orthogonal matrix $\mathbf{Q}$,

$$\mathbf{B} = \mathbf{Q}^T \mathbf{A} \mathbf{Q} = \begin{bmatrix} 2\mathbf{A}_1 & \mathbf{0} \\ \mathbf{0} & \mathbf{0} \end{bmatrix} \tag{4.20}$$

where

$$\mathbf{Q} = \frac{1}{\sqrt{2}} \begin{bmatrix} \mathbf{I} & \mathbf{I} \\ \mathbf{J} & -\mathbf{J} \end{bmatrix} \tag{4.21}$$

The SVD of $\mathbf{B}$ can be written as

$$\mathbf{B} = \begin{bmatrix} \mathbf{U}_1 & \mathbf{0} \\ \mathbf{0} & \mathbf{U}_2 \end{bmatrix} \begin{bmatrix} \mathbf{S}_1 & \mathbf{0} \\ \mathbf{0} & \mathbf{0} \end{bmatrix} \begin{bmatrix} \mathbf{V}_1^T & \mathbf{0} \\ \mathbf{0} & \mathbf{V}_2^T \end{bmatrix} \tag{4.22}$$

where $\mathbf{U}_1$, $\mathbf{S}_1$ and $\mathbf{V}_1$ constitute an SVD of $2\mathbf{A}_1$, and $\mathbf{U}_2$, $\mathbf{V}_2$ are arbitrary $N/2 \times N/2$ orthogonal matrices. Left-mulitplying by $\mathbf{Q}$ and right-multiplying by $\mathbf{Q}^T$ both sides of (4.22) gives an SVD of $\mathbf{A}$,

$$\mathbf{A} = \frac{1}{2} \begin{bmatrix} \mathbf{U}_1 & \mathbf{U}_2 \\ \mathbf{J}\mathbf{U}_1 & -\mathbf{J}\mathbf{U}_2 \end{bmatrix} \begin{bmatrix} \mathbf{S}_1 & \mathbf{0} \\ \mathbf{0} & \mathbf{0} \end{bmatrix} \begin{bmatrix} \mathbf{V}_1 & \mathbf{V}_2 \\ \mathbf{J}\mathbf{V}_1 & -\mathbf{J}\mathbf{V}_2 \end{bmatrix}^T \tag{4.23}$$

In (4.23), not only the eigenvector is of symmetry, but also one-half of the eigenvalues are automatically zero, which greatly simplifies the realization cost. In order to show the efficiency of the proposed structure, the realization errors caused by neglecting the smallest branches are compared with that of a direct SVD decomposition of the original 2-D filter. The comparison is made at the same computational complexity, i.e., the two versions of SVD realization have the same number of 1-D filter coefficients. For example, if one branch is dropped in the direct SVD structure, then two branches are omitted in the proposed structure in order to keep the same complexity of the 1-D subfilters. The maximum errors in the amplitude frequency response with respect to

different numbers of branches used in the structure are listed in Table 4.1. As the designed filter has a quadrantal symmetry, there is only a total of 8 non-zero singular values. The frequency responses for the two realization structures are depicted in Fig. 4.5(a) and (b), respectively, where 4 branches are used in each realization.

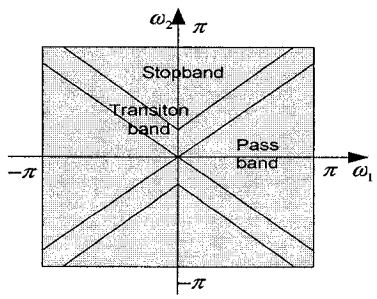

Figure 4.4: Design specification for the quadrantally symmetric fan filter in *Example 4.2.*

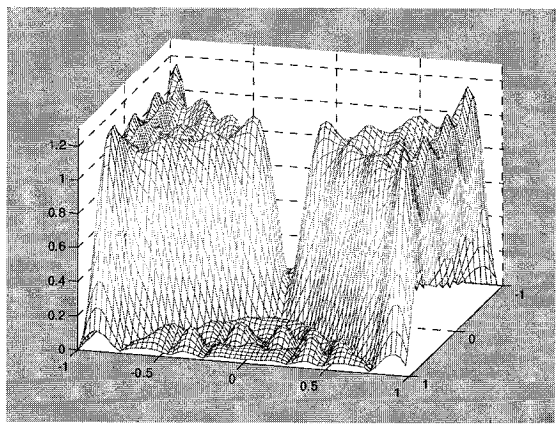

(a)

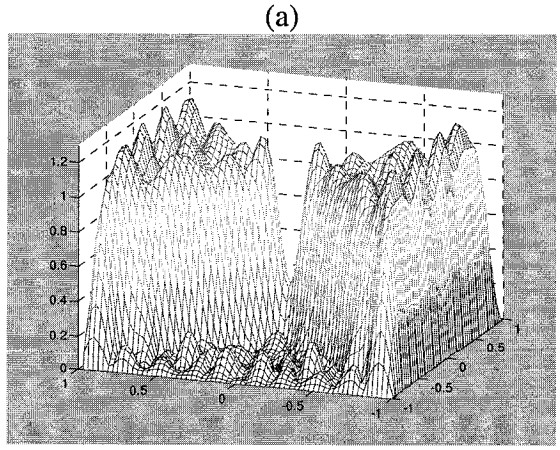

(b)

Figure 4.5: Frequency response of the quadrantally symmetric fan filter designed in *Example 4.2.* (a) Realized by GP structure combined with SVD of four branches. (b) Realized with a direct SVD of four branches.

Table 4.1. Maximum amplitude errors of the two realizations in *Example 4.2*

Number of Branches Used	Proposed GP-SVD Structure	Direct SVD Implementation
4	0.2190	0.2433
5	0.1638	0.1527
6	0.1027	0.1168
7	0.0580	0.0833

Example 4.3: A Centro-Symmetric Fan-Shaped Filter

A 15×15 centro-symmetric fan filter is designed, with the frequency specification depicted in Fig.4.6. This fan filter is decomposed into a 3×3 GP structure with the following transform matrix

$$\mathbf{R}_3 = \begin{bmatrix} 1 & 1 & 1 \\ 1 & 0 & -1 \\ 1 & -1 & 1 \end{bmatrix} \text{ with } \mathbf{R}_3^{-1} = \frac{1}{4}\begin{bmatrix} 1 & 2 & 1 \\ 2 & 0 & -2 \\ 1 & -2 & 1 \end{bmatrix} \tag{4.24}$$

For a centro-symmetric filter, its impulse response satisfies

$$h[m,n] = h[M-1-m, N-1-n] \tag{4.25}$$

The symmetry condition in (4.25) leads to the following relationship for the components in the polyphase structure,

$$\begin{aligned} h_{ij}[m,n] &= h[3m+i, 3n+j] \\ &= h[M-1-i-3m, N-1-j-3n] = h_{(4-i)(4-j)}[K-1-m, L-1-n] \end{aligned} \tag{4.26}$$

Using (4.26) along with the transform matrix in (4.24), it is easy to see that the constituent filters $g_{ij}[m,n]$ also have a centro-symmetry, namely,

$$\mathbf{A} = \begin{bmatrix} \mathbf{A}_1 & \mathbf{J}\mathbf{A}_2\mathbf{J} \\ \mathbf{A}_2 & \mathbf{J}\mathbf{A}_1\mathbf{J} \end{bmatrix} \tag{4.27}$$

By using the orthogonal matrix $\mathbf{Q}$ in (4.21), the matrix $\mathbf{B}$ can be expressed as

$$\mathbf{B} = \mathbf{Q}^T \mathbf{A} \mathbf{Q} = \begin{bmatrix} \mathbf{A}_1 + \mathbf{J}\mathbf{A}_2 & \mathbf{0} \\ \mathbf{0} & \mathbf{A}_1 - \mathbf{J}\mathbf{A}_2 \end{bmatrix} \tag{4.28}$$

Assuming that the SVD of $\mathbf{B}$ is given by

$$\mathbf{B} = \begin{bmatrix} \mathbf{U}_1 & \mathbf{0} \\ \mathbf{0} & \mathbf{U}_2 \end{bmatrix} \begin{bmatrix} \mathbf{S}_1 & \mathbf{0} \\ \mathbf{0} & \mathbf{S}_2 \end{bmatrix} \begin{bmatrix} \mathbf{V}_1^T & \mathbf{0} \\ \mathbf{0} & \mathbf{V}_2^T \end{bmatrix} \tag{4.29}$$

from (4.28) and (4.29), we obtain the SVD of $\mathbf{A}$,

$$\mathbf{A} = \frac{1}{2} \begin{bmatrix} \mathbf{U}_1 & \mathbf{U}_2 \\ \mathbf{J}\mathbf{U}_1 & -\mathbf{J}\mathbf{U}_2 \end{bmatrix} \begin{bmatrix} \mathbf{S}_1 & \mathbf{0} \\ \mathbf{0} & \mathbf{S}_2 \end{bmatrix} \begin{bmatrix} \mathbf{V}_1 & \mathbf{V}_2 \\ \mathbf{J}\mathbf{V}_1 & -\mathbf{J}\mathbf{V}_2 \end{bmatrix}^T \tag{4.30}$$

Similar to the quadrantally symmetric case, the eigenvectors in the above SVD are either symmetric or anti-symmetric. Also, the centro-symmetry is always guaranteed even if some of the branches are discarded. The maximum amplitude error caused by dropping the insignificant branches in the proposed GP-SVD structure as well as that from a direct SVD realization of the designed 2-D filter are given in Table 4.2. Clearly, compared with a direct SVD implementation with the same computational complexity, the proposed method gives a smaller distortion.

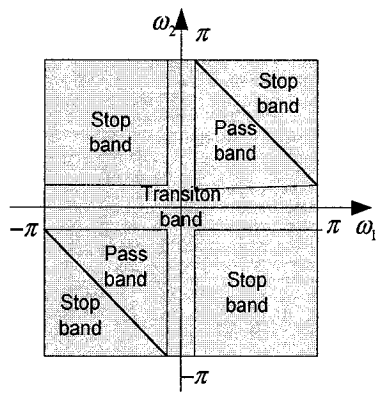

Figure 4.6: Design specification for centro-symmetric fan filter in *Example 4.3*

Table 4.2: Maximum amplitude errors of two realizations in *Example 4.3*

Number of Branches Used	Proposed GP-SVD Structure	Direct SVD Implementation
6	0.1994	0.2318
7	0.1446	0.2264
8	0.1353	0.1736
9	0.1052	0.1515
12	0.0965	0.1381
13	0.0754	0.1008
14	0.0241	0.0691

4.4 Conclusions

In this chapter, a GP structure-based technique has been extended from 1-D to 2-D and used to design 2-D Mth-band FIR filters. Based on the 2×2 sample matrix, a 2-D GP structure is developed. Frequency response specifications for 2-D constituent filters have been derived so that the design problem of a large-size 2-D filter can be simplified as that of a number of short-length 2-D filters. It has been pointed out that the proposed GP-based design is more advantageous when the size of the 2-D filter is large, in which case a direct design of the 2-D impulse response would be much more computationally expensive compared to a small-size 2-D filter. Moreover, a realization technique using the GP structure in conjunction with the SVD has also been proposed for 2-D FIR filters. Owing to the frequency-selective property of the GP decomposition and the energy compaction of the SVD, a high-order 2-D filter can be simplified as a number of short-tap 1-D FIR filters. It has been shown through numerical examples that the proposed GP-SVD structure is superior to the direct SVD realization of a 2-D FIR filter in terms of the maximum approximation error caused by discarding the insignificant parallel branches

for the same number of coefficients of the 1-D constituent filters. It has also been shown that the linear-phase characteristic as well as other symmetry properties that the original 2-D filter has are retained in the resulting 1-D subfilters.

Chapter 5

Perfect Reconstruction Filter Banks with Mirror-Image Symmetry

5.1 Introduction

Filter banks (FBs) provide effective ways to process signals for the purposes of analysis, understanding and compression, and therefore, have been widely used in many fields such as signal processing, communication and control [1]-[3]. A filter bank is said to be *perfect reconstruction* (PR) if $\mathbf{E}(z)\mathbf{R}(z) = \mathbf{I}$. Obviously, perfect reconstruction is a desirable property. As one of the most efficient methods for the design and implementation of PRFBs, lattice factorization has received a great deal of attention over the past two decades [48]-[53]. A lattice structure decomposes $\mathbf{E}(z)$ of a PRFB into a cascade of invertible matrices and delay matrices. This approach provides a fast, efficient, and robust structure for the optimization design as well as implementation of filter banks. A general lattice structure based on order-one factorization is given by

$$\mathbf{E}(z) = \prod_{i=K-1}^{1} (\mathbf{U}_i \mathbf{\Lambda}_i(z)) \mathbf{U}_0 \tag{5.1}$$

where $\mathbf{U}_i$ is an invertible matrix separated by a delay matrix $\mathbf{\Lambda}_k(z) = \mathrm{diag}\left(\mathbf{I}_{M-r_i}, z^{-1}\mathbf{I}_{r_i}\right)$, $(0 \le r_i \le M)$. It is evident that the lattice structure (5.1) gives a PR system, if $\mathbf{R}(z)$ is chosen as

$$\mathbf{R}(z) = [\mathbf{E}(z)]^{-1} = \mathbf{U}_0^{-1} \prod_{i=1}^{K-1} \left(\mathbf{\Lambda}_i(z^{-1})\mathbf{U}_i^{-1}\right) \tag{5.2}$$

As the elements of $\mathbf{\Phi}_i$ can be parameterized and designed by an optimization technique, the lattice structure provides a fast, efficient and robust design and implementation of PRFBs. On the other hand, a tough question remains, namely, is the lattice structure (5.2) complete, or does there always exist a factorization as (5.2) for any given PRFB? The completeness of the lattice structure is a crucial issue in filter bank design and has been intensively studied by many researchers. The lattice structure was first proved to be complete for the PUFBs, in which the invertible matrices $\mathbf{\Phi}_i$ in (5.2) are restricted to be unitary [50], [53].

Although the lattice structure has provided a good solution to the design and implementation problem of PUFBs, it does not work so well for general PRFBs. The difficulty lies in the proof of the completeness. The degree-one factorization has been extended to PRFB, resulting in lattice structures of the biorthogonal lapped transform (BOLT) [51],[52] and the lapped unimodular transform (LUT) [45],[46]. However, the lattice structure for PRFBs is complete for BOLT of order-one only. As such, researchers have turned their attention to a class of PRFBs satisfying certain constraints. For constrained PRFBs, Tran *et al.* [74] have studied the linear-phase perfect reconstruction filter banks (LPPRFBs) as an extension of the famous linear-phase paraunitary filter banks (LPPUFBs). The relaxation of the PU constraint brings more flexibility which can

be exploited for different purposes. Although Tran's structure is not complete [75], it provides an excellent guideline as to how lattice structures for constrained PRFBs are developed. His work triggers a question: is there a complete lattice structure, even though not for general PRFBs, at least for PRFBs with certain constraints?

In this chapter, a class of constrained filter banks is studied. A complete and minimal lattice structure is developed for PRFBs whose analysis filters are mirror-image symmetric. The rest of the chapter is organized as follows. In Section 5.2, the lattice structure of MIS-PUFBs is first briefly reviewed, based on which a simplified structure with fewer parameters is derived. Section 5.3 focuses on the development of a complete lattice structure for even-channel MIS-PRFBs. To this end, a basic invertible order-one building block, which propagates both the PR and mirror-image symmetry properties from a lower-order polyphase matrix to a higher-order one, is developed. It is proved that the lattice structure based on a cascade of such building blocks is complete as well as minimal. In Section 5.4, a lattice structure for odd-channel MIS-PRFBs is developed, where an order-two building block that propagates the PR and MIS properties during the order update of the polyphase matrices of the filter bank, is proposed. Section 5.5 addresses the design problem of MIS-PRFBs, including the parameterization of the lattice structure, the optimization of free parameters and the formulation of the cost function. A few numerical examples are provided to compare the proposed MIS-PRFB with other types of filter banks such as the general PRFB without any constraint, the LPPRFB and the MIS-PUFB. Finally, Section 5.6 gives some of the concluding remarks.

5.2 Lattice Structure of MIS-PUFBs

A filter bank is said to be mirror-image symmetric (MIS), if its analysis filter $H_k(z)$ is symmetric about $\pi/2$ with $H_{M-1-k}(z)$. This symmetry can be described as

$$H_{M-1-k}(z) = z^{-(L-1)} H_k(-z^{-1}),\ (0 \le k \le M-1) \tag{5.3}$$

where M is the number of channels of the filter bank and $L=KM$ is the length of each analysis filter, K being an integer. When M is even, the symmetry constraint in (5.3) can be equivalently written in terms of the polyphase representation as

$$\mathbf{E}(z) = z^{-(K-1)} \mathbf{D}\mathbf{E}(z^{-1})\mathbf{T} \tag{5.4}$$

where

$$\mathbf{D} = \begin{bmatrix} \mathbf{0} & -\mathbf{I}_{M/2} \\ \mathbf{I}_{M/2} & \mathbf{0} \end{bmatrix},\ \mathbf{T} = \begin{bmatrix} \mathbf{0} & -\mathbf{D}_t\mathbf{J}_{M/2} \\ \mathbf{J}_{M/2}\mathbf{D}_t & \mathbf{0} \end{bmatrix},\ \mathbf{D}_t = \begin{bmatrix} 1 & & & \\ & -1 & & \\ & & \ddots & \\ & & & (-1)^{M/2-1} \end{bmatrix}.$$

Note that the order of the analysis filters in (5.4) has been permutated to facilitate the mathematical derivation. The mirror-image symmetry described by (5.4) has been applied to PUFBs in [50], resulting in a lattice structure for the polyphase matrix as given below:

$$\mathbf{E}(z) = \prod_{i=K-1}^{1} \left(\mathbf{\Phi}_i \mathbf{\Lambda}(z)\right) \mathbf{G}_0 \tag{5.5}$$

where

$$\mathbf{\Phi}_i = \begin{bmatrix} \mathbf{U}_i & -\mathbf{V}_i \\ \mathbf{V}_i & \mathbf{U}_i \end{bmatrix},$$

$$\mathbf{\Lambda}(z) = \begin{bmatrix} \mathbf{I}_{M/2} & \mathbf{0} \\ \mathbf{0} & z^{-1}\mathbf{I}_{M/2} \end{bmatrix},$$

$$\mathbf{G}_0 = \begin{bmatrix} \mathbf{U}_0 & -\mathbf{V}_0 \\ \mathbf{V}_0 & \mathbf{U}_0 \end{bmatrix} \begin{bmatrix} \mathbf{I}_{M/2} & \mathbf{0} \\ \mathbf{0} & \Gamma\mathbf{J}_{M/2} \end{bmatrix}.$$

It is interesting to note that the orthogonal matrix $\mathbf{\Phi}_i$ and $\mathbf{G}_0$ contain all the free parameters to be determined, and the delay matrix $\mathbf{\Lambda}(z)$ involves the delay operations only. The lattice structure given by (5.5) has already been proved to be complete and minimal, but it contains redundant parameters. By exploiting Hermitian symmetry of the matrices involved in (5.5), a simplified structure has been obtained in [54], namely,

$$\mathbf{E}(z) = \prod_{i=K-1}^{1} \left(\begin{bmatrix} \mathbf{U}_i & \mathbf{0} \\ \mathbf{0} & \mathbf{U}_i \end{bmatrix} \mathbf{Q}_i \mathbf{\Lambda}(z) \mathbf{Q}_i \right) \mathbf{G}_0 \tag{5.6}$$

where

$$\mathbf{Q}_i = \begin{bmatrix} \mathbf{C}_i & -\mathbf{S}_i \\ \mathbf{S}_i & \mathbf{C}_i \end{bmatrix}$$

with $\mathbf{C}_i$ and $\mathbf{S}_i$ being diagonal matrices whose elements are given by

$$[\mathbf{C}_i]_{k,k} = \cos\alpha_{k,i} \text{ and } [\mathbf{S}_i]_{k,k} = \sin\alpha_{k,i}$$

respectively. All the matrices on the right-hand of (5.6) are orthogonal except $\mathbf{\Lambda}(z)$. As seen from the structure of $\text{diag}(\mathbf{U}_i, \mathbf{U}_i)$ in (5.6), the simplified structure has been able to reduce the number of free parameters to nearly one-half in comparison to $\mathbf{\Phi}_i$ in (5.5). However, there are two $\mathbf{Q}_i$'s involved in each stage of the lattice structure as required by (5.6). We would now like to further simplify the structure of (5.6) in order to reduce the implementation complexity.

According to the C-S decomposition [55], [101], an $M \times M$ orthogonal matrix $\mathbf{A}$ can always be decomposed as

$$\mathbf{A} = \text{diag}(\mathbf{X}_0, \mathbf{X}_1) \mathbf{\Sigma} \text{diag}(\mathbf{Y}_0, \mathbf{Y}_1) \tag{5.7}$$

where $\mathbf{X}_0$ and $\mathbf{Y}_0$ are $(M-\rho)\times(M-\rho)$ orthogonal matrices and $\mathbf{X}_1$ and $\mathbf{Y}_1$ are $\rho\times\rho$ orthogonal matrices. Here, ρ can be any integer between 0 and M. The matrix $\boldsymbol{\Sigma}$ in (5.7) is given by

$$\boldsymbol{\Sigma}=\begin{bmatrix}\mathbf{I}_{M-2\rho} & \mathbf{0} & \mathbf{0}\\ \mathbf{0} & \mathbf{C} & -\mathbf{S}\\ \mathbf{0} & \mathbf{S} & \mathbf{C}\end{bmatrix}$$

when $2\rho < M$, and

$$\boldsymbol{\Sigma}=\begin{bmatrix}\mathbf{C} & -\mathbf{S} & \mathbf{0}\\ \mathbf{S} & \mathbf{C} & \mathbf{0}\\ \mathbf{0} & \mathbf{0} & \mathbf{I}_{2\rho-M}\end{bmatrix}$$

when $2\rho \geq M$, in which $\mathbf{C}$ and $\mathbf{S}$ are $\rho\times\rho$ diagonal matrices with entries $[\mathbf{C}]_{k,k}=\cos\alpha_k$ and $[\mathbf{S}]_{k,k}=\sin\alpha_k$. Applying the C-S decomposition (5.7) to the orthogonal matrix $\boldsymbol{\Phi}_i$ in (5.5) and letting $\rho = M/2$, $\mathbf{X}_0=\mathbf{X}_1$ and $\mathbf{Y}_0=\mathbf{Y}_1$, we have

$$\boldsymbol{\Phi}_i=\begin{bmatrix}\mathbf{U}_i & \mathbf{0}\\ \mathbf{0} & \mathbf{U}_i\end{bmatrix}\begin{bmatrix}\mathbf{C}_i & -\mathbf{S}_i\\ \mathbf{S}_i & \mathbf{C}_i\end{bmatrix}\begin{bmatrix}\mathbf{V}_i & \mathbf{0}\\ \mathbf{0} & \mathbf{V}_i\end{bmatrix} \tag{5.8}$$

Substituting (5.8) into (5.5) gives

$$\mathbf{E}(z)=\prod_{i=K-1}^{1}\left(\begin{bmatrix}\mathbf{U}_i & \mathbf{0}\\ \mathbf{0} & \mathbf{U}_i\end{bmatrix}\begin{bmatrix}\mathbf{C}_i & -\mathbf{S}_i\\ \mathbf{S}_i & \mathbf{C}_i\end{bmatrix}\begin{bmatrix}\mathbf{V}_i & \mathbf{0}\\ \mathbf{0} & \mathbf{V}_i\end{bmatrix}\boldsymbol{\Lambda}(z)\right)\mathbf{G}_0$$

By interchanging the two matrices $\mathrm{diag}(\mathbf{V}_i,\mathbf{V}_i)$ and $\boldsymbol{\Lambda}(z)$ and combining $\mathrm{diag}(\mathbf{V}_i,\mathbf{V}_i)$ with $\mathrm{diag}(\mathbf{U}_{i-1},\mathbf{U}_{i-1})$, the above equation can be rewritten as

$$\mathbf{E}(z)=\prod_{i=K-1}^{1}\left(\mathrm{diag}(\hat{\mathbf{U}}_i,\hat{\mathbf{U}}_i)\mathbf{Q}_i\boldsymbol{\Lambda}(z)\right)\hat{\mathbf{G}}_0 \tag{5.9}$$

where

$$\hat{\mathbf{U}}_i = \begin{cases} \mathbf{V}_{i+1}\mathbf{U}_i, & 0 \le i \le K-2 \\ \mathbf{U}_{K-1}, & i = K-1 \end{cases}$$

$$\hat{\mathbf{V}}_0 = \mathbf{V}_1\mathbf{V}_0$$

$$\hat{\mathbf{G}}_0 = \begin{bmatrix} \hat{\mathbf{U}}_0 & -\hat{\mathbf{V}}_0 \\ \hat{\mathbf{V}}_0 & \hat{\mathbf{U}}_0 \end{bmatrix} \text{diag}(\mathbf{I}, \Gamma\mathbf{J})$$

This simplified lattice structure is depicted in Fig. 5.1. It is clear that the structure in (5.9) is the same as that in (5.6), except that only one $\mathbf{Q}_i$ is needed in each stage of the lattice structure, thus reducing the implementation complexity to a certain degree. Moreover, the further simplified lattice structure in (5.9) is also complete as a result of the straightforward use of the C-S decomposition into the complete structure in (5.5).

The above discussion on the lattice structure is for MIS-PUFBs that have identical analysis and synthesis filters and therefore, the derived simplified structure is shared by the analysis and the synthesis banks. For PRFBs, however, it is in general difficult to develop a complete lattice structure for both the analysis and the synthesis filters. As a matter of fact, to the best knowledge of the author, no disclosure of any complete lattice structure for general PRFBs or the PRFBs with certain constraints has been found in the state of the art literature. In what follows, we will focus on the development of complete lattice structures for a class of PRFBs that are mirror-image symmetric.

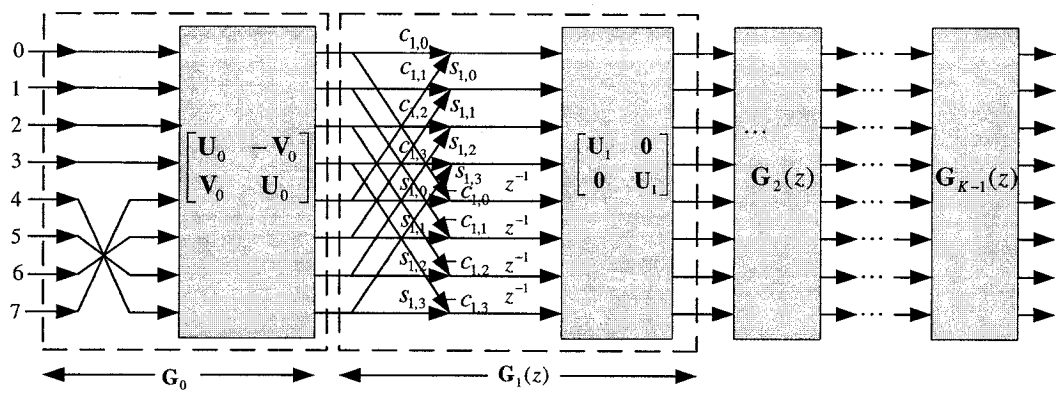

Figure 5.1: Simplified lattice structure for MIS-PUFB

5.3 Lattice Structure of MIS-PRFBs with Even Channel

We first investigate the lattice structure for MIS-PRFBs with an even number of channels. As the analysis and synthesis filters in an MIS-PRFB are closely related to satisfy the PR and MIS conditions, it is necessary to reveal the relation between the polyhase matrix of the analysis bank and that of the synthesis bank. The result is stated in the following Lemma.

Lemma 1: Given the analysis polyphase matrix $\mathbf{E}(z) = \sum_{i=0}^{K-1} \mathbf{E}_i z^{-i}$ of an MIS-PRFB, which satisfies $\mathbf{E}(z)\mathbf{R}(z) = \mathbf{I}$ and (5.4), the corresponding synthesis polyphase matrix $\mathbf{R}(z)$, i.e., the inverse of $\mathbf{E}(z)$, must be of the form $\mathbf{R}(z) = \sum_{i=0}^{K-1} \mathbf{R}_i z^{i}$ and satisfy $\mathbf{R}(z) = z^{K-1}\mathbf{T}\mathbf{R}(z^{-1})\mathbf{D}$.

Proof: Using $\mathbf{E}(z)\mathbf{R}(z) = \mathbf{I}$ and (5.4) and noting that $\mathbf{DD} = -\mathbf{I}$, we have

$$
\begin{aligned}
&\mathbf{I} = \mathbf{R}(z)\mathbf{E}(z) = \mathbf{R}(z^{-1})\mathbf{E}(z^{-1}) \\
&\Leftrightarrow \mathbf{T} = \mathbf{R}(z^{-1})\mathbf{E}(z^{-1})\mathbf{T} \\
&\Leftrightarrow \mathbf{T} = -\mathbf{R}(z^{-1})\mathbf{D}\mathbf{D}\mathbf{E}(z^{-1})\mathbf{T} \\
&\Leftrightarrow \mathbf{T} = -z^{K-1}\mathbf{R}(z^{-1})\mathbf{D}\left(z^{-(K-1)}\mathbf{D}\mathbf{E}(z^{-1})\mathbf{T}\right) \\
&\Leftrightarrow \mathbf{T} = -z^{K-1}\mathbf{R}(z^{-1})\mathbf{D}\mathbf{E}(z) \\
&\Leftrightarrow \mathbf{T}\mathbf{R}(z)\mathbf{E}(z) = -z^{K-1}\mathbf{R}(z^{-1})\mathbf{D}\mathbf{E}(z)
\end{aligned}
\tag{5.10}
$$

With $\mathbf{T}\mathbf{T} = \mathbf{I}$, the last equation in (5.10) can be written as,

$$\mathbf{R}(z) = z^{K-1}\mathbf{T}\mathbf{R}(z^{-1})\mathbf{D} \tag{5.11}$$

Obviously, the constraint in (5.11) imposes the mirror-image symmetry on the synthesis filters. Without loss of generality, we assume $\mathbf{R}(z) = \sum_{i=-K_1}^{K_2} \mathbf{R}_i z^i$. Substituting it into (5.11), and evaluating the terms of the highest and the lowest powers of z on both sides of (5.11), we have

$$K - 1 - K_2 = K_1 \text{ and } K - 1 + K_1 = K_2 \tag{5.12}$$

which gives $K_1 = 0$ and $K_2 = K - 1$. Therefore, $\mathbf{R}(z) = \sum_{i=0}^{K-1} \mathbf{R}_i z^i$.

The above Lemma indicates that the mirror-image symmetry on the analysis filters would automatically lead to a similar symmetry on the synthesis filters. With the knowledge of $\mathbf{E}(z)$ and $\mathbf{R}(z)$, we would like to develop the lattice structure for MIS-PRFB. The idea is to conceive a building block such that a higher-order analysis polyphase matrix can be generated from a lower-order one while the MIS and PR properties are propagated. It is also expected that the inverse of such a building block can be employed to generate in a similar manner the lattice structure for the synthesis polyphase matrix of the filter bank. This idea is similar to the development of LPPRFBs in [74], with the linear-phase constraint being replaced by the mirror-image symmetry.

Suppose we already have an M-channel FIR mirror-image symmetric PRFB, with the analysis and synthesis polyphase matrices of order-(m-1) being given by $\mathbf{E}^{(m-1)}(z)$ and $\mathbf{R}^{(m-1)}(z)$, respectively. Define the order-m polyphase matrices as

$$\mathbf{E}^{(m)}(z) = \mathbf{G}(z)\mathbf{E}^{(m-1)}(z)$$

$$\mathbf{R}^{(m)}(z) = \mathbf{R}^{(m-1)}(z)\mathbf{G}^{-1}(z) \tag{5.13}$$

where $\mathbf{G}(z)$ and $\mathbf{G}^{-1}(z)$ are a pair of inverse propagation building blocks of order-one to be given by

$$\mathbf{G}(z) = \mathbf{A}_0 + z^{-1}\mathbf{A}_1$$

$$\mathbf{G}^{-1}(z) = \mathbf{B}_0 + z\mathbf{B}_1 \tag{5.14}$$

The problem is to determine $\{\mathbf{G}(z), \mathbf{G}^{-1}(z)\}$ such that $\{\mathbf{E}^{(m)}(z), \mathbf{R}^{(m)}(z)\}$ also gives a mirror-image symmetric PRFB.

If $\{\mathbf{E}^{(m)}(z), \mathbf{R}^{(m)}(z)\}$ is of mirror-image symmetry, we have

$$\mathbf{E}^{(m)}(z) = z^{-m}\mathbf{D}\mathbf{E}^{(m)}(z^{-1})\mathbf{T}$$

$$\mathbf{R}^{(m)}(z) = z^{m}\mathbf{T}\mathbf{R}^{(m)}(z^{-1})\mathbf{D} \tag{5.15}$$

From (5.14), we get

$$\mathbf{E}^{(m)}(z^{-1}) = \mathbf{G}(z^{-1})\mathbf{E}^{(m-1)}(z^{-1})$$

$$\mathbf{R}^{(m)}(z^{-1}) = \mathbf{R}^{(m-1)}(z^{-1})\mathbf{G}^{-1}(z^{-1}) \tag{5.16}$$

Recalling that $\{\mathbf{E}^{(m-1)}(z), \mathbf{R}^{(m-1)}(z)\}$ is mirror-image symmetric, i.e.,

$$\mathbf{E}^{(m-1)}(z) = z^{-(m-1)}\mathbf{D}\mathbf{E}^{(m-1)}(z^{-1})\mathbf{T},$$

$$\mathbf{R}^{(m-1)}(z) = z^{(m-1)}\mathbf{T}\mathbf{R}^{(m-1)}(z^{-1})\mathbf{D} \tag{5.17}$$

Substituting (5.16), (5.17) into (5.15), one can obtain

$$\mathbf{G}(z)\mathbf{E}^{(m-1)}(z) = -z^{-1}\mathbf{D}\mathbf{G}(z^{-1})\mathbf{D}\mathbf{E}^{(m-1)}(z)$$

$$\mathbf{R}^{(m-1)}(z)\mathbf{G}^{-1}(z) = -z\mathbf{R}^{(m-1)}(z)\mathbf{D}\mathbf{G}^{-1}(z^{-1})\mathbf{D} \tag{5.18}$$

Since $\{\mathbf{E}^{(m-1)}(z), \mathbf{R}^{(m-1)}(z)\}$ is perfect reconstruction, we may safely remove them from both sides of (5.18). Thus, $\{\mathbf{E}^{m}(z), \mathbf{R}^{m}(z)\}$ is mirror-image symmetric if and only if

$$\mathbf{G}(z) = -z^{-1}\mathbf{D}\mathbf{G}(z^{-1})\mathbf{D}$$

$$\mathbf{G}^{-1}(z) = -z\mathbf{D}\mathbf{G}^{-1}(z^{-1})\mathbf{D} \tag{5.19}$$

Substituting (5.14) into (5.19), we have

$$\mathbf{G}(z) = \mathbf{A}_0 - z^{-1}\mathbf{D}\mathbf{A}_0\mathbf{D} \tag{5.20a}$$

$$\mathbf{G}^{-1}(z) = \mathbf{B}_0 - z\mathbf{D}\mathbf{B}_0\mathbf{D} \tag{5.20b}$$

What is now left is to determine the unknown matrices $\mathbf{A}_0$ and $\mathbf{B}_0$ such that $\mathbf{G}(z)\mathbf{G}^{-1}(z) = \mathbf{I}$. To this end, it is required that

$$\mathbf{A}_0\mathbf{D}\mathbf{B}_0 = \mathbf{0}$$

$$\mathbf{B}_0\mathbf{D}\mathbf{A}_0 = \mathbf{0} \tag{5.21}$$

According to Sylvester's rank theorem [102], from (5.21), it follows that the ranks of $\mathbf{A}_0$ and $\mathbf{B}_0$ must satisfy the relation

$$r(\mathbf{A}_0) + r(\mathbf{B}_0) \le M \tag{5.22}$$

The rank inequality (5.22) imposes a condition on the selection of $\mathbf{A}_0$ and $\mathbf{B}_0$. To maximize the number of free parameters of the filter bank, the total rank is set to the maximum value M. On the other hand, considering that there is, in general, no preference in choosing the number of free parameters for either the analysis or the synthesis part,

one can reasonably assume that $\mathbf{A}_0$ and $\mathbf{B}_0$ have equal rank, namely, $r(\mathbf{A}_0) = r(\mathbf{B}_0) = M/2$. Therefore, we choose $\mathbf{A}_0$ to be of the following form

$$\mathbf{A}_0 = \frac{1}{\sqrt{2}}\begin{bmatrix} \mathbf{U} & \mathbf{U} \\ \mathbf{V} & \mathbf{V} \end{bmatrix} \tag{5.23}$$

Substituting (5.23) into (5.20a), we may write $\mathbf{G}(z)$ as

$$\begin{aligned} \mathbf{G}(z) &= \frac{1}{\sqrt{2}}\begin{bmatrix} \mathbf{U}+z^{-1}\mathbf{V} & \mathbf{U}-z^{-1}\mathbf{V} \\ \mathbf{V}-z^{-1}\mathbf{U} & \mathbf{V}+z^{-1}\mathbf{U} \end{bmatrix} \\ &= \frac{1}{\sqrt{2}}\begin{bmatrix} \mathbf{U} & -\mathbf{V} \\ \mathbf{V} & \mathbf{U} \end{bmatrix}\begin{bmatrix} \mathbf{I} & \mathbf{0} \\ \mathbf{0} & z^{-1}\mathbf{I} \end{bmatrix}\begin{bmatrix} \mathbf{I} & \mathbf{I} \\ -\mathbf{I} & \mathbf{I} \end{bmatrix} \\ &= \mathbf{\Phi}\mathbf{\Lambda}(z)\mathbf{W} \end{aligned} \tag{5.24}$$

where

$$\mathbf{\Phi} = \begin{bmatrix} \mathbf{U} & -\mathbf{V} \\ \mathbf{V} & \mathbf{U} \end{bmatrix},\ \mathbf{\Lambda}(z) = \begin{bmatrix} \mathbf{I} & \mathbf{0} \\ \mathbf{0} & z^{-1}\mathbf{I} \end{bmatrix},\ \mathbf{W} = \frac{1}{\sqrt{2}}\begin{bmatrix} \mathbf{I} & \mathbf{I} \\ -\mathbf{I} & \mathbf{I} \end{bmatrix}$$

Comparing with (5.20a), the order-one building block given by (5.24) is of a product form, which significantly facilitates the inversion of $\mathbf{G}(z)$. It is seen that $\mathbf{\Lambda}(z)$ is a diagonal matrix with one-half of its entries being a pure delay, and $\mathbf{W}$ is the well-known butterfly structure. In particular, both $\mathbf{\Lambda}(z)$ and $\mathbf{W}$ are nonsingular with their inverses being readily given by

$$\mathbf{\Lambda}^{-1}(z) = \mathbf{\Lambda}(z^{-1}) = \begin{bmatrix} \mathbf{I} & \mathbf{0} \\ \mathbf{0} & z\mathbf{I} \end{bmatrix}$$

$$\mathbf{W}^{-1} = \mathbf{W}^T = \frac{1}{\sqrt{2}}\begin{bmatrix} \mathbf{I} & -\mathbf{I} \\ \mathbf{I} & \mathbf{I} \end{bmatrix}$$

It is also noted that all the free parameters of the order-one building block $\mathbf{G}(z)$ are contained in $\mathbf{\Phi}$, which is to be determined. Evidently, $\mathbf{G}(z)$ is invertible if and only if $\mathbf{\Phi}$ is nonsingular. Writing the inverse of $\mathbf{\Phi}$ as

$$\mathbf{\Phi}^{-1} = \begin{bmatrix} \tilde{\mathbf{U}} & \tilde{\mathbf{V}} \\ -\tilde{\mathbf{V}} & \tilde{\mathbf{U}} \end{bmatrix} \tag{5.25}$$

where $\tilde{\mathbf{U}}$ and $\tilde{\mathbf{V}}$ satisfy

$$\mathbf{U}\tilde{\mathbf{U}} + \mathbf{V}\tilde{\mathbf{V}} = \mathbf{I}$$

$$\mathbf{U}\tilde{\mathbf{V}} - \mathbf{V}\tilde{\mathbf{U}} = \mathbf{0} \tag{5.26}$$

with (5.25), we obtain $\mathbf{G}^{-1}(z)$ as

$$\begin{aligned} \mathbf{G}^{-1}(z) &= \mathbf{W}^T \mathbf{\Lambda}(z^{-1}) \mathbf{\Phi}^{-1} \\ &= \frac{1}{\sqrt{2}} \begin{bmatrix} \mathbf{I} & -\mathbf{I} \\ \mathbf{I} & \mathbf{I} \end{bmatrix} \begin{bmatrix} \mathbf{I} & \mathbf{0} \\ \mathbf{0} & z\mathbf{I} \end{bmatrix} \begin{bmatrix} \tilde{\mathbf{U}} & \tilde{\mathbf{V}} \\ -\tilde{\mathbf{V}} & \tilde{\mathbf{U}} \end{bmatrix} \\ &= \begin{bmatrix} \tilde{\mathbf{U}} & \tilde{\mathbf{V}} \\ \tilde{\mathbf{U}} & \tilde{\mathbf{V}} \end{bmatrix} + z \begin{bmatrix} \tilde{\mathbf{V}} & -\tilde{\mathbf{U}} \\ -\tilde{\mathbf{V}} & \tilde{\mathbf{U}} \end{bmatrix} \end{aligned} \tag{5.27}$$

Comparing (5.20b) with (5.27), the matrix $\mathbf{B}_0$ can be determined,

$$\mathbf{B}_0 = \begin{bmatrix} \tilde{\mathbf{U}} & \tilde{\mathbf{V}} \\ \tilde{\mathbf{U}} & \tilde{\mathbf{V}} \end{bmatrix} \tag{5.28}$$

Obviously, the rank of $\mathbf{B}_0$ is not greater than *M*/2, confirming that the rank inequality (5.22) is satisfied. Thus far, we have reached a pair of order-one building blocks, i.e., $\mathbf{G}(z)$ in (5.24) and $\mathbf{G}^{-1}(z)$ in (5.27), for the analysis and synthesis polyphase matrices respectively, which is capable of propagating both PR and MIS properties.

We would now like to construct the lattice structure for MIS-PRFB based on the order-one building block. Accordingly, an analysis polyphase matrix of order *K*-1 can be written as

$$\begin{aligned} \mathbf{E}(z) &= \mathbf{G}_{K-1}(z)\mathbf{G}_{K-2}(z)\cdots\mathbf{G}_1(z)\mathbf{G}_0 \\ &= \prod_{i=K-1}^{1} \left(\mathbf{\Phi}_i \mathbf{\Lambda}(z) \mathbf{W}\right) \mathbf{G}_0 \end{aligned} \tag{5.29}$$

where $\mathbf{G}_i(z)\,(i=1,\ldots,K-1)$ is the order-one building block given by (5.24) and $\mathbf{G}_0$ a constant matrix satisfying the mirror-image symmetry

$$\mathbf{G}_0=\begin{bmatrix}\mathbf{U}_0 & -\mathbf{V}_0\\ \mathbf{V}_0 & \mathbf{U}_0\end{bmatrix}\begin{bmatrix}\mathbf{I}_{M/2} & \mathbf{0}\\ \mathbf{0} & \Gamma\mathbf{J}_{M/2}\end{bmatrix} \tag{5.30}$$

With (5.29), it is easy to get the corresponding synthesis polyphase matrix $\mathbf{R}(z)$ as given below

$$\mathbf{R}(z)=\mathbf{G}_0^{-1}\prod_{i=1}^{K-1}\mathbf{G}_i^{-1}(z)=\mathbf{G}_0^{-1}\prod_{i=K-1}^{1}\left(\mathbf{W}^T\mathbf{\Lambda}(z^{-1})\mathbf{\Phi}_i^{-1}\right) \tag{5.31}$$

Fig. 5.2 depicts the lattice structure (5.29) and (5.31) for the analysis as well as synthesis parts of an eight-channel MIS-PRFB. It should be noted that each stage $\mathbf{G}_i(z)$ (or $\mathbf{G}_i^{-1}(z)$) of the lattice structure has the same form, except for the initial one $\mathbf{G}_0$ (or $\mathbf{G}_0^{-1}$).

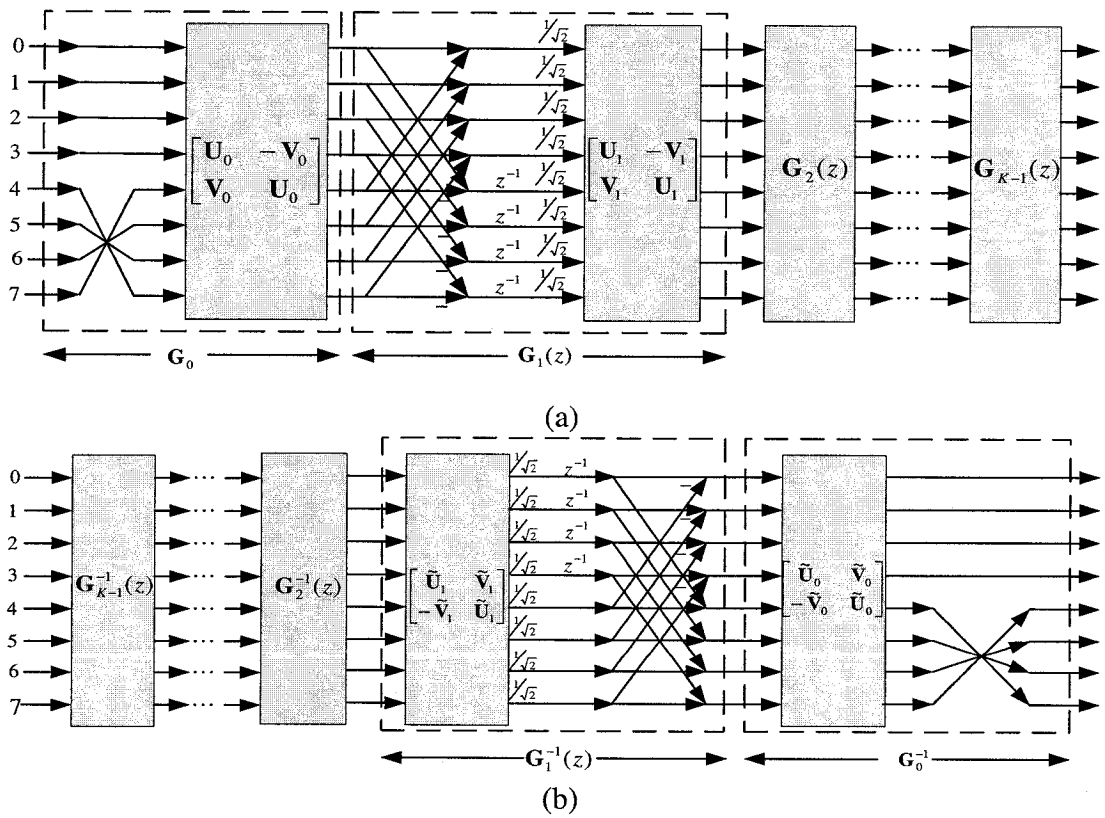

Figure 5.2: Lattice structure of even-channel MIS-PRFB.
(a) Analysis bank. (b) Synthesis bank.

The above discussion indicates that an MIS-PRFB can be constructed by a cascade of a number of lower-order building blocks. We now address the converse issue, namely, for any given MIS-PRFB, does there always exist a factorization form like (5.29)? The answer to this question is provided in the following theorem.

Theorem 5.1: For any even-channel FIR mirror-image PRFB with all analysis filters of length $L=KM$, the associated analysis polyphase matrix $\mathbf{E}(z)=\sum_{i=0}^{K-1}\mathbf{E}_i z^{-i}$ satisfying perfect reconstruction and (5.4), can be factored as (5.29), while the corresponding synthesis polyphase matrix $\mathbf{R}(z)$ is given by (5.31).

Proof: The proof is inductive. Assume that we have an order-m polyphase matrix $\mathbf{E}^{(m)}(z)=\sum_{i=0}^{m}\mathbf{A}_i z^{-i}$ satisfying the PR condition and the mirror-image symmetry. From *Lemma 1*, the inverse of $\mathbf{E}^{(m)}(z)$ can be written as $\mathbf{R}^{(m)}(z)=\sum_{i=0}^{m}\mathbf{B}_i z^{i}$. The key idea is to show there exists a pair of invertible matrices $\mathbf{G}(z)$ and $\mathbf{G}^{-1}(z)$ that peel off the order of $\mathbf{R}^{(m)}(z)$ and $\mathbf{E}^{(m)}(z)$, respectively, by unity each time they are employed, i.e.,

$$\mathbf{E}^{(m-1)}(z)=\mathbf{G}^{-1}(z)\mathbf{E}^{(m)}(z),$$

$$\mathbf{R}^{(m-1)}(z)=\mathbf{R}^{(m)}(z)\mathbf{G}(z). \tag{5.32}$$

Moreover, we would like the left-hand side $\mathbf{E}^{(m-1)}(z)$ and $\mathbf{R}^{(m-1)}(z)$ of (5.32) to retain the desirable perfect reconstruction and mirror-image symmetry (PR-MIS) properties so that the order-reduction procedure in (5.32) can be repeated until the zero-order polyphase matrices are reached. According to the discussion in Section 5.3, the order-one building blocks $\mathbf{G}(z)$ and $\mathbf{G}^{-1}(z)$ given by (5.24) and (5.27) are capable of producing PR-MIS $\mathbf{R}^{(m-1)}(z)$ and $\mathbf{E}^{(m-1)}(z)$. Substituting (5.24) and (5.27) into (5.32) yields

$$\mathbf{E}^{(m-1)}(z)=\sum_{i=0}^{m-1}\tilde{\mathbf{A}}_i z^{-i}=\left(\begin{bmatrix}\tilde{\mathbf{U}} & \tilde{\mathbf{V}}\\ \tilde{\mathbf{U}} & \tilde{\mathbf{V}}\end{bmatrix}+z\begin{bmatrix}\tilde{\mathbf{V}} & -\tilde{\mathbf{U}}\\ -\tilde{\mathbf{V}} & \tilde{\mathbf{U}}\end{bmatrix}\right)\left(\sum_{i=0}^{m}\mathbf{A}_i z^{-i}\right),$$

$$\mathbf{R}^{(m-1)}(z)=\sum_{i=0}^{m-1}\tilde{\mathbf{B}}_i z^{i}=\left(\sum_{i=0}^{m}\mathbf{B}_i z^{i}\right)\left(\begin{bmatrix}\mathbf{U} & \mathbf{U}\\ \mathbf{V} & \mathbf{V}\end{bmatrix}+z^{-1}\begin{bmatrix}\mathbf{V} & -\mathbf{V}\\ -\mathbf{U} & \mathbf{U}\end{bmatrix}\right). \tag{5.33}$$

By evaluating the coefficients of the terms z and z^{-m} on both sides of the above equations, we obtain the following conditions:

$$\text{i)}\begin{bmatrix}\tilde{\mathbf{V}} & -\tilde{\mathbf{U}}\\ -\tilde{\mathbf{V}} & \tilde{\mathbf{U}}\end{bmatrix}\mathbf{A}_0=\mathbf{0} \qquad \text{ii)}\begin{bmatrix}\tilde{\mathbf{U}} & \tilde{\mathbf{V}}\\ \tilde{\mathbf{U}} & \tilde{\mathbf{V}}\end{bmatrix}\mathbf{A}_m=\mathbf{0}$$

$$\text{iii)}\,\mathbf{B}_0\begin{bmatrix}\mathbf{V} & -\mathbf{V}\\ -\mathbf{U} & \mathbf{U}\end{bmatrix}=\mathbf{0} \qquad \text{iv)}\,\mathbf{B}_m\begin{bmatrix}\mathbf{U} & \mathbf{U}\\ \mathbf{V} & \mathbf{V}\end{bmatrix}=\mathbf{0}.$$

Now, the problem reduces to proving that there exist $\mathbf{U}$, $\mathbf{V}$, $\tilde{\mathbf{U}}$ and $\tilde{\mathbf{V}}$ such that the above four conditions are met. It is easily observed that conditions i) and iii) are to guarantee the causality of $\mathbf{E}^{(m-1)}(z)$ and the anti-causality of $\mathbf{R}^{(m-1)}(z)$, while conditions ii) and iv) are to reduce the orders of $\mathbf{E}^{(m)}(z)$ and $\mathbf{R}^{(m)}(z)$ by unity.

We first examine conditions i) and ii). From the PR and MIS properties, we have

$$\mathbf{B}_0\mathbf{A}_m=\mathbf{0} \tag{5.34}$$

$$\mathbf{A}_0=\mathbf{D}\mathbf{A}_m\mathbf{T} \tag{5.35}$$

leading to

$$\mathbf{B}_0\mathbf{A}_m=\mathbf{B}_0\mathbf{D}\mathbf{A}_0\mathbf{T}=\mathbf{0}\Leftrightarrow\mathbf{B}_0\mathbf{D}\mathbf{A}_0=\mathbf{0} \tag{5.36}$$

In a manner similar to the previous rank discussion, we can choose

$$r(\mathbf{A}_0)=r(\mathbf{B}_0)\le M/2 \tag{5.37}$$

which implies that the dimension of the null space of $\mathbf{A}_0$ is larger than or equal to $M/2$. Accordingly, one can choose $M/2$ linearly independent vectors from the null

space of $\mathbf{A}_0$ to form $[\tilde{\mathbf{V}} \ -\tilde{\mathbf{U}}]$ such that condition i) is satisfied. As for condition ii), by substituting (5.35) into condition i) and noting that $\mathbf{D}\begin{bmatrix} \tilde{\mathbf{V}} & -\tilde{\mathbf{U}} \\ -\tilde{\mathbf{V}} & \tilde{\mathbf{U}} \end{bmatrix}\mathbf{D} = \begin{bmatrix} \tilde{\mathbf{U}} & \tilde{\mathbf{V}} \\ \tilde{\mathbf{U}} & \tilde{\mathbf{V}} \end{bmatrix}$, we obtain

$$\begin{bmatrix} \tilde{\mathbf{V}} & -\tilde{\mathbf{U}} \\ -\tilde{\mathbf{V}} & \tilde{\mathbf{U}} \end{bmatrix}\mathbf{D}\mathbf{A}_m\mathbf{T} = -\mathbf{D}\begin{bmatrix} \tilde{\mathbf{U}} & \tilde{\mathbf{V}} \\ \tilde{\mathbf{U}} & \tilde{\mathbf{V}} \end{bmatrix}\mathbf{A}_m\mathbf{T} = \mathbf{0} \Leftrightarrow \begin{bmatrix} \tilde{\mathbf{U}} & \tilde{\mathbf{V}} \\ \tilde{\mathbf{U}} & \tilde{\mathbf{V}} \end{bmatrix}\mathbf{A}_m = \mathbf{0}$$

Therefore, the $\tilde{\mathbf{U}}$ and $\tilde{\mathbf{V}}$ chosen to satisfy condition i) also meet condition ii).

Next, we come to the proof of conditions iii) and iv). With the perfect reconstruction property, we have $\mathbf{B}_0\mathbf{A}_m = \mathbf{0}$, implying that the row vectors of $\mathbf{B}_0$ belong to the null space of $\mathbf{A}_m$. From condition ii), the matrix $[\tilde{\mathbf{U}} \ \tilde{\mathbf{V}}]$ consists of $M/2$ linearly independent row vectors of the null space of $\mathbf{A}_m$. From (5.37), we also know that the rank of $\mathbf{B}_0$ is not greater than $M/2$, which means all the row vectors of $\mathbf{B}_0$ can be expressed as a linear combination of the row vectors of $[\tilde{\mathbf{U}} \ \tilde{\mathbf{V}}]$. Accordingly, $\mathbf{B}_0$ can be written as

$$\mathbf{B}_0 = \mathbf{X}_1\begin{bmatrix} \tilde{\mathbf{U}} & \tilde{\mathbf{V}} \\ \tilde{\mathbf{U}} & \tilde{\mathbf{V}} \end{bmatrix} \tag{5.38}$$

where $\mathbf{X}_1$ is an $M \times M$ matrix. Using (5.38) and recalling that $\mathbf{U}\tilde{\mathbf{V}} - \mathbf{V}\tilde{\mathbf{U}} = \mathbf{0}$, we have

$$\mathbf{B}_0\begin{bmatrix} \mathbf{V} & -\mathbf{V} \\ -\mathbf{U} & \mathbf{U} \end{bmatrix} = \mathbf{X}_1\begin{bmatrix} \tilde{\mathbf{U}} & \tilde{\mathbf{V}} \\ \tilde{\mathbf{U}} & \tilde{\mathbf{V}} \end{bmatrix}\begin{bmatrix} \mathbf{V} & -\mathbf{V} \\ -\mathbf{U} & \mathbf{U} \end{bmatrix} = \mathbf{0} \tag{5.39}$$

thus justifying condition iii). Similarly, writing $\mathbf{B}_m$ as

$$\mathbf{B}_m = \mathbf{X}_2\begin{bmatrix} \tilde{\mathbf{V}} & -\tilde{\mathbf{U}} \\ -\tilde{\mathbf{V}} & \tilde{\mathbf{U}} \end{bmatrix},$$

where $\mathbf{X}_2$ is an $M \times M$ matrix, we obtain

$$\mathbf{B}_m\begin{bmatrix}\mathbf{U} & \mathbf{U}\\ \mathbf{V} & \mathbf{V}\end{bmatrix}=\mathbf{X}_2\begin{bmatrix}\tilde{\mathbf{V}} & -\tilde{\mathbf{U}}\\ -\tilde{\mathbf{V}} & \tilde{\mathbf{U}}\end{bmatrix}\begin{bmatrix}\mathbf{U} & \mathbf{U}\\ \mathbf{V} & \mathbf{V}\end{bmatrix}=\mathbf{0}, \tag{5.40}$$

indicating that condition iv) is satisfied.

The above discussion indicates the $\mathbf{G}(z)$ and $\mathbf{G}^{-1}(z)$ given by (5.29) and (5.31) can always reduce the order of PR-MIS $\mathbf{R}^{(m)}(z)$ and $\mathbf{E}^{(m)}(z)$ by unity while preserving the PR and MIS properties of the resulting lower-order polyphase matrices $\mathbf{R}^{(m-1)}(z)$ and $\mathbf{E}^{(m-1)}(z)$. Clearly, this order-reduction-based factorization can be repeated until a zero-order polyphase matrix is reached.

We now proceed to show the minimal property of the proposed lattice structure. A structure is said to be minimal if the number of delays involved in the structure is equal to the degree of the given transfer function [1]. With the mirror-image symmetry, the degree of the system function (5.29) can be easily calculated below,

$$\begin{aligned}\deg(\mathbf{E}(z)) &= \deg(|\mathbf{E}(z)|)=\deg\left(z^{-(K-1)}|\mathbf{D}||\mathbf{E}(z^{-1})||\mathbf{T}|\right)\\ &= M(K-1)-\deg(|\mathbf{E}(z)|)\end{aligned} \tag{5.41}$$

leading the degree of the system to $M(K-1)/2$, where $\deg(\cdot)$ represents the degree of a transfer function. On the other hand, in our factorization, there are $(K-1)$ building blocks $\mathbf{G}_i(z)$, each having $M/2$ delays. As such, the total number of delays of our structure equals the degree of the transfer function, thus justifying the following theorem.

Theorem 5.2: The factorization in (5.29) is minimal, i.e., the resulting lattice structure is realized with the minimum number of delays.

We now make some comments on the above results regarding MIS-PRFBs in comparison to general PRFBs without MIS as well as the PUFB with MIS.

1. Noticing that

$$\mathbf{W}\boldsymbol{\Phi}_i = \frac{1}{\sqrt{2}}\begin{bmatrix} \mathbf{I} & \mathbf{I} \\ -\mathbf{I} & \mathbf{I} \end{bmatrix}\begin{bmatrix} \mathbf{U}_i & -\mathbf{V}_i \\ \mathbf{V}_i & \mathbf{U}_i \end{bmatrix}$$
$$= \frac{1}{\sqrt{2}}\begin{bmatrix} \mathbf{U}_i + \mathbf{V}_i & \mathbf{U}_i - \mathbf{V}_i \\ -\mathbf{U}_i + \mathbf{V}_i & \mathbf{U}_i + \mathbf{V}_i \end{bmatrix}$$
$$= \frac{1}{\sqrt{2}}\begin{bmatrix} \mathbf{U}'_i & -\mathbf{V}'_i \\ \mathbf{V}'_i & \mathbf{U}'_i \end{bmatrix} = \boldsymbol{\Phi}'_i$$

one can fold the butterfly structure $\mathbf{W}$ into the matrix $\boldsymbol{\Phi}'_i$. Therefore, (5.29) can be simplified as

$$\mathbf{E}(z) = \prod_{i=K-1}^{1} \mathbf{G}'_i(z)\,\mathbf{G}_0 = \prod_{i=K-1}^{1} \left(\boldsymbol{\Phi}'_i\,\boldsymbol{\Lambda}(z)\right)\mathbf{G}_0 \tag{5.42}$$

2. Comparing the resulting building block in (5.39) with that in (5.1) for a general PRFB without MIS, one can see that the mirror-image symmetry has led the invertible matrix $\boldsymbol{\Phi}'$ to a special form of $\begin{bmatrix} \mathbf{U}' & -\mathbf{V}' \\ \mathbf{V}' & \mathbf{U}' \end{bmatrix}$, thus reducing the number of parameters by one-half. Also, the number of delays in $\boldsymbol{\Lambda}(z)$ is fixed to $M/2$ instead of r_i ranging from 0 to M.

3. Unlike the MIS-PUFB in (5.5), where $\boldsymbol{\Phi}_i$ is an orthogonal matrix, $\boldsymbol{\Phi}'_i$ in the MIS-PRFB (5.29) is, in general, an invertible matrix, implying that (5.5) is a special case of (5.29). This result is quite obvious since the MIS-PUFB is a special case of MIS-PRFB. Although the lattice structure can be simply reached by replacing the orthogonal matrices in (5.5) for MIS-PUFB with the invertible matrices in (5.29) for MIS-PRFB, we have to emphasize this is not a straightforward extension. The major contribution in this section is to prove, for the first time, that the lattice structure is complete, i.e., the factorization as (5.29) is not only necessary but also a sufficient condition for the analysis matrix of MIS-PRFBs.

5.4 Lattice Structure for MIS-PRFB with Odd Channel

For an MIS filter bank with an odd number of channels, the symmetry constraint in (5.4) can be equivalently written in its analysis polyphase matrix as

$$\mathbf{E}(z) = z^{-(K-1)}\mathbf{D}\mathbf{E}(-z^{-1})\mathbf{T} \tag{5.43}$$

where

$$\mathbf{D} = \begin{bmatrix} \mathbf{0} & \mathbf{0} & \mathbf{I}_{\lceil M/2 \rceil} \\ \mathbf{0} & 1 & \mathbf{0} \\ \mathbf{I}_{\lceil M/2 \rceil} & \mathbf{0} & \mathbf{0} \end{bmatrix}$$

Although the MIS constraint given by (5.43) possesses a similarity with that given for the even-channel case, the derivation of the lattice structure for the odd-channel case would be significantly different due to the replacement of $\mathbf{E}(z^{-1})$ on the right side of (5.4) to $\mathbf{E}(-z^{-1})$ in (5.43). In what follows, we first show that the order-one building block no longer exists for the odd-channel case.

Assume that an order-m polyphase matrix $\mathbf{E}^{(m)}(z)$ is generated from a lower order matrix $\mathbf{E}^{(m-1)}(z)$ using a order-one building block $\mathbf{G}(z)$ as given by (5.19), namely, $\mathbf{E}^{(m)}(z) = \mathbf{G}(z)\mathbf{E}^{(m-1)}(z)$. Following the idea of obtaining $\mathbf{G}(z)$ in the even-channel case and considering that both $\mathbf{E}^{(m)}(z)$ and $\mathbf{E}^{(m-1)}(z)$ satisfy (5.43), one may impose the MIS property on the propagation matrix $\mathbf{G}(z)$, i.e.,

$$\mathbf{G}(z) = z^{-1}\mathbf{P}\mathbf{G}(-z^{-1})\mathbf{P} \tag{5.44}$$

Using (5.19) in (5.44) and comparing the coefficients with respect to the zero- and first-order terms of z on both sides of (5.44), we obtain

$$-\mathbf{P}\mathbf{A}_1\mathbf{P} = \mathbf{A}_0 \text{ and } \mathbf{P}\mathbf{A}_0\mathbf{P} = \mathbf{A}_1 \tag{5.45}$$

It is obvious from (5.45) that the only solution to $\mathbf{A}_0$ and $\mathbf{A}_1$ is a zero matrix, implying that the order-one building block $\mathbf{G}(z) = \mathbf{A}_0 + z^{-1}\mathbf{A}_1$ does not exist for odd-channel MIS filter banks. Therefore, the basic building block should at least be of order two.

To facilitate the analysis of the perfect reconstruction of the filter bank, we would like the order-two building block to be factorable, i.e., it can be expressed as a product of two order-one building blocks,

$$\begin{aligned}\mathbf{G}(z) &= \mathbf{G}_a(z)\mathbf{G}_b(z) = (\mathbf{A}_0 + z^{-1}\mathbf{A}_1)(\mathbf{B}_0 + z^{-1}\mathbf{B}_1) \\ &= \mathbf{A}_0\mathbf{B}_0 + z^{-1}(\mathbf{A}_0\mathbf{B}_1 + \mathbf{A}_1\mathbf{B}_0) + z^{-2}\mathbf{A}_1\mathbf{B}_1\end{aligned} \tag{5.46}$$

Using (5.46) into (5.44) and evaluating the coefficients of the polynomial function of z, we have the following relations,

$$\mathbf{A}_0\mathbf{B}_0 = \mathbf{P}\mathbf{A}_1\mathbf{B}_1\mathbf{P}, \text{ and } \mathbf{A}_0\mathbf{B}_1 = -\mathbf{P}\mathbf{A}_1\mathbf{B}_0\mathbf{P} \tag{5.47}$$

Note that all the matrices involved in (5.47) are of odd-dimension and any matrix with odd dimension can be expressed as

$$\mathbf{Q} = \begin{bmatrix} \mathbf{Q}_0 & \mathbf{q}_0 & \mathbf{Q}_1 \\ \mathbf{q}_1^T & \gamma & \mathbf{q}_2^T \\ \mathbf{Q}_2 & \mathbf{q}_3 & \mathbf{Q}_3 \end{bmatrix}$$

where $\mathbf{Q}_i$ is a square matrix of size $(M-1)/2$, $\mathbf{q}_i$ is a $(M-1)/2$-dimensional column vector ($i = 0,1,2,3$), and γ is a scalar. To facilitate the construction of $\mathbf{A}_i$ and $\mathbf{B}_i$, we now present a two-step scheme. In the first step, we treat all the matrices involved as even-dimension matrices like $\mathbf{Q} = \begin{bmatrix} \mathbf{Q}_0 & \mathbf{Q}_1 \\ \mathbf{Q}_2 & \mathbf{Q}_3 \end{bmatrix}$ by ignoring their center column and row vectors and then construct even-dimensional $\mathbf{A}_i$ and $\mathbf{B}_i$ to obtain a shrunk $\mathbf{G}(z)$. In the

second step, the missing central column and row vectors are taken into consideration to complete the construction of the odd-dimensional $\mathbf{G}(z)$.

Considering that the constraint in (5.47) remains true for the shrunk even-dimension version, one can let

$$\mathbf{A}_1 = \mathbf{P}\mathbf{A}_0\mathbf{D} \text{ and } \mathbf{B}_1 = -\mathbf{D}\mathbf{B}_0\mathbf{P},$$

where

$$\mathbf{P} = \begin{bmatrix} \mathbf{0} & \mathbf{I} \\ \mathbf{I} & \mathbf{0} \end{bmatrix}$$

$$\mathbf{D} = \begin{bmatrix} \mathbf{0} & -\mathbf{I} \\ \mathbf{I} & \mathbf{0} \end{bmatrix}$$

to simplify the construction of $\mathbf{A}_i$ and $\mathbf{B}_i$ while meeting the requirement of (5.47). Thus, $\mathbf{G}(z)$ can be established as

$$\mathbf{G}(z) = \mathbf{G}_a(z)\mathbf{G}_b(z) \tag{5.48}$$

where

$$\mathbf{G}_a(z) = \mathbf{A}_0 + z^{-1}\begin{bmatrix} \mathbf{0} & \mathbf{I} \\ \mathbf{I} & \mathbf{0} \end{bmatrix}\mathbf{A}_0\begin{bmatrix} \mathbf{0} & -\mathbf{I} \\ \mathbf{I} & \mathbf{0} \end{bmatrix}$$

$$\mathbf{G}_b(z) = \mathbf{B}_0 - z^{-1}\begin{bmatrix} \mathbf{0} & -\mathbf{I} \\ \mathbf{I} & \mathbf{0} \end{bmatrix}\mathbf{B}_0\begin{bmatrix} \mathbf{0} & \mathbf{I} \\ \mathbf{I} & \mathbf{0} \end{bmatrix} \tag{5.49}$$

It should be pointed out that although the order-one building blocks in (5.49) have the same form as that in (5.20a), except for the replacement of $\mathbf{D}$ in (5.20a) with $\mathbf{P}$ in (5.49), the shrunk order-two building block $\mathbf{G}(z)$ of the even-dimension case could not have been obtained by a straightforward cascade of two order-one building blocks as (5.20).

We now determine $\mathbf{A}_0$ and $\mathbf{B}_0$ in a manner similar to that in the discussion of the order-one PR building block in Section 5.3. It is clear from (5.46) that $\mathbf{G}(z)$ is PR if and only if both the order-one blocks involved are PR. Accordingly, we assume that $\mathbf{A}_0$ and $\mathbf{B}_0$ each have a rank of $(M-1)/2$, resulting in

$$\mathbf{A}_0 = \begin{bmatrix} \mathbf{U} & \mathbf{U} \\ \mathbf{V} & \mathbf{V} \end{bmatrix}, \ \mathbf{B}_0 = \begin{bmatrix} \mathbf{X} & \mathbf{Y} \\ \mathbf{X} & \mathbf{Y} \end{bmatrix} \tag{5.50}$$

Substituting (5.50) into (5.49) yields

$$\mathbf{G}_a(z) = \begin{bmatrix} \mathbf{U} & \mathbf{V} \\ \mathbf{V} & \mathbf{U} \end{bmatrix} \begin{bmatrix} \mathbf{I} & \mathbf{0} \\ \mathbf{0} & z^{-1}\mathbf{I} \end{bmatrix} \begin{bmatrix} \mathbf{I} & \mathbf{I} \\ \mathbf{I} & -\mathbf{I} \end{bmatrix}$$

$$\mathbf{G}_b(z) = \begin{bmatrix} \mathbf{I} & \mathbf{I} \\ \mathbf{I} & -\mathbf{I} \end{bmatrix} \begin{bmatrix} \mathbf{I} & \mathbf{0} \\ \mathbf{0} & z^{-1}\mathbf{I} \end{bmatrix} \begin{bmatrix} \mathbf{X} & \mathbf{Y} \\ \mathbf{Y} & \mathbf{X} \end{bmatrix} \tag{5.51}$$

Thus far, we have obtained the transfer function of the shrunk even-dimensional order-two building block. We now construct the complete odd-dimensional building block by adding a column and a row in the center of $\mathbf{G}(z)$ obtained above, namely,

$$\begin{aligned} \mathbf{G}(z) = & \begin{bmatrix} \mathbf{U} & \mathbf{u}_1 & -\mathbf{V} \\ \mathbf{u}_2^T & \alpha & \mathbf{v}_2^T \\ \mathbf{V} & \mathbf{v}_1 & \mathbf{U} \end{bmatrix} \begin{bmatrix} \mathbf{I}_{M/2} & \mathbf{0} & \mathbf{0} \\ \mathbf{0} & 1 & \mathbf{0} \\ \mathbf{0} & \mathbf{0} & z^{-1}\mathbf{I}_{M/2} \end{bmatrix} \begin{bmatrix} \mathbf{I}_{M/2} & \mathbf{0} & \mathbf{I}_{M/2} \\ \mathbf{0} & \sqrt{2} & \mathbf{0} \\ -\mathbf{I}_{M/2} & \mathbf{0} & \mathbf{I}_{M/2} \end{bmatrix} \\ & \times \begin{bmatrix} \mathbf{I}_{M/2} & \mathbf{0} & \mathbf{I}_{M/2} \\ \mathbf{0} & \sqrt{2} & \mathbf{0} \\ -\mathbf{I}_{M/2} & \mathbf{0} & \mathbf{I}_{M/2} \end{bmatrix} \begin{bmatrix} \mathbf{I}_{M/2} & \mathbf{0} & \mathbf{0} \\ \mathbf{0} & z^{-1} & \mathbf{0} \\ \mathbf{0} & \mathbf{0} & z^{-1}\mathbf{I}_{M/2} \end{bmatrix} \begin{bmatrix} \mathbf{X} & \mathbf{x}_1 & \mathbf{X} \\ \mathbf{x}_2^T & \beta & \mathbf{y}_2^T \\ \mathbf{Y} & \mathbf{y}_1 & -\mathbf{Y} \end{bmatrix} \end{aligned} \tag{5.52}$$

By expanding $\mathbf{G}(z)$ in (5.52) as an equivalent form in (5.48) and using the constraints in (5.45), one can have

$$\mathbf{u}_1 = \mathbf{v}_1, \mathbf{u}_2 = \mathbf{v}_2, \mathbf{x}_1 = -\mathbf{y}_1, \ \mathbf{x}_2 = -\mathbf{y}_2$$

As a result, an order-two building block that is capable of propagating both PR and MIS properties for odd-channel MIS-PRFB is finally obtained as

$$\mathbf{G}(z) = \mathbf{\Psi}_a \mathbf{\Lambda}(z) \mathbf{\Psi}_b \tag{5.53}$$

where

$$\mathbf{\Psi}_a = \begin{bmatrix} \mathbf{U} & \mathbf{u} & \mathbf{V} \\ \mathbf{v}^T & \alpha & \mathbf{v}^T \\ \mathbf{V} & \mathbf{u} & \mathbf{U} \end{bmatrix}, \tag{5.54a}$$

$$\mathbf{\Psi}_b = \begin{bmatrix} \mathbf{X} & \mathbf{x} & \mathbf{Y} \\ \mathbf{y}^T & \beta & -\mathbf{y}^T \\ \mathbf{Y} & -\mathbf{x} & \mathbf{X} \end{bmatrix}, \tag{5.54b}$$

$$\mathbf{\Lambda}(z) = \begin{bmatrix} \mathbf{I}_{\lceil M/2 \rceil} & \mathbf{0} & \mathbf{0} \\ \mathbf{0} & z^{-1} & \mathbf{0} \\ \mathbf{0} & \mathbf{0} & z^{-2}\mathbf{I}_{\lceil M/2 \rceil} \end{bmatrix}. \tag{5.54c}$$

In (5.54), $\mathbf{\Psi}_a$ and $\mathbf{\Psi}_b$ are invertible matrices and $\mathbf{\Lambda}(z)$ is the modified delay matrix of odd dimension. Obviously, the inverse of the order-two building block, which can be used to generate the synthesis part of the filter bank, is simply given by

$$\mathbf{G}^{-1}(z) = \mathbf{\Psi}_b^{-1} \mathbf{\Lambda}(z^{-1}) \mathbf{\Psi}_a^{-1} \tag{5.55}$$

With (5.53) and (5.55), the analysis and synthesis polyphase matrices of the MIS-PRFB of odd channel can be constructed by cascading a number of order-two building blocks as

$$\begin{aligned} \mathbf{E}(z) &= \mathbf{G}_{K-2}(z)\mathbf{G}_{K-4}(z)\cdots\mathbf{G}_3(z)\mathbf{G}_1(z)\mathbf{G}_0, \\ \mathbf{R}(z) &= \mathbf{G}_0^{-1}\mathbf{G}_1^{-1}(z)\mathbf{G}_3^{-1}(z)\cdots\mathbf{G}_{K-4}^{-1}(z)\mathbf{G}_{K-2}^{-1}(z), \end{aligned} \tag{5.56}$$

where $\mathbf{G}_0$ is a constant matrix satisfying MIS-PRFB condition

$$\mathbf{G}_0 = \begin{bmatrix} \mathbf{U}_0 & \mathbf{u}_0 & \mathbf{V}_0 \\ \mathbf{v}_0 & \alpha_0 & \mathbf{v}_0 \\ \mathbf{V}_0 & \mathbf{u}_0 & \mathbf{U}_0 \end{bmatrix} \begin{bmatrix} \mathbf{I}_{M/2} & \mathbf{0} & \mathbf{0} \\ \mathbf{0} & 1 & \mathbf{0} \\ \mathbf{0} & \mathbf{0} & \Gamma\mathbf{J}_{M/2} \end{bmatrix}$$

and $\mathbf{G}_0^{-1}$ is the inverse of $\mathbf{G}_0$. The whole lattice structure for odd-channel MIS-PRFB is shown in Fig.5.3. Recalling that each building block in the above polyphase matrices is of order-two, the order of both the analysis and synthesis banks must be even, implying that all the filters involved in the MIS-PRFB must be of odd length. It should be mentioned that the polyphase structure obtained as (5.56) for odd-channel filter banks is in general not complete, since the factorized form of order-two building block in (5.48) is not necessarily obtainable for any given MIS-PRFB. However, it can be verified that the above lattice structure is minimal, as summarized in the following theorem.

Theorem 5.3: The factorization given by (5.56) is minimal, i.e., the resulting lattice structure for odd-channel MIS-PRFB is realized with the minimum number of delays.

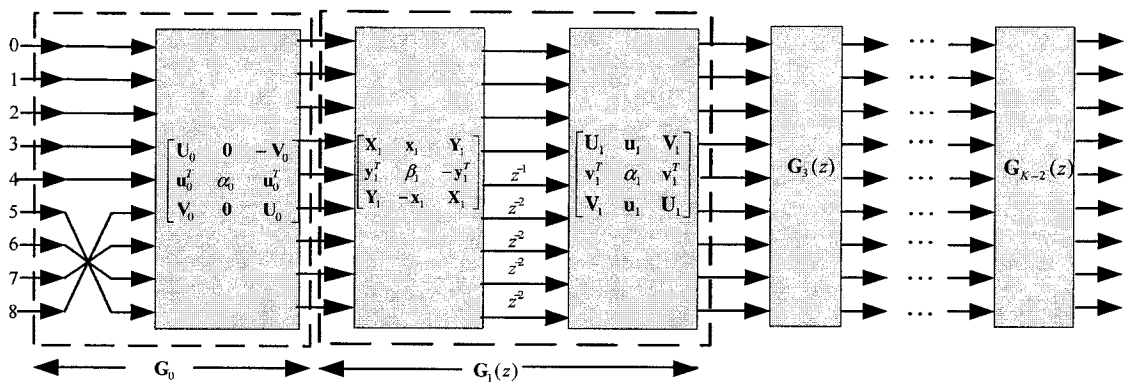

Figure 5.3: Lattice structure of odd-channel MIS-PRFB

5.5 Design of MIS-PRFBs

In addition to the PR and MIS properties that are guaranteed by the proposed lattice structure, some other desirable features, such as large stopband attenuation and coding

gain, should be considered in the design problem so as to obtain high-performance filter banks for practical applications. In this section, we will parameterize the invertible matrices $\mathbf{\Phi}_i$ and optimize the free parameters of the lattice structure by employing the stopband attenuation and the coding gain as a cost function to complete the design of MIS-PRFBs.

5.5.1 Parameterization

We now represent the invertible matrix $\mathbf{\Phi}_i$ with a set of parameters. Several general requirements should be considered in a good parameterization scheme. 1) The matrix must always be invertible, even after the quantization of the lattice parameters. This is to avoid the occurrence of the singular or nearly-singular matrices during the optimization process. 2) The parameterization should give the fewest possible parameters and lead to a fast implementation. 3) Matrix inversion should be avoided in order to minimize the computational complexity. Two commonly-used parameterization schemes, namely, the singular-value decomposition (SVD) [74] and the lifting scheme [84], [85], have been proposed in literature. For the SVD scheme, an invertible matrix $\mathbf{\Phi}_i$ is written as a product of two orthogonal matrices and one diagonal matrix , $\mathbf{\Phi}_i = \mathbf{U}_i\mathbf{\Gamma}_i\mathbf{V}_i$. Since each of the two $M \times M$ orthogonal matrices can be factorized into $M(M-1)/2$ rotation angles and there are M diagonal entries in $\mathbf{\Gamma}_i$, the total number of free parameters of $\mathbf{\Phi}_i$ with the SVD representation is M^2. As for the lifting scheme, with the Gauss-Jordan elimination process, it is not difficult to prove that any $M \times M$ invertible matrix can be completely characterized by $M(M-1)$ lift steps and M scaling factors [84]. Both the SVD and the lifting scheme provide a robust invertible matrix and have the same number

of free parameters. However, the lifting scheme outperforms the SVD in the following aspects. First, the implementation cost for the lifting scheme is less than that of SVD. A lifting step requires one multiplier and one adder, whereas each plane rotation in SVD involves four multipliers and two adders. Thus, the realization cost for an invertible matrix under the lifting scheme is M^2 multipliers plus $M(M-1)$ adders, compared to a total of $2M^2-M$ multipliers and $M(M-1)$ adders for the SVD structure. Secondly, the coefficients in the lifting scheme can be approximated by dyadic values, i.e., rationales in the format of $k/2^m$ (k and m are integers), which is favorable in view of hardware implementations. In what follows, we will focus on the lifting parameterization scheme and show that the number of free parameters in the proposed structure can be reduced as a result of the MIS property.

Taking the even-channel MIS-PRFB as an example, the invertible matrix $\mathbf{\Phi}_i$ has been specialized as $\mathbf{\Phi}_i = \begin{bmatrix} \mathbf{U}_i & -\mathbf{V}_i \\ \mathbf{V}_i & \mathbf{U}_i \end{bmatrix}$ due to the mirror-image symmetry. It can be shown that $\mathbf{\Phi}_i$ is invertible if and only if the complex matrix $\mathbf{U}_i + j\mathbf{V}_i$ is invertible with its inverse being given by $\tilde{\mathbf{U}}_i - j\tilde{\mathbf{V}}_i$. As a result, the parameterization of the invertible $M \times M$ matrix $\mathbf{\Phi}_i$ is equivalent to that of the $\frac{M}{2} \times \frac{M}{2}$ complex matrix $\mathbf{U}_i + j\mathbf{V}_i$. Noting that this complex matrix can be parameterized to $M^2/2$ real-valued coefficients, the number of free parameters is reduced by one-half compared to M^2 parameters required by a general invertible matrix.

5.5.2 Objective Function

In our design, the stopband attenuation as well as the coding gain is used to form the objective function for the optimization of the free parameters, namely, the overall criteria for the maximization problem is given by

$$C_{overall} = \gamma_1 C_{\text{analysis}} + \gamma_2 C_{\text{synthesis}} + \gamma_3 C_{\text{coding gain}} \tag{5.57}$$

where γ_i $(i = 1,2,3)$ is the weighting coefficient, C_{analysis} the stopband attenuation of the analysis filters, $C_{\text{synthesis}}$ that of the synthesis ones and $C_{\text{coding gain}}$ the coding gain of the filter bank. Among these criteria, the stopband attenuations are defined as

$$C_{\text{analysis}} = -10\log_{10} \sum_{k=0}^{M-1} \int_{\omega \in \Omega_k} \left| H_k(e^{j\omega}) \right|^2 d\omega$$

$$C_{\text{synthesis}} = -10\log_{10} \sum_{k=0}^{M-1} \int_{\omega \in \Omega_k} \left| F_k(e^{j\omega}) \right|^2 d\omega \tag{5.58}$$

where the stopbands are set to be

$$\Omega_k = [0, \max(0, (k-0.6)\pi/M)] \cup [\pi, \min(\pi, (k+1.6)\pi/M)]$$

The coding gain, which measures the energy compaction capability of a filter bank, is given by [104],

$$C_{\text{coding gain}} = 10\log_{10} \frac{\sigma_x^2}{\left(\prod_{k=0}^{M-1} \sigma_{x_k}^2 \left\| f_k \right\|^2 \right)^{1/M}} \tag{5.59}$$

where σ_x^2 represents the variance of the input signal $x[n]$, $\sigma_{x_k}^2$ the variance of the kth subband signal $x_k[n]$ and $\left\| f_k \right\|^2$ the norm of the kth synthesis filter. It is worth-mentioning that (5.59) is the generalized version of the conventional coding gain defined for PUFB. It has been modified for PRFB by incorporating the norm of the synthesis filters [106]. The input signal $x[n]$ is assumed to be the commonly-used AR(1) process with the

intersample autocorrelation coefficient $\rho = 0.95$. In this paper, a nonlinear unconstrained optimization technique termed as *fminuc* provided in Matlab software is used to solve the maximization problem in (5.57), in which equal weights are considered.

5.5.3 Numerical Examples

With the PR and MIS structurally satisfied by the lattice structure, we may determine the parameter coefficients by the unconstrained optimization with the given objective function.

Example 1: Four-Channel MIS-PRFBs

In the first example, several four-channel MIS-PRFBs with different filter lengths 4, 8, 12 and 16 are designed and compared with other types of PRFBs such as the general PRFB without any symmetry constraint and the LPPRFBs in [74]. To make a fair comparison, the delay matrices for the three types of filter banks are fixed as $\mathbf{\Lambda}(z) = \mathrm{diag}\left(\mathbf{I}_{M/2}, z^{-1}\mathbf{I}_{M/2}\right)$, the only difference among them being the invertible matrix $\mathbf{\Phi}_i$. In the general PRFB, $\mathbf{\Phi}_i$ has M^2 parameters, whereas in the other two it contains only $M^2/2$ parameters. The stopband attenuation and the coding gain of the three types of filter banks designed under different filter lengths are listed in Tables 5.1 and 5.2, respectively. It is seen that, regardless of the value of K, the stopband attenuation of MIS-PRFB is comparable with that of the general PRFB, but much better than that of the LPPRFB. The coding gain of MIS-PRFB is also better than that of LPPRFB except for K=1. Also, for the three types of filter banks, as the order K increases, the stopband attenuation increases linearly, while the gain of coding improves only marginally. This result is natural, since a longer filter length gives a better stopband attenuation, while the coding gain, measuring the ability of energy compaction, is more relevant to the number

of channels. Fig. 5.4 shows the frequency response of the analysis and synthesis parts of the resulting three types of filter banks of length 8. It is interesting to note that the general PRFB tends to have a nearly mirror-image symmetric frequency response, even though no such symmetry has been utilized in the design. The LPPRFB gives a poor performance in terms of the stopband attenuation, although it has a reduced number of parameters. As a compromise, the MIS-PRFB has decreased the number of free parameters by one-half while providing as a good performance as the general PRFB.

Table 5.1: Stopband attenuation (dB) of PRFB, LPPRFB and MIS-PRFB with different filter lengths

K	PRFB	LPPRFB	MIS-PRFB
1	9.5115	9.2884	9.7755
2	18.8216	15.0978	19.0840
3	27.5564	17.5530	27.9373
4	30.8569	20.2468	31.0289

Table 5.2: Coding gain (dB) of PRFB, LPPRFB and MIS-PRFB with different filter lengths

K	PRFB	LPPRFB	MIS-PRFB
1	7.6426	7.5825	7.5516
2	8.2083	7.9605	8.1361
3	8.5163	8.2157	8.3493
4	8.6912	8.3693	8.4781

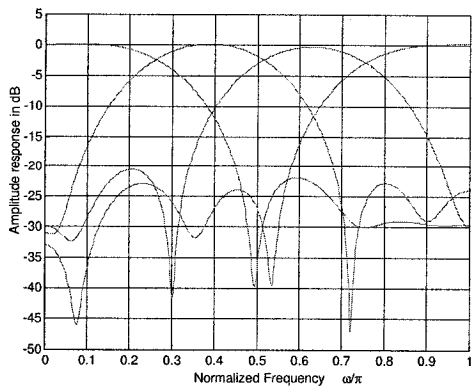

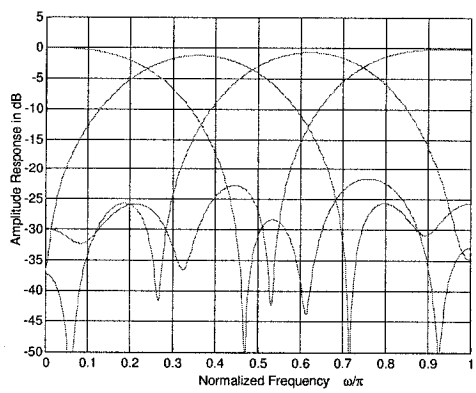

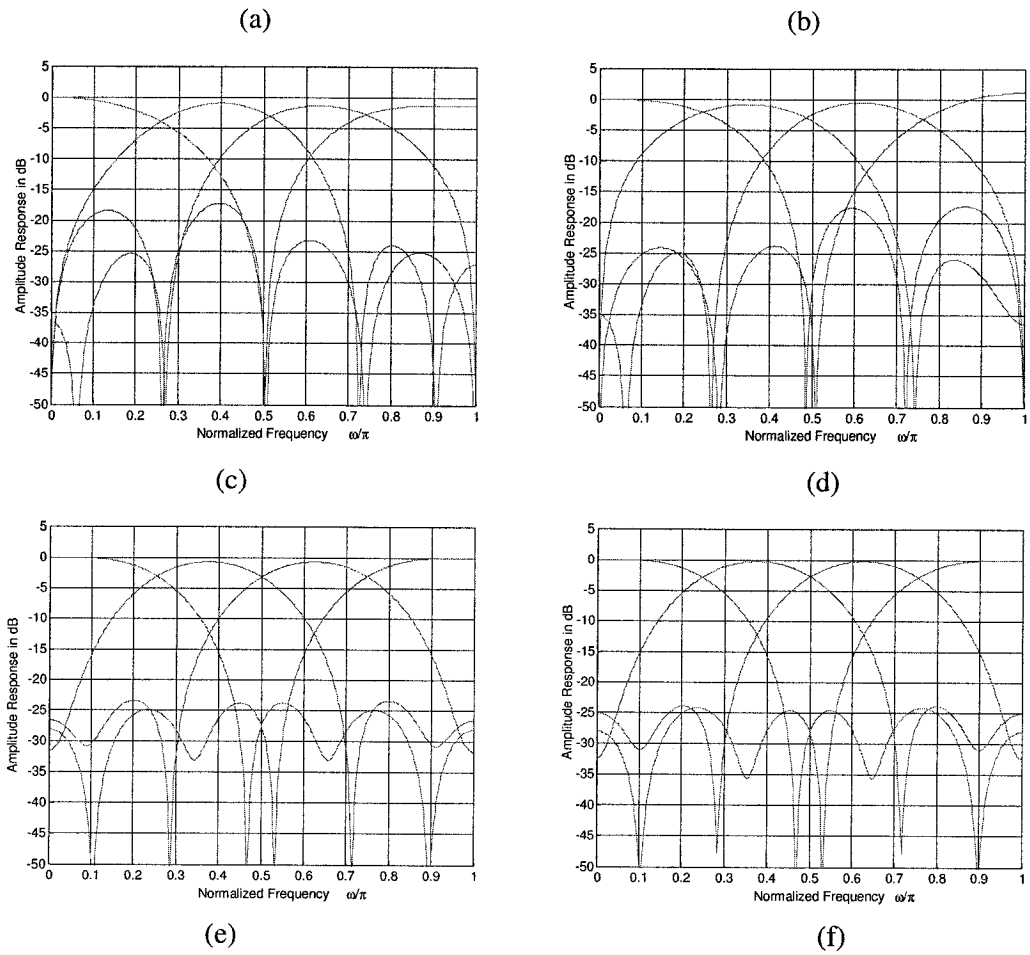

Figure 5.4: Frequency response of four-channel PRFBs.
From top to bottom row, (a) and (b) for PRFB, (c) and (d) for LPPRFB, (e) and (f) for MIS-PRFB, respectively. From left to right column, (a), (c) and (e) for analysis filters, (b), (d) and (f) for synthesis filters, respectively.

Example 2: An Eight-Channel MIS-PRFB

In the second example, an eight-channel MIS-PRFB having 16-tap individual filters is designed, resulting in the amplitude response of both the analysis and the synthesis filters shown in Fig. 5.5. For comparison, we have also designed an eight-channel MIS-PUFB with 16-tap filters and shown its amplitude response in Fig. 5.5 together with that of the designed MIS-PRFB. It is found that the stopband attenuation of MIS-PRFB is 17.7494

dB in the analysis bank and 18.4446 dB in the synthesis bank, and the coding gain is 9.7614 dB. The stopband attenuation and the coding gain of the MIS-PUFB are 17.7692dB and 9.8412dB, respectively. Clearly, the MIS-PRFB and the MIS-PUFB both provide a similar performance in terms of the two criteria employed despite the fact that the MIS-PRFB is a more general case where the analysis and synthesis banks could be designed separately to meet the requirements of particular applications. It is also noted that the eight-channel MIS-PRFB has a much better coding gain compared with that of the four-channel bank of the same filter length.

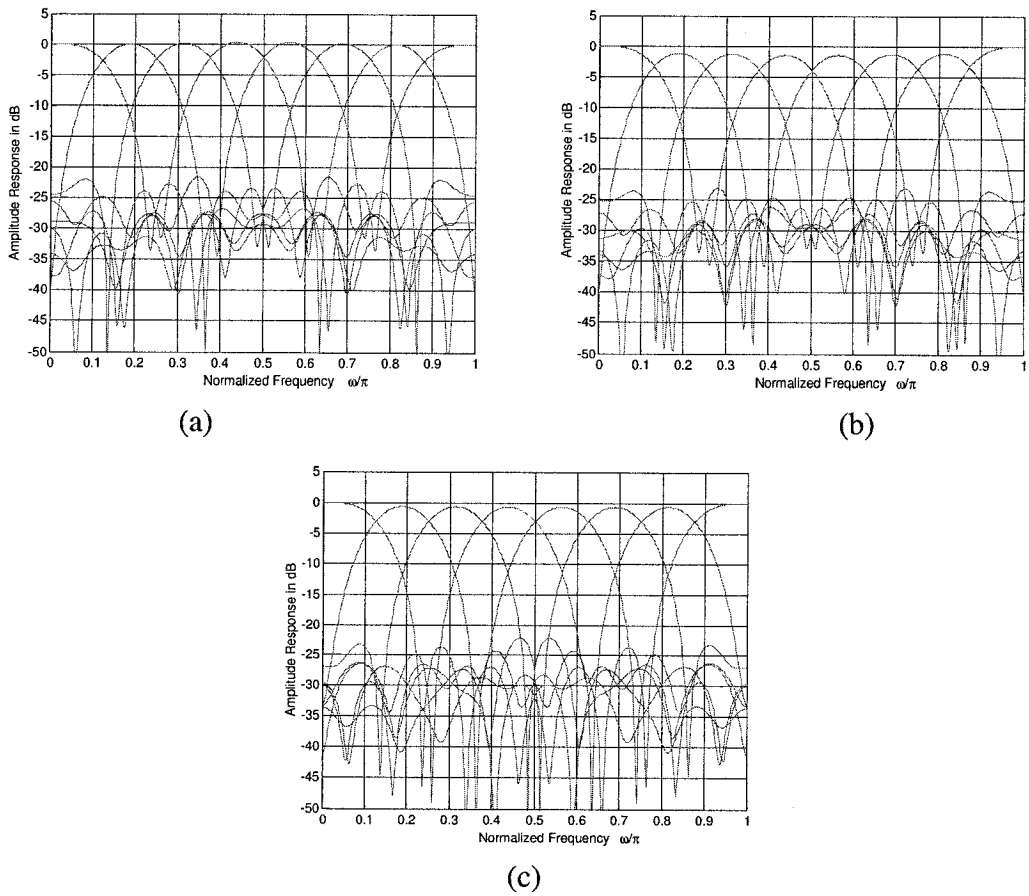

Figure 5.5: Frequency response of eight-channel filter banks with length 16. (a) Analysis filters of MIS-PRFB. (b) Synthesis filters of MIS-PRFB. (c) Analysis and synthesis filters of MIS-PUFB

Example 3: A Three-Channel MIS-PRFB

As another example, an odd-channel MIS-PRFB is designed to complete the proposed lattice structure. Recalling that the order of an odd-channel MIS-PRFB has to be odd, the number of channels is set to 3 and the length of the individual filters chosen as 9 in this example. The designed MIS-PRFB has its amplitude response as shown in Fig. 5.6, in which the stopband attenuation is found to be 12.0135 dB in the analysis bank and 12.3226 dB in the synthesis part, while the coding gain is 6.3842 dB.

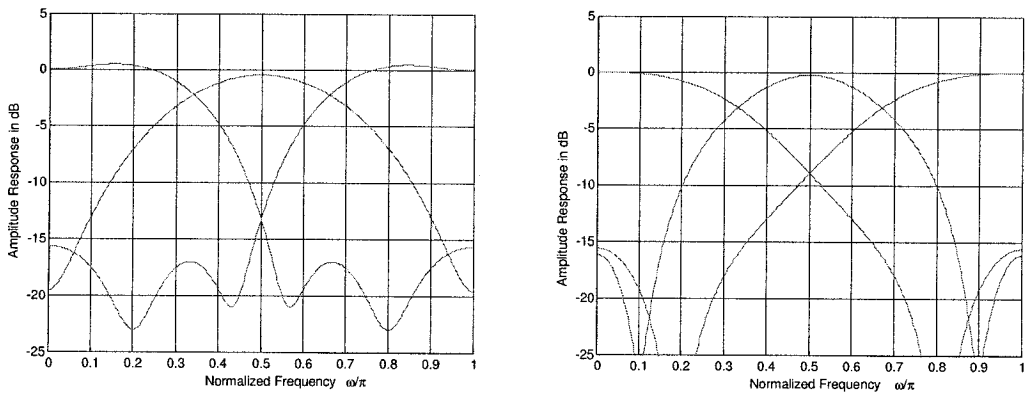

(a) (b)

Figure 5.6: Frequency response of a three-channel MIS-PRFB.
(a) Analysis filters. (b) Synthesis filters.

5.6 Conclusion

The lattice structure of perfect-reconstruction filter banks with mirror-image symmetry has been investigated. By developing an order-one building block that is capable of propagating both the MIS and the PR properties, a complete and minimal lattice structure for an even-channel MIS-PRFB has been obtained. It has also been shown that the basic building block has to be at least of order two to construct the lattice

structure of an odd-channel MIS-PRFB. Using the lifting scheme in conjunction with two optimization criteria, the proposed MIS-PRFB has been designed and compared with general PRFBs, linear-phase PRFBs and MIS-PUFBs. Simulation results have shown that the proposed MIS-PRFB is superior to the LPPRFB with the same number of free parameters in terms of the stopband attenuation, while it is comparable to the general PRFB of the same filter order which however has twice the number of free parameters as the MIS-PRFB does. In comparison with the MIS-PUFB, the MIS-PRFB has relaxed the unitary requirement to the invertible one while yielding a similar performance in both the stopband attenuation and the coding gain.

Chapter 6

Cosine-Modulated Filter Banks with Perfect Reconstruction

6.1 Introduction

As seen in Chapter 5, the design and implementation of PUFBs is a formidable task due to a considerable number of free parameters and the highly complicated nonlinear optimization involved. As such, Nguyen *et al.* [49] have introduced the MIS property on PRFBs, which is able to reduce the number of parameters by almost one-half. Fig. 6.1 shows the frequency response of a typical M-channel filter bank, where the entire frequency is evenly divided into M bands by analysis filters. This uniform separation endorses certain symmetry on both the analysis and synthesis filters. Note that the frequency responses of the analysis filters are symmetric about the center point $\pi/2$. Moreover, each analysis filter is a frequency-shifted duplication of the same prototype filter. This observation has triggered the idea of using the cosine-modulated filter banks (CMFBs), where all the analysis filters are generated from identical low-pass prototype filters through a proper modulation [87]-[89]. With only one filter to be designed instead of all the M analysis filters, the design and implementation complexity of CMFBs has

been significantly reduced. The CMFB with perfect reconstruction, which belongs to PUFBs, was proposed by Koilpillai *et al.* [89],

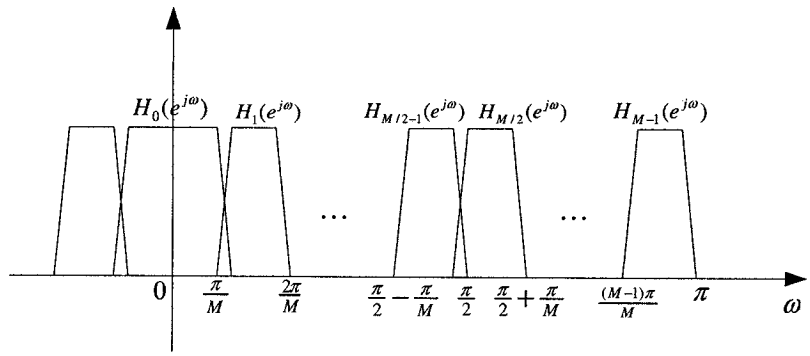

Figure 6.1: Typical frequency response of an M-channel filter banks

Although it is quite obvious that the CMFB also satisfies the MIS property, the relationship between the MIS-PUFBs and CMFBs have not been explicitly investigated. From the modulation perspective, a MIS-PUFB has M independent analysis filters while a CMFB contains only one, leaving a gap between them. In this chapter, we attempt to fill this gap. First, we show that the implementation structure of CMFB in [89] is redundant. By exploiting the linear-phase property of the prototype filter, the lattice structure of the CMFBs is rewritten and simplified in the form of order-one factorization. Based on this factorization, CMFB and PUFB are then encompassed in a uniform expression. Under this framework, the computational simplicity of CMFBs is explicitly demonstrated via the unitary matrices with bidiagonal sparse coefficients. Then, by introducing more prototype filters, in conjunction with a proper modulation, new CMFBs are generated, whose unitary matrices have more parameters than the bidiagonal sparse one in the conventional CMFB. In this sense, the CMFBs are generalized and a bridge is built between the CMFB and MIS-PUFBs.

6.2 CMFBs and MIS-PUFBs

6.2.1 Conventional Implementation of CMFBs

In [89], the analysis filters $h_k[n]$ and synthesis filters $f_k[n]$ are given by

$$h_k[n]=2h[n]\cos\left[(2k+1)\frac{\pi}{2M}\left(n-\frac{N-1}{2}\right)+(-1)^k\frac{\pi}{4}\right], \tag{6.1}$$

$$f_k[n]=2h[n]\cos\left[(2k+1)\frac{\pi}{2M}\left(n-\frac{N-1}{2}\right)-(-1)^k\frac{\pi}{4}\right], \tag{6.2}$$

$$n=0,1,\cdots,N-1,k=0,1,\cdots,M-1$$

where $h[n]$ is a linear-phase filter with length $N=2mM$. Note that the cosine modulation has a periodicity of $2M$, the polyphase matrix of the corresponding analysis filters can be written as

$$\mathbf{E}(z)=\sqrt{M}\mathbf{C}[(\mathbf{I}-\mathbf{J}) \quad -(\mathbf{I}+\mathbf{J})]\begin{bmatrix}\mathbf{G}_0(-z^2)\\ z^{-1}\mathbf{G}_1(-z^2)\end{bmatrix} \tag{6.3}$$

where $\mathbf{C}$ is the modulation matrix whose elements are given by

$$[\mathbf{C}]_{k,l}=\sqrt{\frac{2}{M}}\cos\left(\frac{\pi}{M}\left(k+\frac{1}{2}\right)\left(l+\frac{1}{2}\right)\right)$$

and

$$\mathbf{G}_0(z)=\mathrm{diag}(G_0(z) \quad G_1(z) \quad \cdots \quad G_{M-1}(z))$$

$$\mathbf{G}_1(z)=\mathrm{diag}(G_M(z) \quad G_{M+1}(z) \quad \cdots \quad G_{2M-1}(z))$$

Note that the matrix $\mathbf{C}$ is the famous type-IV M-point DCT and $G_l(z)$ is the $2M$-polyphase subfilter of the prototype filter. It is easy to check that the synthesis filters are the time-reverse of the analysis filters and the necessary and sufficient condition for the cosine-modulated FB to be perfect reconstruction is then given by

$$\tilde{G}_k(z)G_k(z)+\tilde{G}_{M+k}(z)G_{M+k}(z)=\frac{1}{2M},\quad 0\le k\le M/2-1 \tag{6.4}$$

Obviously, the condition in (6.4) can be realized through the following lattice structure:

$$\begin{bmatrix} G_k(z) \\ G_{M+k}(z) \end{bmatrix}=\prod_{k=0}^{m-1}\left(\begin{bmatrix} \cos\theta_k & \sin\theta_k \\ \sin\theta_k & -\cos\theta_k \end{bmatrix}\begin{bmatrix} 1 & 0 \\ 0 & z^{-1} \end{bmatrix}\right)\begin{bmatrix} 1 \\ (-1)^m \end{bmatrix} \tag{6.5}$$

The implementation of (6.3) is shown in Fig. 6.2. It should be noticed that in (6.3) the linear-phase property of the prototype filter is not exploited, leaving a room for the development of a more efficient structure.

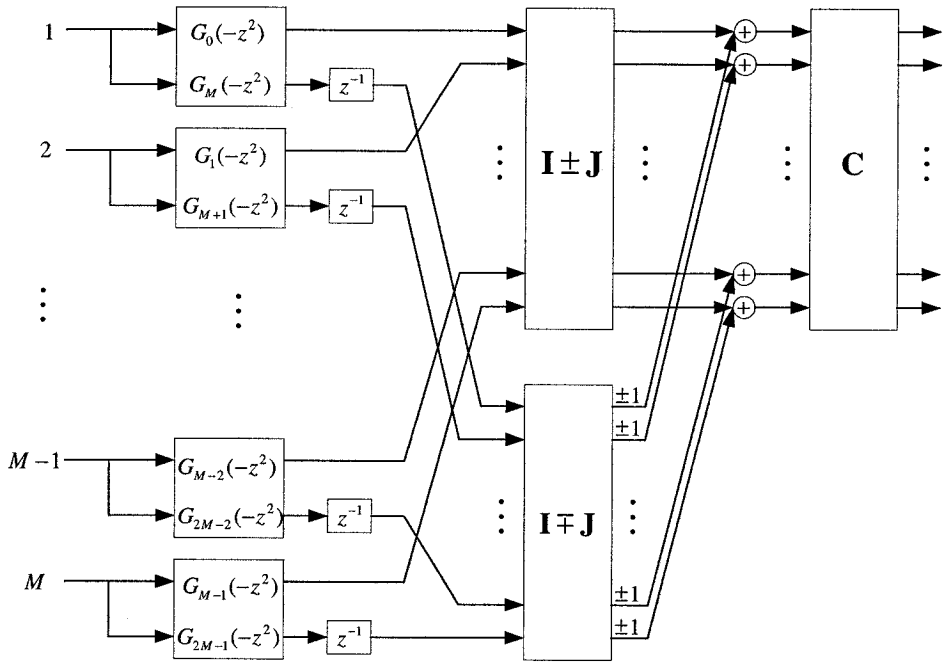

Figure 6.2: Implementation of CMFB with perfect reconstruction

6.2.2 Simplified Implementation of CMFBs

For the DCT-IV transform, we have

$$\begin{aligned}
&\cos\left(\frac{\pi}{M}\left(k+\frac{1}{2}\right)\left(l+\frac{1}{2}\right)\right)+\cos\left(\frac{\pi}{M}\left(k+\frac{1}{2}\right)\left(M-1-l+\frac{1}{2}\right)\right)\\
&=2\cos\left(\frac{\pi}{2M}\left(k+\frac{1}{2}\right)(2l-M+1)\right)\cos\left(\frac{\pi}{2M}\left(k+\frac{1}{2}\right)M\right)\\
&=\rho\sqrt{2}\cos\left(\frac{\pi}{M}\left(k+\frac{1}{2}\right)\left(\frac{M-1}{2}-l\right)\right)
\end{aligned} \tag{6.6}$$

$$\begin{aligned}
&\cos\left(\frac{\pi}{M}\left(k+\frac{1}{2}\right)\left(l+\frac{1}{2}\right)\right)-\cos\left(\frac{\pi}{M}\left(k+\frac{1}{2}\right)\left(M-1-l+\frac{1}{2}\right)\right)\\
&=2\cos\left(\frac{\pi}{2M}\left(k+\frac{1}{2}\right)M\right)\cos\left(\frac{\pi}{2M}\left(k+\frac{1}{2}\right)(2l-M+1)\right)\\
&=\rho\sqrt{2}\cos\left(\frac{\pi}{M}\left(k+\frac{1}{2}\right)\left(l-\frac{M-1}{2}\right)\right)
\end{aligned} \tag{6.7}$$

Using (6.6) and (6.7), and noticing the symmetry of DCT,

$$\cos\left(\frac{\pi}{M}\left(k+\frac{M}{2}+\frac{1}{2}\right)\left(l+\frac{1}{2}\right)\right)=\cos\left(\frac{\pi}{M}\left(k+\frac{1}{2}\right)\left(l+\frac{M}{2}+\frac{1}{2}\right)\right) \tag{6.8}$$

the polyphase matrix in (6.3) can be rewritten as

$$\mathbf{E}(z)=\sqrt{M}\mathbf{DC}\boldsymbol{\Lambda}(z)\mathbf{G}(z^2) \tag{6.9}$$

where

$$\mathbf{G}(z)=\begin{bmatrix}
 & G_{M/2-1}(z) & G_{M/2}(z) & \\
\iddots & & & \ddots \\
G_0(z) & & & G_{M-1}(z) \\
G_M(z) & & & -G_{2M-1}(z) \\
\ddots & & & \iddots \\
 & G_{M+M/2-1}(z) & -G_{M+M/2}(z) &
\end{bmatrix}$$

$$\boldsymbol{\Lambda}(z)=\begin{bmatrix}
1 & & & & \\
 & \ddots & & & \\
 & & 1 & & \\
 & & & z^{-1} & \\
 & & & & \ddots \\
 & & & & z^{-1}
\end{bmatrix}$$

In (6.9), the polyphase matrix is decomposed into a cascade of a modulation matrix $\mathbf{C}$, a delay matrix $\mathbf{\Lambda}(z)$ and a sparse polyphase matrix $\mathbf{G}(z^2)$. Since $\mathbf{C}$ is orthogonal, the paraunitary condition for CMFB then becomes $\tilde{\mathbf{G}}(z)\mathbf{G}(z)=z^{-n_0}\mathbf{I}$. Notice that $\mathbf{G}(z)$ is a sparse matrix with a diamond pattern, the paraunitary condition for $\mathbf{G}(z)$ is equivalent to the condition that the $M/2$ matrices $\begin{bmatrix} G_k(z) & G_{M-1-k}(z) \\ G_{M+k}(z & -G_{2M-1-k}(z) \end{bmatrix}$ $(k=0,1,\ldots,M/2-1)$ with their order being reduced to 2×2, are paraunitary. This condition can be readily realized by cascading a number of 2×2 lattice structures

$$\begin{bmatrix} G_k(z) & G_{M-1-k}(z) \\ G_{M+k}(z & -G_{2M-1-k}(z) \end{bmatrix} = \prod_{k=0}^{m-1}\left(\begin{bmatrix} \cos\theta_k & \sin\theta_k \\ \sin\theta_k & -\cos\theta_k \end{bmatrix}\begin{bmatrix} 1 & 0 \\ 0 & z^{-1} \end{bmatrix}\right)\begin{bmatrix} 1 & 0 \\ 0 & (-1)^m \end{bmatrix} \tag{6.10}$$

Comparing (6.10) with (6.9), one can see that the two 2×1 matrices are merged into one 2×2 matrix and therefore, one-half of the implementation cost is saved. Substituting (6.10) into (6.9), we get the simplified implementation of the CMFB,

$$\mathbf{E}(z)=\sqrt{M}\mathbf{D}\mathbf{C}\mathbf{\Lambda}(z)\prod_{i=m}^{1}\left(\mathbf{Q}_i\mathbf{\Lambda}(z^2)\right)\mathbf{Q}_0 \tag{6.11}$$

where

$$\mathbf{Q}_i = \begin{bmatrix} & & \cos\theta_{M/2-1,i} & \sin\theta_{M/2-1,i} & & \\ & \iddots & & & \ddots & \\ \cos\theta_{0,i} & & & & & \sin\theta_{0,i} \\ \sin\theta_{0,i} & & & & & -\cos\theta_{0,i} \\ & \ddots & & & \iddots & \\ & & \sin\theta_{M/2-1,i} & -\cos\theta_{M/2-1,i} & & \end{bmatrix}$$

In (6.11), the polyphase matrix is decomposed into a cascade of $M\times M$ unitary matrices with a sparse structure and all the delays are located in separated diagonal matrices. The lattice structure in (6.11) is shown in Fig. 6.3. From the realization in Fig. 6.2 and its

simplified version in Fig. 6.3, one can clearly see that the implementation cost is saved by 50%. This saving is attributed to the linear-phase of the prototype filter and the symmetry of the DCT transform.

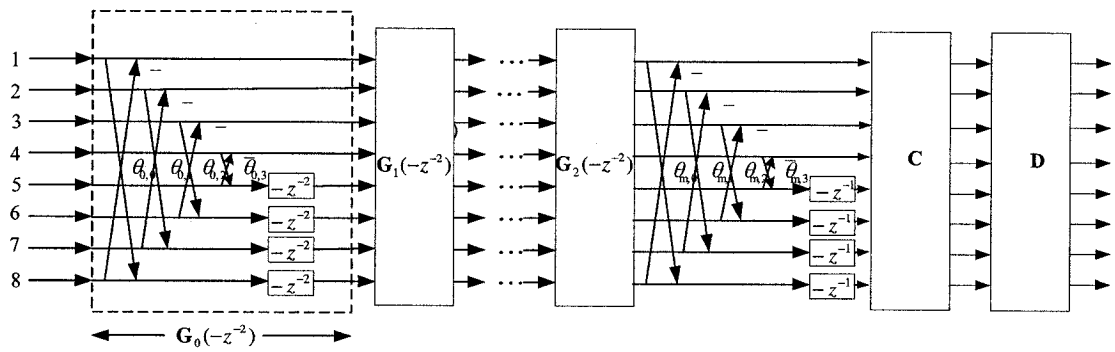

Figure 6.3: Simplified Implementation of CMFB

6.2.3 Order-One Factorization of CMFBs and MIS-PUFBs

Using (6.1) and the linear-phase property $h[N-1-n]=h[n]$, it is not difficult to get the following equation:

$$\begin{aligned}
&h_{M-1-k}[N-1-n] \\
&=2h[N-1-n]\cos\left[(2M-1-2k)\frac{\pi}{2M}\left(N-1-n-\frac{N-1}{2}\right)+(-1)^{M-1-k}\frac{\pi}{4}\right] \\
&=2h[n]\cos\left[\pi\left(\frac{N-1+(-1)^k}{2}-n\right)+(2k+1)\frac{\pi}{2M}\left(n-\frac{N-1}{2}\right)+(-1)^k\frac{\pi}{4}\right] \\
&=\pm(-1)^n 2h[n]\cos\left[(2k+1)\frac{\pi}{2M}\left(n-\frac{N-1}{2}\right)+(-1)^k\frac{\pi}{4}\right] \\
&=\pm h_k[n]
\end{aligned} \tag{6.12}$$

This implies that the CMFB is actually a mirror-image symmetric filter bank. In Chapter 5, we have already investigated the order-one factorization of MIS-PUFB. Now with the order-one factorization as (6.11) for CMFBs, it would be interesting to study the difference between CMFBs and MIS-PUFBs from the point of view of the lattice

structure. The new factorization (6.11) not only reduces the implementation complexity, but also provides us with a starting point to establish a relationship between CMFB and PUFB.

In Chapter 5 we have already attained a lattice structure for MIS-PUFBs as

$$\begin{aligned}\mathbf{E}(z) &= \prod_{i=K-1}^{1}(\mathbf{\Phi}_i\mathbf{\Lambda}_i(z))\mathbf{G}_0 \\ &= \prod_{i=K-1}^{1}\left(\begin{bmatrix}\mathbf{U}_i & -\mathbf{V}_i\\ \mathbf{V}_i & \mathbf{U}_i\end{bmatrix}\begin{bmatrix}\mathbf{I}_{M/2} & \mathbf{0}\\ \mathbf{0} & z^{-1}\mathbf{I}_{M/2}\end{bmatrix}\right)\begin{bmatrix}\mathbf{U}_0 & -\mathbf{V}_0\\ \mathbf{V}_0 & \mathbf{U}_0\end{bmatrix}\begin{bmatrix}\mathbf{I}_{M/2} & \mathbf{0}\\ \mathbf{0} & \mathbf{\Gamma J}_{M/2}\end{bmatrix}\end{aligned} \tag{6.13}$$

Comparing (6.11) and (6.13), the following observations pertaining to the similarity as well as the difference between MIS-PUFBs and CMFBs can be made.

1. In both the structures, the free parameters are contained in a matrix at each stage. The only difference is that in CMFB, $\mathbf{Q}_i$ is a sparse matrix with diamond entries while for MIS-PUFB, $\mathbf{\Phi}_i$ is a full matrix with a certain symmetry. Both the matrices are orthogonal and thus, can be represented by a set of plane rotations $\{\theta_{i,k}\}$. Note that $\mathbf{Q}_i$ has $M/2$ free parameters, while $\mathbf{\Phi}_i$ has $M(M-2)/4$ parameters.
2. Each structure has a special matrix, namely, $\mathbf{G}_0$ in MIS-PUFB and $\mathbf{C}$ in CMFB. Obviously, the DCT matrix $\mathbf{C}$ in the CMFB is a special case of $\mathbf{G}_0$ whose general form is given by

$$\mathbf{G}_0 = \begin{bmatrix}\hat{\mathbf{U}}_0 & -\hat{\mathbf{V}}_0\\ \hat{\mathbf{V}}_0 & \hat{\mathbf{U}}_0\end{bmatrix}\text{diag}(\mathbf{I}, \mathbf{\Gamma J})$$

In the case of CMFB, the DCT matrix acts as a modulation matrix located at the left end of the lattice structure, while $\mathbf{G}_0$ is at the right end serving as an initial stage.

3. At each stage, owing to the difference of $\Lambda(z^2)$ in (6.11) and $\Lambda(z)$ in (6.13), the order of the CMFB is reduced by two while that of the MIS-PUFB is reduced by one only.

From (6.11), we can easily realize that the computational efficiency of CMFBs comes from two parts. First, the general unitary matrix is reduced to a sparse diagonal matrix, which saves $M(M-4)/4$ parameters. Second, since the factorization in the CMFB is of order two, one-half of the matrices are saved. Actually, we can rewrite (6.13) in the same form as (6.11), where one can clearly see that the CMFB is a special case of the MIS-PUFB. Through inserting a pair of inverse matrices $\begin{bmatrix}\mathbf{I} & \mathbf{0}\\ \mathbf{0} & \mathbf{D}_t\mathbf{J}\end{bmatrix}\begin{bmatrix}\mathbf{I} & \mathbf{0}\\ \mathbf{0} & \mathbf{J}\mathbf{D}_t\end{bmatrix}$ between $\mathbf{G}_i(z)$ and $\mathbf{G}_{i+1}(z)$, the initial zero-order mirror-image block at the right end of the lattice structure can be moved to the left end,

$$
\begin{aligned}
\mathbf{E}(z) &= \prod_{i=K-1}^{1}\left(\begin{bmatrix}\mathbf{U}_i & -\mathbf{V}_i\\ \mathbf{V}_i & \mathbf{U}_i\end{bmatrix}\begin{bmatrix}\mathbf{I} & \mathbf{0}\\ \mathbf{0} & z^{-1}\mathbf{I}\end{bmatrix}\right)\begin{bmatrix}\mathbf{U}_0 & -\mathbf{V}_0\\ \mathbf{V}_0 & \mathbf{U}_0\end{bmatrix}\begin{bmatrix}\mathbf{I} & \mathbf{0}\\ \mathbf{0} & \mathbf{D}_t\mathbf{J}\end{bmatrix}\\
&= \begin{bmatrix}\mathbf{U}_{K-1} & -\mathbf{V}_{K-1}\\ \mathbf{V}_{K-1} & \mathbf{U}_{K-1}\end{bmatrix}\begin{bmatrix}\mathbf{I} & \mathbf{0}\\ \mathbf{0} & z^{-1}\mathbf{I}\end{bmatrix}\begin{bmatrix}\mathbf{I} & \mathbf{0}\\ \mathbf{0} & \mathbf{D}_t\mathbf{J}\end{bmatrix}\prod_{i=K-2}^{1}\left(\begin{bmatrix}\mathbf{I} & \mathbf{0}\\ \mathbf{0} & \mathbf{J}\mathbf{D}_t\end{bmatrix}\begin{bmatrix}\mathbf{U}_i & -\mathbf{V}_i\\ \mathbf{V}_i & \mathbf{U}_i\end{bmatrix}\begin{bmatrix}\mathbf{I} & \mathbf{0}\\ \mathbf{0} & z^{-1}\mathbf{I}\end{bmatrix}\begin{bmatrix}\mathbf{I} & \mathbf{0}\\ \mathbf{0} & \mathbf{D}_t\mathbf{J}\end{bmatrix}\right)\cdot\\
&\quad \begin{bmatrix}\mathbf{I} & \mathbf{0}\\ \mathbf{0} & \mathbf{J}\mathbf{D}_t\end{bmatrix}\begin{bmatrix}\mathbf{U}_0 & -\mathbf{V}_0\\ \mathbf{V}_0 & \mathbf{U}_0\end{bmatrix}\begin{bmatrix}\mathbf{I} & \mathbf{0}\\ \mathbf{0} & \mathbf{D}_t\mathbf{J}\end{bmatrix}\\
&= \begin{bmatrix}\mathbf{U}_{K-1} & -\mathbf{V}_{K-1}\\ \mathbf{V}_{K-1} & \mathbf{U}_{K-1}\end{bmatrix}\begin{bmatrix}\mathbf{I} & \mathbf{0}\\ \mathbf{0} & \mathbf{D}_t\mathbf{J}\end{bmatrix}\prod_{i=K-2}^{0}\left(\begin{bmatrix}\mathbf{I} & \mathbf{0}\\ \mathbf{0} & z^{-1}\mathbf{I}\end{bmatrix}\begin{bmatrix}\mathbf{U}_i & -\mathbf{D}_t\mathbf{J}\mathbf{V}_i\\ \mathbf{J}\mathbf{D}_t\mathbf{V}_i & \mathbf{J}\mathbf{D}_t\mathbf{U}_i\mathbf{D}_t\mathbf{J}\end{bmatrix}\right)
\end{aligned}
\tag{6.14}
$$

In (6.14), by letting $\begin{bmatrix} \mathbf{U}_{K-1} & -\mathbf{V}_{K-1} \\ \mathbf{V}_{K-1} & \mathbf{U}_{K-1} \end{bmatrix} \begin{bmatrix} \mathbf{I} & \mathbf{0} \\ \mathbf{0} & \mathbf{D}_t\mathbf{J} \end{bmatrix}$ be $\mathbf{C}_M^{IV}$ and noticing that $\mathbf{U}_i = \text{diag}\{\cos\theta_{i,0} \quad \cdots \quad \cos\theta_{i,M/2-1}\}$ and $\mathbf{V}_i = \text{diag}\{\sin\theta_{i,0} \quad \cdots \quad \sin\theta_{i,M/2-1}\}$, one can easily verify that (6.11) is a special case of (6.14).

6.3 CMFBs with Multiple Prototype Filters

It is seen from the above section that the CMFB realized with order-one factorization has the same expression as the general MIS-PUFBs. Moreover, this uniform expression provides us another perspective to study the CMFBs. The advantage of the CMFBs has been justified in the form of sparse unitary matrices. Compared to the general PUFBs, a CMFB contains sparse unitary matrices and in turn involves fewer rotation angles, which reduce the complexity in both design and implementation. On the other hand, there might be a sacrifice in the performance of the filter bank, such as the stopband energy, due to the limited choice of free parameters. From the modulation point of view, the conventional CMFB is generated from one prototype filter only while a general PUFB contains M independent filters. In this sense, the CMFB can be generalized by allowing for multiple filters such that extra parameters are introduced and a tradeoff can be made between the complexity and the performance. Moreover, a bridge has been built between the CMFBs and the general PUFBs and therefore, discussions for the case of multiple prototype filters can be made under the same framework. Of course, the new FB generated from more filters should contain more parameters than the traditional CMFBs. The number of parameters can be determined by the tradeoff between the complexity and the performance of the resulting FB. In this section, we first investigate the polyphase

matrix of a particular sparse pattern of a CMFB obtained from a modulation scheme, and then generate a CMFB with multiple prototype filters by combining the CMFBs with different sparse patterns.

In a conventional CMFB, the sparse matrix has diamond-shaped non-zero entries. It should be noted that the sparse pattern of $\mathbf{G}(z)$ depends on the modulation scheme. By modifying the modulation function, one may get different types of CMFBs with various sparse matrix patterns. For example, a CMFB can be generated by using the following modulation scheme,

$$h_k[n] = 2p[n]\cos\left[(2k+1)\frac{\pi}{2M}\left(n+\frac{1}{2}\right)+(-1)^k\frac{\pi}{4}\right] \tag{6.15}$$

whose polyphase representation can be given by

$$\mathbf{E}(z) = \sqrt{M}\mathbf{D}\mathbf{C}\boldsymbol{\Lambda}(z)\mathbf{G}^{(1)}(z^2) \tag{6.16}$$

where

$$\mathbf{G}^{(1)}(z) = \begin{bmatrix} -G_M(z) & & & & G_{2M-1}(z) \\ & \ddots & & \ddots & \\ & & -G_{\frac{3M}{2}-1}(z) \;\; G_{\frac{3M}{2}}(z) & & \\ & & G_{\frac{M}{2}-1}(z) \;\; G_{\frac{M}{2}}(z) & & \\ & \iddots & & \ddots & \\ G_0(z) & & & & G_{M-1}(z) \end{bmatrix}$$

The polyphase matrix in (6.16) has the same form as that in (6.9), except that $\mathbf{G}^{(1)}(z)$ has bi-diagonal sparse elements while the sparse matrix $\mathbf{G}(z)$ in (6.9) is of diamond shape. Either the diamond or bidiagonal pattern is regular, i.e., its inverse has the same sparse structure. Combining (6.1) and (6.15), we get a new CMFB generated from two prototype filters,

$$h_k[n]=2p[n]\cos\left[(2k+1)\frac{\pi}{2M}\left(n-\frac{N-1}{2}\right)+(-1)^k\frac{\pi}{4}\right] +2q[n]\cos\left[(2k+1)\frac{\pi}{2M}\left(n+\frac{1}{2}\right)+(-1)^k\frac{\pi}{4}\right] \quad (6.17)$$

$$(n=0,1,\cdots,N-1, k=0,1,\cdots,M-1)$$

where $p[n]$ and $q[n]$ are linear-phase filters with length $N=2mM$. From (6.16) and (6.9), the polyphase matrix corresponding to (6.17) is given by

$$\mathbf{E}(z)=\sqrt{M}\mathbf{DC}\Lambda(z)\mathbf{G}^{(2)}(z^2) \quad (6.18)$$

where

$$\mathbf{G}^{(2)}(z)=\begin{bmatrix} G_{0,0}(z) & \cdots & G_{0,M/2-1}(z) & G_{0,M/2}(z) & \cdots & G_{0,M-1}(z) \\ \vdots & \ddots & \vdots & \vdots & \ddots & \vdots \\ G_{M/2-1,0}(z) & \cdots & G_{M/2-1,M/2-1}(z) & G_{M/2-1,M/2}(z) & \cdots & G_{M/2-1,M-1}(z) \\ G_{M/2,0}(z) & \cdots & G_{M/2,M/2-1}(z) & G_{M/2,M/2}(z) & \cdots & G_{M/2,M-1}(z) \\ \vdots & \ddots & \vdots & \vdots & \ddots & \vdots \\ G_{M-1,0}(z) & \cdots & G_{M-1,M/2-1}(z) & G_{M-1,M/2}(z) & \cdots & G_{M-1,M-1}(z) \end{bmatrix}$$

Clearly, introducing one more prototype filter brings more freedom for the design of CMFB. It can be shown that with the above sparse pattern, the CMFB of perfect reconstruction can be realized by the following lattice structure

$$\mathbf{E}(z)=\sqrt{M}\mathbf{DC}\Lambda(z)\prod_{i=m-1}^{1}\left(\mathbf{\Phi}_i\mathbf{\Lambda}(z^2)\right)\mathbf{\Phi}_0 \quad (6.19)$$

where

$$\mathbf{\Phi}_i = \begin{bmatrix} \theta_{0,0} & \cdots & \theta_{0,M/2-1} & \theta_{0,M/2} & \cdots & \theta_{0,M-1} \\ \vdots & \ddots & \vdots & \vdots & \ddots & \vdots \\ \theta_{M/2-1,0} & \cdots & \theta_{M/2-1,M/2-1} & \theta_{M/2-1,M/2} & \cdots & \theta_{M/2-1,M-1} \\ \theta_{M/2,0} & \cdots & \theta_{M/2,M/2-1} & \theta_{M/2,M/2} & \cdots & \theta_{M/2,M-1} \\ \vdots & \ddots & \vdots & \vdots & \ddots & \vdots \\ \theta_{M-1,0} & \cdots & \theta_{M-1,M/2-1} & \theta_{M-1,M/2} & \cdots & \theta_{M-1,M-1} \end{bmatrix}$$

Obviously, the total number of free parameters is then increased from $mM/2$ in (6.9) to $mM^2/4$ in (6.19). A general modulation scheme has been proposed in [90] as

$$h_k[n] = 2h[n]\cos\left[(2k+1)\frac{\pi}{2M}\left(n-\frac{D}{2}\right)+(-1)^k\frac{\pi}{4}\right] \tag{6.20}$$

$$(D = 2mM + d,\ 0 \le d < 2M)$$

By choosing different values of D, different sparse patterns for $\mathbf{G}(z)$ can be achieved. With (6.20), one can continue doubling the number of prototype filters till a total of 2^{μ}, prototype filters is obtained. Thus, a general form of CMFB can be given by

$$h_k[n] = \sum_{l=0}^{2^{\mu}-1} 2h_l[n]\cos\left[(2k+1)\frac{\pi}{2M}\left(n+\frac{D_l}{2}\right)+(-1)^k\frac{\pi}{4}\right] \tag{6.21}$$

It is easy to see that the polyphase matrix $\mathbf{E}(z)$ corresponding to (6.21) has the same form as (6.18) except that the number of nonzero elements in $\mathbf{G}^{(2^{\mu})}(z)$ is increased to $2^{\mu+1}M$. If the number M of channels is a power of two, this procedure can be carried out until $2^{\mu} = M$ and all the elements of $\mathbf{G}(z)$ are non-zero. Eventually, one can obtain a lattice factorization similar to (6.19) except that $\mathbf{\Phi}_i$ is a full matrix.

6.4 Design Examples

To evaluate the performance and the design/implementation complexity of CMFBs with different number of prototype filters, a 4-channel CMFB whose analysis filters each are of length 16 is designed. With the paraunitary property structurally satisfied, we can establish an objective function to determine the optimal rotation angles. In this chapter, the objective function for the minimization problem is set to be the stopband energy outside the specified passbands as defined by

$$\Phi = \sum_{k=0}^{M-1} \int_{\omega \in \Omega_k} \left| H_k(e^{j\omega}) \right|^2 d\omega \tag{6.22}$$

where the stopbands are defined as

$$\Omega_k = [0, \max(0, (k-0.6)\pi/M)] \cup [\pi, \min(\pi, (k+1.6)\pi/M)]$$

Three types of CMFBs with different prototype filters are designed. The conventional CMFB in [89], denoted as CMFB-I, is included in the design for comparison. The CMFB with two prototype filters and a sparse matrix $\mathbf{G}^{(2)}(z)$ as given in (6.18) is called CMFB-II. CMFB-III represents the general MIS-PUFB. Since the CMFB is paraunitary, the analysis and synthesis filters have the same frequency response and thus only the amplitude response of the analysis filters is shown in Fig. 6.4. The performance of the designed CMFBs is measured by the stopband attenuation. The implementation complexity is measured by the number of multiplications per input sample. Table 6.1 shows the performance and the implementation complexity of the designed three CMFBs. It should be noted that in the evaluation of the implementation complexity, the computation of DCT is not taken into account since it is common for all the three cases.

From Table 6.1, one can see that with the increase of rotation angles, the filter bank has a better stop attenuation while sacrificing a little implementation complexity.

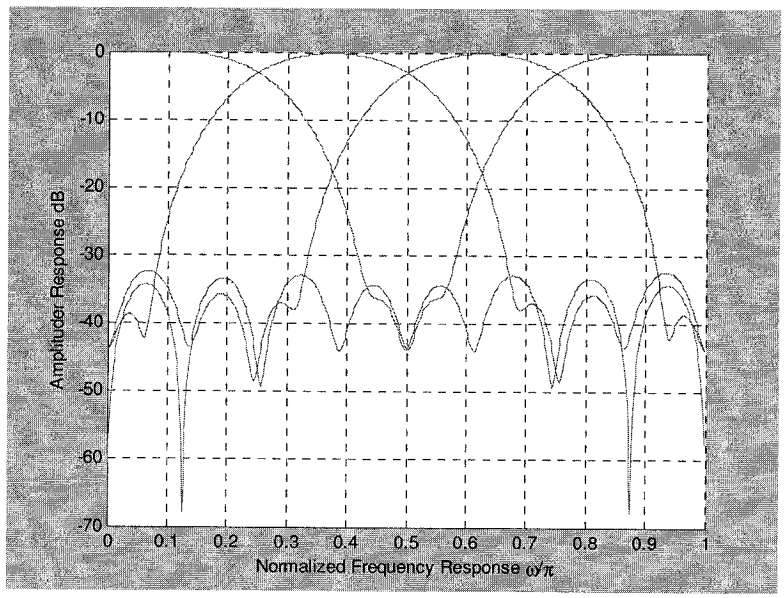

(a)

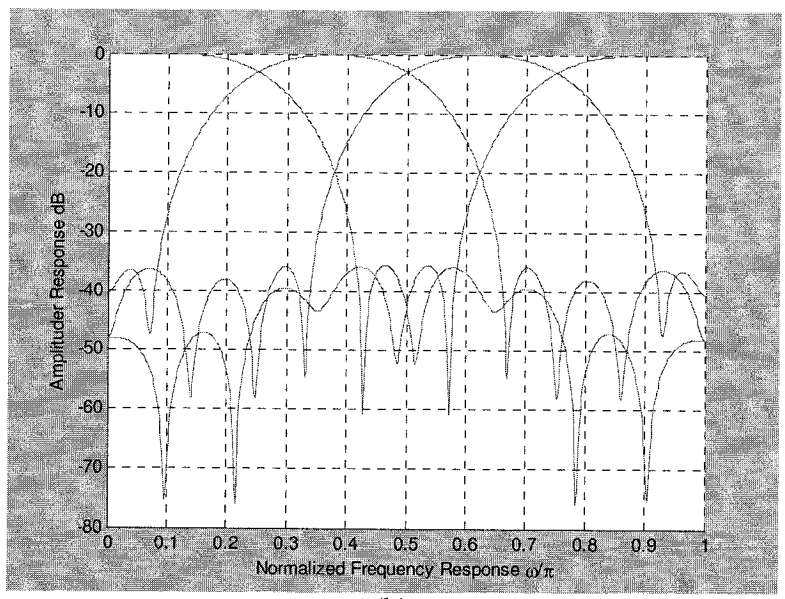

(b)

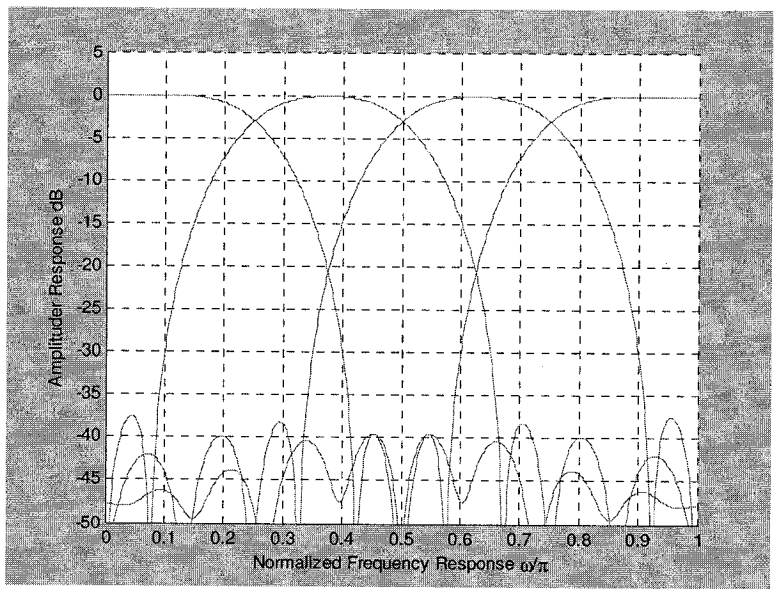

(c)

Figure 6.4: Frequency Responses of three types of CMFBs. (a) Type-I. (b) Type-II. (c) Type-III.

Table 6.1: Performance and complexity of the designed CMFBs

	CMFB-I	CMFB-II	CMFB-III
No. of rotation angles	4	8	24
Multiplications per input	6	10	26
Stopband energy (-dB)	29.1390	31.7543	35.4573

6.5 Conclusion

In this chapter, the conventional CMFB has been formulated first as a cascade of a modulation matrix and a sparse polyphase matrix of diamond shape, resulting in a simplified implementation structure for CMFB. Under this framework, it has been revealed that the CMFB is a special class of MIS-PUFB, whose propagation blocks have less number of coefficients. Then, several new CMFBs have been developed by using multiple prototype filters in conjunction with a proper modulation scheme. The polyphase

matrices of the resulting CMFBs have different sparse pattern and contain more non-zero elements than the conventional CMFB. In this way, the introduction of more prototype filters provides more flexibility in choosing the number of rotation angles. Simulation results have shown that the use of multiple prototype filters makes it possible to have a tradeoff between the implementation complexity and the stopband attenuation of a filter bank according to different applications.

Chapter 7

LPPRFBs with Mirror-Image Symmetry and Application in Image Compression Coding

7.1 Introduction

In some applications, such as image processing, it is essential for all analysis as well as synthesis filters to have linear-phase. Moreover, linear-phase filters allow for the use of simple symmetric extension to easily handle the boundaries of finite-length signals. An important class of filter banks, the linear-phase perfect reconstruction filter banks (LPPRFBs), has thus been extensively studied over the past decades. A great deal of work has been concerned with the design of M-channel LPPRFBs through the lattice factorization [68]-[82]. Soman *et al.* [70] first introduced a complete and minimal factorization that covers a large class of linear-phase paraunitary filter banks (LPPUFBs), namely, even-channel filter banks with all of the filters having the same length MK, where M is the channel number and K is an integer. An equivalent, yet modular, factorization called GenLOT is presented in [71], which includes the DCT [64] and the LOT [68] as the lower-order special cases. More recently, the LPPUFB has been generalized to the LPPRFB in [74]. All these structures have been simplified in [54] and [55], resulting in a considerable reduction in the number of free parameters.

The linear-phase condition is a strong constraint that imposes certain limitation on the choice of the filter's length and symmetry. In [73], through a study of the trace of the polyphase matrix, Trans *et al.* have given permissible solutions of the symmetry and length of the analysis filters for general LPPRFBs with variable length $L_i = K_i M + \beta$, where β is a fixed integer. These solutions are summarized in Table 7.1.

Table 7.1: Possible choices of the length and symmetry for analysis filters of M-channel LPPRFBs

Parity of M and β	No. of Symmetric and Antisymmetric Filters	Parity of $\sum K_i$	Total length of Analysis Bank
M even, β even	$M/2$ symmetric $M/2$ anti-symmetric	even	2mM
M even, β odd	$M/2+1$ symmetric $M/2-1$ anti-symmetric	odd	2mM
M odd, β even	$(M+1)/2$ symmetric $(M-1)/2$ anti-symmetric	odd	(2m+1)M
M odd, β odd	$(M+1)/2$ symmetric $(M-1)/2$ anti-symmetric	even	(2m+1)M

In Chapter 5, we have investigated a class of mirror-image symmetric PRFBs (MIS-PRFBs). This constraint was introduced to reduce the number of parameters and to accelerate the design process of the PRFBs. It has already been observed in Section 5.5.3 that the MIS is a mild constraint which gives a performance similar to that of general filter banks without any constraint. Also, the MIS can be used for filter banks with any length. Therefore, it might be possible to further reduce the number of parameters of filter banks by combining the MIS with other types of constraints such as linear-phase. This idea has already been attempted in [63], yielding a lattice factorization whose number of free parameters is almost the same as that of the simplified structure of a general

LPPRFB in [54] and [55]. However, the properties of LPPUFBs have not yet been fully exploited in the development of the lattice structures of MIS-LPPUFBs in [63]. In this chapter, we apply the C-S decomposition method proposed in [55] to simplify the factorization of MIS-LPPRFBs. The proposed scheme reduces the number of parameters to a large degree without affecting the performance of the filter banks.

7.2 Review of Existing Factorizations

In this section, we first briefly review some of the existing lattice structures for a general LPPRFB, the LPPRFB combined with MIS, and the simplified LPPRFB. Through the comparison of these structures, we will point out that the existing MIS-LPPRFBs still have redundancy, which can be employed for further simplification.

It has been shown in [74] that the even-channel LPPRFB with the polyphase matrix given by (2.34) can always be factorized as

$$\mathbf{E}(z) = \prod_{i=K-1}^{1} \mathbf{G}_i(z)\mathbf{E}_0 = \prod_{i=K-1}^{1} (\mathbf{\Phi}_i \mathbf{W} \mathbf{\Lambda}(z) \mathbf{W}) \mathbf{E}_0 \tag{7.1}$$

where

$$\mathbf{E}_0 = \frac{1}{\sqrt{2}} \begin{bmatrix} \mathbf{U}_0 & \mathbf{0} \\ \mathbf{0} & \mathbf{V}_0 \end{bmatrix} \begin{bmatrix} \mathbf{I} & \mathbf{J} \\ \mathbf{J} & -\mathbf{I} \end{bmatrix}, \tag{7.2a}$$

$$\mathbf{\Phi}_i = \begin{bmatrix} \mathbf{U}_i & \mathbf{0} \\ \mathbf{0} & \mathbf{V}_i \end{bmatrix}, \tag{7.2b}$$

$$\mathbf{\Lambda}(z) = \begin{bmatrix} \mathbf{I} & \mathbf{0} \\ \mathbf{0} & z^{-1}\mathbf{I} \end{bmatrix}, \tag{7.2c}$$

$$\mathbf{W} = \frac{1}{\sqrt{2}} \begin{bmatrix} \mathbf{I} & \mathbf{I} \\ \mathbf{I} & -\mathbf{I} \end{bmatrix}. \tag{7.2d}$$

In (7.2), $\mathbf{U}_i$ and $\mathbf{V}_i$ are invertible matrices to be determined, $\mathbf{\Lambda}(z)$ is a diagonal delay matrix, and $\mathbf{W}$ the well-known butterfly structure. It was proved in [63] that if $\mathbf{U}_i$ in (7.2b) is chosen as

$$\mathbf{U}_i = \begin{cases} \mathbf{\Gamma V}_i \mathbf{\Gamma}, & i = 0,\ldots,K-2 \\ \mathbf{J V}_i \mathbf{\Gamma}, & i = K-1 \end{cases} \tag{7.3}$$

where $\mathbf{\Gamma}$ is a diagonal matrix whose lth diagonal entry is $(-1)^l$, then the above LPPRFB is also mirror-image symmetric (MIS), namely, its analysis filters satisfy

$$H_{M-1-k}(z) = H_k(-z), \quad 0 \le k \le M-1 \tag{7.4}$$

With the MIS property, each propagation matrix $\mathbf{\Phi}_i$ in (7.2b) is now dependent on $\mathbf{V}_i$ only, instead of both $\mathbf{U}_i$ and $\mathbf{V}_i$. This implies that the number of parameters of MIS-LPPRFB is one-half of that of the LPPRFB in (7.1).

On the other hand, it has been recently revealed in [54] that the lattice structure of LPPRFB in (7.1) still has redundancy. This redundancy lying between two consecutive propagation blocks can be removed to obtain a simplified lattice structure. It can be done by rewriting the product $\mathbf{G}_{K-1}(z)\mathbf{G}_{K-2}(z)$ as follows

$$\begin{aligned} &\mathbf{G}_{K-1}(z)\mathbf{G}_{K-2}(z) \\ &= \frac{1}{2}\begin{bmatrix} \mathbf{U}_{K-1} & \mathbf{0} \\ \mathbf{0} & \mathbf{V}_{K-1} \end{bmatrix}\begin{bmatrix} \mathbf{I}+z^{-1}\mathbf{I} & \mathbf{I}-z^{-1}\mathbf{I} \\ \mathbf{I}-z^{-1}\mathbf{I} & \mathbf{I}+z^{-1}\mathbf{I} \end{bmatrix} \\ &\quad \times \frac{1}{2}\begin{bmatrix} \mathbf{U}_{K-2} & \mathbf{0} \\ \mathbf{0} & \mathbf{V}_{K-2} \end{bmatrix}\begin{bmatrix} \mathbf{I}+z^{-1}\mathbf{I} & \mathbf{I}-z^{-1}\mathbf{I} \\ \mathbf{I}-z^{-1}\mathbf{I} & \mathbf{I}+z^{-1}\mathbf{I} \end{bmatrix} \\ &= \frac{1}{2}\begin{bmatrix} \mathbf{I} & \mathbf{0} \\ \mathbf{0} & \mathbf{V}_{K-1}\mathbf{U}_{K-1}^{-1} \end{bmatrix}\begin{bmatrix} \mathbf{U}_{K-1} & \mathbf{0} \\ \mathbf{0} & \mathbf{U}_{K-1} \end{bmatrix}\begin{bmatrix} \mathbf{I} & -\mathbf{I} \\ \mathbf{I} & \mathbf{I} \end{bmatrix}\begin{bmatrix} \mathbf{I} & \mathbf{0} \\ \mathbf{0} & z^{-1}\mathbf{I} \end{bmatrix}\begin{bmatrix} \mathbf{I} & -\mathbf{I} \\ \mathbf{I} & \mathbf{I} \end{bmatrix} \\ &\quad \times \frac{1}{2}\begin{bmatrix} \mathbf{U}_{K-2} & \mathbf{0} \\ \mathbf{0} & \mathbf{V}_{K-2} \end{bmatrix}\begin{bmatrix} \mathbf{I}+z^{-1}\mathbf{I} & \mathbf{I}-z^{-1}\mathbf{I} \\ \mathbf{I}-z^{-1}\mathbf{I} & \mathbf{I}+z^{-1}\mathbf{I} \end{bmatrix} \end{aligned} \tag{7.5}$$

$$
\begin{aligned}
&= \frac{1}{2}\begin{bmatrix} \mathbf{I} & \mathbf{0} \\ \mathbf{0} & \mathbf{V}_{K-1}\mathbf{U}_{K-1}^{-1} \end{bmatrix}\begin{bmatrix} \mathbf{I}+z^{-1}\mathbf{I} & \mathbf{I}-z^{-1}\mathbf{I} \\ \mathbf{I}-z^{-1}\mathbf{I} & \mathbf{I}+z^{-1}\mathbf{I} \end{bmatrix} \\
&\quad \times \frac{1}{2}\begin{bmatrix} \mathbf{U}_{K-1}\mathbf{U}_{K-2} & \mathbf{0} \\ \mathbf{0} & \mathbf{U}_{K-1}\mathbf{V}_{K-2} \end{bmatrix}\begin{bmatrix} \mathbf{I}+z^{-1}\mathbf{I} & \mathbf{I}-z^{-1}\mathbf{I} \\ \mathbf{I}-z^{-1}\mathbf{I} & \mathbf{I}+z^{-1}\mathbf{I} \end{bmatrix} \\
&= \frac{1}{2}\begin{bmatrix} \mathbf{I} & \mathbf{0} \\ \mathbf{0} & \hat{\mathbf{V}}_{K-1} \end{bmatrix}\begin{bmatrix} \mathbf{I}+z^{-1}\mathbf{I} & \mathbf{I}-z^{-1}\mathbf{I} \\ \mathbf{I}-z^{-1}\mathbf{I} & \mathbf{I}+z^{-1}\mathbf{I} \end{bmatrix} \\
&\quad \times \frac{1}{2}\begin{bmatrix} \hat{\mathbf{U}}_{K-2} & \mathbf{0} \\ \mathbf{0} & \hat{\mathbf{V}}_{K-2} \end{bmatrix}\begin{bmatrix} \mathbf{I}+z^{-1}\mathbf{I} & \mathbf{I}-z^{-1}\mathbf{I} \\ \mathbf{I}-z^{-1}\mathbf{I} & \mathbf{I}+z^{-1}\mathbf{I} \end{bmatrix}
\end{aligned}
$$

Note that the component $\mathrm{diag}\{\mathbf{U}_{K-1}, \mathbf{U}_{K-1}\}$ of $\mathbf{G}_{K-1}(z)$ in the second equation of (7.5) has been moved across the delay chain and the butterfly matrices, and then combined with $\mathrm{diag}\{\mathbf{U}_{K-2}, \mathbf{V}_{K-2}\}$ of the subsequent stage $\mathbf{G}_{K-2}(z)$ in the third equation. As $\mathbf{U}_{K-1}$, $\mathbf{U}_{K-2}$, and $\mathbf{V}_{K-2}$ are all free invertible matrices, the product terms $\hat{\mathbf{U}}_{K-2} = \mathbf{U}_{K-1}\mathbf{U}_{K-2}$ and $\hat{\mathbf{V}}_{K-2} = \mathbf{U}_{K-1}\mathbf{V}_{K-2}$ in the last equation of (7.5) are also free invertible matrices. By repeating the above manipulation until i=1, all $\mathbf{U}_i$'s, except $\mathbf{U}_0$, can be removed. Then, a new propagation matrix $\hat{\mathbf{G}}_i(z)$ is given by

$$
\hat{\mathbf{G}}_i(z) = \frac{1}{2}\mathrm{diag}(\mathbf{I}, \hat{\mathbf{V}}_i)\mathbf{W}\boldsymbol{\Lambda}(z)\mathbf{W} \tag{7.6}
$$

where

$$
\hat{\mathbf{V}}_i = \mathbf{V}_i \prod_{l=K-1}^{i} \mathbf{U}_l^{-1}
$$

Thus, a simplified lattice structure is obtained provided that $\mathbf{G}_i(z)$ in (7.1) is replaced with $\hat{\mathbf{G}}_i(z)$ in (7.6). As a consequence, the number of free parameters of LPPRFB in (7.1) has been reduced by almost one-half. It is of interest to note that the simplified LPPRFB has nearly the same number of free parameters as the LPPRFB with MIS, indicating that the lattice structure in (7.1) that satisfies the MIS condition (7.3) still

contains redundant parameters. In the next section, a simplified lattice structure of MIS-LPPRFB with further reduced free parameters will be developed by removing this redundancy.

7.3 Simplified Structure of MIS-LPPRFBs

7.3.1 Simplification of LPPRFBs with MIS

We would now like to apply the MIS constraint as given by (7.3) to further simplify the lattice structure of LPPRFBs. Note that the unitary matrix $\mathbf{U}_i$ has been merged with $\mathbf{V}_i$ in (7.5), making a direct use of (7.3) impossible. Therefore, we first modify the simplification process in (7.5) such that $\mathbf{U}_i$ is preserved and the MIS constraint (7.3) can be exploited.

As $\mathbf{V}_{K-1}$ is invertible, one can rewrite the $\mathbf{U}_{K-1}\mathbf{V}_{K-2}$ in the third equation of (7.5) as

$$\mathbf{U}_{K-1}\mathbf{V}_{K-2} = \mathbf{U}_{K-1}\mathbf{V}_{K-1}^{-1}\mathbf{V}_{K-1}\mathbf{V}_{K-2} \tag{7.7}$$

Substituting (7.7) into (7.5), we have

$$\begin{aligned}
&\mathbf{G}_{K-1}(z)\mathbf{G}_{K-2}(z) \\
&= \frac{1}{2}\begin{bmatrix} \mathbf{I} & \mathbf{0} \\ \mathbf{0} & \mathbf{V}_{K-1}\mathbf{U}_{K-1}^{-1} \end{bmatrix}\begin{bmatrix} \mathbf{I}+z^{-1}\mathbf{I} & \mathbf{I}-z^{-1}\mathbf{I} \\ \mathbf{I}-z^{-1}\mathbf{I} & \mathbf{I}+z^{-1}\mathbf{I} \end{bmatrix}\begin{bmatrix} \mathbf{I} & \mathbf{0} \\ \mathbf{0} & \mathbf{U}_{K-1}\mathbf{V}_{K-1}^{-1} \end{bmatrix} \\
&\quad \times \frac{1}{2}\begin{bmatrix} \mathbf{U}_{K-1}\mathbf{U}_{K-2} & \mathbf{0} \\ \mathbf{0} & \mathbf{V}_{K-1}\mathbf{V}_{K-2} \end{bmatrix}\begin{bmatrix} \mathbf{I}+z^{-1}\mathbf{I} & \mathbf{I}-z^{-1}\mathbf{I} \\ \mathbf{I}-z^{-1}\mathbf{I} & \mathbf{I}+z^{-1}\mathbf{I} \end{bmatrix} \\
&= \frac{1}{2}\begin{bmatrix} \mathbf{I} & \mathbf{0} \\ \mathbf{0} & \mathbf{V}_{K-1}\mathbf{U}_{K-1}^{-1} \end{bmatrix}\begin{bmatrix} \mathbf{I}+z^{-1}\mathbf{I} & \mathbf{I}-z^{-1}\mathbf{I} \\ \mathbf{I}-z^{-1}\mathbf{I} & \mathbf{I}+z^{-1}\mathbf{I} \end{bmatrix}\begin{bmatrix} \mathbf{I} & \mathbf{0} \\ \mathbf{0} & \mathbf{U}_{K-1}\mathbf{V}_{K-1}^{-1} \end{bmatrix} \\
&\quad \times \frac{1}{2}\begin{bmatrix} \mathbf{U}'_{K-2} & \mathbf{0} \\ \mathbf{0} & \mathbf{V}'_{K-2} \end{bmatrix}\begin{bmatrix} \mathbf{I}+z^{-1}\mathbf{I} & \mathbf{I}-z^{-1}\mathbf{I} \\ \mathbf{I}-z^{-1}\mathbf{I} & \mathbf{I}+z^{-1}\mathbf{I} \end{bmatrix}
\end{aligned} \tag{7.8}$$

Note that the component $\mathrm{diag}(\mathbf{U}_{K-1},\mathbf{V}_{K-1})$, instead of $\mathrm{diag}(\mathbf{U}_{K-1},\mathbf{U}_{K-1})$, is merged with $\mathrm{diag}(\mathbf{U}_{K-2},\mathbf{V}_{K-2})$. From $\mathbf{U}_{K-1}=\mathbf{J}\mathbf{V}_{K-1}\boldsymbol{\Gamma}$ and $\mathbf{U}_{K-2}=\boldsymbol{\Gamma}\mathbf{V}_{K-2}\boldsymbol{\Gamma}$, one can verify that

$$\mathbf{U}'_{K-2}=\mathbf{U}_{K-1}\mathbf{U}_{K-2}=\mathbf{J}\mathbf{V}_{K-1}\mathbf{V}_{K-2}\boldsymbol{\Gamma}=\mathbf{J}\mathbf{V}'_{K-2}\boldsymbol{\Gamma}, \tag{7.9}$$

implying that (7.8) successfully removes a redundant $\mathbf{U}_{K-1}$ and preserves the relationship between $\mathbf{U}_{K-1}$ and $\mathbf{V}_{K-1}$ as required by (7.3) in the form of $\mathbf{U}'_{K-2}$ and $\mathbf{V}'_{K-2}$. Repeating the above process till $\mathbf{G}_2(z)\mathbf{G}_1(z)$, one can obtain a new structure which is equivalent to (7.1) as given below

$$\mathbf{E}(z)=\prod_{i=K-1}^{1}\mathbf{G}'_i(z)\mathbf{E}'_0 \tag{7.10}$$

$$\mathbf{G}'_i(z)=\frac{1}{2}\mathrm{diag}(\mathbf{I},\mathbf{X}_i)\mathbf{W}\boldsymbol{\Lambda}(z)\mathbf{W}\mathrm{diag}(\mathbf{I},\mathbf{X}_i^{-1}) \tag{7.11}$$

$$\mathbf{E}'_0=\frac{1}{\sqrt{2}}\mathrm{diag}(\mathbf{U}'_0,\mathbf{V}'_0)\begin{bmatrix}\mathbf{I} & \mathbf{I}\\ \mathbf{I} & -\mathbf{J}\end{bmatrix} \tag{7.12}$$

In (7.11), $\mathbf{X}_i$ is given by

$$\mathbf{X}_i=\mathbf{V}'_i\mathbf{U}'^{-1}_i \quad (i=1,\ldots,K-1) \tag{7.13}$$

$$\mathbf{U}'_i=\prod_{l=K-1}^{i}\mathbf{U}_l,\quad \mathbf{V}'_i=\prod_{l=K-1}^{i}\mathbf{V}_l \tag{7.14}$$

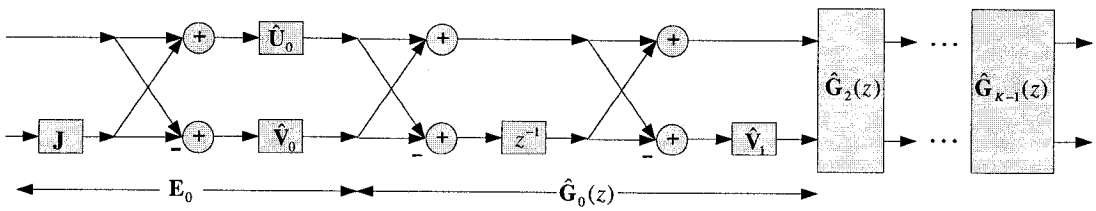

(a)

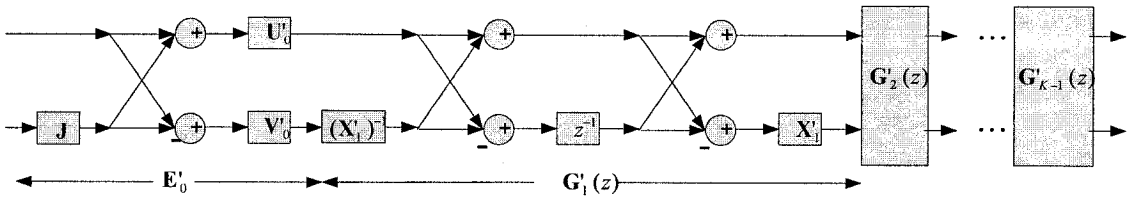

(b)

Figure 7.1: Lattice structures of LPPRFBs. (a) for (7.6) and (b) for (7.10).

Fig. 7.1 shows the lattice implementation structures given by (7.6) and (7.11), respectively. It is clear that the two adjacent $\mathbf{X}_i$ and $\mathbf{X}_{i-1}^{-1}$ can be merged into one invertible matrix and the structures in (7.6) and (7.10) would have the same implementation complexity. It is to be noted that, unlike $\hat{\mathbf{V}}_i$ in $\hat{\mathbf{G}}_i(z)$, $\mathbf{X}_i$ in $\mathbf{G}'_i(z)$ is not an arbitrary invertible matrix. As will be shown later, there exists certain symmetry in $\mathbf{X}_i$, which can be exploited to reduce the free parameters.

7.3.2 Exploitation of MIS via QR Factorization

We now show that the relationship between $\mathbf{U}_i$ and $\mathbf{V}_i$ in (7.4) imposes certain constraints on $\mathbf{X}_i$. Noting that

$$\begin{aligned}\mathbf{U}'_i &= \prod_{l=K-1}^{i} \mathbf{U}_l \\ &= \mathbf{J}\mathbf{V}_{K-1}\boldsymbol{\Gamma}\prod_{l=K-2}^{i}\boldsymbol{\Gamma}\mathbf{V}_l\boldsymbol{\Gamma} \\ &= \mathbf{J}\left(\prod_{l=K-1}^{i}\mathbf{V}_l\right)\boldsymbol{\Gamma} = \mathbf{J}\mathbf{V}'_i\,\boldsymbol{\Gamma}\end{aligned} \tag{7.15}$$

(7.13) can be rewritten as

$$\mathbf{X}_i = \mathbf{V}'_i\,\mathbf{U}'^{-1}_i = \mathbf{V}'_i\,\boldsymbol{\Gamma}\mathbf{V}'^{-1}_i\,\mathbf{J} = \mathbf{X}'_i\,\mathbf{J} \tag{7.16}$$

where

$$\mathbf{X}'_i = \mathbf{V}'_i\,\boldsymbol{\Gamma}\mathbf{V}'^{-1}_i \tag{7.17}$$

One can verify that $\mathbf{X}'_i$ in (7.17) is a special symmetric invertible matrix, i.e.,

$$\mathbf{X}'_i = (\mathbf{X}'_i)^{-1} \tag{7.18}$$

Obviously, $\mathbf{X}'_i$ contains fewer parameters than the general invertible matrix $\hat{\mathbf{V}}_i$ does. Next, we will discuss the parameterization issue of $\mathbf{X}'_i$.

According to the QR decomposition, a square matrix $\mathbf{A}$ can be factorized as

$$\mathbf{A} = \mathbf{QR} \tag{7.19}$$

where $\mathbf{Q}$ is an orthogonal matrix and $\mathbf{R}$ an upper triangular matrix. If $\mathbf{A}$ is invertible, then the QR factorization is unique and the diagonal elements of $\mathbf{R}$ are positive. Performing the QR decomposition on $\mathbf{V}'_i$ in (7.17), one has

$$\mathbf{X}'_i = \mathbf{R}_i^{-1}\mathbf{Q}_i^T\boldsymbol{\Gamma}\mathbf{Q}_i\mathbf{R}_i \tag{7.20}$$

where both $\mathbf{R}_i$ and $\mathbf{R}_i^{-1}$ are invertible upper triangular matrices and $\mathbf{Q}_i^T\boldsymbol{\Gamma}\mathbf{Q}_i$ is a Hermitian orthogonal matrix. Recall that in the C-S decomposition [55], $\mathbf{Q}_i^T\boldsymbol{\Gamma}\mathbf{Q}_i$ can be completely characterized as

$$\mathbf{Q}_i^T\boldsymbol{\Gamma}\mathbf{Q}_i = \mathrm{diag}(\mathbf{Y}_{i,0}, \mathbf{Y}_{i,1})\boldsymbol{\Sigma}_i\mathrm{diag}(\mathbf{Y}_{i,0}^T, \mathbf{Y}_{i,1}^T) \tag{7.21}$$

where $\boldsymbol{\Sigma}_i$ is a special orthogonal matrix defined as

$$\boldsymbol{\Sigma}_i = \begin{cases} \begin{bmatrix} \mathbf{C}_i & -\mathbf{S}_i \\ \mathbf{S}_i & \mathbf{C}_i \end{bmatrix}, & M/2 \text{ even} \\ \begin{bmatrix} \mathbf{1} & \mathbf{0} & \mathbf{0} \\ \mathbf{0} & \mathbf{C}_i & -\mathbf{S}_i \\ \mathbf{0} & \mathbf{S}_i & \mathbf{C}_i \end{bmatrix}, & M/2 \text{ odd} \end{cases} \tag{7.22}$$

in which $\mathbf{C}_i$ and $\mathbf{S}_i$ are $\lfloor M/4 \rfloor$-dimensional diagonal matrices whose entries are given by $\mathbf{C}_i(l,l) = \cos\alpha_{i,l}$ and $\mathbf{S}_i(l,l) = \sin\alpha_{i,l}$, respectively, where $\lfloor x \rfloor$ denotes the floor

operation which gives the largest integer less than or equal to x. Although the number of free parameters is reduced in the new structure, the implementation cost is not accordingly saved. This is because the two matrices $\mathbf{X}_i$ and $\mathbf{X}_i^{-1}$ at each stage could not be merged into the following stages in order to keep the symmetry property of $\mathbf{X}_i$ as seen from (7.10). The presence of this matrix has introduced extra implementation burden. We may observe that this implementation cost can be saved after the QR parameterization. Noticing that in (7.20) the symmetry property has already been exploited, and $\mathbf{R}_i$ and $\mathbf{R}_i^{-1}$ are general upper triangular matrices without any special property, one can merge $\mathbf{R}_i^{-1}$ with the following $\mathbf{R}_{i-1}$, yielding a new upper triangular invertible matrix $\mathbf{R}'_i = \mathbf{R}_i^{-1}\mathbf{R}_{i-1}$. This way, one would save one-half of the upper triangular matrices. Due to the existence of $\mathbf{R}'_i$ between the two adjacent stages, $\mathbf{Q}_i$ and $\mathbf{Q}_{i-1}^T$ cannot be written in one orthogonal matrix. As such, the total implementation cost of the simplified structure in (7.10) is almost the same as that of (7.6).

We now compare the LPPRFB in (7.6) with the MIS-LPPRFB in (7.10) in terms of the degree of design freedom, namely, the number of free parameters to be determined. It is easy to see that $\mathbf{E}_0$ and $\mathbf{E}'_0$ hold the same design freedom since they each have two free invertible matrices $\hat{\mathbf{U}}_0$ and $\hat{\mathbf{V}}_0$ or $\mathbf{U}'_0$ and $\mathbf{V}'_0$. Hence, their difference lies in $\hat{\mathbf{G}}_i(z)$ and $\mathbf{G}'_i(z)$. For notational simplicity, let m, m_0 and m_1 be $M/2$, $\lfloor M/4 \rfloor$ and $M/2-\lfloor M/4 \rfloor$, respectively. In $\hat{\mathbf{G}}_i(z)$, each $\hat{\mathbf{V}}_i$ requires m^2 rotational angles and m signed parameters for a complete parameterization. On the other hand, the Hermitian orthogonal matrix $\mathbf{G}'_i(z)$ is represented by one upper triangular matrix $\mathbf{R}_i$, two

orthogonal matrices $\mathbf{Y}_{i,0}$ and $\mathbf{Y}_{i,1}$, and one special orthogonal matrix $\mathbf{\Sigma}_i$. Since $\mathbf{R}_i$ can be completely characterized by $m(m-1)/2$ lifting steps, $\mathbf{Y}_{i,0}$, $\mathbf{Y}_{i,1}$, and $\mathbf{\Sigma}_i$ contain $m_0(m_0-1)/2$, $m_1(m_1-1)/2$, and m_1 rotational angles, respectively. As a result, the total number of parameters is $m(m-1)/2+m^2/4$ for even m and $m(m-1)/2+(m^2-1)/4$ for odd m. Based on this analysis, the number of free parameters in each structure is listed in Table. 7.2.

Table 7.2: Number of free parameters in LPPRFBs and MIS-LPPRFBs with even channel M=$2m$ and filter length L=KM

Structure	m even	m odd
I: LPPRFB	$(K+1)m^2$	$(K+1)m^2$
II: MIS-LPPRFB	$\frac{(K-1)(3m^2-2m)}{4}+2m^2$	$\frac{(K-1)(3m^2-2m-1)}{4}+2m^2$
Difference of I and II	$\frac{(K-1)(m^2+2m)}{4}$	$\frac{(K-1)(m^2+2m+1)}{4}$

7.4 Design Examples

Several filter banks with various number of channels M and filter lengths L are designed based on the nonlinear optimization of the proposed lattice coefficients. The cost function is set as a weighted combination of the reciprocal of the coding gain, the DC leakage and the stopband attenuation in the form

$$C = 0.4/C_{\text{coding gain}} + 0.2C_{\text{DC}} + 0.2C_{\text{anlysis stopband}} + 0.2C_{\text{synthesis stopband}} \tag{7.23}$$

The above combined criterion is mainly proposed to achieve a high performance transform for its use in image compression coding. When searching for the minimum solution of the cost function, the coding gain is maximized while the DC leakage and the stopband energy are minimized. Among these criteria, the coding gain is directly

associated with the objective performance of compressed images. Low DC leakage is not as essential to the coder's objective performance as the coding gain. However, a low DC leakage does improve the visual quality of the reconstructed image significantly by eliminating annoying blocking and checkerboard artifacts. Finally, the stopband attenuation helps in improving the signal decorrelation and decreasing the amount of aliasing. In the cost function (7.23), the coding gain is the same as that defined in Chapter 5, and the other terms are defined as

$$C_{\mathrm{DC}} = \sum_{i=0}^{M-1} \sum_{n=0}^{L-1} h_i[n] \tag{7.24}$$

$$C_{\text{analysis stopband}} = \sum_{i=0}^{M-1} \int_{\omega \in \Omega_{\text{stopband}}} \left| H_i(e^{j\omega}) \right|^2 d\omega \tag{7.25}$$

$$C_{\text{synthesis stopband}} = \sum_{i=0}^{M-1} \int_{\omega \in \Omega_{\text{stopband}}} \left| F_i(e^{j\omega}) \right|^2 d\omega \tag{7.26}$$

Figs. 7.2-7.5 show the frequency and impulse responses of four MIS-LPPRFBs corresponding to M=4, 8 and K=2, 3. The impulse response of the analysis and synthesis filters decays asymptotically to zero, which is helpful for reducing the block artifact in compressed images. The performances of the designed MIS-LPPRFBs as well as those of general LPPRFBs are listed in Table 7.3 and 7.4, respectively. Different filter banks are denoted by $M \times L$, where M is the number of channels and $L = M \times K$ the filter length. Scrutinizing the results in Table 7.3 and 7.4, we can conclude that the coding gain increases significantly with increasing number of channels, but only marginally with the filter length. On the other hand, the stopband attenuation is largely dependent on the filter length.

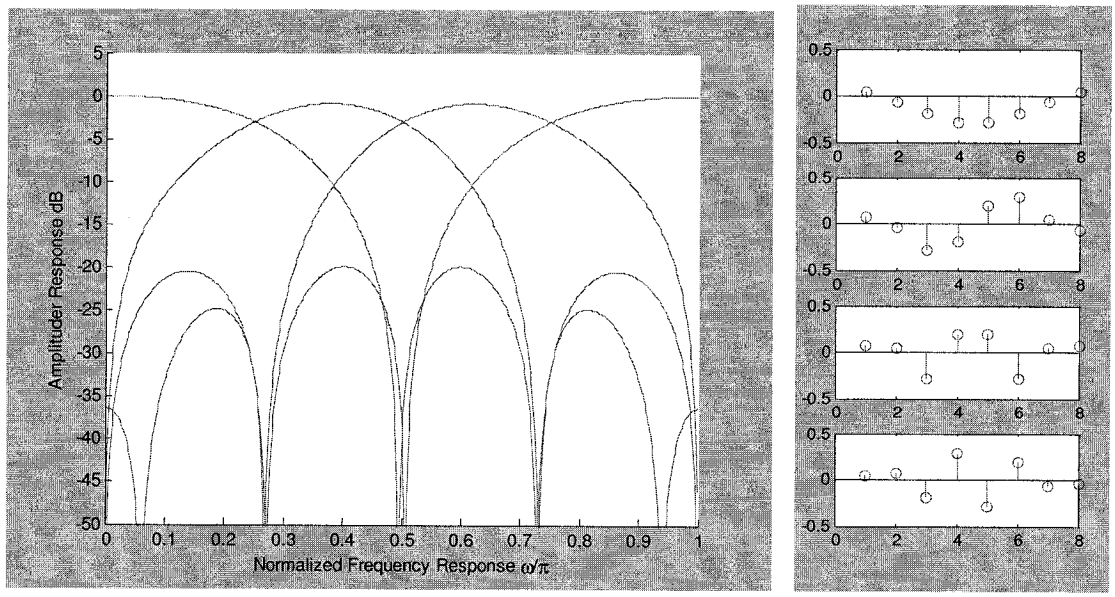

Figure 7.2: Frequency and impulse responses of MIS-LPPRFB with M=4 and L=8

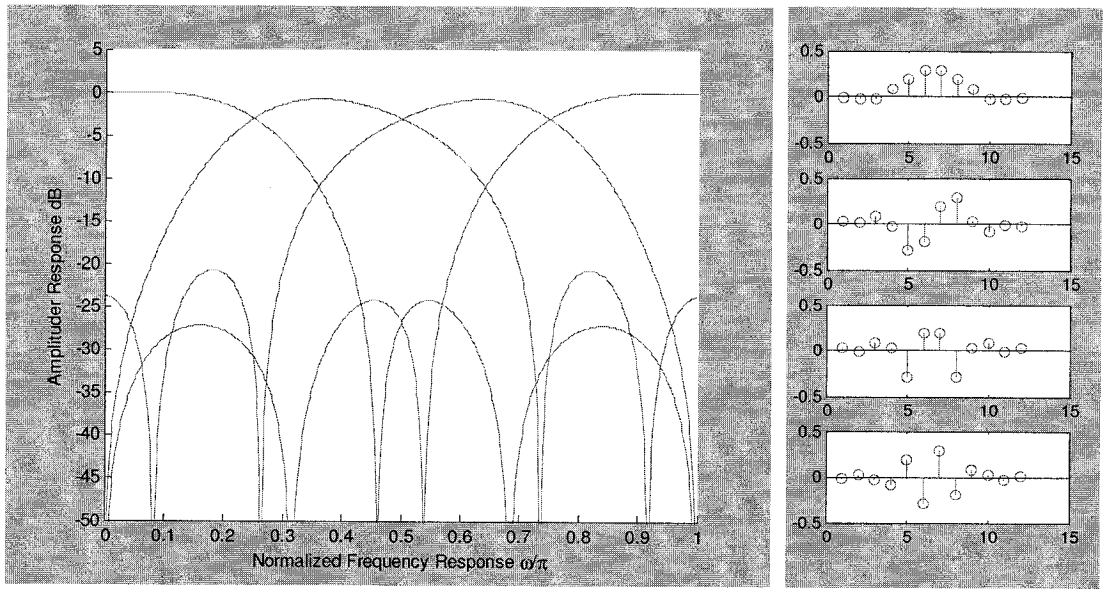

Figure 7.3: Frequency and impulse responses of MIS-LPPRFB with M=4 and L=12

Table 7.3: Performance comparison of MIS-LPPRFBs with different sizes

MIS-LPPRFB ($M \times L$)	4×8	4×12	8×16	8×24
Coding Gain (dB)	6.46	6.71	9.26	9.35
DC Attenuation (-dB)	84.42	87.96	88.33	90.02
Stopband Attenuation (-dB)	15.87	17.62	16.54	18.65

Table 7.4: Performance comparison of LPPRFBs with different sizes

LPPRFB ($M \times L$)	4×8	4×12	8×16	8×24
Coding Gain (dB)	6.54	6.79	9.58	9.59
DC Attenuation (-dB)	86.13	88.67	89.67	91.23
Stopband Attenuation (-dB)	15.89	17.65	16.78	18.67

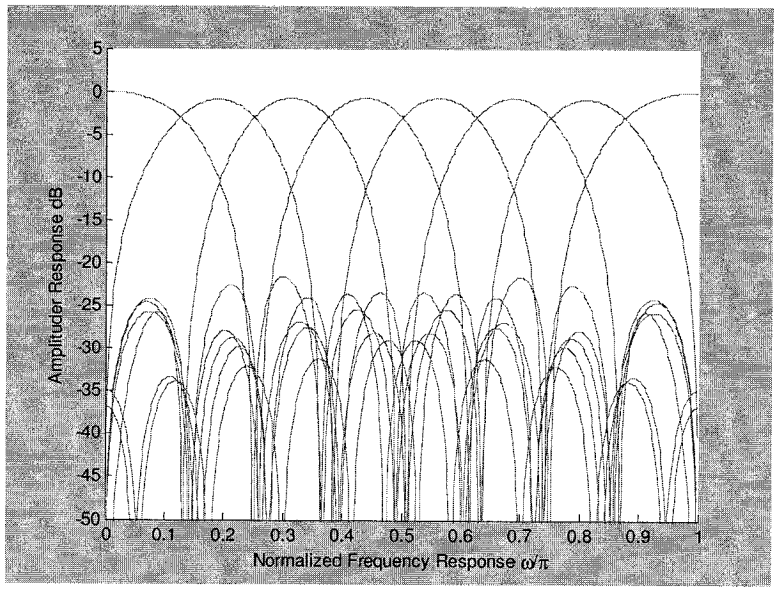

(a)

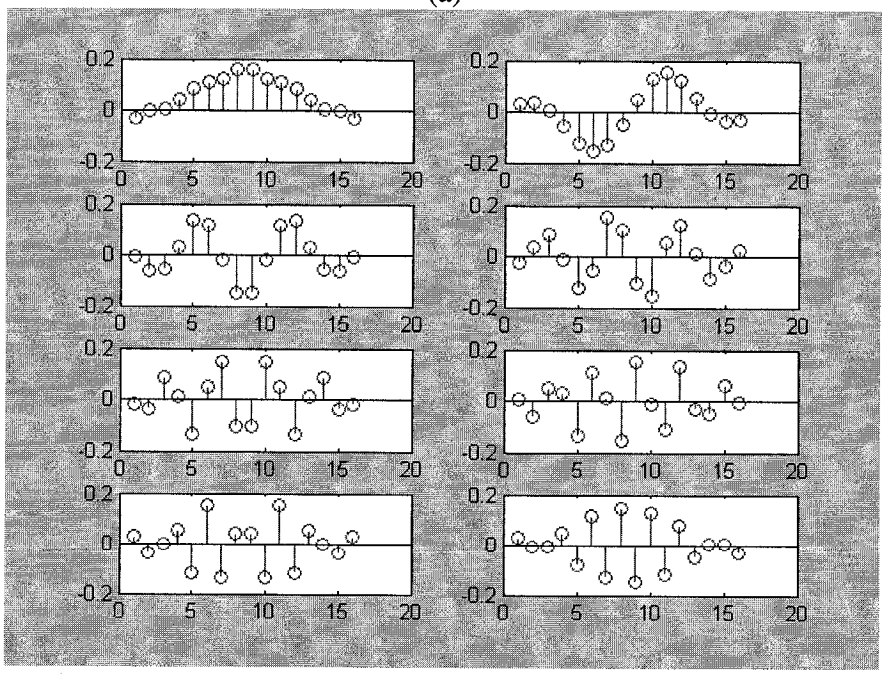

(b)

Figure 7.4: Designed MIS-LPPRFB with M=8 and L=16.
(a) Frequency response. (b) Impulse response

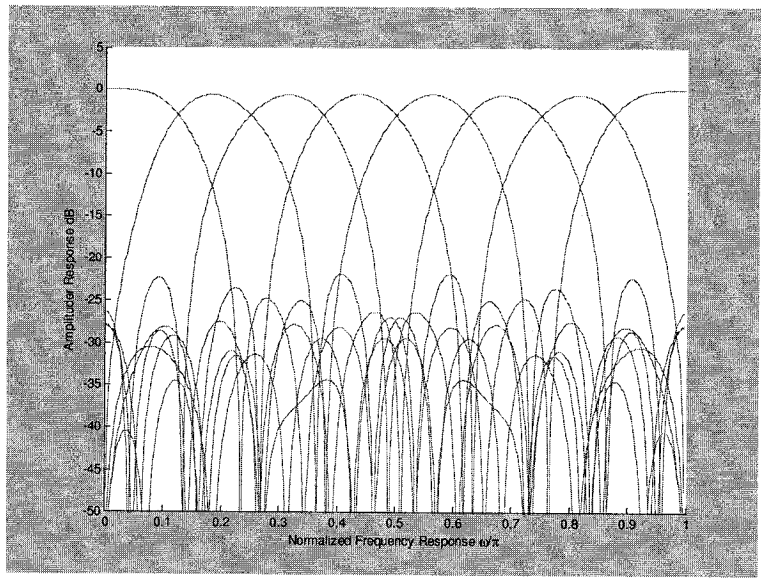

(a)

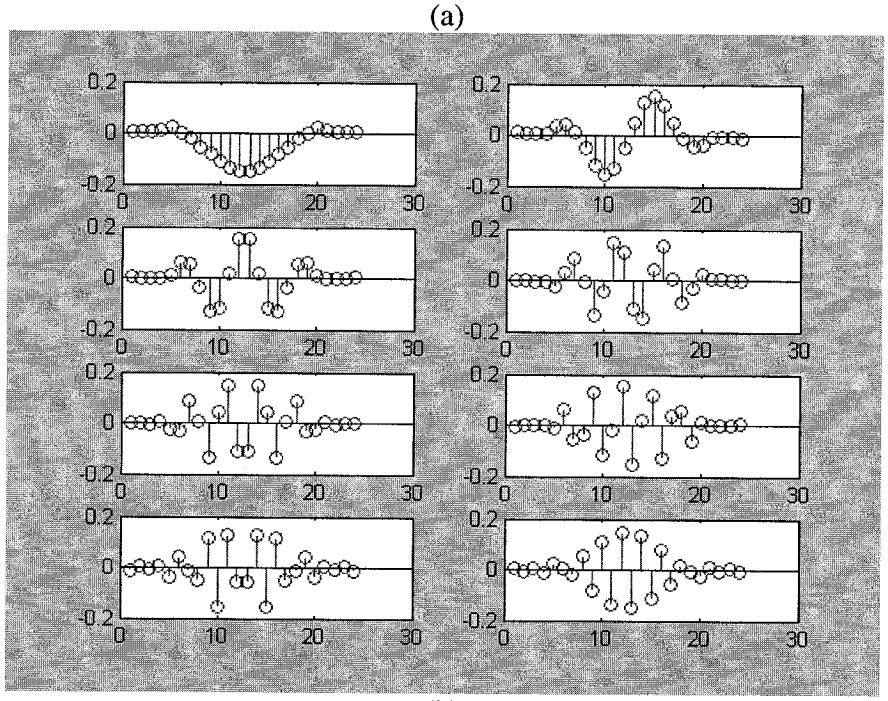

(b)

Figure 7.5: Designed MIS-LPPRFB with M=8 and L=24.
(a) Frequency response. (b) Impulse response

It is clear from the design results that the performance of the proposed MIS-LPPRFB is comparable to that of general LPPRFBs, yet a considerable saving in the number of parameters has been achieved in the proposed structure. It should be pointed out that the little sacrifice in the performance of MIS-LPPRFB in comparison to that of the LPPRFB

is mainly attributed to the first stage. While in most of LPPRFBs the first stage is set to the DCT matrix, there is no good initial matrix for MIS-LPPRFBs, whose performance is similar or equal to DCT. For a fair comparison of both the structures, we set the initial stage of both the structures as the Walsh-Hadamard transform. For an 8-channel and 40-tap FB (i.e., M=8 and K=5), it is seen from Table. 7.2 that the number of free parameters is 96 in LPPRFB and 72 in MIS-LPPRFB. On a 1.8G Hz Pentium IV computer, the execution times for the design of the two FBs with Matlab are 162 and 91 seconds, respectively. Their performances are compared in Table. 7.5. Clearly, the MIS-LPPRFB outperforms the LPPRFB in all respects. By reducing the number of parameters, our lattice structure not only speeds up the optimization, but also more effectively avoids being trapped in a local minimum.

Table 7.5: Performance comparison of LPPRFB and MIS-LPPRFB (M=8, K=5)

Filter Bank	LPPRFB	MIS-LPPRFB
Coding Gain (dB)	9.35	9.38
DC Attenuation (dB)	91.22	94.64
Stopband Attenuation (dB)	24.34	24.69

7.5 Application in Image Compression Coding

Fig. 7.6 shows a typical scheme for image compression coding, including transform, quantization and entropy coding. In most international standards, such as JPEG [65] for still image compression and H.263 [66] as well as MPEG-1 [67] for video compression, an image is divided into small blocks and then the DCT is employed for each block. The DCT is well known for its fast implementation and good energy compaction property. Despite its tremendous success, the DCT still has its limitations. For example, since each block is processed independently by the DCT, the inter-block correlation is not exploited,

thus reducing the compression efficiency. This independent process also leads to annoying blocking artifacts after the quantization, due to a lack of continuity between the block boundaries.

Figure 7.6: Scheme of image compression

Later, the wavelet transform [69] as a powerful means of time-frequency analysis has been intensively studied, and has become one of the most commonly used image compression methods. Implemented as a hierarchical tree structure, the wavelet transform decomposes an image into a dyadic representation. Fig. 7.7 demonstrates a 3-level wavelet decomposition. At each level i, an image is decomposed both horizontally and vertically, yielding four subbands LL_i, HL_i, LH_i and HH_i representing, respectively, the low-frequency, horizontal high-frequency, vertical high-frequency, and diagonal high-frequency subimages. This process can be repeated on the subband LL_i to reach a higher-level decomposition. The frequency-region occupied by the subband images at a higher-level is roughly one-half of that at a lower-level and so is the resolution. After three decompositions, most of the energy is concentrated on the lowest-band LL_3 with the coarsest resolution, leaving the high-frequency components of a finer resolution in the other bands.

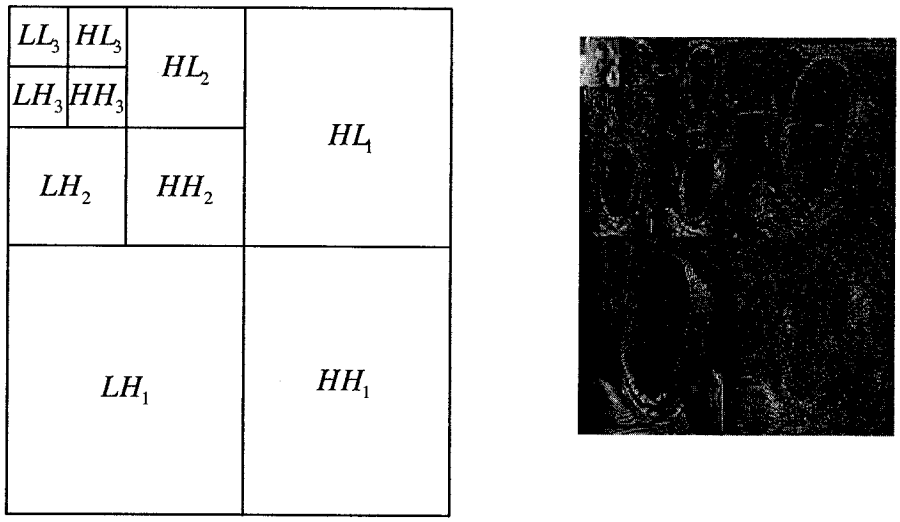

Figure 7.7: Three-level wavelet decomposition

The success of the wavelet transform can be explained from several aspects. 1. Compared to the DCT, the wavelet transform is processed on the whole image instead of the small blocks, which totally solves the block artifact problem. 2. The hierarchical tree structure gives a longer-length filter to compact the low-frequency energy and shorter-length filters to capture the high-frequency information. 3. The subband exhibits a logarithm distribution in both frequency and resolution, which complies with the human visual system. The observation of the fact that different subbands contain the information of the original image at different resolutions brings quite an interesting feature of the wavelet transform. To reconstruct the original image at a low resolution, one needs only the wavelet coefficients from some of the subbands. For a 3-level wavelet decomposition, to get the coarsest resolution, one needs only the coefficients of subband LL_3. With additional information from HL_3, LH_3 and HH_3, one can increase the resolution of the image. This idea is illustrated in Fig. 7.8.

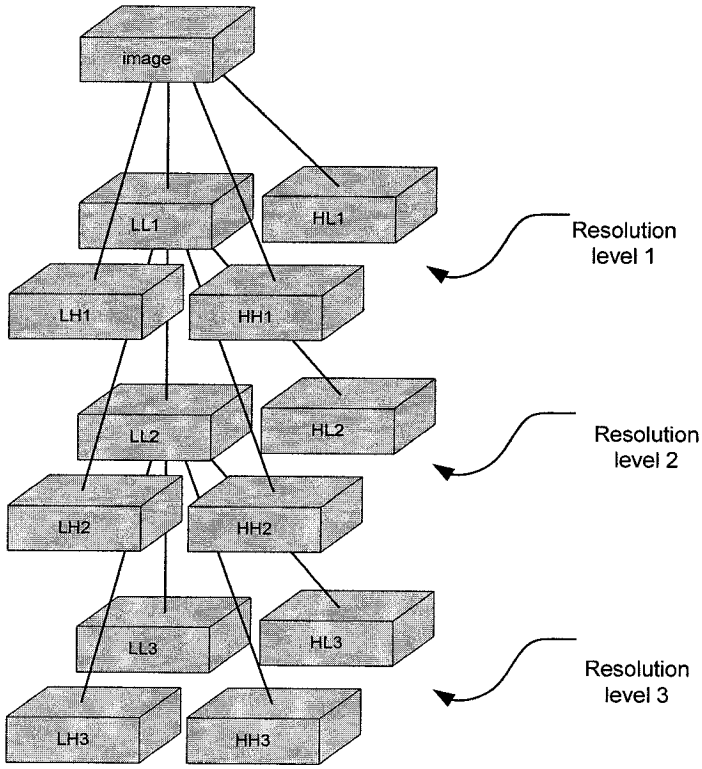

Figure 7.8: Scalable resolution in wavelet decomposition

By exploiting the spatial similarity between the different bands, many codecs have been proposed using wavelet transforms [105-107]. Said and Pearlman [106] proposed the Spatial Partitioning of Images into Hierarchical Trees (SPIHT) algorithm to efficiently organize the wavelet coefficients. Besides its amazing compression performance, an important feature called scalability has been realized. The scalability refers to the generation of a bit-stream containing embedded subsets, each of which represents an efficient compression of the original image at a reduced resolution or increased distortion.

It is well known that the wavelet transform is basically a two-channel LPPRFB. The hierarchical tree structure of the wavelet roughly divides the whole frequency into some "octave" subbands, as shown in Fig. 7.9(a). On the other hand, an M-channel LPPRFB

evenly divides the frequency band and gives a more detailed representation of the high-frequency component as shown in Fig. 7.9(b). In this section, we use the M-channel LPPRFB to replace the wavelet transform for image compression. In order to make use of the efficient wavelet-based SPIHT codec, we need to rearrange the coefficients of the LPPRFB such that the high-frequency subbands are merged together to implement an uneven frequency partition similar to that obtained from a wavelet transform. The reorganization is demonstrated in Fig. 7.10.

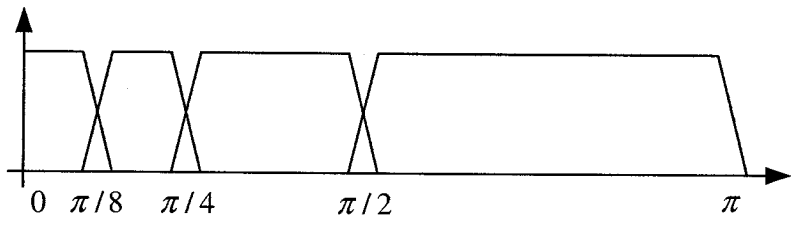

(a)

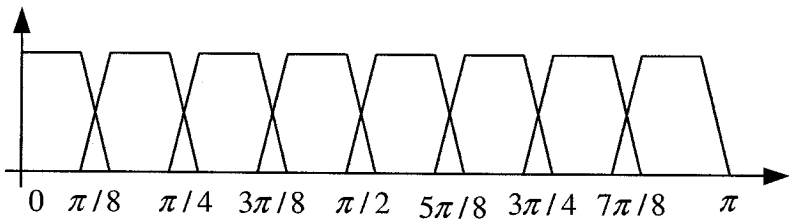

(b)

Figure 7.9: Typical frequency responses. (a) Three-level wavelet transform. (b) 8-channel LPPRFB

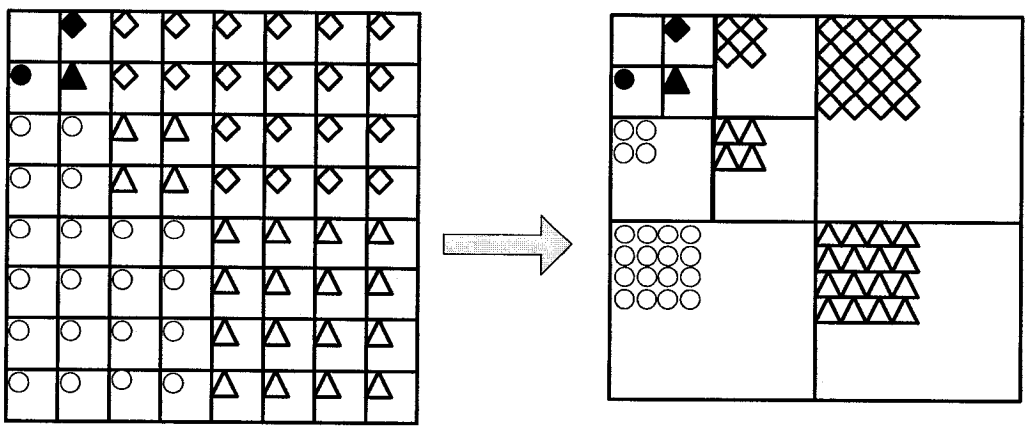

Figure 7.10: Rearrangement of LPPRFB coefficients to mimic wavelet processing

We have employed 8×16 and 8×24 MIS-LPPRFBs to replace the wavelet transform in the SPIHT algorithm for the compression of three images, Lena, Barbara and Goldhill. The resulting objective performances in terms of the peak signal-to-noise ratio (PSNR) under various compression ratios are listed in Table 7.6. The famous 9/7 wavelet and the corresponding 8×16 and 8×24 LPPRFBs are also employed as the transform in the SPIHT algorithm for the purpose of comparison. From Table 7.6, we notice that for a smooth image like Lena, the wavelet transform can sufficiently reduce the redundancy between the pixels. The LPPRFB has a higher complexity than the 9/7 wavelet, but gives comparable results. As compared to the LPPRFB, the MIS-LPPRFB saves 6 and 12 parameters for the filter bank configurations of 8×16 and 8×24, respectively, but the improvement in the PSNR is only about 0.1~0.2dB. For a highly textured image like Barbara, which contains rich high-frequency details, the LPPRFB and the MIS-LPPRFB provide a PSNR gain of around 2.5dB and 2.0dB, respectively, over the 9/7 wavelet transform under a wide range of bit rates. This significant improvement is due to the refined partition on the high frequency region. Under low and medium compression ratio, the high-frequency information is well preserved in LPPRFB and MIS-LPPRFB. The subjective results of the compressed Lena and Barbara images at a certain value of the PSNR are shown in Figs. 7.11 and 7.12. The table cloth part of the Barbara input is detailed in Fig. 7.13 to demonstrate the superiority of the MIS-LPPRFB in visual quality over the 9/7 wavelet. Obviously, under the compression ratio of 1:32, the refined detail of the table cloth, which is blurred when the 9/7 wavelet is used, is preserved in the MIS-LPPRFB compression. Over all the tested images at various compression ratios, the extension of the filter length could help to decorrelate the adjacent pixels and improve the

compression performance. However, with the increase of the filter length, the improvement in the PSNR is just marginal while the complexity would boost exponentially. Therefore, a medium filter length, such as K=2 or 3, is recommended.

Table 7.6: PSNR in dB of three compressed images under different transforms

Compress. Ratio	9/7 Wavelet	8×16 LPPRFB	8×16 MIS-LPPRFB	8×24 LPPRFB	8×24 MIS-LPPRFB
Lena (512×512)					
1:8	40.41	40.35	40.12	40.39	40.18
1:16	37.21	37.28	37.08	37.29	37.12
1:32	34.11	34.14	34.02	34.18	34.06
1:64	31.10	31.04	31.00	31.09	31.05
1:128	28.38	28.19	28.12	28.22	28.14
Barbara (512×512)					
1:8	36.41	37.84	37.15	38.01	37.26
1:16	31.40	33.02	32.67	33.21	33.10
1:32	27.58	29.04	28.53	29.33	28.64
1:64	24.86	26.00	25.74	26.17	25.88
1:128	23.35	23.49	23.38	23.81	23.51
Goldhill (512×512)					
1:8	36.55	36.69	36.56	36.72	36.59
1:16	33.13	33.31	33.17	33.33	33.20
1:32	30.56	30.70	30.61	30.71	30.63
1:64	28.48	28.58	28.52	28.59	28.54
1:128	26.73	26.71	26.69	26.73	26.71

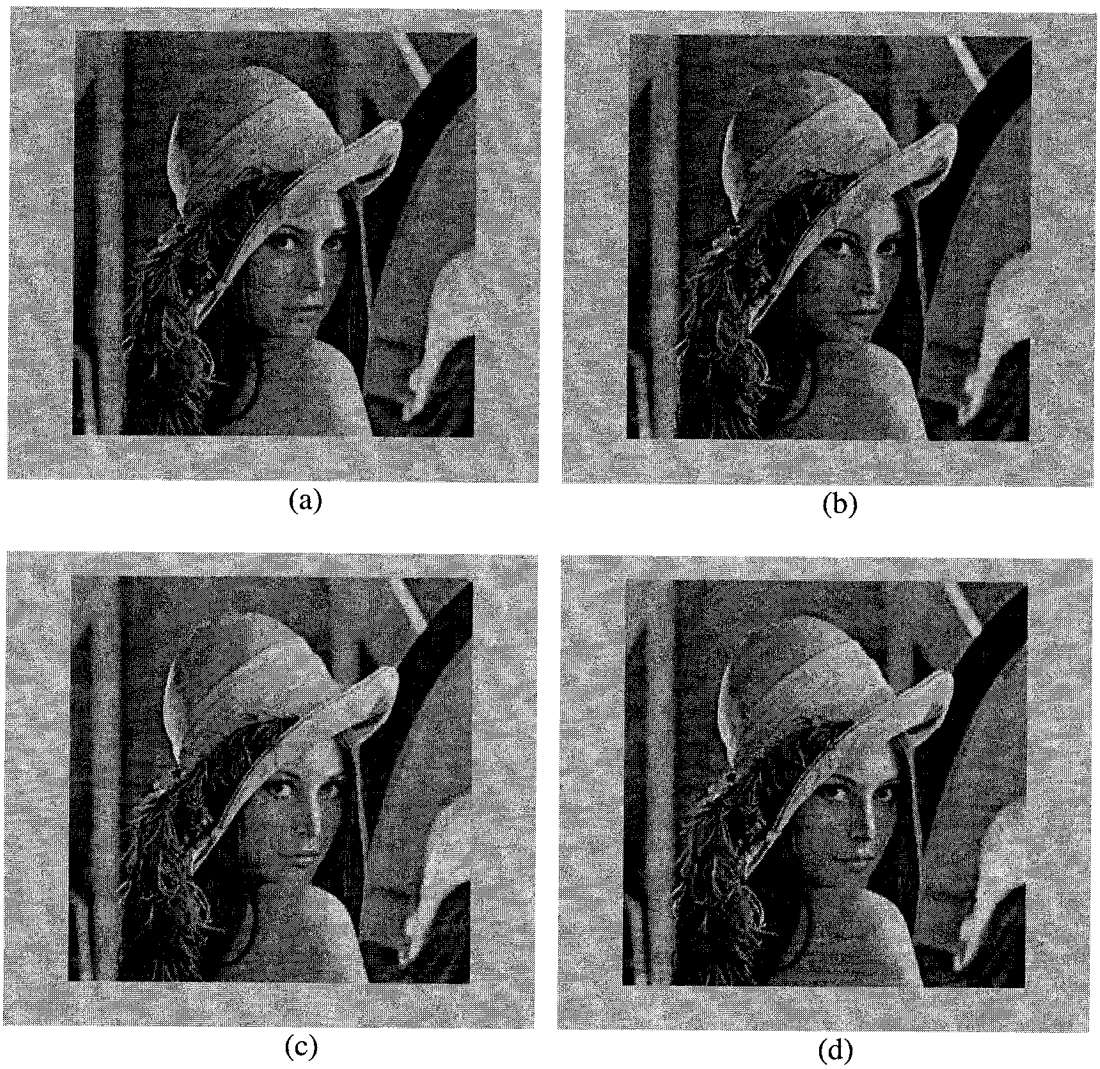

Figure 7.11: Coding results of Lena under 1:32 compression ratio. (a) Original image. (b) 9/7 wavelet at 34.11dB. (c) 8×16 LPPRFB at 34.14dB. (d) 8×16 MIS-LPPRFB at 34.10dB

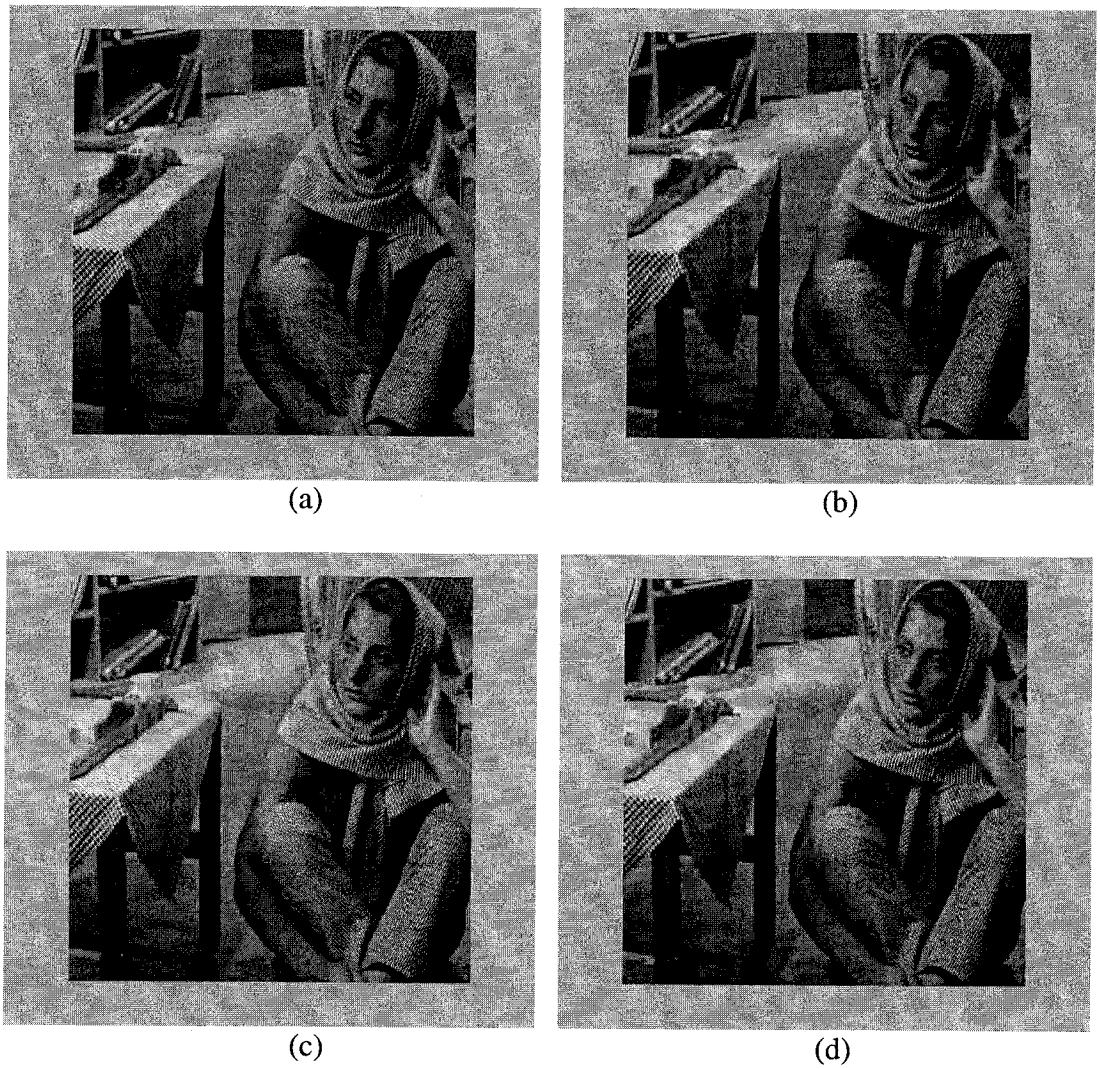

Figure 7.12: Coding results of Barbara under 1:32 compression ratio. (a) Original image. (b) 9/7 wavelet at 27.58dB. (c) 8×16 LPPRFB at 29.04dB. (d) 8×16 MIS-LPPRFB at 28.53dB

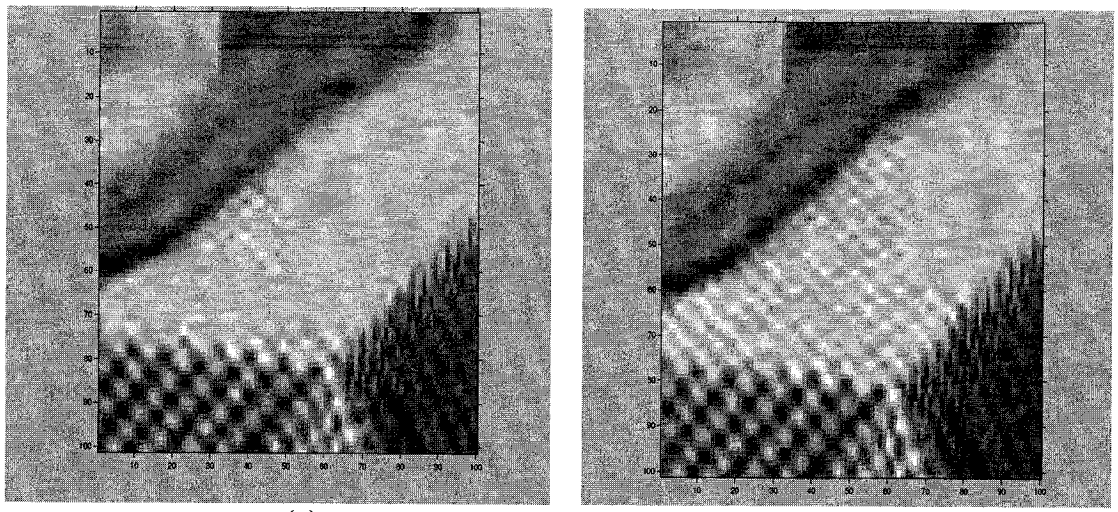

(a) (b)

Figure 7.13: Table cloth detail in Barbara under 1:32 compression ratio. (a) 9/7 wavelet at 27.58dB. (b) 8×16 MIS-LPPRFB at 28.53dB

7.6 Conclusion

In this chapter, a class of filter banks, MIS-LPPRFB, that possesses both the linear-phase property and the mirror-image symmetry, has been investigated. By combining the MIS and LP constraints, a lattice structure with fewer parameters has been proposed. It has been shown that the introduction of MIS has imposed certain constraints on the invertible matrices in the lattice structure of LPPRFB. A new simplification scheme has been developed to remove the redundancy in the traditional lattice structure of the LPPRFB without forfeiting the constraint imposed by the MIS property. This constraint has then been further exploited through the QR factorization, yielding a presentation with fewer parameters. It has been shown through numerical examples that the reduction of free parameters not only speeds up the filter bank design process, but also efficiently decreases the possibility of being trapped in a local minimum. The MIS-LPPRFB has also been employed as a transform in the image compression coding. The coding results

from the 9/7 wavelet and the LPPRFB have also been provided for comparison. It has been shown that under various compression ratios, the MIS-LPPRFB and the LPPRFB give comparable objective and subject performances, but the former has fewer parameters. For the compression of images with rich details, both the LPPRFB and the MIS-LPPRFB are superior to the 9/7 wavelet as a result of their provision of finer frequency partitions.

Chapter 8

Conclusions and Future Study

8.1 Concluding Remarks

In this dissertation, we have studied the design and implementation of a class of multirate systems, namely, the Mth-band filters and the constrained PRFBs (perfect reconstruction filter banks), from the point of view of a polyphase structure. An approach for the design of linear-phase Mth-band filters satisfying an interpolation condition has been first developed based on the generalized polyphase (GP) structure, and then extended to the design of 2-D FIR Mth-band filters. By employing the polyphase representation of analysis and synthesis filters, some new lattice structures have been developed for PRFBs with linear-phase and mirror-image symmetric constraints. It has been shown that all the desirable properties have been satisfied by exploiting the polyphase or the generalized polyphase structures, leading to a reduced design/implementation complexity of the Mth-band filters and filter banks.

The first part of the thesis has been devoted to the design of Mth-band filters that satisfy the time-domain interpolation condition. Although the interpolation condition could be easily accommodated in the conventional polyphase structure, the resulting subfilters therein are no longer linear-phase, thus hindering a direct design of linear-phase

filters via the polyphase structure. This observation motivated us to propose the GP-based design approach. With the insertion of a pair of inverse transform matrices between the delay chain and the subfilters in the conventional polyphase structure, a GP structure consisting of a number of linear-phase constituent filters has been obtained. Some seed transform matrices, which share some of the desirable properties with the Hadamard transform such as the structural simplicity and the frequency-selectivity, have been proposed [103]. Based on these seed matrices, the restriction to an even-order in using Hadarmard transforms has been relaxed to an arbitrary order. With the closed-form frequency specifications being derived, the linear-phase constituent filters can be designed easily and separately, leading to a reduced overall computational complexity [104]. Moreover, the interpolation condition can easily be satisfied by fixing one of the constituent filters in the proposed approach.

To demonstrate the flexibility of the proposed GP-based method, another useful property, the regularity, has also been incorporated in the design, yielding very satisfactory design results without increasing the filter order. The GP-based approach has further been extended to the design of 2-D Mth-band filters [105]. To obtain a very efficient implementation, we have also employed the singular-value decomposition (SVD) in the GP structure, resulting in considerable savings in the number of filter coefficients, yet giving a performance close to that obtained from the optimal minimax design.

The second part of the dissertation has been focused on the development of new lattice factorization for the constrained filter banks, including the MIS-PRFBs, the CMFBs, and the MIS-LPPRFBs. All the desirable properties, such as the linear-phase,

the mirror-image symmetry (MIS) and the perfect reconstruction, are structurally satisfied in the derived lattice structure. Moreover, these constraints have been exploited to reduce the number of parameters and in turn to reduce the design/implementation complexity of filter banks.

First, a basic building block, which is capable of propagating both the MIS and PR properties, has been proposed to develop the lattice structure for the MIS-PRFBs. It has been shown that an order-one factorization would be sufficient for even-channel MIS-PRFBs, while the basic building block for odd-channel MIS-PRFBs has to be at least of order two. The importance of our work is that, for the first time, a lattice structure has been proved to be complete for a class of PRFBs [111]. By using the lifting scheme in conjunction with given optimization criteria, the proposed MIS-PRFB has been designed and compared with general PRFBs, LPPRFBs and MIS-PUFBs. Simulation results show that the MIS-PRFB is superior to the LPPRFB with the same number of free parameters in terms of the stopband attenuation, while being comparable to the general PRFB of the same filter order, which however has twice the number of free parameters as the MIS-PRFB does. In comparison with the MIS-PUFB, the MIS-PRFB has relaxed the unitary requirement to the invertible one, while yielding a similar performance in both the stopband attenuation and the coding gain.

Secondly, the conventional CMFB has been formulated as a cascade of a modulation matrix and a polyphase matrix with a diamond sparse pattern, resulting in a simplified implementation. Under this framework, it has then been shown that the proposed new CMFBs are a special class of MIS-PUFBs. Observing that the conventional CMFB is generated from one prototype filter, new CMFBs have been proposed by introducing

multiple prototype filters in conjunction with a proper modulation scheme [112]. The proposed CMFBs fill the gap between the CMFB and MIS-PRFB. It has been shown that the number of the free parameters can be determined as a tradeoff between the implementation complexity and the performance of a filter bank depending on the particular applications.

Thirdly, we have combined the linear-phase and MIS properties as a stronger constraint to reduce the number of parameters in the lattice structure of MIS-PRFB and that of LPPRFB [113]. The simulation results have shown that the introduction of MIS does not jeopardize the performance of LPPRFB. In fact, ignoring the effect of the DCT, the MIS-LPPRFB has a better performance than the LPPRFB. As a result, the saving of the parameters owing to the stronger constraint can not only speed up the filter bank design, but also efficiently avoid the trap of local minimum.

The relationship amongst the filter banks discussed in this thesis is illustrated by Fig. 8.1. Obviously, all the constrained filter banks, the MIS-PRFB, CMFB, LPPRFB and MIS-LPPRFB, belong to the general PRFB. The MIS-PRFB includes the conventional CMFB as a subclass and the LPPRFB has an overlap with MIS-PRFB, i.e., the MIS-LPPRFB. Overall, the MIS-PRFB as highlighted in the figure is the subfield of filter banks which the dissertation has mainly contributed to.

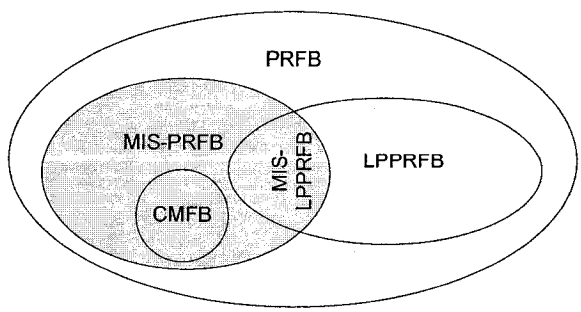

Figure 8.1: Relationship between several constrained PRFBs

In the thesis, some experimental work has also been carried out to validate the applications of Mth-band filters and the MIS-LPPRFBs. An Mth-band filter designed via the GP-based approach has been employed as an interpolation filter for image resizing [114]. It is seen that using the Mth-band filter designed by the proposed method yields a much sharper edge compared to that obtained from other methods. For example, the eigenfilter approach suffers from ringing artifacts at the vicinity of major edges.

The MIS-LPPRFB has been adopted as a lapped block transform in image compression coding. The transformed coefficients have been reorganized to mimic the wavelet transform to exploit the efficiency provided by an existing compression scheme like SPIHT. The MIS-LPPRFB consistently gives a superior performance for a bunch of images at a wide range of compression rate. In comparison to the LPPRFB, the MIS-LPPRFB has saved a considerable amount of implementation cost, yet causing a performance loss like the signal-to-noise ratio (SNR) that is only marginal. It has also been observed that for complicated images with rich details and textures like Barbara, thanks to the more precise high frequency resolution, the MIS-LPPRFB outperforms the famous 9/7 wavelet transform.

8.2 Suggestions for Further Investigation

The major contributions of the thesis to filter banks originate from a key idea, namely, to develop new lattice structures, by incorporating the desirable constraints such as the linear-phase and the MIS, in order to reduce the number of parameters. This idea can be further extended in two directions. One is to consider other types of useful

constraints in the design and implementation of the lattice-based filter banks. The other is to impose the linear-phase and MIS constraints on other types of filter banks.

In Chapter 3, we have considered another type of constraint — the regularity. This constraint is very useful in the wavelet area and has already been investigated for the design of filter banks in recent publications. In [78], the regularities of (K_a, K_s) for the analysis and synthesis filters of a PUFB have been imposed onto the lattice structure of LPPUFBs. These conditions are expressed in terms of the rotation angles of the lattice components, which guarantee the resulting filterbanks to have one or two degrees of regularity. Based on these new regular filterbanks, a large family of symmetric M-band orthonormal wavelets could be generated. Following this idea, the regularity condition can be further combined with the MIS and linear-phase constraints to yield new filter banks with more desirable features.

As another extension of the proposed approach, various implementation structures of 2-D filter banks could be developed by exploiting the afore-mentioned constraints. The idea of sampling a multi-dimensional signal is based on the mathematical concept of *lattices*. The use of lattices has been extended to the discrete-time decimation and interpolation and later to multi-dimensional filter banks. In subband-based image processing, an image is normally decomposed horizontally and vertically by a 1-D filter bank. The decomposed subband images have only three orientations: horizontal, vertical and diagonal directions. In some applications, like fingerprint identification, the interested information may not have major energy distribution in these three directions. In 1992, Bamberger and Smith [117] proposed the so-called directional filter bank (DFB) for an efficient directional decomposition of 2-D signals.

The DFBs have the ability to extract features with a particular frequency and resolution of arbitrary directions and have found important applications in fingerprint feature extraction and matching [118-120]. However, a 2-D DFB would even worsen the already exacerbated complexity concern. Recalling in our thesis, various constraints have been introduced and efficiently reduced the design/implement complexity, it would be urgent to introduce some extra desirable constraints, such as the MIS, for this kind of 2-D filter banks. The expansion of the dimension from one to two makes the mirror-image symmetry is no longer unique and leaves more room for the future investigation. Imposing the MIS constraint on the DFB, I believe there are many work to be carried out in the development of the lattice structures for MIS-PR-DFBs.

Another suggestion for future study is to develop lattice structures for oversampled filter banks. Note that all the FBs considered in this thesis are critically sampled, i.e., the downsampling rate for each branch of the analysis bank is the same and equal to the number M of channels. This is the most popular choice for many applications where one would like to keep the sampling rate unchanged, before and after the subband processing, in the multirate system. More recently, however, the oversampled FB, where the sampling rate in the analysis bank is smaller than the channel number M, has attracted more research attention [121-122]. In this class of FBs, the sampling rate of the synthesis bank is greater than the channel number. Therefore, there must be some redundancy in the processed signal. This redundancy can be manipulated such that the signal is error-robust to possible attacks. It would be an interesting topic to study the lattice structure of the oversampled FB, as well as its variations when the relevant symmetry constraints are considered.

Bibliography

[1] R. E. Crochiere and L. R. Rabiner, "Interpolation and decimation of digital signals: a tutorial review," *Proc. IEEE*, vol. 69, pp. 300-331, March 1981.

[2] R. E. Crochiere, "Subband coding," *Bell System Tech. J.*, vol. 60, pp. 1633-1654, Sept. 1981.

[3] R. E. Crochiere and L. R. Rabiner, *Multirate digital signal processing*, Englewood Cliffs, NJ: Prentice Hall, 1983.

[4] M. Vetterli and J. Kovacevic, *Wavelets and Subband Coding*, Englewood Cliffs, NJ: Prentice Hall, 1995.

[5] P. P. Vaidyanathan, *Multirate Systems and Filter Banks*, Prentice Hall, 1993.

[6] J. F. Kaiser, "Nonrecursive digital filter design using the I_0-sinh window function," *Proc. IEEE Int. Symp. on Circuits and Sys.*, San Francisco, pp. 2—23, April 1974.

[7] A. V. Oppenheim and R. W. Schafer, *Discrete-time signal processing*, Prentice Hall, Inc., Englewood Cliffs, NJ, 1989.

[8] Y. Lim, "Efficient special purpose linear programming for FIR filter design," *IEEE Trans. on Signal Processing*, vol. 31, pp. 963-968, Aug. 1983.

[9] A. T. Johnso, "Optimal linear phase digital filter design by one-phase linear programming," *IEEE Trans. on Circuits and Systems*, vol. 37, pp. 554-558, April 1990.

[10] W. –S. Lu, "A unified approach for the design of 2-D digital filters via semidefinite programming," *IEEE Trans. Circuits and Systems I: Fundamental Theory and Applications*, vol. 49, pp. 814-826, June 2002.

[11] A. Ben-Tal and A. Nemirovski, *Lectures on Modern Convex Optimization: Analysis, algorithms, and engineering applications*, MPS-SIAM, Philadelphia, PA, 2001.

[12] Z. Lin and Y. Liu, "FIR filter design with group delay constraint using semdefinite programming," *Proc. IEEE Symposium on Circuits and Systems 2006*, pp. 2505-2508, May 2006.

[13] S. C. Chan and K. M. Tsui, "On the design of real and complex FIR filters with flatness and peak error constraints using semidefinite programming," *Proc. IEEE Symposium on Circuits and Systems 2004*, pp. III 125-128, May 2004.

[14] R. A. Gopinath, "Lowpass delay filters with flat magnitude and group delay constraints," *IEEE Trans. Signal Processing*, vol. 51, pp. 182-192, Jan. 2003.

[15] L. R. Rabiner and B. Gold, *Theory and application of digital signal processing*, Prentice Hall, Inc., Englewood Cliffs, 1975.

[16] T. W. Parks and J. H. McClellan, "Chebyshev approximation for nonrecursive digital filters with linear phase," *IEEE Trans. on Circuit Theory*, vol. CT-19, pp. 189-194, March 1972.

[17] P. P. Vaidyanathan and T. Q. Nguyen, "Eigenfilters: a new approach to least-squares FIR filter design and applications including Nyquist filters," *IEEE Trans. on Circuits and Systems*, vol. 34, pp. 11-23, Jan. 1987.

[18] T. Q. Nguyen, "The design of arbitrary FIR digital filters using the eigenfilter method," *IEEE Trans. on Signal Processing*, vol. 41, pp. 1128-1139, March 1993.

[19] Y. Neuvo, C.-Y. Dong, and S. Mitra, "Interpolated finite impulse response filters," *IEEE Trans. Signal Processing*, vol. 32, pp. 563-570, Jun 1984.

[20] Y. C. Lim, and L. Yong, "Frequency-response masking approach for digital filter design: complexity reduction via masking filter factorization," *IEEE Trans. Circuits and Systems II*, vol. 41, pp. 518-525, Aug. 1994.

[21] Y. C. Lim, Y. J. Yu, T. Saramaki, "Optimum masking levels and coefficient sparseness for Hilbert transformers and half-band filters designed using the frequency-response masking technique," *IEEE Trans. Circuits and Systems I*, vol. 52, pp. 2444-2453, Nov. 2005.

[22] S. K. Mitra, A. Mahalanobis, and T. Saramaki, "A generalized structural subband decomposition of FIR filters and its application in efficient FIR filter design and implementation," *IEEE Trans. Circuits and Systems II*, vol. 40, pp. 363-374, June 1993.

[23] S. K. Mitra and U. Heute, "Structural sub-band decomposition of sequences and its applications in signal processing," in *IEE Proceeding, Vision, Image and Signal Processing*, vol. 146, pp. 109-123, June 1999.

[24] T.-B. Deng, E. Saito, and E. Okamoto, "Efficient design of SVD-based 2-D digital filters using specification symmetry and order-selecting criterion," *IEEE Trans. Circuits & Systems I*, vol. 50, pp. 217-226, Feb. 2003.

[25] W. –P. Zhu, M. O. Ahmad and M. N. S. Swamy, "Realization of 2-D linear-phase FIR filters by using the singular-value decomposition," *IEEE Trans. Signal Processing*, vol. 47, pp.1349-1358, May 1999.

[26] W. –S. Lu, H. –P. Wang and A. Antoniou, "Design of two-dimensional FIR digital filters by using the singular-value decomposition," *IEEE Trans. Circuit Syst.*, vol. 37, pp. 35-46, Jan. 1990.

[27] S. –C. Fei, W. –S. Lu, and C. –C. Tseng, "Two-dimensional FIR notch filter design using singular value decomposition," *IEEE Trans. Circuit Syst. I*, vol. 45, pp. 290-294, March 1998.

[28] F. Mintzer, "On half-band, third-band, and *N*th-band FIR filters and their design," *IEEE Trans. Acous. Speech, and Signal Processing*, vol. 30, pp. 734-738, Oct 1982.

[29] P. Vaidyanathan and T. Nguyen, "A 'trick' for the design of FIR half-band filters," *IEEE Trans. Circuits & Systems*, vol. 34, pp. 297-300, Mar 1987.

[30] S. Jayasimha and P. V. R. Narasimha, "An iteration scheme for the design of equiripple *M*th-band FIR filters," *IEEE Trans. Signal Processing*, vol. 43, pp. 1998-2002, Aug. 1995.

[31] C. Wu, W.-P. Zhu and M. N. S. Swamy, "Some new results in the design of *M*th-band FIR filters," in *Proc. IEEE Int. Midwest Symp. Circuits and Syst.*, Japan, July 2004, pp. II.53-II.56.

[32] Y. Wisutmethangoon, T. Q. Nguyen, "A method for design of *M*th-band filters," *IEEE Trans. Signal Processing*, vol. 47, pp. 1669-1678, June 1999.

[33] H. L. Seo and L. Y. Yong, "A new approach to synthesize sharp 2D half-band filters," *IEEE Trans. Circuits & Systems II: Analog and Digital Signal Processing*, vol. 46, pp. 1104-1110, Aug. 1999.

[34] Y. Seungjoon, T. Q. Nguyen, "Interpolated *M*th-band filters for image size conversion," *IEEE Trans. Signal Processing*, vol. 50, pp. 3028-3035, Dec. 2002.

[35] S. Oraintara and T. Q. Nguyen, "A simple mapping between *M*th-band FIR filters using cosine modulation," *IEEE Signal Processing Letters*, vol. 10, pp. 125-128, May 2003.

[36] M. J. T. Smith and T. P. Barnwell III, "A procedure for designing exact reconstruction filter banks for tree structured subband coders," *Proc. IEEE Int. Conf. Acoust. Speech and Signal Proc.*, pp. 27.1.1-27.1.4, San Diego, CA, March 1984.

[37] F. Mintzer, "Filters for distortion-free two-band multirate filter banks," *IEEE Trans. on Acoust., Speech and Signal Proc.*, vol. 33, pp. 626-630. June 1985.

[38] H. J. Nussbaumer, "Pseudo QMF filter bank," *IBM Tech. disclosure Bulletin*, vol. 24, pp. 3081-3087, Nov. 1981.

[39] T. A. Ramstad, "Analysis/synthesis filter banks with critical sampling," *Int. Conf. on Digital Signal Processing*, Florence, Sept. 1984.

[40] M. J. T. Smith and T. P. Barnwell III, "A unifying framework for analysis/synthesis systems based on maximally decimated filter banks," *Proc. IEEE Int. Conf. Acoust., Speech and Signal Processing*, pp. 521-524, Tampa, FL, March 1985.

[41] M. Vetterli, "Filter banks allowing for perfect reconstruction," *Signal Processing*, vol. 10, pp. 219-244, April 1986.

[42] J. P. Princen and A. P. Bradley, "Analysis/synthesis filter bank design based on time domain aliasing cancellation," *IEEE Trans. on Acoust., Speech and Signal Processing*, vol. 34, pp. 1153-1161, Oct. 1986.

[43] P. Saghizadeh, and A. N. Willson, "A new approach to the design of critically sampled M-channel uniform-band perfect-reconstruction linear-phase FIR filter banks," *IEEE Trans. Signal Processing*, vol. 46, pp. 1544-1557, June 1998.

[44] Y. –J. Chen, and K. S. Amaratunga, "M-channel lifting factorization of perfect reconstruction filter banks and reversible M-band wavelet transforms," *IEEE Trans. on Circuits and Systems-II: Analog and Digital Signal Processing*, vol. 50. pp. 963-976, Dec. 2003.

[45] R. Kumar, Y. –J. Chen, S. Oraintara, and K. Amaratunga, "Lapped unimodular transforms: Lifting factorization and structural regularity," *IEEE Trans. Signal Processing*, vol. 54, pp. 921-931, March 2006.

[46] S. –M. Phoong and Y. –P. Lin, "Lapped unimodular transform and its factorization," *IEEE Trans. Signal Processing*, vol. 50, pp. 2695-2701, Nov. 2002.

[47] L. Gan, "On parameterizations of first-order unimodular filter banks," in *Proc. IEEE Int. Conf. Acoust. Speech, Signal Processing*, pp. III-233-236, 2006.

[48] P. P. Vaidyanathan, "Theory and design of M-channel maximally decimated quadrature mirror filter banks with arbitrary M, having perfect reconstruction property," *IEEE Trans. on Acoust., Speech and Signal Proc.*, vol. 35, pp. 476-492, April 1987.

[49] T. Q. Nguyen and P. P. Vaidyanathan, "Maximally decimated perfect-reconstruction FIR filter banks with pairwise mirror-image analysis (and synthesis)

frequency responses," *IEEE Trans. on Acoust., Speech and Signal Processing*, vol. 36, pp. 693-706, May 1988.

[50] A. K. Soman and P. P. Vaidyanathan, "A complete factorization of paraunitary matrices with pairwise mirror-image symmetry in the frequency domain," *IEEE Transactions on Signal Processing*, vol. 43, no. 4, pp. 1002–1004, 1995.

[51] P. P. Vaidyanathan and T. Chen, "Role of anticausal inverses in multirate filter-banks--part I: Systems-Theoretic fundamentals," *IEEE Trans on Signal Processing*, vol. 43, pp. 1092-1102, May 1995.

[52] P. P. Vaidyanathan and T. Chen, "Role of anticausal inverses in multirate filter-banks—Part II: The FIR case, factorizations, and biorthogonal lapped transforms," *IEEE Trans. on Signal Processing*, vol. 43, pp. 1103-1115, May 1995.

[53] P. Rault and C. Guillemot, "Symmetric Delay factorization: Generalized framework for paraunitary filter banks," *IEEE Trans. on Signal Processing*, vol. 47, pp. 3315-3325, Dec. 1999.

[54] X. –Q. Gao, T. Q. Nguyen, and G. Strang, "On factorization of *M*-channel paraunitary filterbanks," *IEEE Trans. on Signal Processing*, vol. 49, pp. 1433-1446, July 2001.

[55] L. Gan and K. –K. Ma, "On simplified order-one factorizations of paraunitary filterbanks," *IEEE Trans. Signal Processing*, vol. 52, pp. 674-686, March 2004.

[56] T. Q. Nguyen and P. P. Vaidyanathan, "Two-channel perfect reconstruction FIR QMF structures which yields linear phase FIR analysis and synthesis filters," *IEEE Trans. Acoustics, Speech and Signal Processing*, vol. 37, pp. 676-690, May 1989.

[57] S. –M. Phoong, C. W. Kim, P. P. Vaidyanathan, and R. Ansari, "A new class of two-channel biorthogonal filter banks and wavelet bases," *IEEE Trans. Signal Processing*, vol. 43, pp. 649-665, March 1995.

[58] S. Mallat, "A theory for multiresolution signal decomposition: the wavelet representation," *IEEE Trans. Pattern Anal., and Machine Intell.*, vol. 11, pp. 674-693, July 1989.

[59] Z. –J. Mou, "Symmetry exploitation in digital interpolators/decimators," *IEEE Trans. Signal Processing*, vol. 44, pp. 2611-2615, Oct. 1996.

[60] I. Daubechies, *Ten lectures on wavelets*, SIAM, CBMS series, April 1992.

[61] P. –L. Shui and Z. Bao, "*M*-band biorthogonal interpolating wavelets via lifting scheme," *IEEE Trans. Signal Processing*, vol. 52, pp. 2500-2512, Sept. 2004.

[62] M. Vetterli, and C. Herley, "Wavelets and filter banks: Theory and design," *IEEE Trans. Signal Processing*, vol. 40, pp. 2207-2232, Sept. 1992.

[63] G. Strang and T. Q. Nguyen, *Wavelets and Filter Banks*, Wellesley-Cambridge Press, 1997.

[64] K. R. Rao and P. Yip, *Discrete Cosine Transform: Algorithms, Advantages, Applications*, Academic Press, New York, 1990.

[65] W. B. Pennebaker and J. L. Mitchell, *JPEG Still Image Data Compression Standard*, Van Nostrand Reinhold, New York, 1993.

[66] G. Cote, B. Erol, M. Gallant, and F. Kossentini, "H.263+: video coding at low bit rates," *IEEE Trans. CSVT*, vol. 8, pp. 849-866, Nov. 1998.

[67] ISO/IEC 13818: "Generic coding of moving pictures and associated audio (MPEG-2)".

[68] H. S. Malvar and D. H. Staelin, "The LOT: Transform coding without blocking effects," *IEEE Trans. Acoust., Speech, Signal Processing*, vol. 37, pp. 553-559, April 1989.

[69] H. S. Malvar, *Signal Processing with Lapped Transforms*, Norwood, MA: Artech House, 1992.

[70] A. K. Soman, P. P. Vaidyanathan, and T. Q. Nguyen, "Linear phase paraunitary filter banks: Theory, factorizations and designs," *IEEE Trans. on Signal Processing*, vol. 41, pp. 3480-3496, Dec. 1993.

[71] R. L. de Queiroz, T. Q. Nguyen, and K. R. Rao, "The GenLOT: Generalized linear-phase lapped orthogonal transform," *IEEE Trans. on Signal Processing*, vol. 44, pp. 497-507, March 1996.

[72] T. D. Tran, M. Ikehara, and T. Q. Nguyen, "Linear phase paraunitary filter bank with filters of different lengths and its application in image compression," IEEE Trans. Signal Processing, vol. 47, pp. 2730-2744, Oct. 1999.

[73] T. D. Tran and T. Q. Nguyen, "On *M*-channel linear phase FIR filter banks and application in image compression," *IEEE Trans. on Signal Processing*, vol. 45, pp. 2175-2187, Sep. 1997.

[74] T. D. Tran, R. L. de Queiroz, and T. Q. Nguyen, "Linear-phase perfect reconstruction filter bank: Lattice structure, design, and application in image coding," *IEEE Trans. Signal Processing*, vol. 48, pp. 133-147, Jan. 2000.

[75] L. Gan and K. –K. Ma, "A simplified lattice factorization for linear-phase paraunitary filter banks with pairwise mirror image frequency responses," *IEEE Trans. on Circuits and Systems II: Express Briefs*, vol. 51, pp. 3-7, Jan. 2004.

[76] T. D. Tran, R. L. de Queiroz, and T. Q. Nguyen, "The variable-length generalized lapped biorthogonal transform,"

[77] C. W. Kok, T. Nagai, M. Ikehara and T. Q. Nguyen, "Lattice structures parameterization of linear phase paraunitary matrices with pairwise mirror-image symmetry in the frequency domain with an odd number of rows," *IEEE Trans. Circuits and Systems-II: Analog and Digital Signal Processing*, vol. 48, pp. 633-636, June 2001.

[78] S. Oraintara, T. D. Tran, P. N. Heller, and T. Q. Nguyen, "Lattice structure for regular paraunitary linear-phase filterbanks and *M*-band orthogonal symmetric wavelets," *IEEE Trans. on Signal Processing*, vol. 49, pp. 2659-2672, Nov. 2001.

[79] J. Liang, T. D. Tran and R. L. de Queiroz, "DCT-based general structure for linear-phase paraunitary filterbanks," *IEEE Trans. Signal Processing*, vol. 51, pp.1572-1580, June 2003.

[80] T. D. Tran, J. Liang, and C. Tu, "Lapped transform via time-domain pre- and post-processing," *IEEE Trans. Signal Processing*, vol. 51, pp. 1557-1571, June 2003.

[81] T. Tanaka, Y. Hirasawa, and Y. Yamashita, "Variable-length lapped transforms with a combination of multiple synthesis filter banks for image coding," *IEEE Trans. Signal Processing*, vol. 15, pp. 81-88, Jan. 2006.

[82] L. Gan, K. –K. Ma, T. Q. Nguyen, T. D. Tran, and R. L. de Queiroz, "On the completeness of the lattice factorization for linear-phase perfect reconstruction filter banks," *IEEE Signal Processing Letters*, vol. 9, pp. 133-136, April 2002.

[83] T. D. Tran, "The BinDCT: Fast multiplierless approximation of the DCT," *IEEE Signal Processing Letters*, vol. 7, pp. 141-144, June 2000.

[84] T. D. Tran, "The LiftLT: Fast-lapped transforms via lifting steps," *IEEE Trans. on Signal Processing Letters*, vol. 7, pp. 145-148, June 2000.

[85] J. Liang and T. D. Tran, "Multiplierless approximations of the DCT with the lifting scheme," *IEEE Trans. on Signal Processing*, vol. 49, pp.3032-3044, Dec. 2001.

[86] T. D. Tran, "*M*-channel linear phase perfect reconstruction filter bank with rational coefficients," *IEEE Trans. Circuits and Systems-I: Fundamental Theory and Applications*, vol. 49, pp. 914-925, July 2002.

[87] R. V. Cox, "The design of uniformly and nonuniformly spaced pseudo QMF," *IEEE Trans. Acoust., Speech, Signa Processing*, vol. 34, pp. 1090-1096, Oct. 1986.

[88] H. S. Malvar, "Extended lapped transforms: properties, applications, and fast algorithms," *IEEE Trans. Signal Processing,* vol. 40, pp. 2703-2714, Nov. 1992.

[89] R. D. Koilpillai and P. P. Vaidyanathan, "Cosine-modulated FIR filter banks satisfying perfect reconstruction," *IEEE Trans. Signal Processing*, vol. 40, pp. 770-782, April 1992.

[90] P. N. Heller, T. Karp and T. Q. Nguyen, "A general formulation of modulated filter banks," *IEEE Trans. Signal Processing*, vol. 47, pp. 986-1002, April 1999.

[91] G. D. T. Schuller, and M. J. T. Smith, "New framework for modulated perfect reconstruction filter banks," *IEEE Trans. Signal Processing*, vol. 44, pp. 1941-1954, August 1996.

[92] R. A. Gopinath, and C. S. Burrus, "On cosine-modulated wavelet orthogonal bases," *IEEE Trans. Image Processing*, vol. 4, pp. 162-176, Feb. 1995.

[93] A. Mertins, "Frame analysis for biorthogonal cosine-modulated filterbanks," *IEEE Trans. Signal Processing*, vol. 51, pp. 172-181, Jan. 2003.

[94] R. B. Casey and T. Karp, "Performance analysis and prototype filter design for perfect-reconstruction cosine-modulated filter banks with fixed-point implementation," *IEEE Trans. on Circuits and Systems II: Express Briefs*, vol. 52, pp. 452-456, August 2005.

[95] R. Bregovic and T. Saramaki, "A systematic technique for designing linear-phase FIR prototype filters for perfect-reconstruction cosine-modulated and modified DFT filterbanks," *IEEE Trans. Signal Processing*, vol. 53, pp. 3193-3201, August 2005.

[96] X. Q. Gao, Z. Y. He, and X. –G. Xia, "Efficient implementation of arbitrary-length cosine-modulated filter bank," *IEEE Trans. Signal Processing*, vol. 47, pp. 1188-1192, April 1999.

[97] Y. –P. Lin and P. P. Vaidyanathan, "Linear phase cosine modulated maximally decimated filter banks with perfect reconstruction," IEEE Trans. Signal Processing, vol. 42, pp. 2525-2539, Nov. 1995.

[98] J. F. Sturm, SeDuMi MATLAB Software for Semidefinite Programming (Version 1.04), Available on: http://fewcal.kub.nl/sturm/software/sedumi.html

[99] K. C. Toh, M. J. Tood, and R. H. Tutuncu, SDPT3 Version 2.1-A. MATLAB Software for Semidefinite Programming, Available: http://www.math.nus.edu.sg/~mattohkc/sdpt3.htmal.

[100]H. S. Hou and H. C. Andrews, "Cubic splines for image interpolation and digital filtering," *IEEE Trans. Acoust., Speech, Signal Processing*, vol. ASSP-26, pp. 508-517, 1978.

[101]C. C. Paige and M. Wei, "History and generality of the CS decomposition," *Linear Algebra Applicat.*, vol. 209, pp. 303-326, 1982.

[102]R. A. Horn and C. R. Johnson, *Matrix Analysis.* Cambridge, U. K.: Cambridge Univ. Press, 1985.

[103]C. Wu, W. –P. Zhu, and M. N. S. Swamy, "Design of *M*th-band FIR filters based on generalized polyphase structure," *Proc. 2006 Int. Symposium on Circuits and Systems*, pp. 2037-2040, Kos, Greece, May 2006.

[104]C. Wu, W. –P. Zhu, and M. N. S. Swamy, "Design of *M*th-band FIR filters based on generalized polyphase structure," *IEEE Trans. Circuits & Systems I: Regular Papers,* submitted.

[105]W. –P. Zhu, C. Wu, and M. N. S. Swamy, "Realization of 2-D FIR filters using generalized polyphase structure combined with singular-value decomposition," *Proc. 2006 Int. Symposium on Circuits and Systems*, pp. 2821-2824, Kos, Greece, May 2006.

[106]J. Katto and Y. Yasuda, "Performance evaluation of subband coding and optimization of its filter coefficients," in *SPIE Proc. Visual Commun. Image Process.*, Boston, MA, Nov. 1991, pp. 95-106.

[107]J. M. Shapiro, "Embedded image coding using zerotrees of wavelet coefficients," *IEEE Trans. Signal Processing*, vol. 41, pp. 3445-3462, Dec. 1993.

[108]A. Said and W. A. Pearlman, "A new fast and efficient image codec based on set partitioning in hierarchical trees," *IEEE Trans. on Circuits & Systems Video Tech.*, vol. 6, pp. 243-250, June 1996.

[109]D. S. Taubman, "High performance scalable image compression with EBCOT," *IEEE Trans. Image Processing*, vol. 9, no. 7, pp. 1158-1170, Jul. 2000.

[110]C. Wu, W.-P. Zhu and M. N. S. Swamy, "A Watermark Embedding Scheme in Wavelet Transform Domain," in *Conf. Proc. TENCON 2004*, Thailand, pp. A279-A282, Nov., 2004.

[111]C. Wu, W. –P. Zhu, and M. N. S. Swamy, "Perfect reconstruction filter banks with mirror-image symmetry: Lattice structure, design, and implementation," *IEEE Trans. Circuits & Systems I: Regular Papers,* submitted.

[112]C. Wu, W. –P. Zhu, and M. N. S. Swamy, "A class of cosine-modulated filter banks with multiple prototype filters," *Proc. 2007 IEEE Int. Circuits and Systems*, May 2007, New Orleans, USA.

[113]C. Wu, W. –P. Zhu, and M. N. S. Swamy, "Linear-phase perfect reconstruction filter bank with mirror-image constraints and its application in image coding," *IEEE Trans. Circuits & Systems II: Express Briefs*, in preparation.

[114]C. Wu, W. –P. Zhu, and M. N. S. Swamy, "GP structure-based *M*th-band filter design and application to image interpolation," in *Proc. IEEE Int. Midwest Symp. Circuits and Syst.*, Montreal, Canada, August 5-8, 2007, pp. II.78- II.81.

[115]C. Wu, W. –P. Zhu, and M. N. S. Swamy, "A Complete Lattice Structure for a Class of Perfect Reconstruction Filter Banks," submitted to ISCAS'08, Seattle, USA, 18-21 May 2008.

[116]C. Wu, W. –P. Zhu, and M. N. S. Swamy, "A Lattice Structure for Linear-Phase Perfect Reconstruction Filter Banks with Mirror Image," submitted to ISCAS'08, Seattle, USA, 18-21 May 2008.

[117]R. H. Bamberger and M. J. T. Smith, "A filter bank for the directional decomposition of images: Theory and design," IEEE Trans. Signal Process., vol. 40, pp. 882-893, April 1992.

[118]C. –H. Park, J. –J. Lee, M. J. T. Smith, S. –I. Park, and K. –H. Park, "Directional filter bank-based fingerprint feature extraction and matching," *IEEE Trans. Circuits and Systems for Video Tech.*, vol. 14, pp. 74-85, Jan. 2004.

[119]T. T. Nguyen and S. Oraintara, "A class of multiresolution directional filter banks," *IEEE Trans. Signal Processing*, vol. 55, pp. 949-961, March 2007.

[120]R. Eslami and H. Radha, "A new family of nonredudant transforms using hybrid wavelets and directional filter banks," *IEEE Trans. Image Processing*, vol. 16, pp. 1152-1167, April 2007.

[121]Z. Cvetkovic and M. Vetterli, "Oversampled filter banks," *IEEE Trans. Signal Processing*, vol. 46, pp. 1245-1255, May 1998.

[122]F. Labeau, J.-C. Chiang, M. Kieffer, P. Duhamel, L. Vandendorpe, and B. Macq, "Oversampled filter banks as error correcting codes: Theory and impulse noise correction," *IEEE Trans. Signal Processing*, vol. 53, pp. 4619-4630, Dec. 2005.